Electrochemical characterization of biologically important electroactive metal ligand complexes with multi-electron transfer reaction

by

Md. Matiar Rahman

A thesis submitted in partial fulfillment of the requirements for the degree of
Master of Philosophy (M. Phil.) in Chemistry

Khulna University of Engineering & Technology
Khulna 9203, Bangladesh.
July 2014

Declaration

This is to certify that the thesis work entitled "Electrochemical Characterization Of Biologically Important Electroactive Metal Ligand Complexes With Multi-electron Transfer Reaction" has been carried out by Md. Matiar Rahman in the Department of Chemistry, Khulna University of Engineering & Technology, Khulna, Bangladesh. The above thesis work or any part of this work has not been submitted anywhere for the award of any degree or diploma.

(Dr. Md. Abdul Motin)
Signature of the Supervisor
Professor
Department of Chemistry
Khulna University of Engineering &
Technology
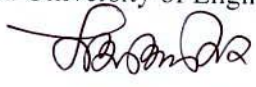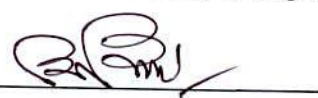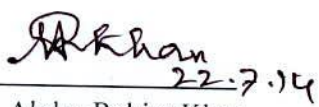
(Md. Matiar Rahman)
Signature of the Candidate
Roll No. 1053551

Approval

This is to certify that the thesis work submitted by Md. Matiar Rahman entitled "Electrochemical Characterization Of Biologically Important Electroactive Metal Ligand Complexes With Multi-electron Transfer Reaction" has been approved by the board of examiners for the partial fulfillment of the requirements for the degree of M. Phil. in the Department of Chemistry, Khulna University of Engineering & Technology, Khulna, Bangladesh in July 22, 2014.

BOARD OF EXAMINERS

1. _____

   Dr. Md. Abdul Motin   Chairman
   Professor, Department of Chemistry   (Supervisor)
   Khulna University of Engineering & Technology

2. _____

   Head   Member
   Department of Chemistry
   Khulna University of Engineering & Technology

3. _____

   Dr. Md. Abdul Aziz   Member
   Professor, Department of Chemistry
   Khulna University of Engineering & Technology

4. _____

   Dr. Mohammad Abu Yousuf   Member
   Professor, Department of Chemistry
   Khulna University of Engineering & Technology

5. _____

   Dr. Md. Abdur Rahim Khan   Member
   Professor, Department of Chemistry   (External)
   Rajshahi University

iii

Dedicated

To

My Parents

Acknowledgement

I would like to express my deepest sense of gratitude and sincere thanks to my respected supervisor **Dr. Md. Abdul Motin**, Professor, Department of Chemistry, Khulna University of Engineering & Technology, Khulna, Bangladesh for his proper guidance, co-operation, invaluable suggestions and constant encouragement throughout this research work. I will remember his inspiring guidance and cordial behavior forever in my future life.

I am pleased to express my gratitude to the Departmental Head Professor **Dr. Mohammad Abu Yousuf** for providing me necessary laboratory facilities for the research. I would like to express my thanks to Professor **Dr. M. A. Aziz** for his encouragement and inspiration throughout the work. I should take this opportunity to express my sincere thanks to **all teachers** of this department for their valuable advice and moral support in my research work.

I wish to convey my hearty thanks to all my friends, class fellows and colleagues specially, **Md. Abdul Hafiz Mia, K. M. Salim Reza, Sheikh Ahidul Alam, Mir Hussain Kabir and Md. Joynal Abedin,** all of them helped me according to their ability.

I wish to thank my **mother**, wife **Shilpi** and son **Naiem** for their grate understanding and support.

<div align="right">

Md. Matiar Rahman

</div>

ABSTRACT

The redox behavior of Cu (II) only and Cu (II) with aspartic acid (Apa), L-phenyl alanine (Phe), 3-nitrobenzene sulfonate (NBS); Zn(II) only and Zn(II) with Apa, Phe, NBS and Catechol (Cate) has been studied by Cyclic voltammetry (CV), Differential pulse voltammetry (DPV) and Chronamperometry (CA) techniques. The voltammetric technique demonstrates the interaction of biologically important metals (Cu, Zn) with the ligands (Apa, Phe, NBS, Cate) that is formed of metal-ligand complexes. The interaction studies have been carried out in variation of metal ion concentration, ligand concentration, buffer solution of different pH and scan rate.

In all the studies of Cu(II) and Zn(II) complexes, with some exception, Cu(II)-ligand systems and Zn(II)-ligand systems have been found to undergo quasireversible electrode reaction with EC mechanism. For all the ligands, Apa and Phe are electroinactive ligands whereas Cate and NBS are electroactive ligands. Both the anodic and cathodic voltammetric peaks were shifted and sometimes developed new peaks with the addition of Apa, Phe, NBS, Cate in Cu(II) and Zn(II) solutions.

On the addition of Apa, Phe and NBS in Cu(II) solution, the peak positions of the voltammogram of Cu(II)-Apa, Cu(II)-Phe and Cu(II)-NBS, first anodic peak was shifted positively but the second oxidation peak was shifted negatively with respect to that of only Cu(II). The peak current decreases significantly compared with that for free Cu(II) in the same experimental conditions. This behavior confirms the interaction and complexation between Cu(II) and Apa, Phe.

The effect of pH of Cu(II)-Apa, Cu(II)-Phe and Cu(II)-NBS were studied by varying pH from 3.5 to 7.0. The peak current of Cu(II)-Apa, Cu(II)-Phe and Cu(II)-NBS increases with the decrease of pH indicating that at lower pH the Cu(II)-Apa, Cu(II)-Phe and Cu(II)-NBS is highly electroactive. The maximum peak current was obtained at pH 3.5. This shows that the electrochemical oxidation of Cu(II)-Apa, Cu(II)-Phe and Cu(II)-NBS is facilitated in acid media and hence the rate of electron transfer is faster. The average diffusion coefficient, D of Cu(II)-Apa or Cu(II)-Phe is found to be $4.5 \times 10^{-6} cm^2 s^{-1}$.

The cyclic voltammogram of Zn(II) only and Zn(II) with Apa, Phe, NBS and Cate in aqueous and in buffer solution of different pH were taken at different scan rates. The CV of Zn (II) shows at pH (1.5, 3 and 4.5) one well defined anodic and cathodic peak at different scan rate but in aqueous solution only Zn(II) showed very weak anodic peak.

Upon the addition of Apa, Phe, NBS, Cate with Zn(II) the first anodic peak shifted positively and the cathodic peak is shifted negatively which indicates the formation of Zn(II)-Apa or Zn (II)-Phe complex. The intensity of the anodic and cathodic peak current decreases with the increasing of Apa or Phe or NBS or Cate suggesting that is formed of more Zn(II)-Apa or Zn(II)- Phe or Zn(II)- NBS complex.

The effect of pH of Zn(II)-Apa, Zn(II)-Phe, Zn(II)-NBS and Zn(II)-Cate were studied by varying pH from 1.5 to 11. The peak current decreases with the increase of pH. The maximum peak current was obtained at pH 3-4.5. At higher pH (7-11), the anodic peak disappeared. This shows that the electrochemical oxidation of Zn(II) complexes is hindered in basic media.

For the comparison CV of Zn(II) only and Zn(II) –Asp, Zn(II)-Phe, Zn(II)- Cate, Zn(II)-NBS at similar condition (pH 3, scan rate 0.1V/s), it is seen that the anodic peak current of Zn(II)-Asp and Zn(II)-Phe are lower than that of Zn(II) only whereas the anodic peak current of Zn(II)-Cate and Zn(II)-NBS is higher than that of Zn(II) only. When Cate and NBS are coordinated with Zn(II) both metal and ligands are electroactive, so constructive interference of peak appeared whereas Asp and Phe are coordinated with Zn(II), here ligands are electroinactive so the overall peak currents are lower than Zn(II) only.

The slopes of the plots of E_p against pH of all studied metal ligand complexes were determined graphically as anodic peak 25- 35 mV/pH at 0.1V/s, which is close to the theoretical value of 30 mV for a two-electron, two-proton transfer process which indicates that the oxidation of all metal-ligand complexes proceeded via the $2e^-/2H^+$ processes. This suggests that during the reaction not only electron but also protons are released from the metal-ligand complexes.

For all the studied system, with the increasing of metal: ligand composition from 1: 1 to 1:5 (metal fixed), the current decreases linearly but after more addition of ligands, the current intensity change is constant. This indicates that the availability of metal is limited for the formation of the metal-ligand complex at saturation point. When the composition of metal

increases with the fixed of the composition of ligands from 1:1 to 5:1, after certain concentration, the voltammogram pattern reflected into the only metal, because of the deficiency of ligands in solution. The relation between metal - ligand concentration and cyclic voltammetric anodic and cathodic peak current (I_{pa} and I_{pc}) is linear.

The proportionality of the anodic and cathodic peak currents with square root of scan rate of all the studied metal ligand complexes with few exceptions suggests that the peak current of the different complexes at each redox reaction is controlled by diffusion process. From the studied of all systems it is seen that current functions ($1/v^{-1/2}$) decreased with the increasing of scan rate except Zn(II)- Cate. So the behavior of electrode reaction of all Cu(II)- ligands and Zn(II)- ligands are of ECE mechanism except Zn(II)- Cate is of CE mechanism. .

Contents

LIST OF TABLES

xiv

xvi

xvii

LIST OF FIGURES

CHAPTER I

Introduction

1.1 General

Electrochemistry is a stringent science concerned with the mutual transformation of chemical and electrical energy. It correlates chemical, surface, and electrical properties of the systems. It has strong links to many other fields of science. Modern electrochemistry has uxorious vast applications. These include exploration of new inorganic and organic compounds, biochemical and biological systems, energy applications involving fuel cells and solar cells, and nanoscale investigations. It also finds applications in electroanalysis, industrial electrolysis, electroplating, batteries, electrochemical machining, minimization of corrosion, sensor biosensors nanotechnology and bio- electrochemistry [1]. Electrochemical processes form the basis of large-scale chemical and metallurgical production of a number of materials. Modern electrochemical power sources (primary and secondary batteries) are used in many fields of engineering and their production figures are measured in billions of units. Several electrochemical devices, such as pH or oxygen electrodes, have been used regularly for years in environmental analysis. Recent advances in electrochemical sensor technology will certainly enlarge expand the scope of these devices towards a wide range of organic and inorganic contaminants and will speed their role in field analysis. These advances incorporate the introduction of modified or molecular devices or sensor arrays, and developments in the areas of micro fabrication, computerized instrumentation and flow detectors.

Electrochemical vision have been proved particularly fruitful for studying and interpreting a number of very important biological processes such as cellular respiration, photosynthesis, and in maintaining the redox balance of proteins [2]. Moreover, redox signaling involves the control of cellular processes by redox reactions. The multifunctional activity of many metal complexes has been found to be essential for living organisms. A significant rising interest in the design of electroactive metal ligand complex compounds as drugs and diagnostic reagents is currently observed. Metal complexes with indole derivatives, amino acids, imidazole derivatives, pyridine derivatives, Schiff bases etc. exhibited remarkable biological activity as well as electrochemical activity [1-6].

The organic ligands containing N/S/O- sites provide potential binding sites for metal ions, and any information on their coordinating properties is important to understand the role of the metal ions in biological systems.

Transition metals particularly iron and essential trace metals such as Zn, Cu, Fe, Ni, and Mn etc. are present in animal and human bodies that serve as metalloenzyme or as enzymatic activators. Iron is the most important metal ion usage in hemoglobin for oxygen transport and as an active site for many metalloenzymes. Copper ion is similar to iron as an essential constituent and vital oxidative enzyme include in oxygen transport of protein in animals. Zinc is the trace element necessary for activity of an appreciable number of enzymes like other trace elements. An obvious expect is that the free metal is more toxic than the metal chelate [7]. Thus the chelating agents are applied in medicine for the formation of soluble easily extractable metal chelates by sequestering metal ions in the circulation of blood. There are many familiar chelating agents of amino acids, 3-nitrobenzene sulfonate, imidazole etc. are well known among them.

In order to understand the issue of biological activity of metal ion interaction with these drug based ligands in terms of electron transfer mechanism is necessary. To our knowledge, a very few redox interaction analyses have been carried out in metal ligand complexes [7-12], but the redox behaviors with short-distant and long –distant interaction among the redox sites, the redox interaction with the electron transfer number and stepping number has not been analyzed.

Attempt will be made in the present work to do a systematic study of interaction of biologically significant metal (Fe, Zn, Cu, etc.) complexes with aminoacids, 3-nitrobenzene sulfonate, Catechol etc. based drug derivatives in order to get greater insight about the metal-ligand interactions which could help to understand the role of metal ions in the biological processes.

Electroactive compounds undergo oxidation and/or reduction on the electrode surface within a certain potential range. The electroactivity of such compounds depends upon the pH of the medium, nature of the electrode and active moiety (electrophore) present in their structures. Their redox behavior can be influenced by the change in pH, substituents, concentration and scan rate. The variation in redox behavior can be abused for a number of useful purposes like elucidation of electrode reaction mechanism. Cyclic voltammetry (CV),

differential pulse voltammetry (DPV), Chronoamperometry (CA) have used in the present work to achieve the following two main objectives:

- to understand the role of metal ions in the biological processes and metal–ligand interactions.
- to diagnose the mechanism of the redox processes.

In recent years the electrochemical techniques have led to the preferment over other techniques in the field of analysis owing to their specificity, high sensitivity, efficient selectivity, greater reliability, extensive versatility and fast detection ability. Direct monitoring, simplicity and low cost facilitated the investigation of the electrode reaction mechanism and interaction studies.

1.2 Biologically Important compounds

The elucidation of reaction mechanism at the electrode surface requires the determination of the electroactive moiety (electrophore) of the molecule, number of electrons involved in oxidation and/or reduction processes, number of protons accompanying the transfer of electrons in different pH media and the reversibility/irreversibility of each step [13]. The redox mechanisms of the following biologically important molecules were proposed on the basis of the results obtained from CV, DPV and Chronoamperometry (CA).

1.2.1 L-Phenylalanine

Phenylalanine (abbreviated as Phe) [7,14] is an α-amino acid with the formula $HO_2CCH(NH_2)CH_2C_6H_5$ (Figure 1.1). This essential amino acid is catagoried as non polar because of the hydrophobic nature of the benzyl side chain the codons for L-phenylalanine are UUU and UUC. L-phenylalanine is an electrically-neutral amino acid, one of the twenty common amino acids used to bio-chemically form proteins, coded for by DNA. Phenylalanine is structurally closely related to dopamine, epinephrine (adrenaline) and tyrosine.
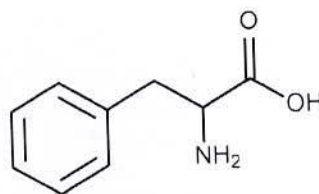
Figure 1.1: Structure of Phenylalanine

Phenylalanine is found naturally in the breast milk of mammals and manufactured for food and drinks products and is also sold as nutritional supplements for their reputed analgesic and antidepressant effects. It is a direct precursor to the neuromodulator phenylethylamine, a commonly used dietary supplement.

1.2.2 Biological functions of phenylalanine

L-phenylalanine can be converted into L-tyrosine, another one of the DNA encoded amino acids L-tyrosine in turn is transformed into L-DOPA, which is further altered into dopamine, norepinephrine (noradrenaline), and epineprine (adrenaline). The latter three are known as the catecholamines.

Phenylalanine uses the same active transport channel as tryptophan to cross the blood-brain barrier, and , in large quantities, interferes with the production of serotonin.

Lignan is derived from phenylalanine and from tyrosine. Phenylalanine is converted to cinamic acid by the enzyme phenylalanine ammonia lyase [15]. The genetic disorder phenylketonuria (PKU) is the inability to metabolize phenylalanine.Individuals with this disorder is known as "phenylketonurics" and must regulate their intake of phenylalanine. Pregnant women with hyperphenylalaninemia may show similar symptoms of the disorder (high levels of phenylalanine in blood) but these indicators will usually disappear at the end of gestation. Individuals who cannot metabolize phenylalanine for whatever reason must monitor their intake of protein to control the buildup of phenylalanine as their bodies convert protein into its component amino acids.

1.2.3 Catechol (Cate)

Catecol (also known as pyrocatechol or 1,2-dihydroxybenzene), is an organic compound with the molecular formula $C_6H_4(OH)_2$ shown in Figure 1.2 . It is the ortho isomer of the three isomeric benzenediols. This colorless compound occurs naturally in trace amounts. About 20M kg are produced annually, mainly as a precursor to pesticides, flavors and fragrances [16]. Catechol occurs as feathery white crystals which are very rapidly soluble in water.
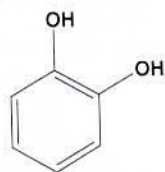
Figure 1.2: Structure of Catechol

1.2.4 Natural Occurrence of Catechol

Small amounts of catechol occur naturally in fruits and vegetables, along with the enzyme polyphenol oxidase (also known as catecholase, or ctechol oxidase).Upon mixing the enzyme with the substrate and exposure to oxygen (as when a potato or apple is cut and left out), the colorless catechol oxidizes to reddish-brown melanoid pigments, derivatives of benzoquinone. the enzyme is inactivated by adding an acid, such as lemon juice, and slowed with cooling . Excluding oxygen also prevents the browning reaction. Benzoquinone is said to be antimicrobial, which slows the spoilage of wounded fruits and other plant parts, Catechol moieites are also found widely within the natural world. Arthropodcutcle consists of chitin linked by a catechol moiety to protein. The cuticle may be strengthened by cross-linking (tanning and sclerotization), particularly in insects, and of course by biomineralozation [17].

1.2.5 Use of Catechol

Approximately 50% of synthetic catechol is consumed in the production of pesticides, the remainder being used as a precursor to fine chemicals such as perfumes and pharmaceuticals [16]. It is a common building block in organic synthesis [18]. Several industrially significant flavors and fragrances are prepared starting from catechol [19]. Guaiacol is prepared by methylation of catechol and is then converted to vanillin on a scale of about 10M kg per year (1990).The related mono ethyl ether of catechol, guethol, is converted to ethylvanillin, a compinent of chocolate confectionaries. 3-trans-Isocamphylcyclohexanol, widely used as a replacement for sandalwood oil, is prepared from catechol via guaiacol and camphor. Piperonal, a flowery scent, is prepared from the methylene diether of catechol followed by condensation with glyoxal and decarboxylation [20]. Catechol is used as a black –and- white photographic developer, but except for some special purpose applications, its use until recently was largely historical. Modern catechol

developing was pioneered by noted photographer Sandy King. His "PyroCat" formulation enjoys widespread popularity among modern black and white film photographers.

1.2.6 Aspartic acid (Apa)

Aspartic acid (abbreviated as Apa) [21] is an α-amino acid with the chemical formula $HOOCCH(NH_2)CH_2COOH$ (Figure 1.3). The carboxylate anion and salts of aspartic acid are known as aspartate. The L-isomer of aspartate is one of the [22] proteinogenic amino acids, i.e., the building blocks of proteins. Its codons are GAU and GAC.
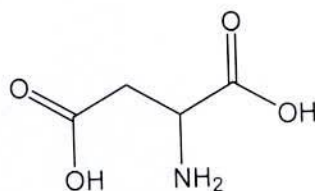
Figure 1.3 : Structure of Aspartic acid

Aspartic acid is, together with glutamic acid, classified as an acidic amino acid with a pK_a of 3.9, however in a peptide the pK_a is highly dependent on the local environment. A pK_a as high as 14 is not at all uncommon. Aspartate is pervasive in biosynthesis. As with all amino acids, the presence of acid protons depends on the residue's local chemical environment and the pH of the solution.

1.2.7 Role in biosynthesis of amino acids

Aspartate is non-essential in mammals, being produced from oxaloacetate by transamination. It can also be generated from ornithine and citrulline in the urea cycle. In plants and microorganisms, aspartate is the precursor to several amino acids, including four that are essential for humans: methionine, threonine, isoleucine, and lysine. The conversion of aspartate to these other amino acids begins with reduction of aspartate to its "semialdehyde," $O_2CCH(NH_2)CH_2CHO$

Aspartate is also a metabolite in the urea cycle and participates in gluconeogenesis. It arries reducing equivalents in the malate-aspartate shuttle, which utilizes the ready interconversion of aspartate and oxaloacetate, which is the oxidized (dehydrogenated) derivative of malic acid. Aspartate donates one nitrogen atom in the biosynthesis of

inosine, the precursor to the purine bases. In addition, aspartic acid acts as hydrogen acceptor in a chain of ATP synthesis.

1.2.8 3-nitrobenzenesulfonate (NBS)

3-nitrobenzenesulfonate (NBS) (Figure 1.4) is a pale yellow powder at standard temperature and pressure. Melting point and boiling point are 52.3° C and 217.5 °C [22], respectively. Vapour pressure is calculated to be 10.3 Pa at 25° C. The partition cofficient between octanol and water is calculted to be -3.13. Water solubility is calculated to be 1.0×10^6 mg/L at 25°C. NBS was used as oxidizing agent for the synthesis of quinoline.
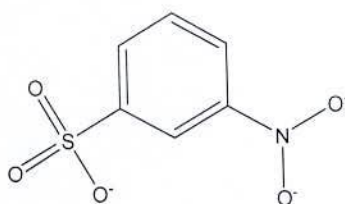
Figure 1.4: Structure of 3-nitrobenzenesulfonate

1.3 Electrochemistry as an analytical tool

Electrochemistry has become a powerful tool to study widely for solving the different problems in the area of inorganic, organic chemistry, nanotechnology, biochemistry, material science, environmental science etc. Many natural and biochemical processes have redox nature. Their redox mechanisms can be easily explained based on the experiment in voltammetry. Cyclic voltammetry is the most widely used modern electro-analytical method available for the mechanistic probing study of redox system.

In our present study we have investigated the redox behavior of biologically important metals (Cu, Zn) with ligands (Apa, Phe, NBS, Cate) in various pH and supporting electrolytes Various ecectrochemical techniques such as Cyclic Voltammetry (CV), Differential Pulse Voltammetry (DPV) and Chronoamperometry (CA) were used for investigation.

1.4 Mass transfer process in voltammetry

The movement of the electro –active substance through solution to the electrode is called mass transfer at the electrode surface. There are different types of mass transport by which a substance may be carried to the electrode surface from bulk solution. Depending on the experimental conditions, any of these or more than one might be operating in a given experiment.

In general, there are three types of mass transfer processes by which a reacting species may be brought to an electrode surface [23], these are,

a) Migration of charged ions in an electric field,

b) Diffusion under the influence of a concentration gradient, and

c) Convection due to the motion of the solution.

1.4.1 Migration

Migration refers to movement of a charged particle in a potential field [7]. In most voltammetric experiments, migration is undesirable but can be eliminated by the addition of a large excess of supporting electrolytes in the electrolysis solution, being charged them, will move towards the charged , i.e. cation to the cathode and anions to the anode. This motion of charged particle through solution, induced by the charges on the electrodes is called migration [24]. The fraction of the current carried by a given cation and anion is known as its transference number. Migration of charged electro-active substances and intermediates may be effectively eliminated by addition to the solution of an electrochemically inactive salt, called supporting electrolyte which does not undergo an electrochemical reaction at the electrode. When the potential is applied, supporting electrolyte remains unchanged and gives diffusion current.

Generally metal ion (cation) of the sample is migrated towards the cathode due to the electrostatic attraction, where they are reduced. When the cations are migrated towards the cathode a special type of current is produced. This current is called migration current. In cyclic voltammetry the effect of migration is usually eliminated by adding a 50 or 100 fold excess of an inert supporting electrilyte such as KCl, KNO_3.

1.4.2 Diffusion

The movement of a substance through solution by random thermal motion is known as diffusion. Whereas a concentration gradient exists in a solution, that is the concentration of

a substance, is not uniform throughout the solution. There is a driving force for diffusion of the substance from regions of high concentration to regions of lower concentration [24]. In any experiment in which the electrode potential is such that the electron transfer rate is very high, the region adjacent to the electrode surface will become depleted of the electro- active species, setting up a concentration in which this species will constantly be arriving at the electrode surface by diffusion from points further away [25].

An electrochemical cell in cyclic voltammetry in which the only mode of mass transfer is diffusion to an electrode surface. Since 50-100 fold excess supporting electrolyte is present in the solution, therefore the electrical force on the reducible in is nullified. When the potential is applied, the metal ions are reduced at the cathode and the concentration of the investigated substance is decrease at the cathode region. Hence a concentration gradient is produced. Under this condition, the reducible ions are diffused from the bulk of the solution and diffusion current is produced.

1.4.3 Convection

Convection or hydrodynamic transport is the movement of a substance through solution by stirring. When the electrolyte is stirred of heated the ions are transported from one space to another. At the same time a type of current is produced. This current is called convection current. Removing the stirring and heating can eliminate this current; Convection is a far more efficient means of mass transport than diffusion [24]. Therefore mass transport limited electrolysis currents are much higher for stirred solution than unstirred solution, where diffusion is the only means of mass transport. So, for minimizing convection unstirred vibration free solutions are required. Under such condition, the current is controlled unequally by diffusion of the reacting species through the concentration gradient adjacent to the electrode.

1.5 Cyclic Voltammetry (CV)

There are several well established electrochemical techniques for the study of electrochemical reactions. We chose the CV technique to study and analyze the redox reactions occurring at the polarizable electrode surface. This technique helps us to understand the mechanism of electron transfer reaction of the compounds as well as the nature of adsorption of reactants or products on the electrode surface.

Cyclic Voltammetry(CV) is perhaps the most effective and versatile electro analytical technique available for the mechanistic study of redox systems. It enables the electrode potential to be rapidly scanned in search of redox couples. Once located, a couple can then be characterized from the potentials of peaks on the cyclic voltammogram and from changes caused by variation of the scan rate. CV is often the first experiment performed in an electrochemical study. CV consists of imposing an excitation potential nature on an electrode immersed in an unstirred solution and measuring the current and its potential ranges varies from a few millivolts to hundreds of millivolts per second in a cycle. This variation of anode and cathodic current with imposed potential is termed as voltammogram. The technique involves under the diffusion controlled mass transfer condition at a stationary electrode utilizing symmetrical triangular scan rate ranging from $1 mVs^{-1}$ to hundreds mVs^{-1} [24].

The Cyclic Voltammetric technique reveals information about the following important phenomena.

i)   Reversibility of a reaction and a very rapid means of analysis of various systems

ii)   Direct investigation of reaction intermediate

iii)   Investigation of stepwise electrochemical and chemical reaction

iv)   Redox characteristic of oxidizing- reducing couple

v)   Investigation of charge transfer reaction at the electrode-solution interface and determination of charge transfer rate constant

1. 6 Differential Pulse Voltammetry (DPV)

Differential Pulse Voltammetry (DPV) is often used to make electrochemical measurement. It can be considered as a derivative of linear sweep voltammetry or staircase voltammetry, with a series of regular voltage pulse superimposed on the potential linear sweep or stair steps [26]. The current is measured immediately before each potential change, and the current difference is plotted as a function of potential. By sampling the current must before the potential is changed, the effect of the charging current can be decreased [24].

1.6.1 Use of DPV

DPV is a very important analytical tool for quantities determination in trace level.This technique can be used to study the redox properties of extremely small amount of chemicals because of the following two features [27]

i)   In these measurements, the effect of the charging current can be minimized, so high sensitivity is achieved.

ii)   Faradaic current is extracted, so electrode reactions can be analyzed more precisely.

1.7 Chronoamperometry

Our aim is to determine so reliable variations of electron transfer number, n with the potential that the redox interaction can be estimated. The technique of evaluating accurate variations at a short time is the analysis of chronoamperograms at a small disk electrode by use of the edge effect of diffusion current [12]. This technique has advantage of without knowing a value of a diffusion coefficient [28, 29]. The electron transfer number, n was determined the ratio of the slope and intercept of the Cottrell plots.

1.8 Electrochemical properties of metal –ligand complexes

In the study of the charge transfer reactions coupled with chemical reactions can give important indication of about actual biological processes occurring in human system. Understanding of such charge-transfer mechanism will help to determine the effectiveness of nutrition, metabolism and treatment of various biological disorders. Electrochemical studies of metal complexes of amino acids and small peptides have been carried in order to obtain a better understanding of transition metal complexes in proteins. In particular Cu(II) complexes were quite often investigated due to the possibility of applying different voltammetric techniques and also to the widespread occurrence of copper proteins, for instance blue proteins [30]. Metal ions can bind to peptides in several ways, depending on the amino acid residues, pH and binding stoichiometry. It has been reported that electrochemical behaviors of some amino acids and transition metal ions studied on Pt electrode [31,32].

Isatin-thiosemicarbazone copper(II) complexes related to the antiviral drug, methisazone were prepared electrochemically or by usual condensation methods, being characterized by different spectroscopic techniques [33]. Also the biological significance of fluvastatin, an indole derivative, is well established [34]. A significant rising interest in the design of metal compounds as drugs and diagnostic agents is currently observed in the area of scientific inquiry appropriately termed medicinal inorganic chemistry [35]. Metal complexes with

Schiff bases of isatin derivatives exhibited remarkable biological activity [36-38]. Redox properties of a drug can give insights into its metabolic fate or pharmaceutical activity [39-41]. The redox behaviour of various amino acids such as *DL*-Leucine, *L*-Proline and *L*-Tryptophan in the presence and absence of copper and iron and biochemically important compounds and their charge transfer reaction and their interaction of metal ions were studied [42].

Iron is an essential element in all organisms but its supply is restricted by its low solubility under physiological conditions. For this reason, microorganisms produce low molecular weight chelating agents, called siderophores, that can solubilize iron from the environment by complexing and transporting it to the cell [43-45]. An important structural feature of siderophores is the incorporation of catechol or hydroxamate groups, which are capable of selectively binding iron(III) in the presence of other biologically important metal ions. Hydroxamate type siderophores generally possess three or two hydroxamate functional groups able to form the hexacoordinate stable iron(III) complexes. The high affinity of siderophores for iron makes them useful as drugs to facilitate iron mobilization in humans, especially in the treatment of iron-overloaded diseases [46]. After complexation, iron must be released by the siderophore either at the cell wall or after penetration into the cell. Several mechanisms have been found or proposed for these processes [47,48]. The simplest is the reduction of iron(III) to a more labile iron(II) species, which results in dissociation of the complex.

The presence of several donor atoms in the molecule and the formation of saccharinate anion make saccharin capable of forming various types of coordination compounds with different metal ions [49]. Saccharin also forms mixed ligand complexes with the metal ions Mn(II), Co(II), Ni(II), Fe(III), Cu(II), Zn(II) and Cd(II) where the secondary ligands are nitrogen donor bases [50–57].

In order to understand the issue of multi-step electron transfer in metal ligand complexes a theoretical and experimental aspect of redox interaction in terms of electrochemical current potential curves analysis is necessary. To our knowledge, a few redox interaction analyses have been carried out in the above metal ligand complex compounds., the redox interaction with the electron transfer number of metal ions (Cu, Zn) with aspartic acid, phenyla alanine, catechol, 3-nitrobenzene sulfonate has not been analyzed before this work.

1.9 Aim of this thesis

Metal (Cu, Zn) complexes with aspartic acid, phenyl alanine, catechol, 3-nitrobenzene sulfonate etc. exhibited remarkable biological activity as well as electrochemical activity The materials, depending on their functionalities, may be used for diverse applications, such as pharmaceuticals, biomedical application, energy sector and electronics.

The specific aims of this study are:

i) to study the interaction of metal ions (Cu, Zn) with aspartic acid, phenyl alanine, catechol, 3-nitrobenzene sulfonate etc. in solution by cyclic voltammetry, differential pulse voltammetry and chronoamperometry method.

ii) to synthesize electrochemically functional biologically important electroactive metal ligand complexes.

iii) to know the redox properties of metals, ligands and metal-ligand complexes with electrochemical significance. The redox properties with electron transfer mechanism of the species will be investigated.

iv) to characterize the new electrochemical features of these synthesizing species by electrochemically.

v) to determine of the electron transfer numbers of metal-ligand complexes with single step and/or multi-step electron transfer reaction.

CHAPTER II

THEORETICAL BACKGROUND

Electrochemistry involves the study of chemical phenomena associated with charge separation. Often this charge separation leads to charge transfer, which can occur homogeneously in solution or heterogeneously on electrode surfaces [58]. To assure electrical neutrality, two or more charge transfer half reactions take place in opposite direction. Except in the transfer case of homogeneous redox reactions, these are separated in space, usually occurring at different electrodes immersed in solution in a cell. These electrodes are linked by conducting paths both externally (via electric wires etc.) and internally in solution (via ionic transport) so that charge can be transported.

If the cell configuration permits, the products of the two electrode reactions can be separated. When the sum of the free energy changes at both electrodes is negative, the electrical energy released can be harnessed (batteries). If it is positive, external electrical energy can be supplied to oblige electrode reaction to take place and convert chemical substances (electrolysis) [59].

Electrode reactions are heterogeneous and take place in the interfacial region between electrode and solution, the region where charge distribution differs from that of the bulk phase. The electrode process is affected by the structure of this region. At each electrode, charge separation can be represented by a capacitance and the difficulty of charge transfer by a resistance.

The electrode can act as a source (for reduction) or a sink (for oxidation) of electrons transferred to or from the species in solution:

$$O + ne \rightarrow R$$
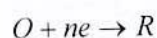
Where, O and R are the oxidized and reduced species. In order for the electron transfer to occur, there must be a correspondence between the energies of the electron orbitals where transfer takes place in the donor and acceptor. In the electrode this level is the highest filled orbital, which in a metal is Fermi energy level. In the soluble species it is the orbital of the valence electron to be given or received. Thus:

14

• for reduction, there is a minimum energy that the transferable electrons from the electrode must have before the transfer can occur, which corresponds to a sufficiently negative potential.

• for an oxidation there is a maximum energy that the lowest unoccupied level in the electrode can have in order to receive electrons from the species in solution, corresponding to a sufficiently positive potential.

The values of the potentials can be controlled externally in order to control the extent and the direction of the reaction. Electrode reactions are half reactions and they are, by convention, expressed as reductions. Each has associated standard electrode potential, E^0 measured relative to the normal hydrogen electrode (NHE), with all species at unit activity ($a_i = 1$).

For half reaction at equilibrium, the potential, E, can be related to the standard electrode potential through the Nernst equation

$$E = E^0 - \frac{RT}{nF} \sum v_i \ln a_i \quad \dots\dots\dots\dots\dots\dots\dots\dots\dots\dots\dots 2.1$$

Where, v_i are the stoichiometric numbers, positive for products (reduced species) and negative for reagents (oxidized species).

If the oxidized and reduced species involved in an electrode reaction are in equilibrium at the electrode surface, the Nernst equation can be applied. The electrode reaction is known as reversible when it obeys the condition of thermodynamic reversibility.

The concentration of the species at the interface depends on the mass transport of these species from bulk solution, described by the mass transfer coefficient k_d. A reversible reaction corresponds to the case where the kinetics of the electrode reaction is much faster than the transport. The kinetics is expressed by a rate constant, k which is the rate constant at any potential. So the criterion for a reversible reaction is:

$k >> k_d$

By contrast, an irreversible reaction is the one where the electrode reaction cannot be reversed, and in such a case

$k << k_d$

Quasi-reversible reactions exhibit behavior intermediate between reversible and irreversible reactions.

In order to study electrode reactions, reproducible experimental conditions must be created which enable minimization of all unwanted factors that can contribute to the measurements and diminish their accuracy. That means to suppress migration effects, confine the

interfacial region as close as possible to the electrode, and minimize solution resistance. These objectives are achieved by the addition of large amount (around 1 mol dm^{-3}) of inert electrolyte, the electroactive species being at a concentration of 5 mM or less [59].

Since an electrode predominantly attracts positively and negatively charged species, which may or may not undergo reaction at the surface, it should be remembered that the species may adsorb at the electrode surface. This makes it clear that in the description of any electrode process we have to consider the transport of species to the electrode surface as well as the electrode reaction itself. This transport can occur by diffusion, convection or migration. Diffusion is the transport of species due to the concentration gradient, convection is the imposition of mechanical fluid movement and migration is the movement of species under an electric field gradient.

For electroanalytical purposes, conditions are usually created in solution so that migration of the electroactive species can be neglected, through the addition of a large excess of supporting electrolyte. This electrolyte transports nearly all the charge movement by ion transport from one electrode to the other through the solution and the electroactive species are left unaffected by migration effects. Thus one is left with diffusion and convection. If there is convection, usually externally controlled, it is usually supposed to occur only as close to the surface at a distance known as the diffusion layer thickness. Closer to the surface there is only transport by diffusion.

The mechanism consists of the steps shown in Figure 2.1. [58]
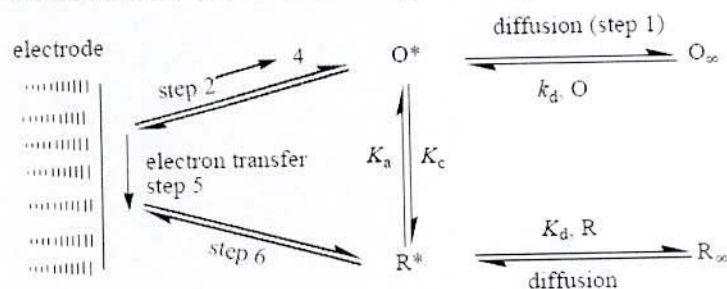
Figure 2.1. Process of electron transfer at an electrode.

Step 1: diffusion of the species to where the reaction occurs;

Step 2: rearrangement of the ionic atmosphere (10^{-8}s);

Step 3: reorientation of the solvent dipoles (10^{-11}s);

Step 4: alteration in the distances between the central ion and the ligands;

Step 5: electron transfer (10^{-16}s);

Step 6: relaxation in the opposite sense.

Diffusion step is the rate determining step.

The anodic and cathodic rate constants, k_a and k_c, describe the kinetics of the electrode reaction.

These are described by the Butler-Volmer equations:

$$k_a = k^0 \exp[\alpha_a nF(E - E^0) / RT] \dots\dots\dots\dots\dots\dots\dots 2.2$$

$$k_c = k^0 \exp[\alpha_c nF(E - E^0) / RT] \dots\dots\dots\dots\dots\dots\dots 2.3$$

where α_a and α_c are the anodic and cathodic transfer coefficients and E^0 is the formal potential for the system when the activities are replaced by concentrations, c_i ($a_i = \gamma_i c_i$; γ_i being the activity coefficient of species i).

Voltammetric methods have been used to identify the species present in solution to obtain qualitative and quantitative data and to study the nature and the mechanism of reactions that occur in the electrochemical system. Analyzing and interpreting the voltammograms enable determination of thermodynamic and kinetic parameters. The recorded current is a measure of the electrochemical reaction rate, which occurs in the interfacial region between the electrode and the solution and gives information about the electrochemical reaction mechanism.

In the present work three voltammetric techniques (CV, DPV and CA) have been employed.

2.1 Cyclic Voltammetry

A triangular potential-time waveform (Figure 2.2) with equal positive and negative slope where, usually the initial potential ($E_{initial}$) and final potential (E_{final}) are kept the same, give rise to the term cyclic voltammetry (CV). While the potential sweep is carried out, potentiostat measures the current resulting from the applied potential. The resulting plot of current *vs.* potential is termed as cyclic voltammogram. During a single potential cycle, the expected *I-E* response of a reversible redox couple is illustrated in Figure 2.3.

Simply stated, in the forward scan, the reaction is $O + e^- \rightarrow R$, R is electrochemically generated as indicated by the cathodic current. In the reverse scan, $R \rightarrow O + e^-$, R is oxidized back to O as indicated by the anodic current. The CV is capable of rapidly generating a new species during the forward scan and then probing its fate on the reverse scan. This is a very important aspect of the technique [60].
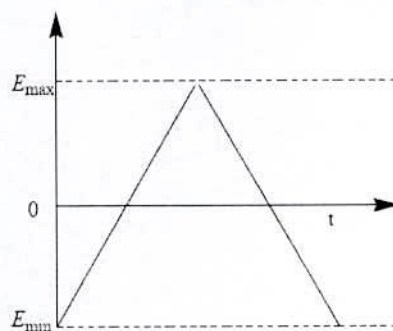
Figure 2.2. Variation of potential with time in cyclic voltammetry

A characteristic feature is the occurrence of peaks, identified by the peak potential E_p, which corresponds to electron transfer reactions. The repetitive triangular potential excitation signal for CV causes the potential of the working electrode to sweep backward and forward between two designate values (the switching potentials).

In cyclic voltammetry of reversible system, the product of the initial oxidation or reduction is then reduced or oxidized, respectively, on reversing the scan direction.
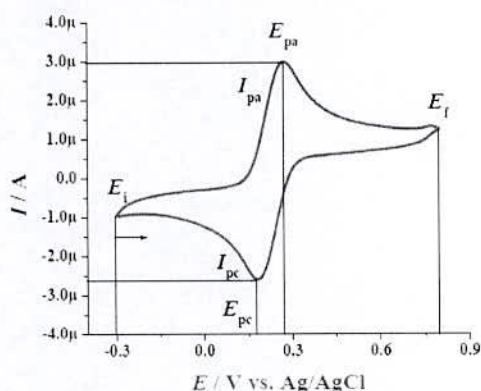
Figure 2.3. Cyclic voltammogram of Potasium Ferrocianide in 0.1 M acetate buffer (pH 4.5) at a potential scan rate of 100 mV s⁻¹.

The important parameters of a cyclic voltammogram are the magnitude of the peak currents, I_{pa}, and I_{pc}, and the potentials (E_{pa} and E_{pc}) at which the peaks occur. The two parameters give the peak hight and peak position in the voltammogram.

A redox couple in which both species rapidly exchange electrons with the working electrode is termed as electrochemically reversible couple. Such a couple can be identified from a cyclic voltammogram by measurement of the potential difference between the two peak potentials. The following equation applies to an electrochemically reversible system:

$$\Delta E_p = E_{pa} - E_{pc} \approx \frac{0.058}{n} \quad \text{at 298K} \ldots\ldots\ldots\ldots 2.4$$

where n is the number of electrons transferred, E_{pa} and E_{pc}, are the anodic and cathodic peak potentials in volts respectively. The separation of peak potentials with a value of 0.058/n is independent of scan rate for a reversible couple, but is slightly dependent on switching potential and cycle number.

The potential midway between the two potentials is the formal reduction potential of the couple:

$$E^0 = \frac{E_{pa} + E_{pc}}{2} \ldots\ldots\ldots\ldots\ldots\ldots\ldots\ldots\ldots\ldots 2.5$$

This equation holds only for a reversible electron transfer reaction having $\alpha = 0.5$. Electrochemical irreversibility is caused by slow electron exchange of the redox species with the working electrode. It is characterized by a separation of peak potentials that is greater than $\frac{0.058}{n}$ V and is dependent on the scan rate.

Adsorbed species lead to changes in the shape of the cyclic voltammogram, since they do not have to diffuse from the electrode surface. In particular, if only adsorbed species are oxidized or reduced, in the case of fast kinetics the cyclic voltammogram is symmetrical, with coincident oxidation and reduction peak potentials [61].

Cyclic voltammetry is one of the most versatile techniques for the study of electroactive species, as it has a provision for mathematical analysis of an electron transfer process at the electrode [62-65]. It is an electroanalytical tool for monitoring and recognition of many electrochemical processes taking place at the surface of electrode and can be used to study redox processes in biochemistry and macromolecular chemistry [66].

2.1.1 Single electron transfer process

Based upon the values of electrochemical parameters, i.e., peak potential E_p, half peak potential ($E_{p/2}$), half wave potential ($E_{1/2}$), peak current (I_p), anodic peak potential E_{pa}, cathodic peak potential E_{pc} etc, it can be ascertained whether a reaction is reversible, irreversible or quasi-reversible. The electrochemical parameters can be graphically obtained from the voltammogram as shown in the Figure 2.3.

Three types of single electron transfer process can be studied.

a. Reversible process. b. Irreversible process and c. Quasi-reversible.

2.1.1 (a) Reversible processes

The heterogeneous transfer of electron from an electrode to a reducible species and vice versa is a form of Nernstian electrode reaction with assumption that at the surface of electrode, rate of electron transfer is so rapid that a dynamic equilibrium is established and Nernstian conditions hold i.e.;

$$C_O(0,t)/ C_R(0,t)= Exp[(nF/RT)(E_i - vt - E^0)]............2.6$$

In eq. (2.6) concentration of oxidized and reduced species, C_o and C_R are function f time, E^0 is the standard electrode potential, E_i is the initial potential. Under these conditions, the oxidized and reduced species involved in an electrode reaction are in equilibrium at the electrode surface and such an electrode reaction is termed as a "reversible reaction. Due to difference in concentration of electroactive species at the surface of electrode and the concentration in the bulk, diffusion controlled mass transport takes place. We can apply Fick's second law to obtain time dependent concentration distribution in one dimension of expanding diffusion layer;

$$\partial C_i(x,t)/\partial t = D_i\partial^2 C_i(x,t)/\partial x^2 ....2.7$$

where C_i and D_i are concentration and diffusion coefficient of species i.

Peak current is a characteristic quantity in reversible cyclic voltammetric process. The expression for current (I) is obtained by solving Fick's law equation [67]

$$I = nFAC_o^* (\pi D_o\sigma)\chi(\sigma t) ....2.8$$

Where $\sigma = (nF/RT)v$

and $\sigma t = nF/RT(E_i - E)$

At this value of χ (σt) the current is maximum and is referred as I_p. Substituting the maximum value of χ (σt), the current expression for forward potential scan becomes,

$$I_p = 0.4463nFAC_0^*\left[\frac{nF}{RT}\right]^{1/2} D_o^{1/2}\upsilon^{1/2} ....2.9$$

where I_p is the peak current or maximum current and all other parameters have their usual significance.

At 298 K, the above equation can be written as:

$$I_p = 2.69\times10^5 n^{3/2} AC_0^* D_o^{1/2}\upsilon^{1/2} ....2.10$$

Eq (2.10) is called Randle's Sevcik equation [63,64]. The value of numerical constant of Eq (2.10) determined by Sevcik was little low. The correct value of this constant was determined by Randle and was experimentally verified by Delahay, Muller and Adams [67].

Diagnostic criteria of reversibility

Certain well-defined characteristic values can be obtained from the voltammogram, for a reversible electrochemical reaction [68].

- Relationship between peak potential (E_p) and half wave potential ($E_{1/2}$) for a reversible reaction is given by;

$$E_{pc} = E_{1/2} - (1.109 \pm 0.002)RT/nF \quad ....2.11a$$

$$E_{pa} = E_{1/2} - (1.109 \pm 0.002)RT/nF \quad ....2.11b$$

where $E_{1/2}$ is potential corresponding to $I = 0.8817I_p$. For reversible reaction $E_{1/2} = E^0$ At 298 K

$$E_{pa} = E_{1/2} + 0.0285/nV \quad ....2.11c$$

From Eq(2.11a) and (2.11b) one obtains,

$$\Delta E_p = E_{pc} - E_{pa} = -2.22RT/nF \quad ....2.12a$$

At 298 K

$$\Delta E_p = E_{pc} - E_{pa} = -\frac{0.057}{n}V \quad ....2.12b$$

- The peak position (voltage) does not alter as scan rate varies. In some cases, the precise determination of peak potential E_p is not easy because the observed CV peak is some what broader. So it is sometimes more convenient to report the potential at $I = 0.5I_p$ called half peak potential, $E_{p/2}$ which is used for $E_{1/2}$ determination [69] by the following expression:

$$E_{pc/2} = E_{1/2} + 1.09RT/nF \quad ....2.13a$$

At 298 K

$$E_{pc/2} = E_{1/2} + 0.028/n \quad ....2.13b$$

$$E_{pa/2} = E_{1/2} - 0.028/n \quad ....2.13c$$

From equation (2.11a) and (2.13a) we obtain,

$$\left| E_{pc} - E_{pc/2} \right| = 2.2RT/nF \quad ....2.14a$$

At 298 K

$$\Delta E = \left| E_{pc} - E_{pc/2} \right| = 0.0565/n ....2.14b$$

These act as diagnostic criteria for reversibility. Eq (2.14b) shows that with increase in number of electrons transferred peak separation (E_{pc} - E_{pa}) decreases. For one, two and three electrons it is 57 mV, 29 mV and 19 mV respectively. E_p and ΔE_p i.e., (E_{pc}-E_{pa}) are independent of scan rate for a reversible system [70]. However, ΔE_p may increase lightly with υ because of presence of finite solution resistance between the reference electrode and working electrode.

2.1.1 (b) Irreversible processes

For a totally irreversible process, reverse reaction of the electrode process does not occur. For such a process, stationary electrode voltammetric curves were described by Delahay [67], Matsuda and Ayabe [71] and Reinmuth [72].

The process can be expressed by the following reaction:

$$O + ne \rightarrow R$$
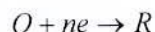
Irreversibility can be diagnosed by three major criteria.

(a)   A shift in peak potential occurs as the scan rate varies.

(b)   Peak width for irreversible process is given by

$$\left| E_p - E_{p/2} \right| = 1.857 \frac{RT}{\alpha n' F} \dots\dots\dots\dots\dots\dots\dots\dots\dots 2.15$$

where n' being the number of electrons transferred in the rate determining step and α is the charge transfer coefficient.

$$\left| E_p - E_{p/2} \right| = \frac{47.7}{\alpha n'} \text{ mV at 298 K} \dots\dots\dots\dots\dots 2.16$$

$$I = nFAC_o^*(\pi D_o b)^{1/2} \chi(bt) \dots\dots\dots\dots\dots\dots 2.17a$$

where $b = \alpha n' F \upsilon / RT$

An examination of Table 2.2 reveals that the function $\chi(bt)$ goes through a maximum at $\pi^{1/2}\chi(bt) = 0.4958$. Introduction of this value in equation (2.17a) yields the expression (2.17b):

$$I_p = 2.99 \times 10^5 n(\alpha n')^{1/2} AC_o D_o^{1/2} \upsilon^{1/2} \dots\dots\dots\dots 2.17b$$

For an irreversible process, I_p in terms of $k^0 sh$ is given as:

$$I_p = 0.227nFAC_o^* k_{sh}^o \exp\left[-\left(\frac{\alpha n'F}{RT}\right)(E_p - E^o)\right] \dots\dots 2.18$$

The unknown E^o (standard potential) can be determined by using Eq (2.18) [68];

$$E_p - E^o = -0.78\frac{RT}{\alpha n'F} + \frac{RT}{\alpha n'F}\ln\frac{k_{sh}^o}{(D_o)^{1/2}} - \frac{RT}{2\alpha n'F}\ln \alpha n'\upsilon \dots 2.19$$

Reinmuth [72] reported an alternative expression

$$\frac{I_p}{nFA} = C_o^* k_{sh}^o \dots\dots\dots\dots\dots\dots\dots\dots\dots\dots\dots\dots 2.20$$

where k_{sh}^o is standard heterogeneous rate constant for forward reaction. For totally irreversible process, the standard heterogeneous electron transfer rate constant has a value of $\leq 10^{-5}$ cm sec^{-1} with extremely low value of charge transfer coefficient and the current is mainly controlled by the rate of charge transfer reaction. Nernst equation is not applicable for such type of reactions. Cyclic voltammogram for irreversible process is shown in Figure [2.4] [58].
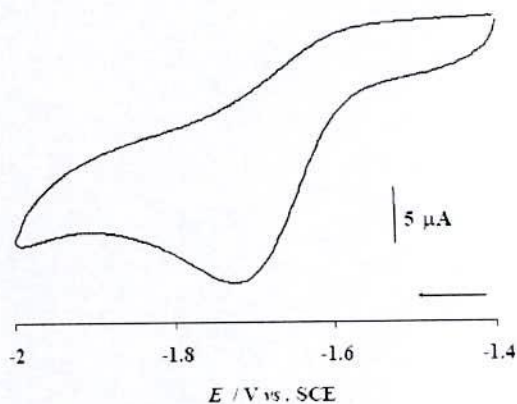
Figure 2.4. Cyclic voltammogram of irreversible redox process.

2.1.1 (c) Quasi-reversible process

Quasi-reversible process is termed as a process, which shows intermediate behavior between reversible and irreversible processes. In such a process the current is controlled by both the charge transfer and mass transfer.

Cyclic voltammogram for quasi-reversible process is shown in Figure [2.5]. [58]
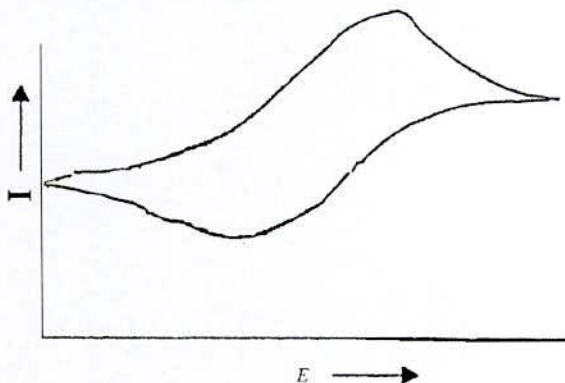
Figure 2.5. Cyclic voltammogram of quasi-reversible redox process.

For quasi-reversible process the value of standard heterogeneous electron transfer rate constant, k_{sh}^o lies in the range of 10^{-1} to 10^{-5} cm sec^{-1} [73]. An expression relating the current to potential dependent charge transfer rate was first provided by Matsuda and Ayabe [71].

$$I(t) = C_{o(0,t)}k_{sh}^o Exp\left[-\frac{\alpha nF}{RT}\left\{E(t) - E^o\right\}\right] - C_{R(0,t)}k_{sh}^o Exp\left[-\frac{\beta nF}{RT}\left\{E(t) - E^o\right\}\right]....2.21$$

where k_{sh}^o is the heterogeneous electron transfer rate constant at standard potential E^0 of redox system. α is the transfer coefficient and $\beta = 1-\alpha$. In this case, the shape of the peak and the various peak parameters are functions of α and the dimensionless parameter, Λ, defined as [74]

$$\Lambda = \frac{k_{s,h}}{D^{1/2}(nF/RT)^{1/2}\upsilon^{1/2}} \ldots \ldots \ldots 2.22$$

when $D_o = D_R = D$

D_o and D_R are the diffusion coefficients of oxidized and reduced species respectively.

For quasi-reversible process current value is expressed as a function of $\psi(E)$ [74].

$$I = nFAC_o^* \frac{k_{sh}^o}{\Lambda}\psi(E) \ldots \ldots \ldots 2.23$$

where $\psi(E)$ is expressed as

$$\psi(E) = \frac{I}{nFAC_o^* D_o^{1/2}(nF/RT)^{1/2}\upsilon^{1/2}} \ldots \ldots \ldots 2.24$$

It is observed that when $\Lambda \geq 10$, the behavior approaches that of a reversible system [68]. For three types of electrode processes, Matsuda and Ayabe [71] suggested following zone boundaries.

24

- Reversible (Nernstian)

$$k_{sh}^o \geq 0.3 \upsilon^{1/2} \text{ cm s}^{-1}$$

- Quasi-reversible

$$0.3\upsilon^{1/2} \geq k_{sh}^o \geq 2 \times 10^{-5} \upsilon^{1/2} \text{ cm s}^{-1}$$

- Totally irreversible

$$k_{sh}^o \leq 2 \times 10^{-5} \upsilon^{1/2} \text{ cm s}^{-1}$$

2.1.2 Multi electron transfer processes

Multi-electron transfer process usually takes place in different steps. A two-step mechanism each characterized by its own electrochemical parameters is called an "EE mechanism".

A two step reversible "EE mechanism" is represented as;

$$O + n_1 e \leftrightarrow R_1 \qquad\qquad (E_1^o)\text{.....................}2.25$$

$$R + n_1 e \leftrightarrow R_2 \qquad\qquad (E_2^o)\text{....................}2.26$$

Each heterogeneous electron transfer step is associated with its own electrochemical parameters i.e., k_{sh}^o and α_i, where $i = 1, 2$ for the 1st and 2nd electron transfer respectively. The value of k_{sh}^o for first reversible electron transfer limiting case can be calculated as [75]:

$$k_{sh} = k_{sh}^o \exp\left[-\alpha 1 F \Delta E^o / 2RT\right]\text{...........................}2.27$$

where

$$\Delta E^o = E_2^o - E_1^o$$

For ΔE^0 greater than 180 mV, shape of wave does not dependent on the relative values of E^0, otherwise shapes of peak and peak currents depend upon ΔE^0 [76]. Based on the value of ΔE^0, we come across different types of cases as shown in the Figure 2.6.

Types of two electron transfer reactions

Case 1: $\Delta E^0 \geq 150$ mV peaks separation

When $\Delta E^0 \geq 150$ mV the EE mechanism is termed as "disproportionate mechanism [77]. Cyclic voltammogram consists of two typical one-electron reduction waves. The heterogeneous electron transfer reaction may simultaneously be accompanied by homogenous electron transfer reaction, which in multi-electron system leads to disproportionation which can be described as:

$$R_1 \rightarrow O + n_1 e \dotfill 2.28a$$

$$R_1 + n_2 e \rightarrow R_2 \dotfill 2.28b$$

$$2R_1 \leftrightarrow O + R_2 \dotfill 2.28c$$

$$k_{disp} = \frac{[O][R_2]}{[R_1]^2} \dotfill 2.29$$

$$\ln k_{disp} = \left[\frac{nF}{RT} \right] (E_2^o - E_1^o) \dotfill 2.30$$

Case 2: $\Delta E^0 < 100$ mV ----- Peaks overlapped

In this case, the individual waves merge into one broad distorted wave whose peak height and shape are no longer characteristics of a reversible wave. The wave is broadened similar to an irreversible wave, but can be distinguished from the irreversible voltammogram, in that the distorted wave does not shift on the potential axis as a function of the scan rate.

Case 3: $\Delta E^0 = 0$ mV ----- Single peak

In this case, in cyclic voltammogram, only a single wave would appear with peak current intermediate between those of a single step one electron and two electron transfer reactions and E_p-$E_p/2 = 56$ mV.
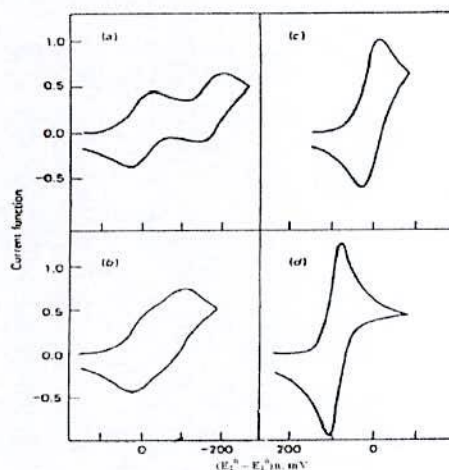
Figure 2.6. Cyclic voltammograms for a reversible two-step system. (a) $\Delta E^0 = -180$ mV, (b) $\Delta E^0 = -90$ mV, (c) $\Delta E^0 = 0$ mV, (d) $\Delta E^0 = 180$ mV. (Taken from ref. 78)

Contrary to the convention the direction of the current in these voltammograms has been shown cathodic above the base line and anodic below the base line.

26

Case 4: $E^0_1 < E^0_2$ ----2nd Reduction is easy than 1st one

If the energy required for the second electron transfer is less than that for the first, one wave is observed, having peak height equal to $2^{3/2}$ times that of a single electron transfer process. In this case, E_p-$E_p/2$ = 29 mV. The effective E^0 for the composite two electron

wave is given by $\dfrac{(E^o_1 + E^o_2)}{2}$ as reported in literature [78]

2.1.3 Determination of heterogeneous electron transfer rate constant by CV

Cyclic voltammetry provides a systematic approach to solution of diffusion problems and determination of different kinetic parameters including $k_{s,h}$. Various methods have been reported in literature for the determination of heterogeneous rate constants. Nicholson [73,89], Gileadi [80] and Kochi [81] developed different equations to calculate heterogeneous electron transfer rate constants.

2.1.4 Coupled chemical reactions

Although charge transfer processes are an important part of the entire spectrum of chemical reactions, yet they seldom occur as isolated elementary steps. Electron transfer reactions coupled with new bond formation or bond breaking steps are very frequent. The occurrence of such chemical reactions, which directly affect the available surface concentration of the electroactive species, is common to redox processes of many important organic and inorganic compounds. Changes in the shape of the cyclic voltammogram resulting from the chemical competition for the electrochemical reactant or product, can be extremely useful for elucidating the reaction pathways and for providing reliable chemical information about reactive intermediates [82].

2.2 Pulse techniques

The basis of all pulse techniques is the difference in the rate of decay of the charging and the faradaic currents following a potential step (or pulse). The charging current decays considerably faster than the faradaic current. A step in the applied potential or current represents an instantaneous alteration of the electrochemical system. Analysis of the evolution of the system after perturbation permits deductions about electrode reactions and their rates to be made. The potential step is the base of pulse voltammetry. After applying a

pulse of potential, the capacitative current dies away faster than the faradic one and the current is measured at the end of the pulse. This type of sampling has the advantage of increased sensitivity and better characteristics for analytical applications. At solid electrodes there is an additional advantage of discrimination against blocking of the electrode reaction by adsorption [59].

2.2.1 Differential pulse voltammetry (DPV)

DPV is considered as a derivative of staircase voltammetry with a series of regular voltage pulses superimposed on the stair steps. The base potential is incremented between the pulses, the increment being always the same; the current is measured immediately before pulse application and at the end of the pulse. The difference between the two currents is registered. The application of potential is illustrated in Figure 2.7 [58]

Since DPV is a differential method, the response is similar to the first derivative of a conventional voltammogram, which is a peak. The waveform is shown in Figure 2.8 [58]. DPV is a more sensitive voltammetric technique than CV.

The peak potential, E_p can be approximately identified with $E_{1/2}$, for a reversible system but with increasing irreversibility E_p moves away from $E_{1/2}$, at the same time as peak width increases and its height diminishes [59].

Quantitative treatments for reversible systems demonstrated that, with only R (positive sign) or only O (negative sign) initially present, the following equation can be written as

$$E_{max} = E_{1/2} \pm \frac{\Delta E}{2} \quad \dots\dots\dots\dots\dots\dots\dots\dots\dots\dots\dots\dots\dots\dots\dots\dots\dots 2.31$$

where ΔE is the pulse amplitude.
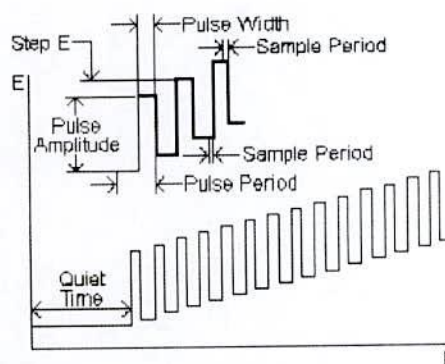
Figure 2.7. Scheme of application of potential.

28
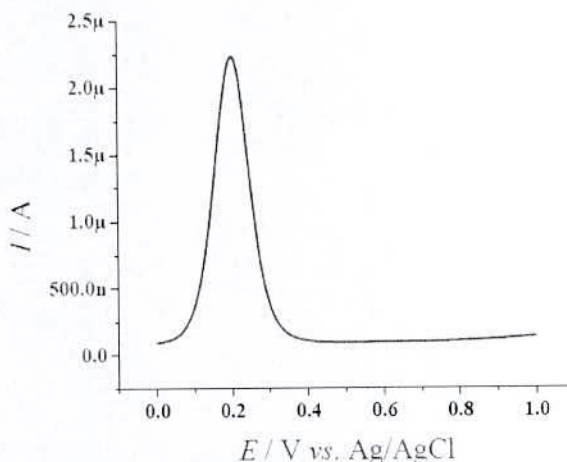
Figure. 2.8. Differential pulse voltammogram of 10 μM K₄Fe(CN)₆ in 0.1 M phosphate buffer pH 7.0. Scan rate: 5 mV s⁻¹. (My own work)

The use of pulse width larger than about 100 mV is not viable, as the peak width at half height, $W_{1/2}$, also increases, leading to a loss of resolution. At the limit, when $\Delta E \rightarrow 0$

$$W_{1/2} = 3.52\frac{RT}{nF} = \frac{90.4}{n} \quad\dots\dots\dots\dots\dots\dots\dots\dots\dots\dots\dots.2.32$$

2.3 Chronoamperometry (CA)

A chronoamperometric curve at a disk microelectrode varies from the Cottrell behavior to the steady state current. When potential is stepped to a diffusion-controlled potential domain at the disk electrode with radius, a, in the solution including electroactive species with the concentration, c^*, and the diffusion coefficient, D, the responding current, I, at the electrolysis time, t, has been expressed as [83,84]

$$I = 4nFc^*Da\left(1 + 0.71835\tau^{-1/2} + 0.05626\tau^{-3/2} - 0.00646\tau^{-5/2}\right)\dots 2.33$$

$$I = 4nFc^*Da\left[(\pi/4\tau)^{1/2} + \pi/4 + 0.094\tau^{1/2}\right]\dots\dots\dots\dots\dots.2.34$$

where $\tau = 4Dt/a^2$. Equations 2.33 and 2.34 are valid for $\tau > 1.44$ and $\tau < 0.82$, respectively. Some expressions for the chronoamperometric curves obtained by finite difference or the related methods [85-90] are closed to Eq.2.33 and 2.34. When τ is small enough to neglect the third term in Eq. 2.34, the potential-depending current for the reversible case is expressed by

29

$$I = \left(\pi^{1/2}nFD^{1/2}a^2t^{-1/2} + \pi nFDa\right)c^*(1+e^{-\varsigma})^{-1} \ldots\ldots\ldots 2.35$$

where

$$\varsigma = (F/RT)(E - E^{0'})$$

The Cottrell plot (I vs. $t^{-1/2}$) gives the slope and the intercept, respectively

$$s = \pi^{1/2}nFD^{1/2}a^2c^*(1+e^{-\varsigma})^{-1}$$

$$p = \pi nFDa\,c^*(1+e^{-\varsigma})^{-1}$$

The ratio of the square of the slope to the intercept is

$$s^2/p = nFa^3\,c^*(1+e^{-\varsigma})^{-1} \text{ or } n\left(1+e^{-\varsigma}\right)^{-1} = s^2/pFa^3\,c^* \ldots 2.36$$

This equation does not include D, and hence is the basic equation of evaluating n without knowing D from the chronoamperometric curves.

CHAPTER III

Experimental

During the course of the present work a number of techniques were involved which were in general standard ones. Constant efforts for attaining the ideal conditions for the experiments were always attempted. The thoroughly cleaned glass pieces were dried in electric oven. The smaller pieces of apparatus were dried in electric oven and stored in a desiccator, while larger pieces of apparatus were used directly from the oven.

The redox behavior of metals (Cu and Zn) with different ligands such as Aspartic acid, L-Phenylalanine, Catechol, 3-nitro benzenesulfonate and electrochemical reactions in aqueous solution and buffer solution at different pH has been measured using Cyclic Voltammetry (CV) and Differential Pulse Voltammetry (DPV) at glassy carbon (Gc) or platinum electrode (Pt). Details of the instrumentation are given in the following sections. The source of different chemicals, the instruments and brief description of the methods are given below.

3.1 Chemicals

All chemicals, solvents and ligands used in the electrochemical synthesis and analytical work were analytical grade obtained from E. Merck Germany, British Drug House (BDH) of England and Sigma-Aldrich Chemical Company. The used chemicals were-

SL. No.	Chemicals	Molecular formula	Molar mass	Reported purity	Producer
1.	L-Phenylalanine	$HO_2CCH(NH_2)CH_2C_6H_5$	165.19	99%	Loba Chemie Pvt. Ltd. Mumbai, India.
2.	Aspartic acid	$HO_2CCH(NH_2)CH_2C\,O_2H$	133.1	98%	Sigma-Aldrich Co. USA.
3.	Catechol	$C_6H_4(OH)_2$	110.11	99%	Fisher Scientific UK Ltd.
4.	3-Nitro benze sulphonate	$C_6H_4SO_5N$	202.17	99%	Sigma-Aldrich Co. USA.
5.	Glacial Acetic acid	CH_3COOH	60.05	99.5%	Loba Chemie Pvt. Ltd. Mumbai, India.

SL. No.	Chemicals	Molecular formula	Molar mass	Reported purity	Producer
6.	Sodium acetate	CH_3COONa	136.08	99%	E-Merck, Germany.
7.	Potasium Chloride	KCl	74.6	99.5%	E-Merck, Germany.
8.	Sodium di Hydrogen Ortho Phophate.	$NaH_2PO_4.2H_2O$	156.01	98-100%	Loba Chemie Pvt. Ltd. Mumbai, India.
9.	Di-Sodium Hydrogen Ortho Phophate.	$Na_2HPO_4.2H_2O$	177.99	97-100%	Fisher Scientific UK Ltd.
10.	Sodiun Hydroxide	$NaOH$	40.0	97%	E-Merck, Germany.
11.	Ammonium Chloride	NH_4Cl	53.5	99%	Loba Chemie Pvt. Ltd. Mumbai, India.
12.	Ammonium Hydroxide	NH_4OH	35	99%	Loba Chemie Pvt. Ltd. Mumbai, India.
13.	Copper (II) Chloride	$CuCl_2.2H_2O$	170.48	99%	E-Merck, Germany.
14.	Zinc Chloride	$ZnCl_2.$	136.28	98%	E-Merck, Germany.

3.2 Equipments

During this research work the following instruments were used.

i) The electrochemical studies (CV, DPV and CA) were performed with a PC controlled μstat 400 Potentiostats/Galvanostats (Drop Sens, Spain) (Figure 3.1),

ii) A Pyrex glass micro cell with Teflon cap,

iii) Glassy carbon(Gc)/ Pt working electrode,

iv) Ag/ AgCl reference electrode,

v) Pt wire counter electrode,

vi) A pH meter (pH Meter, Hanna Instuments, Italy) was employed for maintaining the pH of the solutions. Preparation of the solutions was done by ordinary laboratory glassware, and

vii) A HR 200 electronic balance with an accuracy of ± 0.0001g was used for weighting.

3.3 Cyclic Voltammetry (CV)

There are several well established electrochemical techniques for the study of electrochemical reactions. We have chose the CV technique to study and analyze the redox reactions occurring at the polarizable electrode surface. This technique helps us to understand the mechanism of electron transfer reaction of the compounds as well as the nature of adsorption of reactants or products on the electrode surface. CV is often the first experiment performed in an electrochemical study. CV consists of imposing an excitation potential nature on an electrode immersed in an unstirred solution and measuring the current and its potential ranges varies from a few millivolts to hundreds of millivolts per second in a cycle. This variation of anodic and cathodic current with imposed potential is termed as votammogram [91].

The technique involves under the diffusion controlled mass transfer condition at a stationary electrode utilizing symmetrical triangular scan rate ranging from 1 mV s^{-1} to hundreds millivolts per second.

In CV the current function can be measured as a function of scan rate. The potential of the working electrode is controlled vs a reference electrode such as Ag / AgCl electrode. The electrode potential is ramped linearly to a more negative potential and then ramped is reversed back to the starting voltage. The forward scan produces a current peak for any analyte that can be reduced through the range of potential scan. The current will increase as the current reaches to the reduction potential of the analyte [92]

The current at the working electrode is monitored as a triangular excitation potential is applied to the electrode. The resulting voltammogram can be analyzed for fundamental information regarding the redox reaction. The potential at the working electrode is controlled vs a reference electrode, Ag / AgCl((s) (standard KCl) electrode. The excitation signal varies linearly with time. First scan positively and then the potential is scanned in reverse, causing a negative scan back to the original potential to complete the cycle. Signal on multiple cycles can be used on the scan surface. A cyclic voltammogram is plot of response current at working electrode to the applied excitation potential.

3.4 Importent Features of Cyclic Voltammetrty

An electrochemical system containing species 'O' capable of being reversibly reduced to 'R' at the electrode is given by,

$$O + ne^- = R \quad \dots\dots\dots\dots\dots\dots\dots 3.1$$

Nernst equation for the system is

$$E = E^0 + \frac{0.059}{n} \log \frac{C_0^s}{C_R^s} \quad \ldots\ldots\ldots\ldots\ldots\ldots\ldots\ldots 3.2$$

Where,

E = Potential applied to the electrode

E^0 = Standard reduction potential of the couple versus reference electrode

n = Number of electrons in Eq.(3.1)

C_0^s = Surface concentration of species 'O'

C_R^s = Surface concentration of species 'R'

A redox couple that changes electrons rapidly with the working electrode is termed as electrochemically reverse couple. The relation gives the peak current i_{pc}

$$i_{pc} = 0.4463 \, nFA \, (D\alpha)^{1/2} C \ldots\ldots\ldots\ldots\ldots\ldots 3.3$$

$$\alpha = \left(\frac{nFv}{RT}\right) = \left(\frac{nv}{0.026}\right)$$

Where,

i_{pc} = peak current in amperes

F= Faraday's constant (approximately 96500)

A = Area of the working electrode in cm^2

v= Scan rate in volt/ sec

C= Concentration of the bulk species in mol/L

D= Diffusion coefficient in cm^2 /sec

In terms of adjustable parameters, the peak current is given by the Randless- Sevcik equation,

$$i_{pc} = 2.69 \times 10^5 \times n^{3/2} AD^{1/2} Cv^{1/2} \quad \ldots\ldots\ldots\ldots\ldots\ldots\ldots 3.4$$

The peak potential E_p for reversible process is related to the half wave potential $E_{1/2}$, by the expression,

$$E_{pc} = E_{1/2} - 1.11\left(\frac{RT}{nF}\right), \quad \text{at } 25^0C \ldots\ldots\ldots\ldots\ldots 3.5$$

$$E_{pc} = E_{1/2} - \left(\frac{0.0285RT}{n}\right) \ldots\ldots\ldots\ldots\ldots\ldots\ldots\ldots 3.6$$

The relation relates the half wave potential to the standard electrode potential

$$E_{1/2} = E^0 - \frac{RT}{nF} \ln \frac{f_{red}}{f_{ox}} \left(\frac{D_{ox}}{D_{ox}}\right)^{1/2}$$

$$E_{1/2} = E^0 - \frac{RT}{nF} \ln\left(\frac{D_{ox}}{D_{red}}\right)^{1/2} \quad \ldots\ldots\ldots\ldots\ldots\ldots\ldots\ldots 3.7$$

Assuming that the activity coefficient f_{ox} and f_{red} are equal for the oxidized and reduced species involved in the electrochemical reaction.

From equation (3.6), we have,

$$E_{pa} - E_{pc} = 2.22\left(\frac{RT}{nF}\right) \quad \text{at } 25^0C \ldots\ldots\ldots\ldots\ldots 3.8$$

$$\text{or } E_{pa} - E_{pc} = \left(\frac{0.059}{n}\right) \quad \text{at } 25^0C \ldots\ldots\ldots\ldots\ldots 3.9$$

This is a good criterion for the reversibility of electrode process. The value of i_{pa} should be close for a simple reversible couple,

$$i_{pa}/i_{pc} = 1 \ldots\ldots\ldots\ldots\ldots\ldots\ldots\ldots\ldots 3.10$$

And such a system $E_{1/2}$ can be given by,

$$E_{1/2} = \frac{E_{pa} + E_{pc}}{2} \quad \ldots\ldots\ldots\ldots\ldots\ldots\ldots 3.11$$

For irreversible processes (those with sluggish electron exchange), the individual peaks are reduced in size and widely separated, Totally irreversible systems are characterized by a shift of the peak potential with the scan rate [93];

$$E_p = E^0 - (RT/\alpha n_a F)[0.78 - \ln(k^0/(D)^{1/2}) + \ln(\alpha n_a F \alpha/RT)^{1/2}] \ldots\ldots 3.12$$

Where α is the transfer coefficient and n_a is the number of electrons involved in the charge transfer step. Thus E_p occurs at potentials higher than E^0, with the over potential related to k^0 (standard rate constant) and α. Independent of the value k^0, such peak displacement can be compensated by an appropriate change of the scan rate. The peak potential and the half-peak potential (at 25^0 C) will differ by $48/\alpha n$ mV. Hence, the voltammogram becomes more drawn-out as αn decreases.

The peak current, given by

$$i_p = (2.99 \times 10^5)n(\alpha n_a)^{1/2}ACD^{1/2}v^{1/2} \ldots\ldots\ldots\ldots 3.13$$

is still proportional to the bulk concentration , but will be lower in height (depending upon the value of α) . Assuming $\alpha = 0.5$, the ratio of the reversible –to – irreversible current peaks is 1.27 (i.e. the peak current for the irreversible process is about 80% of the peak for a reversible one). For quasi- reversible systems (with $10^{-1} > k^0 > 10^{-5}$ cm/s) the current is controlled by both the charge transfer and mass transport [24]. The shape of the cyclic voltammogram is a function of the ratio $k^0 (\pi v n F D/RT)^{1/2}$. As the ratio increases, the process

approaches the reversible case. For small values of it, the system exhibits an irreversible behavior. Overall, the voltammograms of a quasi-reversible system are more drawn out and exhibit a larger separation in peak potential compared to a reversible system.

Unlike the reversible process in which the current is purely mass transport controlled, currents due to quasi-reversible process are controlled by a mixture of mass transport and charge transfer kinetics [94,95]. The process occurs when the relative rate of electron transfer with respect to that of mass transport is insufficient to maintain Nernst equilibrium at the electrode surface.

3.5 Differential Pulse Voltammetry (DPV)

Differential Pulse Voltammetry (DPV) is often used to make electrochemical measurement. It can be considered as a derivative of linear sweep voltammetry or staircase voltammetry, with a series of regular voltage pulse superimposed on the potential linear sweep or stair steps. The current is measured immediately before each potential change, and the current difference is plotted as a function of potential. By sampling the current must before the potential is changed, the effect of the charging current can be decreased.

By contrast, in normal pulse voltammetry the current resulting from a series of ever larger potential pulse is compared with the current at a constant 'baseline' voltage. Another type of pulse voltammetry is square wave voltammetry, which can be considered a special type of differential pulse voltammetry in which equal time is spent at the potential of the ramped baseline and potential of the superimposed pulse. The potential wave form consists of small pulses (of constant amplitude) superimposed upon a staircase wave form [96]. Unlike NPV, the current is sampled twice in each pulse Period (once before the pulse, and at the end of the pulse), and the difference between these two current values is recorded and displayed.

3.6 Important features of differential pulse voltammetry

Differential pulse voltammetry has these characteristics:

i)   Reversible reactions show symmetrical peaks and irreversible reaction show asymmetrical peaks.

ii)   The peak potential is equal to $E_{1/2}^{r}$-ΔE in reversible reactions, and the peak current is proportional to the concentration.

iii)   The detection limit is about 10^{-8} M.

3.7 Chronoamperometry

To determine the variations of electron transfer number, n with the potential that the redox interaction can be estimated. The technique of evaluating accurate variations at a short time is the analysis of chronoamperograms at a disk electrode by use of the edge effect of diffusion current [91]. This technique has advantage of without knowing a value of a diffusion coefficient [23,97]. When potential is stepped from a non-reacting domain to E, a Cottrell plot (I vs. $t^{-1/2}$) shows the slope by the linear diffusion

$$s = \pi^{1/2} n F D^{1/2} a^2 c^*$$

together with the intercept for the edge effect

$$p = \pi n F D a c^*$$

where a is the radius of the electrode, c^* is the concentration of the electroactive species, D is the diffusion coefficient. The ratio of the square of the slope, s, to the intercept, p, is

$$n = s^2 / p F a^3 c^* \quad \dots\dots\dots\dots\dots\dots\dots\dots\dots\dots\dots\dots\dots\dots 3.14$$

Since this equation does not include D, values of n can be determined from s and p without knowing D values.

3.8 Computer controlled potentiostat (for CV and DPV experiment)

In this study the current voltage system was a µstat 400 Potentiostats/Galvanostats (Drop Sens) developed by Drop View, Spain (Figure 3.1). A potentiostat system sets the control parameters of the experiments. Its purpose is to impose a cyclic linear potential sweep on the working electrode and to output the resulting current potential curve. This sweep is described in general by its initial (E_i), switching (E_s) and final (E_f) potentials and scan rate (V/s).

3.9 Electrochemical cell

This research work was performed by a three electrode electrochemical cell. The voltammetric cell also contains a Teflon cap. The electrochemical reaction of interest takes place at the working electrode and the electrical current at this electrode due to electron transfer is termed as faradic current. The counter electrode is driven by the potentiostatic circuit to balance the faradic process at the working electrode with an electron transfer of opposite direction (Figure 3.1).

3.10 Electrodes

i)   Working electrode is a glassy carbon (Gc) or Platinum (Pt) electrode with 1.6 mm diameter disc.

ii)   Ag/ AgCl (standard NaCl) electrode used as reference electrode from BASi, USA.

iii)   Counter electrode is a Pt wire.

The working electrode is an electrode where the redox reactions of the substances take place. The reference electrode provides the current required to sustain in electrolysis at the working electrode so that is behavior remains essentially constant with the passage of small current. The counter electrode in the three electrode system is made of an inert metal.

3.11 Preparation of Electrode

The working electrode used in this study is glassy carbon (Gc) or Platinum (Pt) electrode procured from the Bioanalytical System (BASi), USA. This electrode preparation includes the polishing and conditioning of the electrode. The electrode was polished with fine alumina powder (0.05μm) on a wet polishing cloth. To do so a part of the cloth was made wet with deionized water and alumina powder was sprinkled n it. The electrode was then polished on this surface by softly pressing the electrode against the polishing surface in the end for 5-10 minutes. The electrode was then thoroughly washed with deionized water. At this point the electrode surface would look like a shiny mirror.

3.12 Removing Dissolved Oxygen from Solution

Before the experiment, it is necessary to remove the dissolved oxygen, which has a cathodic signal that can interfere with observed current response, This was done by purging an inert gas N_2 (99.99% pure and dry) (BOC, Bangladesh) through the solution for about 10 minutes .

3.13 Electrode polishing

After each experiment species may be adsorbed onto the surface of the electrode. So it is essential to remove the adsorbed species by polishing the electrode on wet polishing cloth using alumina powder. To do so a part of the cloth was made wet with deionized water and alumina powder was sprinkled on it. The electrode was then polished on this surface by soft pressing the electrode against the polishing surface. The electrode was then washed with copious amount of deionized water.

3.14 Experimental procedure

The cell was assembled and filled with solution containing analyte, supporting electrolyte and acetate buffer or phosphate buffer. The surface of the electrodes is completely immersed. The cell is dearated for 5 minutes with high purity nitrogen gas. The solution has been kept quite for 10 seconds. To determine the potential window of the scanning is initially carried out with the supporting electrolyte solution to obtain the background voltammogram. The voltammogram containing the analyte in supporting electrolyte is taken under two different modes, at i) various scan rates and ii) various concentrations. Then we have applied potential from the Drow View Software and measured Cyclic voltammetry, Differential pulse voltammetry and Chronoamperometry.

3.15 Preparation of Buffer Solutions

Phosphate Buffer Solution: Phosphate buffer solution (pH 7.0-11) was prepared by mixing a solution of 0.2M NaOH with a solution of 0.2 M KH_2PO_4. The pH of the prepared solution was measured with pH Meter,

Acetate Buffer Solution: To prepare acetate buffer (pH 2-6) solution definite amount of sodium acetate was dissolved in 2M acetic acid in a volumetric flask and the pH was measured. The pH of the buffer solution was adjusted by further addition of acetic acid and / or sodium acetate.
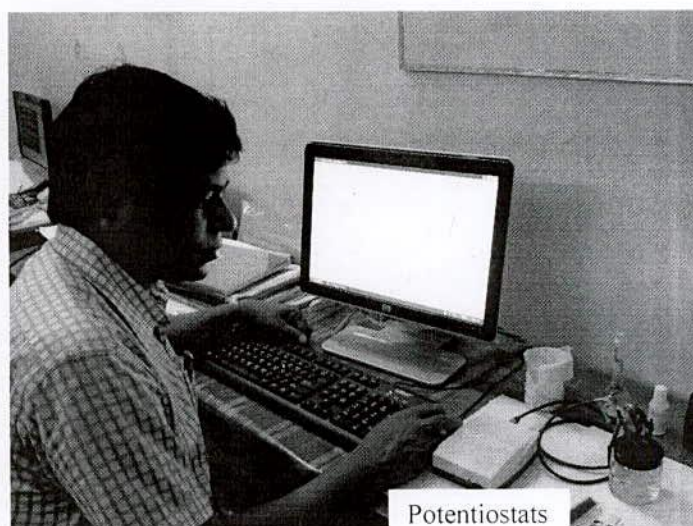
Figure 3.1: Electrochemical setup (Software controlled Potentiostats/Galvanostats (µstat 400))

CHAPTERE IV

Results and Discussion

The redox behavior of Cu (II) only and Cu (II) with aspartic acid, L-phenyl alanine, 3-nitrobenzene sulfonate; Zn(II) only and Zn(II) with aspartic acid, L-phenyl alanine, 3-nitrobenzene sulfonate and Catechol has been studied by Cyclic voltammetry (CV), Differential pulse voltammetry (DPV) and Chronamperometry techniques. The voltammetric techniques provide important information about the mode of redox interaction between metals and ligands and their electron transfer mechanism.

4.1 Cu (II) System

The cyclic voltammogram of 2mM Cu(II) only, Cu (II) with aspartic acid, Cu (II) with L-phenylalanine and Cu (II) with 3-nitrobenzene sulfonate in aqueous and aqueous buffer solution in different pH were taken at different scan rates at Glassy carbon (GC) or Platinum (Pt) electrode. The CV of 2mM Cu (II) in 1M KCl at different scan rates in aqueous solution are shown in Figure 4.1. The potential window was -0.8 to 0.8 V.

The CV of Cu(II) shows two anodic peaks at potential -0.12V and 0.31 V and corresponding two cathodic peaks at potential -0.57V and 0.16V at 0.1V/s scan rate, respectively. The first reduction peak is ascribed to formation of the Cu^{1+} and the second reduction formation of Cu^0 and corresponding first oxidation formation of Cu^{1+} and second oxidation formation of Cu^{2+}.
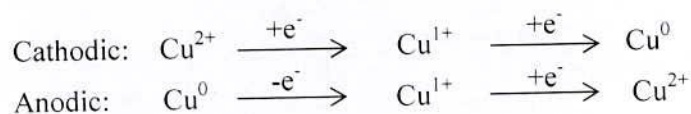
Cathodic: $Cu^{2+} \xrightarrow{+e^-} Cu^{1+} \xrightarrow{+e^-} Cu^0$

Anodic: $Cu^0 \xrightarrow{-e^-} Cu^{1+} \xrightarrow{+e^-} Cu^{2+}$

The second corresponding anodic and cathodic peak current ratios (I_{pa}/I_{pc}) at different scan rates are tabulated in Table 4.1. The current ratio is close to one and independent of scan rate. It indicates that the voltammetic reactions of Cu (II) in aqueous solutions are reversible at any scan rate. The corresponding peak potential differences (ΔE_{cor}) of second peaks at

different scan rate are tabulated in Table 4.1. From the Table 4.1 it is seen that the corresponding peak potentials are above 0.1V which is higher than theoretical one electron transfer reaction. The theoretical separation between peaks is given by $\Delta E_{pcor} = 0.059/n$ V (for a n electron transfer reaction) at all scan rates [23]. The corresponding peak potentials differences are usually independent of scan rate and concentration. The measured value for a reversible process is generally higher due to uncompensated solution resistance between the reference and working electrodes, and non-linear diffusion [98]. From the Table 4.1, it is seen that the corresponding peak potential separation increases with the increase in scan rate. It indicates that there is a limitation due to charge transfer kinetics or ohmic potential (iR) drop [97].

The half wave potential difference ($\Delta E_{1/2}$) of Cu(II) in aqueous solution at different scan rate is tabulated in Table 4.1. The $\Delta E_{1/2}$ value of Cu(II) in aqueous solution is ≈ 0.4V which is independent of scan rate. The differences in formal potential ($\Delta E_{1/2}$) of successive one electron systems commonly depend upon the extent of redox interaction [99].

From Table 4.1 it is apparent that the peak current increases with the scan rate. This can be rationalized by considering the size of the diffusion layer and the time taken to record the scan. The voltammogram takes longer to record as the scan rate is decreased. Therefore, the size of the diffusion layer above the electrode surface becomes different depending upon the scan rate used. In a slow voltage scan the diffusion layer grows much further from the electrode incomparison to a fast scan. Consequently, the flux to the electrode surface is considerably smaller at slow scan rates than it is at faster rates. As the current is proportional to the flux towards the electrode the magnitude of the current becomes lower at slow scan rates and higher at high scan rates [91].

Current passage through either a Galvanic or an electrolytic cell requires a driving force or a potential to overcome the resistance of the ions to move towards the anode or the cathode. Just an metallic conduction, this force follows Ohm's law and is equal to the product of current in amperes and the resistance of the cell in Ohms. The force is generally referred to as the ohmic potential or the IR drop [92].

4.1.1 Scan rate effect of Cu(II)

Figure 4.2 shows plots of two kinds of the anodic and the cathodic net peak currents against the square-root of the scan rates, where the net current means the second peak subtracted from the first one by the scan-stopped method [23]. The proportionality of the first and the second peaks suggests that the peak current of the reactant at each redox reaction is controlled by diffusion process.

4.1.2 pH effect of Cu(II)

Figure 4.3-4.4 shows the voltammogram of 2 mM $CuCl_2$ in acetate buffer solution at different pH and different scan rate solution containing 1M KCl. The peak current increases with the increase of scan rate. The CV of Cu(II) shows at pH 3.0, two anodic peaks at potential -0.14V and 0.31 V and corresponding two cathodic peaks at potential -0.65V and 0.16V at 0.1V/s scan rate, respectively. The second corresponding anodic and cathodic peak current ratios (I_{pa}/I_{pc}) at different scan rates are tabultated in Table 4.2-4.3. The current ratio is close to one and ascribed that the voltammetric reactions of Cu(II) in buffer solutions are reversible. The corresponding peak potential differences (ΔE_{cor}) of second peaks are tabulated in Table 4.2. From the table 4.2 it is seen that the corresponding peak potentials are $\approx 0.1V$ and the ΔE_{cor} value in buffer solution is slightly lower than aqueous solution ascribed that the electron transfer in buffer solution (pH 3.0) is easier than aqueous solution.

The half wave potential difference ($\Delta E_{1/2}$) of Cu(II) in buffer solution at different scan rate is tabulated in Table 4.2. The $\Delta E_{1/2}$ value of Cu(II) in buffer solution is 0.44V at 0.1V/s scan rate that is slightly higher than Cu(II) in aqueous solution . This indicates that the redox interaction in buffer solution is higher than aqueous solution. Figure 4.5-4.6 shows the plots of the anodic and cathodic peak currents against the square root of scan rate. The proportionality of the peaks suggests that the peak current of the reactant at each step is diffusion controlled process.

Figure 4.7-4.9 shows the comparison of voltammogram of 2 mM $CuCl_2$ in acetate buffer solution at different pH (3.0, 4.5, 6.0) at different scan rate of solution containing 1M KCl.

The anodic peak current increases with the decrease of pH indicating that at lower pH the Cu(II) is highly electroactive. For other scan rate Cu(II) in buffer solution similar behavior are showed.

The effect of pH was studied by varying pH from 3.0 to 7.0. In the pH range studied sharp two anodic peaks and one cathodic peak appeared as like neutral solution. For comparative evaluation and characterization at all pHs, the anodic peak was found to be better than cathodic peak. The peak current was plotted against pH and is given in the Figures 4.10-4.12. From the figure it is seen that the first oxidation peak current increased with decrease in pH. The maximum peak current was obtained at pH 3. This shows that the electrochemical oxidation of Cu(II) is facilitated in acid media and hence the rate of electron transfer is faster. A plot was made between oxidation peak potential and pH as shown in Figures 4.13-4.15. The peak potential is almost unchanged with the increase in pH.

4.1.3 Concentration effect of Cu(II)

Figure 4.16 shows the cyclic voltammograms of different concentrations of the Cu(II) in aqueous buffer solution of pH 3 at 0.1 Vs^{-1} scan rate. The intensity of the anodic and cathodic peak current increases with increasing of Cu(II) concentration (Table 4.4) . The effect of concentration can be shown by recording the CV at each concentration (1, 3, 4 and 5 mM) and plotting i_p *vs.* concentration for either the anodic peak or the cathodic peak (Figure 4.17). The relation between Cu(II) concentration and cyclic voltammetric anodic and cathodic peak current (I_{pa}) is linear. The linear dependence of peak current on Cu(II) concentration is depicted from the calibration curve shown Figure 4.17. From the Figure 4.17 it is seen that , with the increase in concentration there is a gradual linear increase in peak current, which may be due to the presence of a large amount of electroactive species at higher concentration. The slope of the first oxidation peak is 3.18 and second oxidation peak is 0.60. The increase of peak current with concentration also gives the idea that the system may be diffusion controlled [23].

4.1.4 Differential pulse voltammetry

Differential pulse voltammetry (DPV) is an important analytical tool for more precise determination in electoactive species. Sometimes, the peak could not be resolved by cyclic voltammetry. In this measurement, the effect of the charging current can be minimized, so high sensitivity achieved.

The effect of pulse amplitude was varied from 0.01V to 0.04V. Peak current increased with increasing of pulse amplitude. There was peak broadening when the amplitude was greater than 0.02V. So, 0.02V of amplitude was chosen for these investigations.(Table 4.5)

As the pulse time increases the peak current decreases. On the other hand at very low pulse time the peak current increases accompanied by peak broadening. When the pulse time is less than 20 ms, the peak broadening started. Hence, a pulse time of 20ms was chosen for these investigations. Figures 4.18-4.19 shows the DPV of Cu(II) in buffer solution at different concentration and different scan rate.

The DPV of Cu(II) shows two anodic peaks at potential -0.19V and 0.32 V at E_{puls} 0.02 V, t_{puls}= 20ms and scan rate 0.1V/s in aqueous buffer solution (pH = 3.0) (acetate buffer) (Figure 4.18). The natures of anodic peaks are similar to cyclic voltammogram peak but the peak intensity of DPV is sharp.

Two anodic peak potential differences (ΔE_p) of Cu(II) in aqueous solution is ~ 0.51V which is almost independent of scan rate. The differences in potential (ΔE) of successive one electron systems commonly depend upon the extent of redox interaction [99].

4.1.5 Concentration effect DPV of Cu(II)

Figure 4.20-4.21 shows the DPV of different concentrations of the Cu(II) in aqueous buffer solution of pH 3 at 0.1 Vs^{-1} scan rate. The intensity of the anodic and cathodic peak current increases with increasing of Cu(II) concentration (Table 4.6). The effect of concentration can be shown by recording the DPV at each concentration (1, 2, 3, 4 and 5 mM) and plotting i_p *vs.* concentration for either the anodic peak or the cathodic peak. The relation between Cu(II) concentration and DPV of anodic and cathodic peak current (Ip) is linear. The linear dependence of peak current on Cu(II) concentration is depicted from the calibration curve shown Figs 4.22-4.23 similar to CV.

4.1.6 Chronoamperometry of Cu(II)

Determination of electron transfer number, n at different stepping potential is very essential for the estimation of redox interaction. The technique of evaluating accurate variations at a short time is the analysis of chronoamperograms at disk electrode by use of the edge effect of diffusion current. This technique has advantage of without knowing a value of a diffusion coefficient[23,31.100-102]. When potential is stepped from a non-reacting domain to E, a Cottrell plot (I vs. $t^{-1/2}$) shows the slope by the linear diffusion

$$s = \pi^{1/2} n F D^{1/2} a^2 c^*$$

together with the intercept for the edge effect

$$p = \pi n F D a c^*$$

where a is the radius of the electrode, c^* is the concentration of the electroactive species, D is the diffusion coefficient. The ratio of the square of the slope, s, to the intercept, p, is

$$n = s^2 / p F a^3 c^* \quad \text{.................................4.1}$$

Since this equation does not include D, values of n can be determined from s and p without knowing D values. Figure 4.24 shows the chronoamperogram of Cu(II) in buffer solution. The Cottrell plots of the background-subtracted current for species fell on straight line for a certain time interval, as is shown in Figure 4.25 at stepping potential 0.4V. Values of n thus obtained from the slope and intercept from equation 4.1. This technique reproducibility for Cu(II) system is very low. This is may be due to the adsorption of Cu(II) on the electrode surface.

Chronoamperometry was also used for the determination of diffusion coefficient (D) of Cu(II) system at different pH. The Cottrell plots (I vs t) of the background-subtracted current for Cu(II) system at different pH is shown in Figure 4.24. In order to determine the diffusion coefficient of Cu(II) in different pH, the plots of I vs. $t^{-1/2}$ were drawn using the data obtained from the chronoamperograms (Figure 4.25). According to the Cottrell equation [23]

$$I = n F A C D^{1/2} \pi^{1/2} t^{-1/2} \quad \text{.................................4.2}$$

The value of D can be obtained from the slopes of the linear plots of I vs. $t^{-1/2}$.

The mean value of D was found to be 2×10^{-5} $cm^2 s^{-1}$, considering n=2 at different pH.

4.1.7 Cu(II)-ligand systems

4.1.7.1 Redox behavior of Cu(II) in presence of Aspartic acid

Only aspartic acid are electrochemically inactive in thedifferent pH and potential range investigated (Figure 4.26). Figure 4.27 shows the cyclic voltammogram of Cu(II) in presence of Aspartic acid (Apa) in 1M KCl at 0.1V/s scan rate. It is observed that the peak positions of the voltammogram of Cu(II) with aspartic acid was shifted with respect to that of only Cu(II) (Figure 4.27). The peak current decreases significantly compared with that for free Cu(II) in the same experimental conditions, which may be due to the complexation of free Cu(II) with aspartic acid. This behavior confirms the interaction between Cu(II) and aspartic acid.

For coordinated Cu(II) with aspartic acid (Apa), the two anodic peaks were found at -0.08V and 0.22 V and corresponding two cathodic peaks were found at potential -0.62 V and 0.08V at 0.1V/s scan rate, respectively. On the other hand, the uncoordinated Cu(II) shows two anodic peaks at potential -0.12V and 0.31 V and corresponding two cathodic peaks at potential -0.57V and 0.16V at 0.1V/s scan rate, respectively. The anodic first oxidation peak shifts positively towards 0.04V and second oxidation peak shift 0.1 Volt negatively and first reduction peak shift negatively -0.05V and second reduction peak negatively 0.08V. The second oxidation peak is shifted more than first oxidation peak. This indicate that first oxidation of Cu-Apa is difficult than that of Cu only whereas second oxidation of Cu(I)-Apa is easier than that of Cu(I) only. The first and second reduction potential of Cu(II)-Apa is more negative than that of Cu(II) only. This indicate that Cu(II) ion is more stabilized by the complexation with aspartic acid, so further electron accepting is not favored except Cu(II) only.

The observation of 2-stage reduction Cu(II) $\leftrightarrow$ Cu (I) and Cu (I) $\leftrightarrow$ Cu (0) of Copper ions depends on the structure of the ligand. If preferential stabilization of Copper (II) species takes place due to complex formation, a redox reaction in 2 steps will occur i.e Cu(II) +1e $\leftrightarrow$ Cu (I) and Cu(I) + 1e $\leftrightarrow$ Cu(0) instead of the direct reaction of Cu (II) + 2e $\leftrightarrow$ Cu (0).

However, the stabilization of Cu species may also be due to d-π interactions between the copper d orbitals and the π system.

$$Cu(II)Apa + e \leftrightarrow Cu(I)Apa + e \leftrightarrow Cu(0) + Apa$$

The second corresponding anodic and cathodic peak current ratios (I_{pa}/I_{pc}) of Cu(II)-Apa at different scan rates are tabulated in Table 4.7. The current ratio is one and independent of scan rate. It indicates that voltammetic reactions of Cu(II)-Apa in aqueous solutions are reversible at any scan rate. The corresponding peak potential difference (ΔE_{cor}) of second peak is tabulated in Table 4.7. The corresponding peak potential differences are usually independent of scan rate and concentration. The theoretical separation between peaks is given by $\Delta E_{pcor} = 0.059/n$ V (for a n electron transfer reaction) at all scan rates [23]. From the Table 4.7 it is seen that the corresponding peak potentials are ≈ 0.1V which is higher than theoretical one electron transfer reaction. The measured value for a reversible process is generally higher due to uncompensated solution resistance between the reference and working electrodes and non-linear diffusion [98]. From the Table 4.7, it is seen that the corresponding peak potential separation increases with the increase in scan rate. It indicates that there is a limitation due to charge transfer kinetics or ohmic potential (iR) drop [97]. When current passage through the cell containing electrolytes requires a driving force or a potential to overcome the resistance of the ions to move towards the anode or the cathode. The force is generally referred to as the ohmic potential or the IR drop.

The half wave potential difference ($\Delta E_{1/2}$) of Cu(II)-Apa in aqueous solution at different scan rate is tabulated in Table 4.7. The $\Delta E_{1/2}$ value of Cu(II)-Apa in aqueous solution is almost 0.3V which is lower than only Cu(II) in aqueous solution (0.4V). The redox interaction of Cu(II)-Apa is lower than only Cu(II) in aqueous solution.

The CV after interaction of Cu(II) with aspartic acid in 1M KCl at different scan rates were observed and the current – potential data, peak separation, peak current ratio of the voltammograms are recorded in Table 4.7. The voltammogram of Cu(II)-Apa interaction at different scan rate show that with the increase of scan rate the peak current of both the anodic and cathodic peaks increases. The cathodic peaks are shifted towards right and the anodic peaks are shifted to the left direction with increase in scan rate.

Figure 4.28 shows plots of the two kinds of the anodic and the cathodic net peak currents of Cu(II)–Apa against the square-root of the scan rates, where the net current means the second peak subtracted from the first one by the scan-stopped method [23]. The proportionality of

the first and the second peaks suggests that the peak current of the reactant at each redox reaction is controlled by diffusion process.

4.1.7.2 pH effect of Cu(II)-Apa

Figure 4.29-4.31 shows the comparison voltammogram of 2 mM Cu(II)-Apa in acetate buffer solution at different pH (3.5, 4.5, 5.5) and different scan rate of solution containing 1M KCl. The peak current increases with the increase of scan rate (Table 4.8-4.10). The anodic and cathodic peak current varies proportionally with the square root of scan rate (Figure 4.32-4.34) indicating that the peak currents are controlled by diffusion process. Figure 4.35-4.37 shows the comparison of voltammogram of Cu(II)-Apa in buffer solution at different pH and different scan rate. The first anodic peak current decreases with the increase of pH indicating that at the lower pH, the Cu(II)-Apa is highly electroactive.

The effect of pH was studied by varying pH from 3.5 to 7.0. In the pH range studied two anodic peaks and one cathodic peak appeared. The peak current increases with the decrease of pH indicating that at the lower pH the Cu(II)-Apa is highly electroactive. The position of the redox couple was found to be dependent upon pH. The peak current was plotted against pH and is given in the Figures 4.38-4.40. The maximum peak current was obtained at pH 3.5. This shows that the electrochemical oxidation of Cu(II)-Apa is facilitated in acid media and hence the rate of electron transfer is faster. A plot was made between oxidation peak potential and pH as shown in Figure 4.41-4.43. The first anodic peak potential increased with decrease in pH indicating higher energy requirement for oxidation at acid pH. The peak current of Cu(II)-Apa is lower than the only Cu(II) at the same condition. The trend of increasing intensity indicates the formation of more Cu(II)-aspartic acid complex. The formation of more Cu(II)-aspartic acid complex with decreasing pH is due to the increasing of coordination sites of the amino group of the aspartic acid molecule through protonation.

The voltammograms exhibit a couple of redox peaks, but the second oxidation peak potential is shifted negatively as pH increases, and studies at pH > 9 voltammetric peaks are disappeared. The peak separation of two anodic peak increases with the decrease of pH. The electrochemical response is sensitive to the pH, and the waves shift to more negative potentials as the pH is increased. Figure 4.41-4.43 shows the plot of E_p values against pH. The slopes of the plot was determined graphically as 40 mV/pH though the peak separation was about 40 mV at 0.1V/s, which is somewhat larger than the theoretical value of 30 mV

for a two-electron, two-proton transfer process which indicate that the oxidation of the Cu(II)-Apa proceeded via the 2e−2H+ processes. This also suggest that during the reaction not only electron but also protons are released from the Cu(II)-Apa [103].

The most reasonable explanation for this concerns the influence of the coordinated amino acid in that the amido group can combine protons. In accordance with this, the proton dissociation constants for the NH_2 group of aspartic acid (pKb, Apa = 9.8). So, the number of protons integrated with coordinated aspartic acid is dependent on pH.

The electrochemical properties of these complexes are pH-dependent and the reduction of coordinated aspartic acid proceeded via the 2e−2H+(pH < 7) processes, being modulated by the amino acid ligands through combining protons on the NH_2 groups [103]. This behavior could be an advantage for research into the mechanism of proton pumps.

4.1.7.3 Effect of Aspartic acid composition on the Cu(II) voltammogram

Figures 4.44-4.45 shows the effect of Aspartic acid composition on the voltammogram of the Cu(II) in aqueous solution. The first anodic peak shifted positively and the second anodic peak is shifted negatively upon the addition of aspartic acid which indicates the formation of Cu(II)-Apa complex. The intensity of the anodic and cathodic peak current decreases with the increasing of aspartic acid (Figure 4.46-4.47) suggests that the formation of more Cu(II)-aspartic acid complex. With the increasing of aspartic acid concentration 1:1 to 1:3, the anodic current decreases linearly (Table 4.11-4.12) (shown in Figure 4.46-4.47) but after more addition of aspartic acid, the current intensity change is constant. This indicate that the availability of Cu(II) is limited for the formation of the Cu(II)-Apa complex at saturation point.

Figure 4.48-4.53 shows the effect of aspartic acid composition on the voltammogram of the Cu(II) in buffer solution at different pH and different scan rate. The intensity of the anodic peak current decreases with the increasing of aspartic acid composition (Table 4.13-4.18) shown in Figure 4.54-4.59 which properties is similar to the properties of aqueous solution.

4.1.7.4 Concentration effect on the voltammogram of Cu(II) - aspartic acid

Figure 4.60 shows the cyclic voltammograms of different concentrations of the metal ions + aspartic acid at 0.1 Vs^{-1} scan rate. The intensity of the new peak increases with increasing of Cu(II) + Aspartic acid concentration. This may be due to the formation of more Cu(II)-Apa

complex with increasing of Cu(II)+Apa concentration. The effect of concentration can be shown by recording the CV at each concentration (2, 3, 4 and 5 mM) and plotting i_p *vs.* concentration for either the anodic peak or the cathodic peak (Figure 4.61). The relation between Cu(II) + Aspartic acid concentration and cyclic voltammetric anodic and cathodic peak current (Ip) is linear. The linear dependence of peak current on Cu(II) + Aspartic acid concentration is depicted from the calibration curve shown in Fig.4.61. (Table 4.19)

4.1.7.5 DPV of Cu(II) - Apa

Figure 4.62-4.63 shows the oxidation and reduction of DPV of Cu(II) in presence of Aspartic acid (Apa) in 1M KCl in aqueous buffer solution (pH = 3.0) (acetate buffer) at E_{puls} 0.02 V, t_{puls}= 20ms and scan rate 0.1V/s using Pt electrode (1.6m) (Table 4.20). It is observed that the peak positions of the DPV of Cu(II) with aspartic acid was shifted from -0.19 to -0.11V and 0.32 to 0.18V with respect to that of only Cu(II). And also a new peak appeared at 0.41V. The peak current decreases significantly compared with that for free Cu(II) in the same experimental conditions. This indicate that the formation of complexation of free Cu(II) with aspartic acid. The anodic peak potential difference (ΔE_p) of Cu(II)-Apa in aqueous solution at 0.1V/s is almost 0.29V which is lower than only Cu(II) in aqueous solution (0.51V). The redox interaction of Cu(II)-Apa is lower than only Cu(II) in aqueous solution.

4.1.7.6 Concentration effect of DPV of Cu-Apa

Figure 4.64-4.65 shows the DPV of different concentrations of the Cu(II)-Apa in aqueous buffer solution of pH 3 at 0.1 Vs^{-1} scan rate. The intensity of the anodic and cathodic peak current increases with increasing of Cu(II)-Apa concentration. The effect of concentration can be shown by recording the DPV at each concentration (1, 2, 3, 4 and 5 mM) and plotting i_p *vs.* concentration for either the anodic peak or the cathodic peak. The relation between Cu (II) concentration and DPV anodic and cathodic peak current (Ip) is linear.

4.1.7.7 Chronoamperometry of Cu-Apa

Figure 4.66 shows the Chronoamperogram of Cu(II)-Apa in buffer solution at pH 3.5.The Cottrell plots of the background-subtracted current for Cu(II)-Apa in aqueous buffer solution at different pH fell on each straight line as is shown in Figure 4.67. Values of *n*

thus obtained from the slope and intercept from equation 4.1. This technique reproducibility for Cu(II)-Apa system is very low. This is may be due to the polymerization of Apa on the electrode surface.

Chronoamperometry was also used for the determination of diffusion coefficient (D) of Cu(II)-Apa system at different pH. The Cottrell plots (*I* vs *t*) of the background-subtracted current for Cu(II)-Apa system at different pH is shown in Figure 4.66. In order to determine the diffusion coefficient of Cu(II)-Apa in different pH, the plots of *I* vs. $t^{-1/2}$ were drawn using the data obtained from the chronoamperograms . According to the Cottrell equation

$$I= nFACD^{1/2}\pi^{1/2}t^{-1/2} \quad \text{...................... 4.3}$$

The mean value of D was found to be 5×10^{-6} cm^{2}s^{-1}, considering n=3 at different pH.

4.1.7.8 Redox behavior of Cu(II) in presence of L-Phenylalanine (Phe)

Phenylalanine is electrochemically inactive in the different pH and potential range investigated (Figure 4.68). Figure 4.69 shows the cyclic voltammogram of Cu(II) in presence of L-phenylalanine (Phe) in 1M KCl at 0.1V/s scan rate. It is observed that the peak positions of the voltammogram of Cu(II) with L-phenylalanine (Phe) was shifted with respect to that of only Cu(II). The peak current decreases significantly compared with that for free Cu(II) in the same experimental conditions, which may be due to the complexation of free Cu(II) with L-phenylalanine (Phe). This behavior confirms the interaction between Cu(II) and L-phenylalanine (Phe).

For coordinated Cu(II) with L-phenylalanine (Phe), the two anodic peaks were found at -0.07 and 0.22 V and corresponding two cathodic peaks were found at potential 0.08 V and -0.056V at 0.1V/s scan rate, respectively in water. On the other hand, the uncoordinated Cu(II) shows two anodic peaks at potential -0.12V and 0.31 V and corresponding two cathodic peaks at potential -0.57V and 0.16V at 0.1V/s scan rate, respectively. The anodic first oxidation peak shifts positively and second oxidation peak shift negatively and first reduction peak shift negatively and second reduction peak negatively similar to aspartic

acid. The second oxidation peak is shifted more than first oxidation peak. This indicate that first oxidation of Cu-Phe is difficult than that of Cu only whereas second oxidation of Cu(I)-Phe is easier than that of Cu(I) only. The first and second reduction of Cu(II)-Phe is more negative than that of Cu(II) only. This indicate that Cu(II) ion is more stabilized by the complexation with L-phenylalanine, so further electron accepting is not favored except Cu(II) only.

The stabilization of Cu species may also be due to d-π interactions between the copper d orbitals and the π system,

Cu(II)-Phe + e ↔ Cu(I)-Phe + e ↔ Cu (0) + Phe
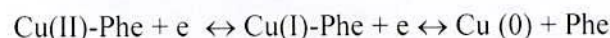
Normally with the addition of increasing concentration of a ligand, the reduction peak potential of metal ion generally shifts to more negative potentials and also the reduction of the metal complex ion becomes more difficult due to stabilization of metal ion by complex formation.

The second corresponding anodic and cathodic peak current ratios (I_{pa}/I_{pc}) of Cu(II)-Phe at different scan rates are tabulated in Table 4.21. The current ratio is one and independent of scan rate. It indicates that voltammetic reactions of Cu(II)-Phe in aqueous solutions are reversible at any scan rate. The corresponding peak potential differences (ΔE_{cor}) of second peaks are tabulated in Table 4.21. The corresponding peak potentials differences are usually independent of scan rate and concentration. The theoretical separation between peaks is given by $\Delta E_{pcor} = 0.059/n$ V (for a n electron transfer reaction) at all scan rates [23]. From the Table 4.21 it is seen that the corresponding peak potentials are ≈ 0.1V which is higher than theoretical one electron transfer reaction. The measured value for a reversible process is generally higher due to uncompensated solution resistance between the reference and working electrodes and non-linear diffusion [98]. From the Table 4.21, it is seen that the corresponding peak potential separation increases with the increase in scan rate. It indicates that there is a limitation due to charge transfer kinetics or Ohmic potential (iR) drop [97].

The half wave potential difference ($\Delta E_{1/2}$) of Cu(II)-Phe in aqueous solution at different scan rate is tabulated in Table 4.21. The $\Delta E_{1/2}$ value of Cu(II)-Phe in aqueous solution is almost 0.29V which is lower than only Cu(II) in aqueous solution (0.4V). The redox interaction of Cu(II)-Phe is lower than only Cu(II) in aqueous solution. This may be due to the localization of electron increased after insertion of ligand.

The CV after interaction of Cu(II) with Phe in 1M KCl at different scan rates were observed and the current – potential data, peak separation, peak current ratio of the voltammograms are recorded in Table 4.21. The voltammogram of Cu-Phe interaction at different scan rate show that with the increase of scan rate the peak current of both the anodic and cathodic peaks increases. The cathodic peaks are shifted towards right and the anodic peaks are shifted to the left direction with increase in scan rate.

The current function $(i_p/v^{1/2})$ is independent of the scan rate and the ratio of second anodic to cathodic peak current, i_{pa}/i_{pc}, is almost equal to unity, indicating that the Cu(II)- Phe complex formed in the electro-reduction is stable within the time scale of the experiment.

Figure 4.70 shows plots of the two kinds of the anodic and the cathodic net peak currents of Cu(II) –Phe against the square-root of the scan rates, where the net current means the second peak subtracted from the first one by the scan-stopped method [23]. The proportionality of the first corresponding peak suggests that the peak current of the reactant at each redox reaction is controlled by diffusion process. But the first oxidation peak current decrease with the increase of scan rate, this is may be due to the complexation of phenylalanine with Cu(II).

4.1.7.9 pH effect of Phenylalanine

Figure 4.71-4.73 shows the comparison voltammogram of 2 mM Cu(II)-Phe in acetate buffer solution at different pH (3.5, 4.5, 5.5) at scan rate 0.1V/s solution containing 1M KCl. The peak current increases with the increase of scan rate. The anodic and cathodic peak current varies proportionally with square root of scan rate (Figure 4.74-4.76) indicating that the peak currents are controlled by diffusion process. In figure 4.76 the peak current is proportional upto 0.4 $v^{1/2}s^{-1/2}$ and then decreases this, is may be due to the chemical complications at higher scan rate. Figure 4.77-78 shows the comparison voltammogram of Cu(II) –Phe in buffer solution at different pH and different scan rate. The peak current decreases with the increase of pH indicating that at the lower pH, the Cu(II)-Phe is highly electroactive.

The effect of pH was studied by varying pH from 3.5 to 7.0. In the pH range studied two anodic peaks and one cathodic peak appeared. The peak current increases with the decrease

of pH shown in Figure 4.79-80 indicating that at lower pH the Cu(II) –Phe is highly electroactive. At pH 6.0 the cathodic peak is disappeared. For comparative evaluation and characterization at all pHs, the anodic peak was found to be better than cathodic peak. The position of the redox couple was found to be dependent upon pH. The peak current was plotted against pH and is given in the figure 4.81-4.82. The maximum peak current was obtained at pH 3.5. This shows that the electrochemical oxidation of Cu(II)-Phe is facilitated in acid media and hence the rate of electron transfer is faster. A plot was made between oxidation peak potential and pH as shown in figure 4.81-82. The peak potential increased with decrease in pH indicating higher energy requirement for oxidation at acid pH. The peak current of Cu(II)-Phe is lower than the only Cu(II) at the same condition. This indicate that only Cu(II) is more electroactive than Cu(II)-Phe in solution.

The trend of increasing intensity indicates the formation of more Cu(II)-Phe complex. The formation of more Cu(II)-Phe complex with decreasing pH is due to the increasing of coordination sites of the amino group of the Phe molecule through protonation. The peak separation of two anodic peak increases with the decrease of pH (Table 4.22-4.24).

The electrochemical response is sensitive to the pH, and the waves shift to more negative potentials as the pH is increased. Figure 4.81-4.82 shows the plot of E_p values against pH. The slopes of the plot was determined graphically as 26 mV/pH at 0.1 V/s, which is close to the theoretical value of 30 mV for a two-electron, two-proton transfer process (Scheme 1)which indicate that the oxidation of the Cu(II)-Phe proceeded via the 2e–/2H+ processes. This also suggest that during the reaction not only electron but also protons are released from the Cu(II)-Phe.

The most reasonable explanation for this concerns the influence of the coordinated amino acid in that the amide group can combine protons. In accordance with this, the proton dissociation constants for the -NH$_2$ group of phenylalanine (pKb,Phe = 9.09). So, the number of protons integrated with coordinated Phenylalanine is dependent on pH.

4.1.7.10 Effect of Phenyl alanine composition on the Cu(II) voltammogram

Figure 4.83 shows the effect of L-Phenylalanine concentration on the voltammogram of the Cu(II) in aqueous solution. The first anodic peak shifted positively and the second anodic

peak is shifted negatively upon the addition of L-Phenylalanine which indicates the formation of Cu(II)-Phe complex. The intensity of the peak current decreases with the increasing of L-Phenylalanine (Figure 4.84) suggests that the formation of more Cu(II)- L-Phenylalanine complex(Table 4.25).

With the increasing of L-Phenylalanine concentration 1:1 to 1:3, the current decreases linearly (shown in Figure 4.84) but after more addition of L-Phenylalanine, the current intensity change is constant. This indicate that the availability of Cu(II) is limited for the formation of the Cu(II)- L-Phenylalanine complex at saturation point. Figure 4.85-4.87 shows the effect of phenylalanine composition on the voltammogram of Cu(II) in buffer solution at different pH and different scan rate. The intensity of the anodic peak current decreases with the increasing of Phe composition shown (Figure 4.88-4.90). The buffer solution behavior is similar to the aqueous solution (Table 4.26-4.28).

4.1.7.11 Concentration effect on the voltammogram of Cu(II) + L-Phenylalanine

Figure 4.91 shows the cyclic voltammograms of different concentrations of the metal ions + L-Phenylalanine at 0.1 Vs^{-1} scan rate. The intensity of the new peak increases with increasing of Cu(II) + Phe concentration. This may be due to the formation of more Cu(II)-Phe complex with increasing of Cu(II) +Phe concentration.

The effect of concentration of Cu(II) and L-Phenylalanine can be shown by recording the CV at each concentration (2, 3, 4 and 5 mM) and plotting i_p *vs.* concentration for either the anodic peak or the cathodic peak (Figure 4.92). The relation between Cu(II) + Phe concentration and cyclic voltammetric anodic and cathodic peak current (Ip) is linear(Table 4.29). The linear dependence of peak current on Cu(II) + Phe acid concentration is depicted from the calibration curve shown in Fig.4.92.

Figure 4.93-95 shows the comparison CV of Cu(II) with different ligands such as Aspartic acid, Phenylalanine at different pH. From the figure it is seen that the peak position shifts with the addition of Ap or Phe and the peak current decreases with addition of Apa or Phe(Table 4.30).

4.1.7.12 DPV of Cu(II) - Phe

Figure 4.96-4.97 shows the DPV of Cu(II) in presence of L-Phenylalanine (Phe) in 1M KCl in aqueous buffer solution (pH = 3.0) (acetate buffer) at E_{puls} 0.02 V, t_{puls}= 20ms and scan

rate 0.1V/s. It is observed that the peak positions of the DPV of Cu(II) with L-Phenylalanine (Phe) was shifted from -0.19 to -0.11V and 0.32 to 0.18V with respect to that of only Cu(II). And also a new peak appeared at 0.41V. The peak current decreases significantly compared with that for free Cu(II) in the same experimental conditions. This indicate that the formation of complexation of free Cu(II) with L-Phenylalanine.

4.1.7.13 Concentration effect of Cu(II)-Phe

Figure 4.98-99 shows the DPV of different concentrations of the Cu(II)-Phe in aqueous buffer solution of pH 3 at 0.1 Vs^{-1} scan rate. The intensity of the anodic and cathodic peak current increases with increasing of Cu(II)-Phe concentration. The effect of concentration can be shown by recording the DPV at each concentration (1, 2, 3, 4 and 5 mM) and plotting i_p *vs.* concentration for either the anodic peak or the cathodic peak. The relation between Cu(II) concentration and DPV anodic and cathodic peak current (Ip) is linear(Table 4.31).

4.1.7.14 Chronoamperometry of Cu(II)-Phe

Figure 4.100 shows the chronoamperogram of Cu(II)-Phe at different concentration at the scan rate 0.4V/s. The Cottrell plots of the background-subtracted current for Cu(II)-Phe in aqueous buffer solution at different pH fell on each straight line as is shown in Figure 4.101. Values of *n* thus obtained from the slope and intercept from equation 4.1. This technique reproducibility for Cu(II)-Phe system is very low. This is may be due to the polymerization of Phe on the electrode surface.

Chronoamperometry was also used for the determination of diffusion coefficient (D) of Cu(II)-Phe system at different pH. The Cottrell plots (*I* vs *t*) of the background-subtracted current for Cu(II)-Phe system at different pH is shown in Figure 4.100. In order to determine the diffusion coefficient of Cu(II)-Phe in different pH, the plots of *I* vs. $t^{-1/2}$ (Figure 4.101) were drawn using the data obtained from the chronoamperograms . According to the Cottrell equation [23]

$$I = nFACD^{1/2}\pi^{1/2}t^{-1/2} \quad \ldots\ldots\ldots\ldots\ldots\ldots\ldots 4.4$$

The mean value of D was found to be 4×10^{-6} cm^{2}s^{-1}, considering n=3 at different pH.

4.1.7.15 Cu (II) with 3-nitrobenzene sulfonate system(NBS)

NBS are electrochemically almost inactive in the potential range investigated (Figure 4.102). Figure 4.103 shows the cyclic voltammogram of Cu(II) in presence of 3-nitrobenzene sulfonate in buffer solution (pH 3.5) and different scan rate. It is observed that the peak positions of the voltammogram of Cu(II) with 3-nitrobenzene sulfonate was shifted with respect to that of only Cu(II). The peak current decreases significantly compared with that for free Cu(II) in the same experimental conditions, which may be due to the complexation of free Cu(II) with 3-nitrobenzene sulfonate. This behavior confirms the interaction between Cu(II) and 3-nitrobenzene sulfonate.

For coordinated Cu(II) with 3-nitrobenzene sulfonate (NBS), the two anodic peaks were found at -0.06 and 0.25 V and corresponding two cathodic peaks were found at potential - 0.71V and -0.18 V at 0.1V/s scan rate, respectively. But the voltammetric Cu(II) with NBS peaks are broad compared to aspartic acid and phenylalanine. On the other hand, the uncoordinated Cu(II) shows two anodic peaks at potential -0.12V and 0.31 V and corresponding two cathodic peaks at potential -0.57V and 0.16V at 0.1V/s scan rate, respectively. The anodic first oxidation peak shifts positively towards 0.05V and second oxidation peak shift 0.06 Volt negatively and first reduction peak shift -0.14V negatively and second reduction peak 0.3V negatively. The second oxidation peak is shifted more than first oxidation peak. This indicate that first oxidation of Cu-NBS is difficult than that of Cu only whereas second oxidation of Cu(I)-NBS is easier than that of Cu(I) only. The first and second reduction of Cu(II)-NBS is more negative than that of Cu(II) only. This indicate that Cu(II) ion is more stabilized by the complexation with NBS, so further electron accepting is not favored except Cu(II) only. The stabilization of Cu species may also be due to d-π interactions between the copper d orbitals and the π system.

Cu(II)NBS + e $\leftrightarrow$ Cu(I)NBS + e $\leftrightarrow$ Cu (0) + NBS
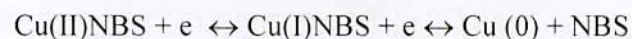
The first corresponding anodic and cathodic peak current ratios (I_{pa}/I_{pc}) of Cu(II)-NBS is one at slow scan rate. It indicates that voltammetic reactions of Cu(II)-NBS in aqueous solutions are reversible at slow scan rate. The corresponding peak potential differences (ΔE_{cor}) of second peaks are tabulated in Table 4.32-4.33. The theoretical value of ΔE_{pcor} is 0.059/n (for a n electron transfer reaction) [23] . From the (Table 4.32-4.33) it is seen that

the corresponding peak potentials are $\approx 0.60V$ at the scan rate 0.02V/s to 0.1V/s and beyond the scan rate the ΔEp values are slightly higher than theoretical one electron transfer reaction. The measured value for a reversible process is generally higher due to uncompensated solution resistance between the reference and working electrodes and non-linear diffusion [98]. From the Table 4.32-4.33, it is seen that the corresponding peak potential separation increases with the increase in scan rate. It indicates that there is a limitation due to charge transfer kinetics or ohmic potential (iR) drop [97]. The $\Delta E_{1/2}$ value of Cu(II)-NBS in aqueous solution is almost 0.26V which is lower than only Cu(II) in aqueous solution (0.4V). The redox interaction of Cu(II)-NBS is lower than only Cu(II) in aqueous solution.

The CV after interaction of Cu(II) with NBS in 1M KCl at different scan rates were observed and the current – potential data, peak separation, peak current ratio of the voltammograms are recorded in Table 4.32-4.33. The voltammogram of Cu (II)-NBS interaction at different scan rate show that with the increase of scan rate the peak current of both the anodic and cathodic peaks increases. The cathodic peaks are shifted towards right and the anodic peaks are shifted to the left direction with increase in scan rate.

4.1.7.16 pH effect of NBS

Figure 4.103-4.105 shows the comparison voltammogram of 2 mM Cu(II)-NBS in acetate buffer solution at different pH (3.5, 4.5, 5.5) at different scan rate. The current function $(i_p/v^{1/2})$ is independent of the scan rate and the ratio of second anodic to cathodic peak current, i_{pa}/i_{pc}, is almost equal to unity, indicating that the Cu(II) complex formed in the electro-reduction is stable within the time scale of the experiment.

Figure 4.106-4.107 shows plots of the two kinds of the anodic and the cathodic net peak currents of Cu(II) –NBS against the square-root of the scan rates. The proportionality of the first and the second peaks suggests that the peak current of the reactant at each redox reaction is controlled by diffusion process.

The effect of pH was studied by varying pH from 3.5 to 6.0 (Figure 4.108). In the pH range studied two broad anodic peaks and two broad cathodic peaks appeared. The peak current increases with the decrease of pH. The position of the redox couple was found to be

dependent upon pH. The peak current was plotted against pH and is given in the figure 4.109. From the figure it is seen that the oxidation peak current is higher at pH 4.5. This indicate that the electrochemical oxidation of Cu(II)-NBS is facilitated in acid media and hence the rate of electron transfer is faster. A plot was made between oxidation peak potential and pH as shown in figure 4.110. The peak potential is almost unaffected with decrease or increase in pH. The peak current of Cu(II)-NBS is lower than the only Cu(II) at the same condition. This indicate that only Cu(II) is more electroactive than Cu(II)-NBS in solution.

4.2 Zn(II) System

The cyclic voltammogram of Zn(II) only and Zn(II) with aspartic acid, L-phenyl alanine, 3-nitrobenzene sulfonate (NBS) and catechol in aqueous and aqueous buffer solution of different pH were taken at different scan rates at Glassy carbon (GC) electrode. The CV of 2mM Zn(II) in 1M KCl at different scan rates are shown in Figure 4.111.

At the slow scan rate 0.02V/s, the CV of Zn(II) shows one anodic peaks at potential -1.0V and corresponding one cathodic peaks at potential -1.27V.
The reduction peak is ascribed to formation of the Zn^{2+} to Zn^0 and corresponding oxidation formation of Zn^0 to Zn^{2+}.

Cathodic: $Zn^{2+} + 2e \longrightarrow Zn^0$

Anodic: $Zn^0 - 2e \longrightarrow Zn^{2+}$
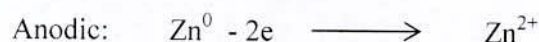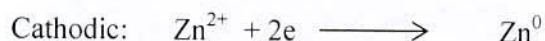
From Table 4.34 it is apparent that the peak current decreases with the increase of scan rate. This can be rationalized by considering the size of the diffusion layer and the time taken to record the scan. The volammogram takes longer to record as the scan rate is decreased. Therefore, the size of the diffusion layer above the electrode surface becomes different depending upon the scan rate used. In a slow voltage scan the diffusion layer grows much further from the electrode incomparison to a fast scan. Consequently, the flux to the electrode surface is considerably smaller at slow scan rates than it is at faster rates. As the

current is proportional to the flux towards the electrode the magnitude of the current becomes lower at slow scan rates and higher at high scan rates [91].

Figure 4.112 shows the plots of the peak current against square root of scan rate in aqueous solution. The peak current is not proportional with the square root of scan rate suggest that the reactant at each redox reaction is controlled by adsorption rather than diffusion.

4.2.1 pH effect of Zn(II)

Figure 4.113-4.117 shows the comparison voltammogram of 2 mM Zn(II) in buffer solution at different pH (1.5, 2, 3, 4.5, 7, 11) at different scan rate.

The CV of Zn (II) shows at pH (1.5, 3 and 4.5) one well defined anodic and corresponding cathodic peak at different scan rate. The anodic and cathodic peak potentials and current ratios (I_{pa}/I_{pc}) at different scan rates are tabulated in Tables 4.35-4.38. The current ratio is very far from one and ascribed that the voltammetic reactions of Zn(II) in buffer solutions are irreversible. The corresponding peak potential differences (ΔE_{cor}) of the peaks are tabulated in Table 4.35-4.38. From the table 4.35-4.38. it is seen that the corresponding peak potentials are less than 60 mV at pH 4.5 but at lower pH (1.5, 3) and higher pH (7, 11) the ΔE_{cor} is higher than 60 mV. The theoretical separation between peaks is given by ΔE_{pcor} = 60 m V for one electron transfer reaction. Figure 4.118-4.121 shows the plots of the anodic peak current against the square root of scan rate at different pH. The proportionality suggest that the peak current is controlled by diffusion process. Figure 4.122 shows the comparison of voltammogram of 2 mM Zn(II) in acetate buffer solution at different pH (1.5, 3, 4.5, 7, 11) at scan rate 0.1V/s of solution containing 1M KCl. The effect of pH was studied by varying pH from 1.5 to 11. In the pH range studied sharp anodic peaks and cathodic peak appeared upto pH 4.5 (Figure 4.122). The peak current was plotted against pH and is given in the figure 4.123. The maximum anodic peak current was obtained at pH 4.5. This shows that the electrochemical oxidation of Zn(II) is facilitated in acid media and hence the rate of electron transfer is faster. A plot was made between oxidation peak potential and pH as shown in figure 4.124. At higher pH, the peak of CV is disappeared. The peak potential is almost unaffected with the charge of pH .

The electrochemical behavior of Zn(II) is dependent on the solution pH. The oxidation peak of Zn(II) increased up to pH 4.5 and at higher pH values the oxidation peak decreased

(Figure 4.123). The reduction peak current of Zn(II) decreased at higher pH. So the oxidation peak was selected for the analytical determination of Zn(II) for further investigations at pH 4.5. The peak current increases at pH 4.5 indicating that at this pH the Zn(II) is highly electroactive.

4.2.2 Differential pulse voltammetry of Zn(II)

In aqueous solution Zn (II) shows very weak DPV peak (Figure 4.125). But in buffer solution (pH <7) the peak is very prominent. The DPV of Zn(II) shows one anodic peaks at potential -0.98V at E_{puls} 0.02 V, t_{puls}= 20ms and at different scan rate in aqueous buffer solution (pH = 4.5) (acetate buffer) (Figure 4.126). The nature of anodic peaks are similar to cyclic voltammogram peak but the peak in DPV is sharp. The peak current is increased with the increase of scan rate. The peak current varies proportionally with the square root of scan rate indicating that the anodic peak current is controlled by diffusion process.

4.2.3 Zn(II)-ligand systems

4.2.3a Redox behavior of Zn(II) in presence of Aspartic acid

Figure 4.127 shows the cyclic voltammogram of Zn(II) in presence of Aspartic acid (Apa) in 1M KCl at different scan rate in aqueous solution. It is observed that the peak positions of the voltammogram of Zn(II) with aspartic acid was shifted with respect to that of only Zn(II). The peak current increases significantly in aqueous solution compared with that for free Zn(II) in the same experimental conditions, which may be due to the complexation of free Zn(II) with aspartic acid. This behavior confirms the interaction between Zn(II) and aspartic acid. Free ligands (aspartic acid and phenyl alanine) are electrochemically inactive in the potential range investigated that has been described previously.

For coordinated Zn(II) with aspartic acid (APa), anodic peaks were found at -0.9V and corresponding cathodic peaks were found at potential -1.53V at 0.1V/s scan rate. On the other hand, the uncoordinated Zn(II) have no peak in aqueous solution at 0.1V/s scan rate but it shows anodic peak and corresponding cathodic peak on the addition of aspartic acid. Figure 4.128 shows the peak current against square root of scan rate. The peak current is varied proportionally indicating that the peak current is controlled by diffusion. In aqueous buffer solution at pH 3.5, the anodic peak current decreases significantly compared with that

for free Zn(II) in the same experimental conditions, which may be due to the complexation of free Zn(II) with aspartic acid shown in Figure 4.129. The anodic and cathodic peaks shifted negatively after the complexation of Zn(II) with aspartic acid. This indicate that Zn(II) ion is more stabilized by the complexation with aspartic acid.

The reduction peak is ascribed to formation of the $Zn^{2+}(L)$ to $Zn^0(L)$ and corresponding oxidation formation of Zn^0 (L) to Zn^{2+} (L).

Cathodic: Zn^{2+} (L) + 2e $\longrightarrow$ Zn^0 (L)

Anodic: Zn^0 (L) - 2e $\longrightarrow$ Zn^{2+} (L)
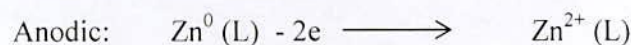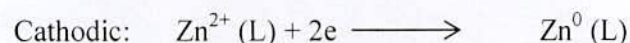
If preferential stabilization of Zn (II) species takes place due to complex formation, a redox reaction in 1 step will occur i.e Zn^{2+} (L) + 2e $\longrightarrow$ Zn^0 (L) and Zn^0 (L) - 2e $\longrightarrow$ Zn^{2+} (L). However, the stabilization of Zn(II) species may also be due to d-π interactions between the copper d orbitals and the π system.

The anodic and cathodic peak current ratios (I_{pa}/I_{pc}) of Zn(II)-Apa at different scan rates are tabulated in Table 4.39-4.40. The current ratio is much higher than one. It indicates that voltammetic reactions of Zn(II)-Apa in aqueous solutions are not reversible at any scan rate. The corresponding peak potential differences (ΔE_{cor}) of second peaks are tabulated in Table 4.39. The theoretical separation between peaks is given by $\Delta E_{pcor} = 0.059/n$ V (for a n electron transfer reaction) at all scan rates [23]. From the Table 4.39 it is seen that the corresponding peak potentials are much higher than theoretical one electron transfer reaction. The measured value for a reversible process is generally higher due to uncompensated solution resistance between the reference and working electrodes and non-linear diffusion [98].

The CV after interaction of Zn(II) with aspartic acid in 1M KCl at different scan rates were observed and the current – potential data, peak separation, peak current ratio of the voltammograms are recorded in Table 4.39-4.40.

The voltammogram of Zn(II)-Apa interaction at different scan rate show that with the increase of scan rate the peak current of both the anodic and cathodic peaks increases. The cathodic peaks are shifted towards right and the anodic peaks are shifted to the left direction with increase in scan rate. Figure 4.128 and 4.130 (only anodic peak) shows plots of the two kinds of the anodic and the cathodic net peak currents of Zn(II) –Apa against the

square-root of the scan rates, where the net current means the second peak subtracted from the first one by the scan-stopped method [23]. The proportionality of the first and the second peaks suggests that the peak current of the reactant at each redox reaction is controlled by diffusion process.

4.2.4 Effect of Aspartic acid composition on the Zn(II) voltammogram

Figure 4.131 shows the effect of Aspartic acid concentration on the voltammogram of the Zn(II). The first anodic peak shifted positively and the second anodic peak is shifted negatively upon the addition of aspartic acid which indicates the formation of Zn(II)-Apa complex. The intensity of the anodic and cathodic peak current decreases with the increasing of aspartic acid   suggests that the formation of more Zn(II)-aspartic acid complex. With the increasing of aspartic acid concentration 1:1 to 1:3, the current decreases linearly but after more addition of aspartic acid, the current intensity change is constant. This indicate that the availability of Cu(II) is limited for the formation of the Cu(II)-Apa complex at saturation point.

In the buffer solution (pH 3), a broad anodic peak and high intense one cathodic peak appeared. The anodic peak current in buffer solutioin is lower than the aqueous solution whereas the cathodic peak in buffer solution is higher than the aqueous solution (Figure 4.132).

4.2.5 Redox behavior of Zn(II) in presence of L-phenylalanine Phe

Figure 4.133 shows the cyclic voltammogram of Zn(II) in presence of L-phenylalanine (Phe) in 1M KCl at different scan rate in aqueous solution. It is observed that the peak positions of the voltammogram of Zn(II) with L-phenylalanine was shifted with respect to that of only Zn(II). The peak current increases significantly in aqueous solution compared with that for free Zn(II) in the same experimental conditions, which may be due to the complexation of free Zn(II) with L-phenylalanine. This behavior confirms the interaction between Zn(II) and L-phenylalanine. Free phenyl alanine are electrochemically inactive in the potential range investigated.

For coordinated Zn(II) with L-phenylalanine (AP), anodic peaks were found at -0.98V and -0.77V and cathodic peaks were found at potential -1.33V at 0.1V/s scan rate. On the other

hand, the uncoordinated Zn(II) have no peak in aqueous solution at 0.1 V/s scan rate but it shows anodic peak and corresponding cathodic peak on the addition of phenyl alanine. The anodic and cathodic peaks shifted negatively after the complexation of Zn(II) with L-phenylalanine. This indicate that Zn(II) ion is more stabilized by the complexation with L-phenylalanine.

The reduction peak is ascribed to formation of the $Zn^{2+}(L)$ to $Zn^{0}(L)$ and corresponding oxidation formation of $Zn^{0}(L)$ to $Zn^{2+}(L)$.

Cathodic: $Zn^{2+}(L) + 2e \longrightarrow Zn^{0}(L)$

Anodic: $Zn^{0}(L) - 2e \longrightarrow Zn^{2+}(L)$
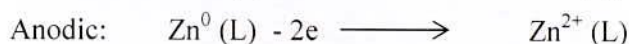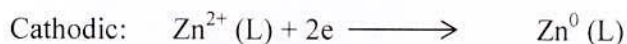
However, the stabilization of Zn species may also be due to d-π interactions between the copper d orbitals and the π system.

The anodic and cathodic peak current ratios (I_{pa}/I_{pc}) of Zn(II)-Phe at different scan rates are tabulated in Table 4.41-4.42. The current ratio is much higher than one. It indicates that voltammetic reactions of Zn(II)- Phe in aqueous solutions are not reversible at any scan rate. The corresponding peak potential differences (ΔE_{cor}) of second peaks are tabulated in Table 4.41-4.42. The theoretical separation between peaks is given by $\Delta E_{pcor} = 0.059/n$ V (for a n electron transfer reaction) at all scan rates [23]. From the Table 4.41-4.42 it is seen that the corresponding peak potentials are much higher than theoretical one electron transfer reaction. The measured value for a reversible process is generally higher due to uncompensated solution resistance between the reference and working electrodes and non-linear diffusion [98]. The CV after interaction of Zn(II) with L Phenylalanine in 1M KCl at different scan rates were observed and the current – potential data, peak separation, peak current ratio of the voltammograms are recorded in Table 4.41-4.42.

The voltammogram of Zn(II)-Phe interaction at different scan rate show that with the increase of scan rate the peak current of both the anodic and cathodic peaks increases. The cathodic peaks are shifted towards right and the anodic peaks are shifted to the left direction with increase in scan rate. Figure 4.134 shows plots of the two kinds of the anodic and the cathodic net peak currents of Zn(II) – Phe against the square-root of the scan rates, where the net current means the second peak subtracted from the first one by the scan-stopped

64

method [23]. The proportionality of the first and the second peaks suggests that the peak current of the reactant at each redox reaction is controlled by diffusion process.

4.2.6 Effect of L-Phenylalanine composition on the Zn(II) voltammogram

Figure 4.135 shows the effect of L-phenyl alanine concentration on the voltammogram of the Zn(II). The first anodic peak shifted positively and the second anodic peak is shifted negatively upon the addition of L-phenyl alanine which indicates the formation of Zn(II)-Phe complex. The intensity of the anodic and cathodic peak current decreases with the increasing of L-phenyl alanine (Figure 4.135) suggests that the formation of more Zn(II)-Phe complex. With the increasing of L-phenyl alanine concentration 1: 1 to 1:3, the current decreases linearly but after more addition of aspartic acid, the current intensity change is constant. This indicate that the availability of Cu(II) is limited for the formation of the Zn(II)-Phe complex at saturation point.

4.2.7 Acetate buffer solution pH 3

In buffer solution (pH 3) a broad anodic peak and high intense cathodic peak appeared. The anodic peak current in buffer solution is lower than in aqueous solution whereas the cathodic peak in buffer solution is higher than aqueous solution (Figure 4.136). The peak potential is shifted positively in the buffer solution. Figure 4.137 shows the CV of Zn(II)-Phe at different scan rate in buffer solution (pH=3.5). The anodic peak current varies linearly with the square root of scan rate indicating that the peak current is controlled by diffusion process (Figure 4.138).

4.2.8 Zn (II) with 3-nitrobenzene sulfonate (NBS) system

Figure 4.139 shows the cyclic voltammogram of Zn(II) in presence of 3-nitrobenzene sulfonate (NBS) in 1M KCl at different scan rate at pH 3.5. In aqueous solution Zn(II)-NBS is electroinactive. It is observed that the peak positions of the voltammogram of Zn(II) with 3-nitrobenzene sulfonate was shifted with respect to that of only Zn(II). The peak current decreases significantly compared with that for free Zn(II) in the same experimental conditions, which may be due to the complexation of free Zn(II) with 3-nitrobenzene sulfonate. This behavior confirms the interaction between Zn(II) and 3-

nitrobenzene sulfonate. Free ligands are electrochemically almost inactive in the potential range investigated.

For coordinated Zn(II) with 3-nitrobenzene sulfonate (NBS), the two broad anodic peaks were found at 0.25V and 0.52 V and corresponding one cathodic peak were found at potential -0.75V at 0.1V/s scan rate, respectively. The peaks are broad compared to aspartic acid and phenylalanine. On the other hand, the uncoordinated Zn(II) shows anodic peaks at potential -1.0V and corresponding cathodic peaks at potential -1.27V at 0.05V/s scan rate, respectively. After coordination of Zn(II) with NBS, the anodic both oxidation and reduction peaks shift positively. This indicate that oxidation of Zn(II)-NBS is easier than that of Zn(II) only. This also suggest that Zn(II) ion is more stabilized by the complexation with NBS, so further electron accepting is not favored except Cu(II) only. The stabilization of Zn species may also be due to d-π interactions between the copper d orbitals and the π system.

Zn(II)NBS + 2e $\leftrightarrow$ Zn(I)NBS + e $\leftrightarrow$ Zn (0) + NBS

The first corresponding anodic and cathodic peak current ratios (I_{pa}/I_{pc}) of Zn(II)-NBS is less than one. It indicates that voltammetic reactions of Zn(II)-NBS in aqueous solutions are not reversible. The corresponding peak potential differences (ΔE_{cor}) of second peaks are tabulated in Table 4.43. The corresponding peak potentials differences are usually independent of scan rate and concentration. The theoretical separation between peaks is given by ΔE_{pcor} = $0.059/n$ V (for a n electron transfer reaction) at all scan rates [23]. From the Table 4.43 it is seen that the corresponding peak potentials are higher than 1.0V at the scan rate 0.1V/s. The measured value for a reversible process is generally higher due to uncompensated solution resistance between the reference and working electrodes and non-linear diffusion [98]. It is also seen that the corresponding peak potential separation increases with the increase in scan rate. It indicates that there is a limitation due to charge transfer kinetics or ohmic potential (iR) drop [97].

The CV after interaction of Zn(II) with NBS in 1M KCl at different scan rates were observed and the current – potential data, peak separation, peak current ratio of the voltammograms are recorded in Table 4.43. The voltammogram of Zn(II)-NBS interaction at different scan rate show that with the increase of scan rate the peak current of both the

anodic and cathodic peaks increases. The cathodic peaks are shifted towards right and the anodic peaks are shifted to the left direction with increase in scan rate.

The plots of the anodic and the cathodic net peak currents of Zn(II)–NBS against the square-root of the scan rates, where the net current means the second peak subtracted from the first one by the scan-stopped method [23] (Figure 4.140). The proportionality of the first and the second peaks suggests that the peak current of the reactant at each redox reaction is controlled by diffusion process.

4.2.9 pH effect of Zn(II)- NBS

Figure 4.141 shows the comparison voltammogram of 2 mM Zn(II)-NBS in buffer solution at different pH (3.5, 4.5, 6.0, 8.0, 10.0) at scan rate 0.1V/s solution containing 1M KCl. The oxidation peak current increases with the decrease of pH indicating that at lower pH the Zn(II) is highly electroactive.

The effect of pH was studied by varying pH from 3.5, 4.5, 6.0, 8.0, 10.0. The position of the redox couple was found to be dependent upon pH. The peak current was plotted against pH and is given in the figure 4.142. From the figure it is seen that the oxidation peak current is higher at pH 4.5. This indicate that the electrochemical oxidation of Zn(II)-NBS is facilitated in acid media and hence the rate of electron transfer is faster. A plot was made between oxidation peak potential and pH as shown in figure 4.143. The peak potential is almost unaffected with decrease or increase in pH. The peak current of Zn(II)-NBS is lower than the only Zn(II) at the same condition.

4.2.10 Redox behavior of Catechol system

Aspartic acid, Phenylalanine are electroinactive ligands but Catechol is electroactive ligand. So, we have studied the electrochemical properties of Catechol before the studied of Zn(II)-Catechol systems. Figure 4.144-4.148 shows the CV of Catechol at different scan rate and different pH. The CV of Catechol shows anodic peak at potential 0.65 V and corresponding cathodic peak at potential 0.14 at 0.1V/s scan rate in buffer solution of pH 3. The first oxidation peak is ascribed to formation of the Cate to $Cate^{+2}$ and reduction peak formation

of Cate^{+2} to Cate. One step two electron transfer reaction is confirmed by the Chronoamperometry of Cottrell plot that will be discussed later.

The corresponding anodic and cathodic peak current ratios (I_{pa}/I_{pc}) at different scan rates are tabulated in Table 4.45-4.49. The current ratio is close to one at higher scan rate but at slower scan rate the current ratio value is little higher than one. It indicates that the voltammetic reactions of Catechol in aqueous buffer solutions are reversible at higher scan rate. The corresponding peak potential differences (ΔE_{cor}) of catechol at different scan rate are tabulated in Table 4.45-4.49. From the Table 4.45-4.49 it is seen that the corresponding peak potentials are above 0.4V which is much higher than theoretical one electron transfer reaction. The theoretical separation between peaks is given by $\Delta E_{pcor} = 0.059/n$ V (for a n electron transfer reaction) at all scan rates [23]. The corresponding peak potentials differences are usually independent of scan rate and concentration. The measured value for a reversible process is generally higher due to uncompensated solution resistance between the reference and working electrodes, and non-linear diffusion [98]. From the Table 4.45-4.49, it is seen that the corresponding peak potential separation increases with the increase in scan rate. It indicates that there is a limitation due to charge transfer kinetics or ohmic potential (iR) drop [97].

Figure 4.149-4.153 shows plots of the anodic and the cathodic net peak currents against the square-root of the scan rates, where the net current means the second peak subtracted from the first one by the scan-stopped method at different pH[23]. The proportionality of the first and the second peaks suggests that the peak current of the reactant at each redox reaction is controlled by diffusion process. The current function ($i_p/v^{1/2}$) is independent of the scan rate and the ratio of anodic to cathodic peak current, i_{pa}/i_{pc} , is almost equal to unity, at higher scan rate at pH 3indicating that the catechol species in the redox process is stable within the time scale of the experiment.

4.2.11 Catechol pH effect

Figure 4.154 shows the comparison voltammogram of 2 mM Catechol in acetate buffer solution at different pH (3.5, 5.5, 6.5, 7.5) at scan rate 0.1V/s solution. The peak current increases with the decrease of pH indicating that at lower pH the Catechol is highly electroactive.

The effect of pH was studied by varying pH from 3.5 to 7.5. In the pH range studied one anodic peak and one cathodic peak appeared. The anodic peak current increases with the decrease of pH. The position of the redox couple was found to be dependent upon pH. The peak current was plotted against pH and is given in the figure 4.155. From the figure it is seen that the oxidation peak current increased with decrease in pH. The maximum peak current was obtained at pH 3.5.

This shows that the electrochemical oxidation of Catechol is facilitated in acid media and hence the rate of electron transfer is faster. A plot was made between oxidation peak potential and pH as shown in figure 4.156. The peak potential increased with decrease in pH indicating higher energy requirement for oxidation at acid medium.

The electrochemical response is sensitive to the pH, and the waves shift to more negative potentials as the pH is increased. Figure 4.156 shows the plot of E_p values against pH. The slopes of the plot was determined graphically as ca. ~ 40 mV/pH though the peak separation was about 40 mV at 0.1V/s, which is somewhat larger than the theoretical value of 30 mV for a two-electron, two-proton transfer process (Scheme 1)which indicate that the oxidation of the Catechol proceeded via the 2e−/2H+ processes. This also suggests that during the reaction not only electron but also protons are released from the Catechol.

The electrochemical properties of these complexes are pH-dependent and the oxidation or reduction of Catechol proceeded via the 2e−/2H+*(pH < 7)* processes, being modulated by the quinone through combining protons on the -O groups [103]. This behaviour could be an advantage for research into the mechanism of proton pumps.

4.2.12 Differential pulse voltammetry of Cate

The DPV of Catechol shows one anodic peaks at potential 0.6 V at at E_{puls} 0.02 V, t_{puls}= 20ms and scan rate 0.1V/s in aqueous buffer solution (pH = 7) (acetate buffer) (Figure 4.157-4.158). The natures of anodic peaks are similar to cyclic voltammogram peak(Table 4.50).

4.2.13 Redox behavior of Zn(II) with Catechol

Figure 4.159 shows the cyclic voltammogram of Zn(II) in presence of Catechol (Cate) in 1M KCl at different scan rate in aqueous solution. It is observed that the peak positions of

the voltammogram of Zn(II) with Catechol (Cate) was shifted with respect to that of only Zn(II). The peak current increases significantly compared with that for free Zn(II) in the same experimental conditions, which may be due to the complexation of free Zn(II) with Catechol (Cate). This behavior confirms the interaction between Zn(II) and Catechol (Cate).

For coordinated Zn(II) with Catechol (Cate), a anodic peaks was found at -0.96 V and cathodic peaks was found at potential -1.69V at 0.1V/s scan rate, respectively in water. On the other hand, the uncoordinated Zn(II) have no anodic peak in aqueous solution at 0.1V/s scan rate but it shows anodic peak and corresponding cathodic peak on the addition of Catechol (Cate). The cathodic peaks shifted negatively after the complexation of Zn with Catechol. This indicate that Zn(II) ion is more stabilized by the complexation with Catechol.

The anodic and cathodic peak current ratios (I_{pa}/I_{pc}) of Zn(II)- Cate at different scan rates are tabulated in Table 4.51. The current ratio is much lower than one. It indicates that voltammetic reactions of Zn(II)- Cate in aqueous solutions are not reversible at any scan rate. The corresponding peak potential differences (ΔE_{cor}) of second peaks are tabulated in Table 4.51. The corresponding peak potentials differences are usually independent of scan rate and concentration. The theoretical separation between peaks is given by $\Delta E_{pcor} = 0.059/n$ V (for a n electron transfer reaction) at all scan rates [23]. From the Table 4.51 it is seen that the corresponding peak potentials are ≈ 60 mV which is close to theoretical one electron transfer reaction. The measured value for a reversible process is generally higher due to uncompensated solution resistance between the reference and working electrodes and non-linear diffusion [98].

The CV after interaction of Zn(II) with Cate in 1M KCl at different scan rates were observed and the current – potential data, peak separation, peak current ratio of the voltammograms are recorded in Table 4.51.

The voltammogram of Zn(II)- Cate interaction at different scan rate show that with the increase of scan rate the peak current of both the anodic and cathodic peaks increases. The cathodic peaks are shifted towards right and the anodic peaks are shifted to the left direction with increase in scan rate. Figure 4.160 shows plots of the two kinds of the anodic and the cathodic net peak currents of Zn(II) – Cate against the square-root of the scan rates, where the net current means the second peak subtracted from the first one by the scan-stopped

method [23]. The proportionality of the first and the second peaks suggests that the peak current of the reactant at each redox reaction is controlled by diffusion process.

4.2.14 pH effect of Zn(II)-Catechol

Figure 4.161-4.165 shows the comparison voltammogram of 2 mM Zn(II)-Cate in buffer solution at different pH (2, 3.0, 4.5, 7.0 and 11) at different scan rate of solution containing 1M KCl. The peak current increases with the decrease of pH indicating that at lower pH the Zn (II) is highly electroactive.

In pH 7 and 11, the CV shows that Zn(II)-Cate is almost electroinactive and do not show any prominent peak. So we have plotted peak current against square root of scan rate at pH 2-4.5. The peak current varied proportionally with the scan rate indicating that the current is controlled by diffusion process.

The effect of pH was studied by varying pH from 2 to 11. Figure 4.169 shows the comparison CV of Zn (II) –Catechol in buffer solution containing pH 2, 3, 5, 7.5 and 11 at scan rate 0.1V/s. At pH 2-5, the anodic and cathodic peak current is prominent but at pH 7 and 11, the anodic and cathodic peak is very weak and shifted positively. In the pH range studied one anodic peak and one cathodic peak appeared. The peak current increases with the decrease of pH shown in Figure 4. 170. In acidic medium (pH 2-4.5), the anodic peak appeared at 0.95V and cathodic peak at about -1.53V. In basic medium (pH 7-11), the anodic peak shifted positively at 0.37V and cathodic peak shifted 0.26V. This comparison shows the dominance of solvation in high-polarity mediums and of ion pairing in low-polarity mediums.

The position of the redox couple was found to be dependent upon pH. The peak current was plotted against pH and is given in the figure 4. 170. From the figure it is seen that the oxidation peak current increased with decrease in pH. The maximum peak current was obtained at pH 3.0. This shows that the electrochemical oxidation of Zn(II)-Cate is facilitated in acid media and hence the rate of electron transfer is faster. A plot was made between oxidation peak potential and pH as shown in figure 4.171 two slopes are appeared. The peak potential decreases with increase in pH then sharply increases and then unaffected indicating higher energy requirement for oxidation at basic medium. Since the electron transfer is associated with proton transfer in Zn(II)-catechol system, in basic medium the proton transfer is restricted, so the potential shifted toward positive direction. The intensity

of the peak current decreases with increasing of pH. The trend of increasing intensity indicates the formation of more Zn(II)-Cate complex(Table 4.52-4.54).

Figure 4. 171 shows the plot of E_p values against pH in acidic range. The slopes of the plot was determined graphically as ca.20 mV/pH at 0.1V/s, (pH 2-5) which is close to the theoretical value of 30 mV for a two-electron, two-proton transfer process which indicate that the oxidation of the Zn(II)-Cate proceeded via the 2e−/2H+ processes. This also suggest that during the reaction not only electron but also protons are released from the Zn(II)-Cate.

.

4.2.15 Effect of composition of Catechol with Zn(II)

Figure 4.172-4.175 shows the effect of Catechol concentration on the voltammogram of the Zn(II) at different pH and scan rate 0.1V/s. The anodic peak shifted positively upon the addition of Catechol which indicates the formation of Zn(II)-Cate complex. The intensity of the peak current decreases with the increasing of Catechol (Figure 4.176-4.179) suggests that the formation of more Zn(II)-Cate complex.

With the increasing of Catechol concentration 1: 1 to 1:5, the current decreases linearly (shown in Figure 4.176-4.179) but after more addition of Catechol, the current intensity change is constant. This indicate that the availability of Zn(II) is limited for the formation of the Zn(II)- Catechol complex at saturation point. Figure 4.180 shows the CV of increase of composition of Zn(II) but the Catechol composition is fixed. When the composition of Zn(II) increases with the fixed of the composition of Catechol, the voltammogram paterns turns into the only Zn(II), because of the deficiency of Catechol that is not sufficient in solution that can be coordinated with Zn(II). With the increase of Zn(II) composition 1:1 to 5:1, the anodic current decreases slowly indicating that the coordinating species decrease in solution (Figure 4.181).

4.2.16 Concentration effect on the voltammogram of Zn(II) + Catechol

Figure 4.182 shows the cyclic voltammograms of different concentrations of the Zn(II) ions + Catechol of pH 2 at 0.1 Vs^{-1} scan rate. The current intensity of the anodic peak is increased upon the addition of Catechol and slightyly shifted toward at the negative direction and the cathodic current increased with the addition of Catechol and slightly shifted toward the positive direction. The shifting of the peaks suggests the formation of

Zn(II)-Cate complex. The effect of concentration of Zn(II) and Catechol can be shown by recording the CV at each concentration (1, 2, 3, 4 and 5 mM) and plotting i_p *vs.* concentration for either the anodic peak or the cathodic peak (Figure 4.183). The relation between Zn(II) + Catechol concentration and cyclic voltammetric anodic and cathodic peak current (Ipa) is linear. The linear dependence of peak current on Zn (II) + Catechol concentration is depicted from the calibration curve shown Fig.4.183.

Figure 4.184 shows the comparison CV of Zn(II) only and Zn(II) –Asp, Zn(II)-Phe, Zn(II)-Cate, Zn(II)-NBS at similar condition (pH 3, scan rate 0.1V). From the figure it is seen that the anodic peak current of Zn(II)-Asp and Zn(II)-Phe are lower than Zn(II) only whereas the anodic peak current of Zn(II)- Cate and Zn(II)-NBS is higher than Zn(II) only. As the Asp and Phe are electroinactive in solution on the other hand the Cate and NBS are electroactive. When Cate and NBS are coordinated with Zn(II) both metal and ligands are electroactive, so constructive interference of peak appeared whereas Asp and Phe are coordinated with Zn(II), here ligands are electroinactive so the overall peak currents are lower than Zn(II) only.

4.2.17 Differential pulse voltammetry of Zn(II)- Cate

Figure 4.185-4.186 shows the DPV of Zn(II) in presence of Catechol in 1M KCl in aqueous buffer solution (pH = 2) (acetate buffer) at E_{puls} 0.02 V, t_{puls}= 20ms and at different scan rate.

It is observed that the peak positions of the DPV of Zn(II) with Catechol was shifted and two anodic peaks appeared and the peak shifted from -1.1 to 0.9 V and new peak appeared at -1.25V with respect to that of only Zn(II). The peak current increases significantly compared with that for free Zn(II) in the same experimental conditions. This indicate that the formation of complexation of free Zn(II) with Catechol.

4.2.18 DPV of Catechol concentration on the Zn(II) voltammogram

Figure 4.187-4.188 shows the effect of Catechol concentration on the DPV of the Zn(II). The anodic peak shifted slightly negatively upon the addition of Catechol which indicates the formation of Zn(II)-Cate complex. The intensity of the peak current decreases with the increasing of Catechol suggests that the formation of more Zn(II)-Cate complex.

With the increasing of Catechol concentration 1: 1 to 1:5, the current decreases linearly but after more addition of Catechol, the current intensity change is constant. This indicate that the availability of Zn(II) is limited for the formation of the Zn(II)- Catechol complex at saturation point.

For the explanation of reaction mechanism of electrode reaction, it is necessary to plot of the current functions $(1/v^{-1/2})$ vs scan rate. From the studied of all systems it is seen that the current functions decreased with the increasing of scan rate (Figure 4.189) except Zn(II)-Cate. So the behavior of electrode reaction of Cu(II)- ligands and Zn(II)- ligands are of ECE mechanism and Zn(II)- Cate is of CE mechanism .

Table 4.1 : Peak potential (E_{pa}), corresponding peak potential difference (ΔE), peak separation ($\Delta E_{1/2}$), peak current Ip (μA), corresponding peak current ratio (I_{pa}/I_{pc}), of 2mM $CuCl_2$ in aqueous solution at different scan rate.

v/Vs^{-1}	E_{pa1} /V	E_{pc1} /V	E_{pa2} /V	$\Delta E = E_{pc1} \sim E_{pa2}$	$\Delta E_{1/2}$/V	I_{pa1} /μA	I_{pc1} /μA	I_{pa2}/μA	I_{pa}/ I_{pc}
0.02	-0.13	0.17	0.29	0.12	0.42	3.870	-0.854	0.820	0.960
0.04	-0.13	0.17	0.28	0.11	0.41	4.501	-1.382	1.372	0.993
0.06	-0.13	0.17	0.28	0.11	0.41	4.884	-1.616	1.625	1.006
0.08	-0.13	0.17	0.29	0.12	0.42	6.007	-1.880	2.007	1.068
0.10	-0.13	0.17	0.29	0.12	0.42	6.284	-2.274	2.272	0.999
0.15	-0.13	0.17	0.29	0.12	0.43	8.148	-2.626	2.539	0.967
0.20	-0.13	0.17	0.30	0.13	0.43	8.891	-2.767	3.081	1.113
0.25	-0.12	0.16	0.31	0.15	0.43	9.354	-3.194	4.151	1.300
0.30	-0.12	0.17	0.31	0.14	0.43	10.100	-3.856	4.334	1.124
0.35	-0.12	0.16	0.31	0.15	0.43	10.632	-4.182	4.950	1.184
0.40	-0.12	0.16	0.31	0.15	0.43	9.897	-4.614	5.098	1.105
0.45	-0.12	0.16	0.31	0.15	0.43	10.820	-4.689	5.579	1.190
0.50	-0.11	0.16	0.31	0.15	0.42	11.152	-5.823	5.886	1.011

Table 4.2 : Peak potential (E_{pa}), corresponding peak potential difference (ΔE), peak separation ($\Delta E_{1/2}$), peak current Ip (μA), corresponding peak current ratio (I_{pa}/I_{pc}), of 2mM $CuCl_2$ in buffer solution (pH = 3.0) (acetate buffer) at different scan rate.

v/Vs^{-1}	E_{pa1} /V	E_{pc1} /V	E_{pa2} /V	$\Delta E = E_{pc1}{\sim}E_{pa2}$	$\Delta E_{1/2}$/V	I_{pa1} /μA	I_{pc1} /μA	I_{pa2} /μA	I_{pa}/ I_{pc}
0.02	-0.16	0.17	0.28	0.11	0.44	2.087	-1.262	1.471	1.166
0.04	-0.15	0.17	0.28	0.11	0.43	3.705	-1.618	1.571	0.971
0.06	-0.15	0.17	0.29	0.12	0.44	4.453	-2.093	1.699	0.812
0.08	-0.15	0.17	0.29	0.12	0.44	4.514	-2.385	1.794	0.752
0.10	-0.15	0.16	0.29	0.13	0.44	4.675	-2.829	1.900	0.672
0.15	-0.14	0.17	0.29	0.12	0.43	6.428	-2.896	2.285	0.789
0.20	-0.13	0.17	0.29	0.12	0.42	7.512	-3.535	2.562	0.725
0.25	-0.13	0.17	0.29	0.12	0.42	8.006	-4.314	2.794	0.648
0.30	-0.13	0.17	0.29	0.12	0.42	8.089	-4.481	2.990	0.667
0.35	-0.12	0.16	0.29	0.13	0.41	8.907	-5.386	3.163	0.587
0.40	-0.12	0.16	0.29	0.13	0.41	9.733	-6.538	3.380	0.517
0.45	-0.12	0.15	0.29	0.14	0.41	10.195	-7.006	4.174	0.596
0.50	-0.11	0.15	0.29	0.14	0.40	10.773	-7.427	4.381	0.589

Table 4.3 : Peak potential (E_{pa}), corresponding peak potential difference (ΔE), peak separation ($\Delta E_{1/2}$), peak current Ip (μA), corresponding peak current ratio (I_{pa}/I_{pc}), of 2mM CuCl$_2$ in buffer solution (pH = 6.0) (acetate buffer) at different scan rate.

v/Vs^{-1}	E_{pa1} /V	E_{pc1} /V	E_{pa2} /V	$\Delta E = E_{pc1} \sim E_{pa2}$	$\Delta E_{1/2}$/V	I_{pa1} /μA	I_{pc1} /μA	I_{pa2} /μA	I_{pa}/ I_{pc}
0.02	-0.17	0.13	0.29	0.16	0.46	1.694	-0.883	1.156	1.309
0.04	-0.15	0.11	0.27	0.16	0.42	2.641	-1.136	1.258	1.107
0.06	-0.15	0.12	0.27	0.15	0.42	3.469	-1.252	1.451	1.159
0.08	-0.15	0.11	0.27	0.16	0.42	3.334	-1.394	1.572	1.128
0.10	-0.16	0.08	0.28	0.20	0.44	-	-1.661	1.760	1.059
0.15	-0.14	0.11	0.27	0.16	0.41	4.600	-1.749	1.922	1.099
0.20	-0.14	0.11	0.27	0.16	0.41	5.055	-2.042	2.078	1.018
0.25	-0.14	0.10	0.27	0.17	0.41	5.269	-2.116	2.218	1.048
0.30	-0.14	0.08	0.27	0.19	0.41	5.579	-2.224	2.310	1.039
0.35	-0.13	0.10	0.26	0.16	0.39	6.295	-2.317	2.525	1.089
0.40	-0.13	0.10	0.26	0.16	0.39	6.604	-2.317	2.753	1.188
0.45	-0.13	0.09	0.27	0.18	0.40	7.214	-2.816	2.887	1.025
0.50	-0.13	0.08	0.27	0.19	0.40	7.422	-2.981	2.957	0.992

Table 4.4 : Peak Current Ip (μA) of CuCl$_2$ in aqueous buffer solution (pH = 3.0) (acetate buffer) at different concentration and at scan rate 0.1V/s.

Conc/mM	Peak Current I$_p$ (μA)				
	1st Oxidn.	2nd Oxidn.	1st Redn.	2nd Redn.	3rd Redn.
1	10.666	7.572	-	-1.144	-3.455
2	40.292	17.627	-1.793	-2.815	-11.256
3	52.088	17.771	-2.520	-4.695	-12.370
4	90.529	24.582	-3.224	-7.206	-22.434
5	99.577	27.195	-4.274	-9.989	-23.727

Table 4.5 : DPV of 2mM $CuCl_2$ for oxidation, E_{pa} and reduction, E_{pc} peak potential at different scan rate.

v/Vs^{-1}	E_{pa1} /V	E_{pa2} /V	E_{pa3} /V	E_{pc1} /V	E_{pc2} /V	E_{pc3} /V
0.06	-0.180	0.275	0.420	0.390	0.240	-0.270
0.08	-0.180	0.300	0.420	0.390	0.240	-0.270
0.10	-0.180	0.295	0.425	0.390	0.245	-0.270
0.15	-0.180	0.295	0.425	0.390	0.235	-0.275
0.20	-0.180	0.300	0.425	0.390	0.240	-0.280
0.25	-0.180	0.295	0.440	0.390	0.210	-0.270

Table 4.6 : DPV of $CuCl_2$ only in different concentration buffer solution (pH = 3.0) (acetate buffer) for oxidation, I_{pa} and reduction, I_{pc} peak current at scan rate 0.1V/s.

Concentration / mM	v/Vs^{-1}	I_{pa1} /μA	I_{pa2} /μA	I_{pc1} /μA	I_{pc2} /μA
1	0.10	19.85	4.70	-3.05	-4.27
2	0.10	21.80	4.18	-6.57	-6.62
3	0.10	21.41	2.58	-3.17	-6.19
4	0.10	28.02	4.53	-6.08	-10.90
5	0.10	39.05	8.91	-11.90	-15.10

Table 4.7 : Peak potential (E_{pa}), corresponding peak potential difference (ΔE), peak separation ($\Delta E_{1/2}$), peak current Ip (μA), corresponding peak current ratio (I_{pa}/I_{pc}), of $CuCl_2$ + aspartic acid (1:3) in aqueous solution at different scan rate.

v/Vs^{-1}	E_{pa1} /V	E_{pc1} /V	E_{pa2} /V	$\Delta E = E_{pc1} \sim E_{pa2}$	$\Delta E_{1/2}$/V	I_{pa1} /μA	I_{pc1} /μA	I_{pa2} /μA	I_{pa}/I_{pc}
0.02	-0.08	0.08	0.22	0.14	0.30	0.846	-0.238	0.226	0.949
0.04	-0.07	0.08	0.22	0.14	0.29	0.916	-0.302	0.319	1.056
0.06	-0.07	0.08	0.22	0.14	0.29	1.086	-0.358	0.386	1.078
0.08	-0.07	0.08	0.22	0.14	0.29	1.156	-0.401	0.439	1.095
0.10	-0.08	0.08	0.22	0.14	0.30	1.289	-0.444	0.487	1.097
0.15	-0.08	0.08	0.22	0.14	0.30	1.561	-0.455	0.491	1.079
0.20	-0.08	0.08	0.22	0.14	0.30	1.664	-0.605	0.564	0.932
0.25	-0.07	0.08	0.23	0.15	0.30	1.713	-0.671	0.634	0.945
0.30	-0.07	0.08	0.23	0.15	0.30	1.832	-0.720	0.696	0.967
0.35	-0.08	0.07	0.23	0.16	0.31	1.901	-0.869	0.746	0.858
0.40	-0.08	0.07	0.22	0.15	0.30	2.061	-0.943	0.936	0.993
0.45	-0.06	0.07	0.23	0.16	0.29	2.270	-1.080	1.000	0.926
0.50	-0.06	0.07	0.23	0.16	0.29	2.313	-1.042	1.037	0.995

Table 4.8: Peak potential (E_{pa}), corresponding peak potential difference (ΔE), peak separation ($\Delta E_{1/2}$), peak current Ip (μA), corresponding peak current ratio (I_{pa}/I_{pc}), of $CuCl_2$ + aspartic acid (1:3) in aqueous buffer solution (pH = 3.5) (acetate buffer) at different scan rate.

v/Vs^{-1}	E_{pa1} /V	E_{pc1} /V	E_{pa2} /V	$\Delta E = E_{pc1} \sim E_{pa2}$	$\Delta E_{1/2}$/V	I_{pa1} /μA	I_{pc1} /μA	I_{pa2} /μA	I_{pa}/I_{pc}
0.02	-0.09	0.06	0.23	0.17	0.32	0.978	-0.252	0.277	1.099
0.04	-0.10	0.08	0.23	0.15	0.33	1.370	-0.346	0.348	1.006
0.06	-0.10	0.07	0.22	0.15	0.32	1.660	-0.508	0.469	0.923
0.08	-0.10	0.07	0.23	0.16	0.33	1.918	-0.591	0.592	1.001
0.10	-0.10	0.07	0.23	0.16	0.33	2.138	-0.658	0.668	1.015
0.15	-0.10	0.05	0.24	0.19	0.34	2.607	-0.768	0.757	0.986
0.20	-0.10	0.06	0.24	0.18	0.34	2.995	-0.885	0.888	1.003
0.25	-0.09	0.01	0.24	0.23	0.33	3.051	-0.910	0.910	1.000
0.30	-0.09	0.03	0.25	0.22	0.34	3.367	-1.020	1.056	1.035
0.35	-0.06	0.02	0.26	0.24	0.32	3.420	-1.141	1.180	1.034
0.40	-0.07	0.03	0.26	0.23	0.33	3.740	-1.293	1.299	1.005
0.45	-0.07	0.07	0.26	0.19	0.33	3.878	-1.353	1.382	1.021
0.50	-0.07	0.10	0.26	0.16	0.33	4.012	-1.561	1.569	1.005

Table 4.9 : Peak potential (E_{pa}), corresponding peak potential difference (ΔE), peak separation ($\Delta E_{1/2}$), peak current Ip (μA), corresponding peak current ratio (I_{pa}/I_{pc}) of $CuCl_2$ + aspartic acid (1:3) in aqueous buffer solution (pH = 4.5) (acetate buffer) at different scan rate.

v/Vs^{-1}	E_{pa1} /V	E_{pc1} /V	E_{pa2} /V	$\Delta E = E_{pc1} \sim E_{pa2}$	$\Delta E_{1/2}$/V	I_{pa1} /μA	I_{pc1} /μA	I_{pa2} /μA	I_{pa}/ I_{pc}
0.02	-0.10	0.05	0.19	0.14	0.29	0.652	-0.244	0.259	1.061
0.04	-0.11	0.05	0.18	0.13	0.29	0.785	-0.301	0.383	1.272
0.06	-0.11	0.05	0.18	0.13	0.29	0.973	-0.409	0.424	1.037
0.08	-0.11	0.05	0.18	0.13	0.29	1.044	-0.446	0.496	1.112
0.10	-0.11	0.05	0.19	0.14	0.30	0.967	-0.487	0.587	1.205
0.15	-0.10	0.05	0.19	0.14	0.29	1.193	-0.625	0.630	1.008
0.20	-0.10	0.05	0.19	0.14	0.29	1.247	-0.695	0.735	1.057
0.25	-0.09	0.06	0.19	0.13	0.28	1.386	-0.837	0.842	1.006
0.30	-0.09	0.05	0.19	0.14	0.28	1.399	-0.939	0.886	0.943
0.35	-0.09	0.06	0.19	0.13	0.28	1.505	-1.036	0.912	0.880
0.40	-0.08	0.06	0.19	0.13	0.27	1.606	-1.113	0.921	0.827
0.45	-0.08	0.05	0.19	0.14	0.27	1.633	-1.210	0.917	0.758
0.50	-0.07	0.06	0.20	0.14	0.27	1.652	-1.270	0.923	0.727

Table 4.10: Peak potential (E_{pa}), corresponding peak potential difference (ΔE), peak separation ($\Delta E_{1/2}$), peak current Ip (μA), corresponding peak current ratio (I_{pa}/I_{pc}) of $CuCl_2$ +M aspartic acid (1:3) in aqueous buffer solution (pH = 5.5) (acetate buffer) at different scan rate.

v/Vs^{-1}	E_{pa1} /V	E_{pc1} /V	E_{pa2} /V	$\Delta E = E_{pc1} \sim E_{pa2}$	$\Delta E_{1/2}$/V	I_{pa1} /μA	I_{pc1} /μA	I_{pa2} /μA	I_{pa}/ I_{pc}
0.02	-0.11	0.05	0.15	0.10	0.26	0.740	-0.119	0.353	2.966
0.04	-0.11	0.05	0.15	0.10	0.26	0.966	-0.149	0.453	3.040
0.06	-0.10	0.05	0.15	0.10	0.25	1.126	-0.167	0.511	3.060
0.08	-0.10	0.05	0.15	0.10	0.25	1.318	-0.215	0.569	2.646
0.10	-0.10	0.05	0.15	0.10	0.25	1.437	-0.229	0.604	2.637
0.15	-0.10	0.05	0.15	0.10	0.25	1.600	-0.261	0.684	2.621
0.20	-0.10	0.05	0.16	0.11	0.26	1.794	-0.332	0.729	2.196
0.25	-0.10	0.05	0.16	0.11	0.26	1.970	-0.36	0.770	2.139
0.30	-0.10	0.05	0.16	0.11	0.26	2.070	-0.385	0.802	2.083
0.35	-0.09	0.05	0.16	0.11	0.25	2.136	-0.397	0.788	1.985
0.40	-0.09	0.05	0.16	0.11	0.25	2.240	-0.436	0.825	1.892
0.45	-0.09	0.05	0.16	0.11	0.25	2.224	-0.524	0.833	1.590
0.50	-0.09	0.05	0.19	0.14	0.28	-	-0.564	0.930	1.649

Table 4.11 : Peak potential (E_p), corresponding peak potential difference (ΔE), peak separation ($\Delta E_{1/2}$), peak current Ip (μA), corresponding peak current ratio (I_{pa}/I_{pc}) of Pure Cu(II), Cu(II)-Aspartic acid (1:1), (1:2) and (1:3) at similar condition (Scan rate = 0.04V/s).

Cu(II)-Aspartic acid	E_{pa1} /V	E_{pc1} /V	E_{pa2} /V	$\Delta E = E_{pc1} \sim E_{pa2}$	$\Delta E_{1/2}$/V	I_{pa1} /μA	I_{pc1} /μA	I_{pa2} /μA	I_{pa}/ I_{pc}
(1:0)	-0.13	0.17	0.28	0.11	0.41	4.501	-1.382	1.372	0.993
(1:1)	-0.10	0.13	0.26	0.13	0.36	2.634	-0.534	0.611	1.144
(1:2)	-0.09	0.11	0.24	0.13	0.33	1.819	-0.459	0.421	0.917
(1:3)	-0.07	0.08	0.22	0.14	0.29	0.916	-0.302	0.319	1.056

Table 4.12 : Peak potential (E_p), corresponding peak potential difference (ΔE), peak separation ($\Delta E_{1/2}$), peak current Ip (μA), corresponding peak current ratio (I_{pa}/I_{pc}) of Pure Cu(II), Cu(II)-Aspartic acid(1:1), (1:2) and (1:3) at similar condition (Scan rate = 0.10V/s).

Cu(II)-Aspartic acid	E_{pa1} /V	E_{pc1} /V	E_{pa2} /V	$\Delta E = E_{pc1}{\sim}E_{pa2}$	$\Delta E_{1/2}$/V	I_{pa1} /μA	I_{pc1} /μA	I_{pa2} /μA	I_{pa}/ I_{pc}
(1:0)	-0.13	0.17	0.29	0.12	0.42	6.284	-2.274	2.272	0.999
(1:1)	-0.10	0.12	0.26	0.14	0.36	3.464	-0.964	0.918	0.952
(1:2)	-0.09	0.12	0.24	0.12	0.33	2.423	-0.621	0.619	0.997
(1:3)	-0.08	0.08	0.22	0.14	0.30	1.289	-0.444	0.487	1.097

Table 4.13 : Peak potential (E_p), corresponding peak potential difference (ΔE), peak separation ($\Delta E_{1/2}$), peak current Ip (μA), corresponding peak current ratio (I_{pa}/I_{pc}) of Pure Cu(II), Cu(II)-Aspartic acid(1:1), (1:2) and (1:3) at similar condition (pH = 3.5,Scan rate = 0.04V/s).

Cu(II)-Aspartic acid	E_{pa1} /V	E_{pc1} /V	E_{pa2} /V	$\Delta E = E_{pc1}{\sim}E_{pa2}$	$\Delta E_{1/2}$ /V	I_{pa1} /μA	I_{pc1} /μA	I_{pa2} /μA	I_{pa}/ I_{pc}
(1:0)	-0.15	0.17	0.28	0.11	0.43	3.705	-1.618	1.571	0.971
(1:1)	-0.12	0.14	0.25	0.11	0.37	1.377	-0.683	0.630	0.922
(1:2)	-0.11	0.10	0.23	0.13	0.34	1.696	-0.648	0.601	0.927
(1:3)	-0.10	0.08	0.23	0.15	0.33	1.370	-0.346	0.348	1.006

Table 4.14 : Peak potential (E_p), corresponding peak potential difference (ΔE), peak separation ($\Delta E_{1/2}$), peak current Ip (μA), corresponding peak current ratio (I_{pa}/I_{pc}) of Pure Cu(II), Cu(II)-Aspartic acid (1:1), (1:2) and (1:3) at similar condition (pH = 3.5, Scan rate = 0.10V/s).

Cu(II)-Aspartic acid	E_{pa1} /V	E_{pc1} /V	E_{pa2} /V	$\Delta E = E_{pc1}{\sim}E_{pa2}$	$\Delta E_{1/2}$/V	I_{pa1} /μA	I_{pc1} /μA	I_{pa2} /μA	I_{pa}/ I_{pc}
(1:0)	-0.15	0.16	0.29	0.13	0.44	4.675	-2.829	1.900	0.672
(1:1)	-0.12	0.10	0.26	0.16	0.38	2.203	-0.574	1.019	1.775
(1:2)	-0.11	0.11	0.23	0.12	0.34	2.634	-0.989	1.090	1.102
(1:3)	-0.10	0.07	0.23	0.16	0.33	2.138	-0.658	0.668	1.015

Table 4.15 : Peak potential (E_p), corresponding peak potential difference (ΔE), peak separation ($\Delta E_{1/2}$), peak current Ip (μA), corresponding peak current ratio (I_{pa}/I_{pc}) of Pure Cu(II), Cu(II)-Aspartic acid (1:1), (1:2) and (1:3) at similar condition (pH = 4.5,Scan rate = 0.04V/s).

Cu(II)-Aspartic acid	E_{pa1} /V	E_{pc1} /V	E_{pa2} /V	$\Delta E = E_{pc1}{\sim}E_{pa2}$	$\Delta E_{1/2}$/V	I_{pa1} /μA	I_{pc1} /μA	I_{pa2} /μA	I_{pa}/ I_{pc}
(1:0)	-0.16	0.15	0.30	0.15	0.46	0.192	-1.697	3.561	2.098
(1:1)	-0.13	0.07	0.25	0.18	0.38	1.639	-0.813	1.109	1.364
(1:2)	-0.11	0.06	0.21	0.15	0.32	1.117	-0.502	0.667	1.329
(1:3)	-0.11	0.05	0.18	0.13	0.29	0.785	-0.301	0.383	1.272

Table 4.16 : Peak potential (E_p), corresponding peak potential difference (ΔE), peak separation ($\Delta E_{1/2}$), peak current Ip (μA), corresponding peak current ratio (I_{pa}/I_{pc}) of Pure Cu(II), Cu(II)-Aspartic acid (1:1), (1:2) and (1:3) at similar condition (pH = 4.5, Scan rate = 0.50V/s).

Cu(II)-Aspartic acid	E_{pa1} /V	E_{pc1} /V	E_{pa2} /V	$\Delta E = E_{pc1}{\sim}E_{pa2}$	$\Delta E_{1/2}$/V	I_{pa1} /μA	I_{pc1} /μA	I_{pa2} /μA	I_{pa}/ I_{pc}
(1:0)	-0.14	0.14	0.28	0.14	0.42	1.266	-7.202	5.812	0.807
(1:1)	-0.09	0.05	0.27	0.22	0.36	1.834	-1.687	2.032	1.205
(1:2)	-0.08	0.05	0.22	0.17	0.30	1.395	-1.402	1.346	0.960
(1:3)	-0.07	0.06	0.20	0.14	0.27	1.652	-1.27	0.923	0.727

Table 4.17 : Peak potential (E_p), corresponding peak potential difference (ΔE), peak separation ($\Delta E_{1/2}$), peak current Ip (μA), corresponding peak current ratio (I_{pa}/I_{pc}) of Pure Cu(II), Cu(II)-Aspartic acid (1:1), (1:2) and (1:3) at similar condition (pH = 5.5, Scan rate = 0.04V/s).

Cu(II)-Aspartic acid	E_{pa1} /V	E_{pc1} /V	E_{pa2} /V	$\Delta E = E_{pc1}{\sim}E_{pa2}$	$\Delta E_{1/2}$/V	I_{pa1} /μA	I_{pc1} /μA	I_{pa2} /μA	I_{pa}/ I_{pc}
(1:0)	-0.15	0.11	0.27	0.16	0.42	2.641	-1.136	1.258	1.107
(1:1)	-0.13	0.05	0.21	0.16	0.34	1.407	-0.251	0.699	2.785
(1:2)	-0.11	0.05	0.17	0.12	0.28	1.251	-0.200	0.527	2.635
(1:3)	-0.11	0.05	0.15	0.10	0.26	0.966	-0.149	0.453	3.040

Table 4.18 : Peak potential (E_p), corresponding peak potential difference (ΔE), peak separation ($\Delta E_{1/2}$), peak current Ip (μA), corresponding peak current ratio (I_{pa}/I_{pc}), of Pure Cu(II), Cu(II)-Aspartic acid (1:1), (1:2) and (1:3) at similar condition (pH = 5.5, Scan rate = 0.10V/s).

Cu(II)-Aspartic acid	E_{pa1} /V	E_{pc1} /V	E_{pa2} /V	$\Delta E = E_{pc1} \sim E_{pa2}$	$\Delta E_{1/2}$/V	I_{pa1} /μA	I_{pc1} /μA	I_{pa2} /μA	I_{pa}/ I_{pc}
(1:0)	-0.16	0.08	0.28	0.20	0.44	2.702	-1.661	1.760	1.059
(1:1)	-0.13	0.06	0.20	0.14	0.33	2.005	-0.382	0.909	2.379
(1:2)	-0.11	0.04	0.17	0.13	0.28	1.830	-0.291	0.738	2.536
(1:3)	-0.10	0.05	0.15	0.10	0.25	1.437	-0.229	0.604	2.637

Table 4.19 : Peak Current Ip (μA) of $CuCl_2$ + aspartic acid (1:3 same concentration) in buffer solution (acetate buffer) pH = 3.5 at different concentration of scan rate 0.1V/s.

Conc/mM	Peak Current I_p (μA)			
	1st Oxidn	2nd Oxidn.	1st Redn.	2nd Redn.
1	-	4.835	-1.668	-
2	4.006	5.155	-1.922	-1.260
3	5.782	5.822	-2.092	-1.889
4	8.782	5.657	-2.222	-2.339
5	13.604	7.469	-2.641	-2.880

Table 4.20 : DPV of 4mM $CuCl_2$ + 4mM aspartic acid (1:3) in aqueous buffer solution (pH = 3.0) (acetate buffer) for oxidation and reduction peak potential at different scan rate.

v/Vs^{-1}	E_{pa1} /V	E_{pa2} /V	E_{pa3} /V	E_{pc1} /V	E_{pc2} /V	E_{pc3} /V
0.06	-0.120	0.230	0.435	0.365	0.160	-0.225
0.08	-0.125	0.225	0.435	0.365	0.165	-0.225
0.10	-0.120	0.230	0.435	0.365	0.155	-0.225
0.15	-0.125	0.230	0.430	0.365	I_{pa}0.150	-0.225
0.20	-0.125	0.235	0.420	0.360	0.145	-0.225
0.25	-0.125	0.235	0.420	0.360	0.135	-0.215

Table 4.21: Peak potential (E_{pa}), corresponding peak potential difference (ΔE), peak separation ($\Delta E_{1/2}$), peak current Ip (μA), corresponding peak current ratio (I_{pa}/I_{pc}) of 2mM $CuCl_2$ + 2mM L-Phenylalanine (1:3) in aqueous solution at different scan rate.

v/Vs^{-1}	E_{pa1} /V	E_{pc1} /V	E_{pa2} /V	$\Delta E = E_{pc1} \sim E_{pa2}$	$\Delta E_{1/2}$/V	I_{pa1} /μA	I_{pc1} /μA	I_{pa2} /μA	I_{pa}/ I_{pc}
0.05	-0.08	0.06	0.21	0.15	0.29	-	-0.357	0.441	1.235
0.10	-0.07	0.07	0.22	0.15	0.29	2.160	-0.565	0.619	1.095
0.15	-0.07	0.06	0.22	0.16	0.29	2.061	-0.681	0.659	0.968
0.20	-0.07	0.06	0.22	0.16	0.29	1.912	-0.746	0.736	0.986
0.25	-0.06	0.06	0.22	0.16	0.28	1.856	-0.826	0.824	0.997
0.30	-0.06	0.06	0.22	0.16	0.28	1.581	-0.969	0.875	0.903
0.35	-0.05	0.06	0.22	0.16	0.27	1.566	-1.043	0.926	0.888
0.40	-0.05	0.07	0.23	0.16	0.28	1.541	-1.127	1.089	0.966
0.45	-0.05	0.06	0.23	0.17	0.28	1.488	-1.189	1.120	0.942
0.50	-0.04	0.06	0.23	0.17	0.27	1.177	-1.233	1.156	0.937
0.60	-0.04	0.06	0.23	0.17	0.27	0.899	-1.339	1.225	0.915
0.70	-0.04	0.06	0.24	0.18	0.28	0.844	-1.428	1.296	0.907
0.80	-0.03	0.06	0.24	0.18	0.27	0.763	-1.520	1.360	0.895

Table 4.22 : Peak potential (E_{pa}), corresponding peak potential difference (ΔE), peak separation ($\Delta E_{1/2}$), peak current Ip(μA), corresponding peak current ratio (I_{pa}/I_{pc}) of $CuCl_2$ + L-Phenylalanine (1:3) in aqueous buffer solution (pH = 3.5) (acetate buffer) at different scan rate.

v/Vs^{-1}	E_{pa1} /V	E_{pc1} /V	E_{pa2} /V	E_{pc2} /V	$\Delta E =$ E_{pc1}~E_{pa2}	$\Delta E =$ E_{pc2}~E_{pa1}	$\Delta E_{1/2}$/V	I_{pa1} /μA	I_{pc1} /μA	I_{pa2} /μA	I_{pc2} /μA	$I_{pa2}/$ I_{pc1}	$I_{pa1}/$ I_{pc2}
0.02	-0.09	0.08	0.22	-0.59	0.14	0.50	0.31	1.038	-0.424	0.427	-0.324	1.007	3.204
0.04	-0.10	0.08	0.22	-0.54	0.14	0.44	0.32	1.261	-0.546	0.556	-0.496	1.018	2.542
0.06	-0.10	0.08	0.22	-0.55	0.14	0.45	0.32	1.516	-0.667	0.671	-0.629	1.006	2.410
0.08	-0.10	0.07	0.23	-0.59	0.16	0.49	0.33	1.701	-0.763	0.766	-0.653	1.004	2.605
0.10	-0.10	0.07	0.23	-0.6	0.16	0.50	0.33	1.901	-0.855	0.866	-0.687	1.013	2.767
0.15	-0.10	0.07	0.23	-0.65	0.16	0.55	0.33	2.131	-1.053	1.066	-0.795	1.012	2.680
0.20	-0.10	0.07	0.23	-0.65	0.16	0.55	0.33	2.47	-1.269	1.262	-0.936	0.994	2.639
0.25	-0.09	0.07	0.24	-0.66	0.17	0.57	0.33	2.828	-1.448	1.424	-0.995	0.983	2.842
0.30	-0.09	0.07	0.24	-	0.17	0.09	0.33	2.722	-1.554	1.561	-	1.004	-
0.35	-0.08	0.06	0.24	-	0.18	0.08	0.32	2.855	-1.641	1.691	-	1.030	-
0.40	-0.08	0.06	0.24	-	0.18	0.08	0.32	3.134	-1.847	1.818	-	0.984	-
0.45	-0.08	0.06	0.24	-	0.18	0.08	0.32	3.205	-1.901	1.869	-	0.983	-
0.50	-0.08	0.06	0.25	-	0.19	0.08	0.33	3.546	-1.992	1.937	-	0.972	-

Table 4.23: Peak potential (E_{pa}), corresponding peak potential difference (ΔE), peak separation ($\Delta E_{1/2}$), peak current Ip (μA), corresponding peak current ratio (I_{pa}/I_{pc}) of $CuCl_2$ + L-Phenylalanine (1:3) in aqueous buffer solution (pH = 4.5) (acetate buffer) at different scan rate.

v/Vs^{-1}	E_{pa1} /V	E_{pc1} /V	E_{pa2} /V	E_{pc2} /V	$\Delta E = E_{pc1} \sim E_{pa2}$	$\Delta E = E_{pc2} \sim E_{pa1}$	$\Delta E_{1/2}$/V	I_{pa1} /μA	I_{pc1} /μA	I_{pa2} /μA	I_{pc2} /μA	$\frac{I_{pa2}}{I_{pc1}}$	$\frac{I_{pa1}}{I_{pc2}}$
0.02	-0.08	0.05	0.20	-0.60	0.15	0.52	0.28	1.062	-0.263	0.313	-0.574	1.190	1.850
0.04	-0.08	0.05	0.20	-0.59	0.15	0.51	0.28	1.116	-0.386	0.439	-0.756	1.137	1.476
0.06	-0.09	0.05	0.21	-0.62	0.16	0.53	0.30	1.278	-0.468	0.510	-0.875	1.090	1.460
0.08	-0.09	0.05	0.21	-0.64	0.16	0.55	0.30	1.432	-0.477	0.570	-1.018	1.195	1.407
0.10	-0.09	0.05	0.21	-0.65	0.16	0.56	0.30	1.578	-0.516	0.601	-1.043	1.165	1.513
0.15	-0.09	0.05	0.21	-0.65	0.16	0.56	0.30	1.786	-0.654	0.667	-1.279	1.020	1.396
0.20	-0.08	0.05	0.22	-	0.17	-	0.30	1.877	-0.741	0.727	-	0.981	-
0.25	-0.08	0.05	0.22	-	0.17	-	0.30	2.071	-0.815	0.769	-	0.943	-
0.30	-0.08	0.06	0.22	-	0.16	-	0.30	1.887	-0.894	0.790	-	0.884	-
0.35	-0.07	0.04	0.23	-	0.19	-	0.30	1.662	-1.021	0.813	-	0.796	-
0.40	-0.07	0.01	0.23	-	0.22	-	0.30	1.689	-1.099	0.822	-	0.748	-
0.45	-0.07	0.02	0.23	-	0.21	-	0.30	1.642	-1.175	0.842	-	0.716	-
0.50	-0.06	0.01	0.23	-	0.22	-	0.29	1.669	-1.263	0.841	-	0.666	-

Table 4.24 : Peak potential (E_{pa}), corresponding peak potential difference (ΔE), peak separation ($\Delta E_{1/2}$), peak current Ip(μA), corresponding peak current ratio (I_{pa}/I_{pc}), of $CuCl_2$ + L-Phenylalanine (1:3) in aqueous buffer solution   (pH = 6.0) (acetate buffer) at different scan rate.

v/Vs^{-1}	E_{pa1} /V	E_{pc1} /V	E_{pa2} /V	$\Delta E = E_{pc1} \sim E_{pa2}$	$\Delta E_{1/2}$/V	I_{pa1} /μA	I_{pc1} /μA	I_{pa2} /μA	I_{pa2}/I_{pc1}
0.02	-0.10	-0.20	0.20	0.40	0.30	0.147	-0.126	0.252	2.000
0.04	-0.12	-0.20	0.17	0.37	0.29	0.264	-0.153	0.406	2.653
0.06	-0.12	-0.20	0.17	0.37	0.29	0.500	-0.237	0.458	1.932
0.08	-0.12	-0.20	0.16	0.36	0.28	0.602	-0.146	0.442	3.027
0.10	-0.12	-0.20	0.17	0.37	0.29	0.683	-0.162	0.459	2.833
0.15	-0.12	-0.20	0.16	0.36	0.28	0.824	-0.254	0.416	1.638
0.20	-0.11	-0.20	0.16	0.36	0.27	0.754	-0.290	0.494	1.703
0.25	-0.11	-0.20	0.16	0.36	0.27	0.621	-0.328	0.496	1.512
0.30	-0.11	-0.21	0.16	0.37	0.27	0.670	-0.400	0.473	1.182
0.35	-0.10	-0.21	0.16	0.37	0.26	0.709	-0.528	0.602	1.140
0.40	-0.10	-0.21	0.16	0.37	0.26	0.532	-0.310	0.513	1.655
0.45	-0.10	-0.21	0.16	0.37	0.26	0.558	-0.517	0.499	0.965
0.50	-0.09	-0.21	0.16	0.37	0.25	0.368	-0.653	0.426	0.652

Table 4.25 : Peak potential (E_p), corresponding peak potential difference (ΔE), peak separation ($\Delta E_{1/2}$), peak current Ip (μA), corresponding peak current ratio (I_{pa}/I_{pc}) of Pure Cu(II), Cu(II)- L-Phenylalanine (1:1), (1:2) and (1:3) at similar condition (Scan rate = 0.1V/s).

Cu(II)-Aspartic acid	E_{pa1} /V	E_{pc1} /V	E_{pa2} /V	$\Delta E = E_{pc1} \sim E_{pa2}$	$\Delta E_{1/2}$/V	I_{pa1} /μA	I_{pc1} /μA	I_{pa2} /μA	I_{pa}/I_{pc}
(1:0)	-0.13	0.17	0.29	0.12	0.42	6.284	-2.274	2.272	0.999
(1:1)	-	-	-	-	-	-	-	-	-
(1:2)	0.09	0.1	0.23	0.13	0.14	0.939	-0.114	1.053	9.237
(1:3)	-0.07	0.07	0.22	0.15	0.29	2.160	-0.565	0.619	1.095

89

Table 4.26 : Peak potential (E_p), corresponding peak potential difference (ΔE), peak separation ($\Delta E_{1/2}$), peak current Ip (μA), corresponding peak current ratio (I_{pa}/I_{pc}) of Pure Cu(II), Cu(II)- L-Phenylalanine (1:1), (1:2) and (1:3) at similar condition (pH = 3.5, Scan rate = 0.1V/s).

Cu(II)-Aspartic acid	E_{pa1} /V	E_{pc1} /V	E_{pa2} /V	$\Delta E = E_{pc1} \sim E_{pa2}$	$\Delta E_{1/2}$ /V	I_{pa1} /μA	I_{pc1} /μA	I_{pa2} /μA	I_{pa}/ I_{pc}
(1:0)	-0.15	0.16	0.29	0.13	0.44	4.675	-2.829	1.900	0.672
(1:1)	-0.10	0.09	0.29	0.20	0.39	3.158	-1.349	1.164	0.863
(1:2)	-0.11	0.09	0.24	0.15	0.35	2.644	-0.980	1.025	1.046
(1:3)	-0.10	0.07	0.23	0.16	0.33	1.901	-0.855	0.866	1.013

Table 4.27 : Peak potential (E_p), corresponding peak potential difference (ΔE), peak separation ($\Delta E_{1/2}$), peak current Ip (μA), corresponding peak current ratio (I_{pa}/I_{pc}) of Pure Cu(II), Cu(II)- L-Phenylalanine (1:1), (1:2) and (1:3) at similar condition (pH = 4.5, Scan rate= 0.1V/s).

Cu(II)-Aspartic acid	E_{pa1} /V	E_{pc1} /V	E_{pa2} /V	$\Delta E = E_{pc1} \sim E_{pa2}$	$\Delta E_{1/2}$ /V	I_{pa1} /μA	I_{pc1} /μA	I_{pa2} /μA	I_{pa}/ I_{pc}
(1:0)	-	-	-	-	-	-	-	-	-
(1:1)	-0.12	0.10	0.23	0.13	0.35	2.464	-1.388	1.221	0.880
(1:2)	-0.11	0.08	0.22	0.14	0.33	1.520	-0.815	1.176	1.443
(1:3)	-0.09	0.05	0.21	0.16	0.30	1.578	-0.516	0.601	1.165

Table 4.28 : Peak potential (E_p), corresponding peak potential difference (ΔE), peak separation ($\Delta E_{1/2}$), peak current Ip (μA), corresponding peak current ratio (I_{pa}/I_{pc}) of Pure Cu(II), Cu(II)- L-Phenylalanine (1:1), (1:2) and (1:3) at similar condition (pH = 6.0, Scan rate = 0.1V/s).

Cu(II)-Aspartic acid	E_{pa1} /V	E_{pc1} /V	E_{pa2} /V	$\Delta E = E_{pc1} \sim E_{pa2}$	$\Delta E_{1/2}$ /V	I_{pa1} /μA	I_{pc1} /μA	I_{pa2} /μA	I_{pa}/ I_{pc}
(1:0)	-0.16	0.08	0.28	0.20	0.44	-	-1.661	1.760	1.060
(1:1)	-0.13	0.06	0.23	0.17	0.36	0.812	-0.456	0.728	1.596
(1:2)	-0.12	-	0.17	-	0.29	1.122	-	0.561	-
(1:3)	-0.12	-0.20	0.17	0.37	0.29	0.683	-0.162	0.459	2.833

Table 4.29 : Peak Current Ip (μA) of CuCl$_2$ + L- Phenyl alanine (1:3 same concentration) in buffer solution (acetate buffer) pH = 3.5 at different concentration of scan rate 0.1V/s.

Conc/mM	Peak Current I$_p$ (μA)			
	1st Oxidn	2nd Oxidn.	1st Redn.	2nd Redn.
1	-	4.463	-1.381	-
2	3.000	5.587	-2.579	-0.986
3	5.855	5.993	-2.719	-1.074
4	14.677	7.743	-3.123	-3.488
5	18.250	8.196	-3.252	-4.250

Table 4.30 : Peak potential (E_p), corresponding peak potential difference (ΔE), peak separation ($\Delta E_{1/2}$), peak current Ip (μA), corresponding peak current ratio (I_{pa}/I_{pc}) of Pure CuCl$_2$, Cu(II)-Aspartic acid(1:3), Cu(II)-L Phenyl alanine (1:3) at similar condition (Scan rate= 0.10V/s, pH=6.0).

Composition	E_{pa1} /V	E_{pc1} /V	E_{pa2} /V	$\Delta E = E_{pc1} \sim E_{pa2}$	$\Delta E_{1/2}$/V	I_{pa1} /μA	I_{pc1} /μA	I_{pa2} /μA	I_{pa}/ I_{pc}
Cu only	-0.16	0.08	0.28	0.20	-0.44	2.702	-1.661	1.760	1.059
Cu + aspartic acid	-0.10	0.05	0.15	0.10	-0.25	1.437	-0.229	0.604	2.638
Cu + phenylalanine	-0.12	-0.20	0.17	0.37	-0.29	0.683	-0.162	0.459	2.833

Table 4.31 : DPV of 3mM CuCl$_2$ + 3mM L- Phenyl alanine (1:3) in aqueous buffer solution (pH = 3.5) (acetate buffer) E (V) for oxidation and reduction peak potential at different scan rate.

v/Vs^{-1}	E_{pa1} /V	E_{pa2} /V	E_{pc1} /V	E_{pc2} /V
0.06	-0.135	0.205	0.160	-0.235
0.08	-0.135	0.205	0.160	-0.235
0.10	-0.135	0.215	0.155	-0.235
0.15	-0.145	0.210	0.155	-0.235
0.20	-0.145	0.215	0.170	-0.250
0.25	-0.145	0.235	0.180	-0.250

Table 4.32 : Peak potential (E_{pa}), corresponding peak potential difference (ΔE), peak current Ip (μA), corresponding peak current ratio (I_{pa}/I_{pc}) of 2mM $CuCl_2$ + 2mM 3-Nitro benzene sulfonate (1:3) in aqueous buffer solution (pH = 3.5) at different scan rate.

v/Vs^{-1}	E_{pa1} /V	E_{pc1} /V	$\Delta E = E_{pc1} \sim E_{pa2}$	I_{pa1} /μA	I_{pc1} /μA	I_{pa}/ I_{pc}
0.02	-0.09	-0.72	0.63	2.460	-1.955	1.258
0.03	-0.09	-0.72	0.63	2.676	-3.266	0.819
0.04	-0.09	-0.73	0.64	3.079	-3.837	0.802
0.05	-0.09	-0.72	0.63	3.409	-4.074	0.837
0.06	-0.09	-0.74	0.65	3.732	-4.443	0.840
0.07	-0.09	-0.77	0.68	3.849	-5.405	0.712
0.08	-0.07	-0.75	0.68	3.919	-6.293	0.623
0.09	-0.07	-0.75	0.68	4.035	-7.349	0.549
0.10	-0.05	-0.75	0.70	4.176	-7.676	0.544
0.20	-0.02	-0.81	0.79	4.794	-10.704	0.448
0.30	-0.02	-0.81	0.79	5.667	-14.066	0.403
0.40	-0.02	-0.81	0.79	5.858	-16.282	0.360
0.50	0.01	-0.81	0.82	6.830	-17.347	0.394

Table 4.33 : Peak potential (E_{pa}), corresponding peak potential difference (ΔE), peak current Ip (μA), corresponding peak current ratio (I_{pa}/I_{pc}) of $CuCl_2$ +3-Nitro benzene sulfonate (1:3) in aqueous buffer solution (pH = 4.5) at different scan rate.

v/Vs^{-1}	E_{pa1} /V	E_{pc1} /V	$\Delta E = E_{pc1} \sim E_{pa2}$	I_{pa1} /μA	I_{pc1} /μA	I_{pa}/ I_{pc}
0.02	-0.08	-0.71	0.63	2.268	-3.171	0.715
0.03	-0.08	-0.71	0.63	2.850	-4.813	0.592
0.04	-0.08	-0.72	0.64	3.205	-5.177	0.619
0.05	-0.08	-0.72	0.64	4.070	-6.093	0.668
0.06	-0.08	-0.72	0.64	4.574	-7.609	0.601
0.07	-0.08	-0.72	0.64	4.952	-8.065	0.614
0.08	-0.06	-0.76	0.70	5.014	-8.628	0.581
0.09	-0.06	-0.80	0.74	5.513	-9.373	0.588
0.10	-0.06	-0.80	0.74	5.595	-9.912	0.564
0.20	-0.05	-0.81	0.76	7.025	-14.55	0.483
0.30	-0.02	-0.82	0.80	8.513	-16.965	0.502
0.40	-0.01	-0.83	0.82	8.739	-17.888	0.488
0.50	-0.01	-0.83	0.82	9.116	-19.895	0.458

Table 4.34 : Peak potential (E_p), corresponding peak potential difference (ΔE), peak current Ip (μA), corresponding peak current ratio (I_{pa}/I_{pc}) of of 2mM $ZnCl_2$ in aqueous solution at different scan rate.

v/Vs^{-1}	E_{pa}/V	$I_{pa}/\mu A$
0.02	-1.01	3.226
0.04	-1.00	1.392
0.06	-1.01	1.055
0.08	-1.00	0.202
0.10	-1.00	0.092
0.15	0.99	0.054
0.20	-0.98	0.083
0.25	-0.99	0.130
0.30	-0.99	0.134
0.35	-0.99	0.208
0.40	-0.99	0.079
0.45	-0.99	0.177
0.50	-0.99	0.102

Table 4.35 : Peak potential (E_p), corresponding peak potential difference (ΔE), peak current Ip (μA), corresponding peak current ratio (I_{pa}/I_{pc}) of 2mM $ZnCl_2$ in aqueous buffer solution (pH = 1.5) (KCl + HCl buffer) at different scan rate.

v/Vs^{-1}	E_{pa1}/V	E_{pc1}/V	$\Delta E = E_{pc1} \sim E_{pa2}$	$I_{pa1}/\mu A$	$I_{pc1}/\mu A$	I_{pa}/I_{pc}
0.05	-0.94	-1.48	0.54	31.43	-83.46	0.376
0.10	-0.94	-1.55	0.61	29.92	-122.40	0.244
0.20	-0.92	-1.61	0.69	36.59	-160.47	0.228
0.30	-0.90	-1.57	0.67	57.49	-199.57	0.288
0.40	-0.91	-1.70	0.79	40.75	-203.73	0.200
0.50	-0.90	-1.74	0.84	42.09	-242.01	0.174

Table 4.36 : Peak potential (E_p), corresponding peak potential difference (ΔE), peak current Ip (μA), corresponding peak current ratio (I_{pa}/I_{pc}) of 2mM $ZnCl_2$ in aqueous buffer solution (pH = 2) (KCl + HCl buffer) at different scan rate.

v/Vs^{-1}	E_{pa1} /V	E_{pc1} /V	$\Delta E = E_{pc1} \sim E_{pa2}$	I_{pa1} /μA	I_{pc1} /μA	I_{pa}/ I_{pc}
0.05	-0.94	-1.65	0.71	0.141	6.88	60.27
0.10	-0.94	-1.75	0.81	0.316	7.92	33.35
0.15	-0.93	-1.72	0.79	0.387	8.73	47.57
0.20	-0.93	-1.74	0.81	0.447	9.02	52.27
0.25	-0.93	-1.75	0.82	0.500	10.86	54.54
0.30	-0.93	-1.77	0.84	0.548	12.09	56.45

Table 4.37: Peak potential (E_p), corresponding peak potential difference (ΔE), peak current Ip (μA), corresponding peak current ratio (I_{pa}/I_{pc}) of 2mM $ZnCl_2$ in aqueous buffer solution (pH = 4.5) (Acetate buffer) at different scan rate.

v/Vs^{-1}	E_{pa1} /V	E_{pc1} /V	$\Delta E = E_{pc1} \sim E_{pa2}$	I_{pa1} /μA	I_{pc1} /μA	I_{pa}/ I_{pc}
0.05	-0.98	-1.30	0.32	61.31	-16.56	3.702
0.10	-0.96	-1.34	0.38	78.31	-13.64	5.741
0.20	-0.94	-1.37	0.43	104.25	-20.95	4.976
0.30	-0.92	-1.40	0.48	119.67	-20.05	5.968
0.40	-0.92	-1.41	0.49	133.55	-26.71	5.000
0.50	-0.92	-1.47	0.55	147.62	-28.69	5.145

Table 4.38 : Peak potential (E_p) and peak current Ip (μA) of 2mM $ZnCl_2$ in buffer solution (pH = 11.0) at different scan rate.

v/Vs^{-1}	E_{pc1} /V	I_{pc1} /μA
0.05	-	-
0.10	0.74	-11.99
0.20	0.73	-31.45
0.30	0.71	-56.96
0.40	0.67	-84.87
0.50	0.64	-106.19

Table 4.39 : Peak potential (E_p), corresponding peak potential difference (ΔE), peak current Ip (μA), corresponding peak current ratio (I_{pa}/I_{pc}) of $ZnCl_2$ + aspartic acid (1:3) in aqueous solution at different scan rate.

v/Vs^{-1}	E_{pa1} /V	E_{pc1} /V	$\Delta E = E_{pc1}{\sim}E_{pa2}$	I_{pa1} /μA	I_{pc1} /μA	I_{pa}/ I_{pc}
0.02	-0.91	-1.48	0.57	1.021	-3.897	0.262
0.04	-0.92	-1.48	0.56	1.911	-4.46	0.428
0.06	-0.91	-1.49	0.58	2.288	-4.787	0.478
0.08	-0.90	-1.51	0.61	2.586	-4.946	0.523
0.10	-0.90	-1.52	0.62	3.334	-5.455	0.611
0.15	-0.90	-1.53	0.63	3.568	-6.242	0.572
0.20	-0.90	-1.57	0.67	4.468	-6.621	0.675
0.25	-0.89	-1.57	0.68	5.319	-7.491	0.710
0.30	-0.89	-1.57	0.68	5.643	-7.694	0.733
0.35	-0.89	-1.57	0.68	5.788	-7.785	0.743
0.40	-0.89	-1.57	0.68	6.247	-8.452	0.739
0.45	-0.89	-1.57	0.68	6.429	-8.863	0.725
0.50	-0.88	-1.57	0.68	6.880	-8.902	0.772

Table 4.40 : Peak potential (E_p), corresponding peak potential difference (ΔE), peak current Ip (μA), corresponding peak current ratio (I_{pa}/I_{pc}) of $ZnCl_2$ + aspartic acid (1:3) in aqueous buffer solution   (pH = 3.5) (acetate buffer) at different scan rate.

v/Vs^{-1}	E_{pa}/V	$I_{pa}/\mu A$
0.02	-0.90	0.379
0.04	-0.90	0.635
0.06	-0.90	0.732
0.08	-0.89	1.038
0.10	-0.89	1.055
0.15	-0.89	1.250
0.20	-0.89	1.293
0.25	-0.94	1.355
0.30	-0.96	1.691
0.35	-0.96	1.564
0.40	-0.96	1.973
0.45	-0.95	2.302
0.50	-0.95	2.045

Table 4.41 : Peak potential (E_p), corresponding peak potential difference (ΔE), peak current Ip (μA), corresponding peak current ratio (I_{pa}/I_{pc}) of $ZnCl_2$ + L-phenyl alanine (1:3) in aqueous solution at different scan rate.

v/Vs^{-1}	E_{pa1}/V	E_{pa2}/V	$\Delta E_{1/2}/V$	$I_{pa1}/\mu A$	$I_{pa2}/\mu A$
0.02	-0.99	-0.84	0.15	0.700	1.106
0.06	-0.99	-0.79	0.20	-	1.186
0.10	-0.99	-0.79	0.20	0.637	1.317
0.20	-0.99	-0.76	0.23	0.609	1.369
0.30	-0.98	-0.74	0.24	0.582	1.397
0.40	-0.97	-0.71	0.26	0.450	1.486
0.50	-0.93	-0.75	0.18	-	1.621

Table 4.42 : Peak potential (E_p), corresponding peak potential difference (ΔE), peak current Ip (μA), corresponding peak current ratio (I_{pa}/I_{pc}) of $ZnCl_2$ + L-phenyl alanine (1:3) in aqueous buffer solution (pH = 3.5) (acetate buffer) at different scan rate.

v/Vs^{-1}	E_{pa}/V	$I_{pa}/\mu A$
0.04	-0.88	0.158
0.06	-0.89	0.362
0.10	-0.88	1.002
0.30	-0.87	3.259
0.50	-0.87	4.529

Table 4.43 : Peak potential (E_p), corresponding peak potential difference (ΔE), peak current Ip (μA), corresponding peak current ratio (I_{pa}/I_{pc}) of $ZnCl_2$ + 3- nitro benzene sulphonate (1:3) in buffer solution(acetate buffer) pH = 3.5 at different scan rate.

v/Vs^{-1}	E_{pa1}/V	E_{pc1}/V	E_{pa2}/V	E_{pc2}/V	$\Delta E = E_{pc1} \sim E_{pa2}$	$\Delta E = E_{pc2} \sim E_{pa1}$	$\Delta E_{1/2}/V$	$I_{pa1}/\mu A$	$I_{pc1}/\mu A$	$I_{pa2}/\mu A$	$I_{pc2}/\mu A$	I_{pa2}/I_{pc1}	I_{pa1}/I_{pc2}
0.04	0.04	0.00	0.50	-0.73	0.50	0.77	0.46	0.980	-4.421	3.422	-8.068	0.774	0.121
0.06	0.05	-0.20	0.51	-0.75	0.71	0.80	0.46	1.533	-7.293	4.384	-9.382	0.601	0.163
0.08	0.16	-0.23	0.56	-0.78	0.79	0.94	0.40	2.362	-9.362	4.082	-10.687	0.436	0.221
0.10	0.18	-0.25	0.56	-0.81	0.81	0.99	0.38	2.517	-10.533	3.738	-11.179	0.355	0.225
0.20	0.19	-0.25	0.67	-0.95	0.92	1.14	0.48	3.779	-17.915	1.046	-18.262	0.058	0.207
0.30	0.27	-0.25	-	-0.95	-	1.22	-	4.412	-22.332	-	-23.083	-	0.191
0.40	0.28	-0.25	-	-	-	-	-	5.442	-27.197	-	-	-	-
0.50	0.35	-0.25	-	-	-	-	-	5.999	-34.938	-	-	-	-

Table 4.44 : Peak potential (E_p), corresponding peak potential difference (ΔE), peak current Ip (μA), corresponding peak current ratio (I_{pa}/I_{pc}) of Zn(II)- 3-Nitro benzene Sulphonate (1:3) in different pH at similar condition (Scan rate= 0.10V/s).

pH	v (V/s)	$E_{pa\,1}$/V	$E_{pa\,2}$/V	E_{pc}/V	$\Delta E = E_{pc} \sim E_{pa}$	I_{pa1} /μA	I_{pc1} /μA	I_{pa2} /μA	I_{pa}/ I_{pc}
3.5	0.10	0.16	0.56	-0.81	1.37	3.529	-13.000	3.738	0.287
4.5	0.10	0.14	0.56	-0.78	1.34	5.448	-12.438	4.040	0.325
6.0	0.10	0.12	0.60	-0.78	1.38	1.932	-9.301	0.829	0.089
8.0	0.10	0.17	0.58	-0.71	1.29	2.159	-9.862	0.838	0.085
10.0	0.10	-0.06	0.56	-0.73	1.29	3.593	-12.88	1.227	0.095

Table 4.45 : Peak potential (E_{pa}), corresponding peak potential difference (ΔE), peak separation ($\Delta E_{1/2}$), peak current Ip (μA), corresponding peak current ratio (I_{pa}/I_{pc}) of 2mM catechol in buffer solution (pH = 2.0) (KCl + HCl buffer) at different scan rate.

v/Vs^{-1}	$v^{1/2}$	E_{pa1} /V	E_{pc1} /V	$\Delta E = E_{pc1} \sim E_{pa2}$	I_{pa1} /μA	I_{pc1} /μA	I_{pa}/ I_{pc}
0.05	0.224	0.63	0.26	0.37	8.11	-4.59	1.767
0.06	0.245	0.63	0.26	0.37	8.91	-4.56	1.953
0.07	0.265	0.62	0.25	0.37	8.79	-6.97	1.261
0.08	0.283	0.63	0.25	0.38	8.69	-7.81	1.113
0.09	0.300	0.63	0.24	0.39	9.11	-8.03	1.134
0.10	0.316	0.63	0.24	0.39	9.21	-8.39	1.098
0.20	0.447	0.65	0.22	0.43	12.59	-13.14	1.134
0.30	0.548	0.65	0.21	0.44	16.71	-16.78	0.996
0.40	0.632	0.66	0.19	0.47	18.54	-19.29	0.961

Table 4.46 : Peak potential (E_{pa}), corresponding peak potential difference (ΔE), peak separation ($\Delta E_{1/2}$), peak current Ip (µA), corresponding peak current ratio (I_{pa}/I_{pc}) of 2mM catechol in aqueous buffer solution (pH = 3.5) (KCl + HCl buffer) at different scan rate.

v/Vs^{-1}	$v^{1/2}$	E_{pa1} /V	E_{pc1} /V	$\Delta E = E_{pc1} \sim E_{pa2}$	I_{pa1} /µA	I_{pc1} /µA	I_{pa}/I_{pc}
0.05	0.224	0.62	0.18	0.44	8.64	-4.82	1.792
0.06	0.245	0.62	0.17	0.45	9.01	-7.65	1.178
0.07	0.265	0.63	0.16	0.47	9.27	-7.78	1.191
0.08	0.283	0.63	0.16	0.47	9.96	-7.30	1.364
0.09	0.300	0.63	0.16	0.47	10.56	-8.64	1.222
0.10	0.316	0.64	0.15	0.49	11.00	-9.96	1.104
0.20	0.447	0.65	0.13	0.52	16.72	-15.14	1.222
0.30	0.548	0.67	0.13	0.54	20.24	-18.42	1.099
0.40	0.632	0.68	0.11	0.57	23.89	-22.01	1.085

Table 4.47 : Peak potential (E_{pa}), corresponding peak potential difference (ΔE), peak separation ($\Delta E_{1/2}$), peak current Ip (µA), corresponding peak current ratio (I_{pa}/I_{pc}) of 2mM catechol in aqueous buffer solution (pH = 5.5) (Acetate buffer) at different scan rate.

v/Vs^{-1}	$v^{1/2}$	E_{pa1} /V	E_{pc1} /V	$\Delta E = E_{pc1} \sim E_{pa2}$	I_{pa1} /µA	I_{pc1} /µA	I_{pa}/I_{pc}
0.05	0.224	0.55	0.11	0.44	7.34	-5.13	1.430
0.06	0.245	0.56	0.11	0.45	7.51	-6.47	1.160
0.07	0.265	0.57	0.10	0.47	7.74	-8.60	0.900
0.08	0.283	0.57	0.09	0.48	7.87	-9.39	0.838
0.09	0.300	0.59	0.09	0.50	9.33	-8.97	1.040
0.10	0.316	0.59	0.09	0.50	8.66	-10.90	0.794
0.20	0.447	0.61	0.08	0.53	11.41	-16.24	1.040
0.30	0.548	0.63	0.06	0.57	16.64	-20.17	0.825
0.40	0.632	0.64	0.04	0.60	18.57	-20.87	0.890

Table 4.48 : Peak potential (E_{pa}), corresponding peak potential difference (ΔE), peak separation ($\Delta E_{1/2}$), peak current Ip (μA), corresponding peak current ratio (I_{pa}/I_{pc}) of 2mM catechol in aqueous buffer solution (pH = 6.5) (Phosphate buffer) at different scan rate.

v/Vs^{-1}	$v^{1/2}$	E_{pa1} /V	E_{pc1} /V	$\Delta E = E_{pc1} \sim E_{pa2}$	I_{pa1} /μA	I_{pc1} /μA	I_{pa}/I_{pc}
0.05	0.224	0.37	0.08	0.29	6.76	-6.28	1.076
0.06	0.245	0.39	0.07	0.32	4.53	-6.55	0.692
0.07	0.265	0.41	0.07	0.34	5.52	-8.66	0.637
0.08	0.283	0.41	0.07	0.34	6.15	-9.35	0.658
0.09	0.300	0.43	0.07	0.36	4.72	-8.83	0.534
0.10	0.316	0.44	0.07	0.37	5.16	-9.27	0.557
0.20	0.447	0.46	0.05	0.41	4.05	-15.37	0.534
0.30	0.548	0.53	0.03	0.50	9.51	-15.19	0.626
0.40	0.632	0.52	0.02	0.50	9.81	-16.63	0.590

Table 4.49: Peak potential (E_{pa}), corresponding peak potential difference (ΔE), peak separation ($\Delta E_{1/2}$), peak current Ip (μA), corresponding peak current ratio (I_{pa}/I_{pc}) of 2mM catechol in aqueous buffer solution (pH = 7.5) (Phosphate buffer) at different scan rate.

v/Vs^{-1}	$v^{1/2}$	E_{pa1} /V	E_{pc1} /V	$\Delta E = E_{pc1} \sim E_{pa2}$	I_{pa1} /μA	I_{pc1} /μA	I_{pa}/I_{pc}
0.05	0.224	0.37	0.04	0.33	5.23	-5.22	1.001
0.06	0.245	0.38	0.04	0.34	5.89	-5.75	1.024
0.07	0.265	0.38	0.04	0.34	3.78	-8.23	0.459
0.08	0.283	0.40	0.04	0.36	3.99	-7.46	0.535
0.09	0.300	0.42	0.03	0.39	5.27	-7.59	0.694
0.10	0.316	0.43	0.03	0.40	3.53	-7.64	0.462
0.20	0.447	0.50	0.01	0.49	3.64	-7.27	0.694
0.30	0.548	0.51	-0.03	0.54	2.52	-10.21	0.247
0.40	0.632	0.52	-0.04	0.56	4.61	-9.99	0.461

101

Table 4.50 : DPV of 2mM catechol in buffer solution (pH = 7.0) (Phosphate buffer) for oxidation and reduction peak potential at different scan rate.

scan rate, v (V/s)	Potential E (V)		
	$E_{1\ oxdn}$	$E_{1\ redn}$	$E_{2\ redn}$
0.10	0.45	0.5	0.01
0.20	0.53	0.55	-0.05
0.30	0.55	0.6	-0.04

Table 4.51 : Peak potential (E_{pa}), corresponding peak potential difference (ΔE), peak separation ($\Delta E_{1/2}$), peak current Ip (μA), corresponding peak current ratio (I_{pa}/I_{pc}) of $ZnCl_2$ + catechol in aqueous at different scan rate.

v/Vs^{-1}	E_{pa1}/V	E_{pc1}/V	$\Delta E = E_{pc1} \sim E_{pa2}$	$I_{pa1}/\mu A$	$I_{pc1}/\mu A$	I_{pa}/I_{pc}
0.05	-0.89	-1.72	0.83	1.45	-56.80	0.025
0.10	-0.88	-1.69	0.81	1.42	-69.92	0.020
0.15	-0.88	-1.69	0.81	2.31	-81.06	0.028
0.20	-0.88	-1.71	0.83	2.32	-90.05	0.026
0.25	-0.88	-1.72	0.84	4.61	-101.52	0.045
0.30	-0.88	-1.73	0.85	5.16	-105.88	0.049

Table 4.52 : Peak potential (E_p), corresponding peak potential difference (ΔE), peak current Ip (μA), corresponding peak current ratio (I_{pa}/I_{pc}) of $ZnCl_2$ + catechol (1:3) in aqueous solution (pH = 2.0) at different scan rate.

v/Vs^{-1}	E_{pa1}/V	E_{pc1}/V	$\Delta E = E_{pc1} \sim E_{pa2}$	$I_{pa1}/\mu A$	$I_{pc1}/\mu A$	I_{pa}/I_{pc}
0.05	-0.89	-1.53	0.64	4.43	-33.40	0.133
0.10	-0.90	-1.53	0.63	10.60	-45.69	0.232
0.20	-0.90	-1.54	0.64	16.14	-59.85	0.270
0.30	-0.89	-1.57	0.68	18.97	-64.84	0.292

Table 4.53 : Peak potential (E_p), corresponding peak potential difference (ΔE), peak current Ip (μA), corresponding peak current ratio (I_{pa}/I_{pc}) of $ZnCl_2$ +Catechol (1:3) in aqueous solution (pH = 3.0) at different scan rate.

v/Vs^{-1}	E_{pa1} /V	E_{pc1} /V	$\Delta E = E_{pc1} \sim E_{pa2}$	I_{pa1} /μA	I_{pc1} /μA	I_{pa}/I_{pc}
0.05	-0.95	-1.52	0.57	10.92	-9.29	1.175
0.10	-0.95	-1.52	0.57	16.95	-11.62	1.459
0.20	-0.94	-1.55	0.61	22.48	-13.81	1.628
0.30	-0.93	-1.54	0.61	27.82	-15.26	1.823
0.40	-0.92	1.55	2.47	30.00	-16.15	1.857
0.50	-	-	-	-	-	-

Table 4.54 : Peak potential (E_p), corresponding peak potential difference (ΔE), peak current Ip (μA), corresponding peak current ratio (I_{pa}/I_{pc}) of $ZnCl_2$ + Catechol (1:3) in aqueous solution (pH = 4.5) at different scan rate.

v/Vs^{-1}	E_{pa1} /V	E_{pc1} /V	$\Delta E = E_{pc1} \sim E_{pa2}$	I_{pa1} /μA	I_{pc1} /μA	I_{pa}/I_{pc}
0.05	-0.95	-1.24	0.29	8.58	-7.820	1.097
0.10	-0.95	-1.26	0.31	21.78	-9.710	2.243
0.20	-0.94	-1.27	0.33	39.04	-15.22	2.565
0.30	-0.93	-1.27	0.34	51.66	-12.70	4.068
0.40	-0.92	-1.30	0.38	61.70	-15.85	3.892
0.50	-0.91	-1.03	.12	70.60	-14.32	4.930

Table 4.55 : Peak potential (E_p), corresponding peak potential difference (ΔE), peak current Ip (μA), corresponding peak current ratio (I_{pa}/I_{pc}) of $ZnCl_2$ + Catechol (1:1), (1:2), (1:3), (1:4) and (1:5) at similar condition (pH = 2, Scan rate= 0.1V/s).

($ZnCl_2$: Catechol)	E_{pa1} /V	E_{pc1} /V	$\Delta E = E_{pc1} \sim E_{pa2}$	I_{pa1} /μA	I_{pc1} /μA	I_{pa}/I_{pc}
(1:1)	-0.90	-1.56	0.66	14.31	-88.73	0.161
(1:2)	-0.92	-1.55	0.63	19.58	-58.21	0.336
(1:3)	-0.90	-1.53	0.63	10.60	-45.69	0.232
(1:4)	-0.89	-1.52	0.63	10.67	-35.41	0.301
(1:5)	-0.91	-1.50	0.59	5.23	-24.42	0.214

Table 4.56 : Peak potential (E_p), peak current Ip (μA), corresponding peak current ratio (I_{pa}/I_{pc}), of $ZnCl_2$ + Catechol (1:1), (1:2) and (1:3) at similar condition (pH = 3.0, Scan rate= 0.1V/s).

$ZnCl_2$: Catechol	E_{pa1} /V	I_{pa1} /μA	I_{pa2} /μA	I_{pa}/I_{pc}
(1:1)	-0.93	33.19	-	-
(1:2)	-0.95	18.13	-	-
(1:3)	-0.95	16.95	-11.62	1.459

Table 4.57 : Peak potential (E_p), peak current Ip (μA), corresponding peak current ratio (I_{pa}/I_{pc}), of $ZnCl_2$ + Catechol (1:1), (1:2) and (1:3) at similar condition (pH = 4.5, Scan rate= 0.1V/s).

$ZnCl_2$: Catechol	E_{pa} /V	E_{pc} /V	$\Delta E = E_{pc} \sim E_{pa}$	I_{pa} /μA	I_{pc} /μA	I_{pa}/I_{pc}
(1:1)	-0.93	-1.29	0.35	33.19	-2.64	2.492
(1:2)	-0.95	-1.26	0.31	18.13	-7.53	0.851
(1:3)	-0.95	-1.26	0.31	16.95	-9.71	2.243

Table 4.58 : Peak potential (E_p), corresponding peak potential difference (ΔE), peak current Ip (μA), corresponding peak current ratio (I_{pa}/I_{pc}), of Zn(II)-Catechol(1:1), (1:2), (1:3), (1:4) and (1:5) at similar condition (pH = 2.0, Scan rate= 0.30V/s).

$ZnCl_2$: Catechol	E_{pa1} /V	E_{pc1} /V	$\Delta E = E_{pc1} \sim E_{pa2}$	I_{pa1} /μA	I_{pc1} /μA	I_{pa}/I_{pc}
(1:1)	-0.90	-1.57	0.67	28.245	-116.212	0.243
(1:2)	-0.90	-1.62	0.72	26.552	-88.492	0.300
(1:3)	-0.89	-1.56	0.67	18.974	-65.350	0.290
(1:4)	-0.89	-1.54	0.65	17.236	-49.146	0.351
(1:5)	-0.89	-1.55	0.66	10.194	-30.596	0.333

Table 4.59 : Peak potential (E_p), corresponding peak potential difference (ΔE), peak current Ip (μA), corresponding peak current ratio (I_{pa}/I_{pc}) of $ZnCl_2$ + Catechol (1:1), (2:1), (3:1), (4:1) and (5:1) at similar condition (pH = 2.0, Scan rate= 0.1V/s).

$ZnCl_2$: Catechol	E_{pa1} /V	E_{pc1} /V	$\Delta E = E_{pc1} \sim E_{pa2}$	I_{pa1} /μA	I_{pc1} /μA	I_{pa}/ I_{pc}
(1:1)	-0.96	-1.65	0.69	6.65	-63.69	0.104
(2:1)	-0.91	-1.76	0.85	3.65	-44.71	0.082
(3:1)	-0.9	-1.75	0.85	6.58	-63.01	0.104
(4:1)	-0.88	-1.79	0.91	0.75	-54.69	0.014
(5:1)	-0.92	-1.84	0.92	3.71	-44.96	0.082

Table 4.60 : Peak Current Ip (μA) of $ZnCl_2$ + Catechol (1:3 same concentration) in aqueous buffer solution (acetate buffer) at different concentration of scan rate 0.1V/s.

Conc / mM	Peak Current I_p (μA)	
	1st Oxidn	1st Redn.
1	-	-34.98
2	1.42	-69.92
3	3.16	-5.80
4	5.98	-88.74
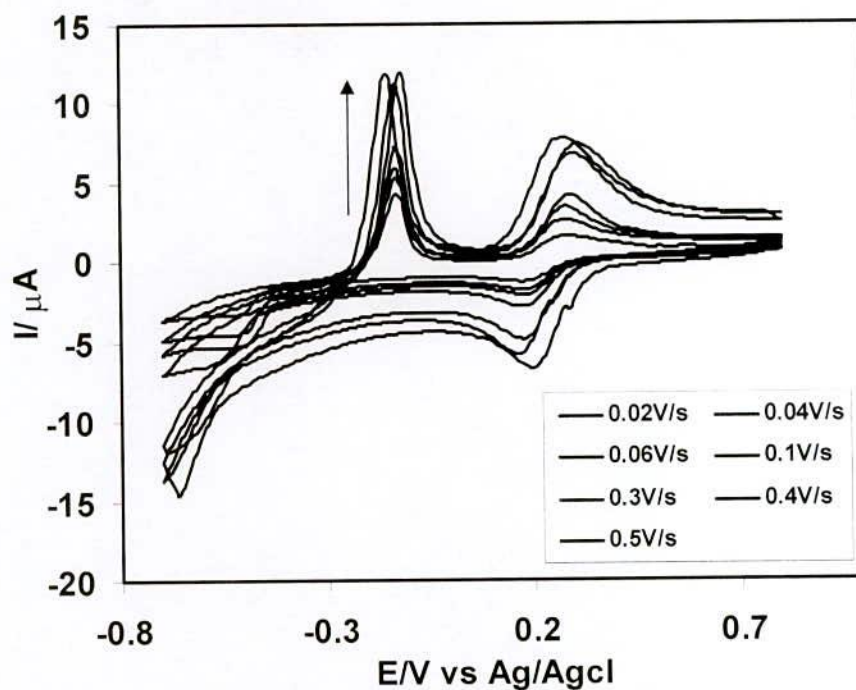
Figure 4.1 : Cyclic voltammogram of 2mM $CuCl_2$ in aqueous solution at different scan rate.
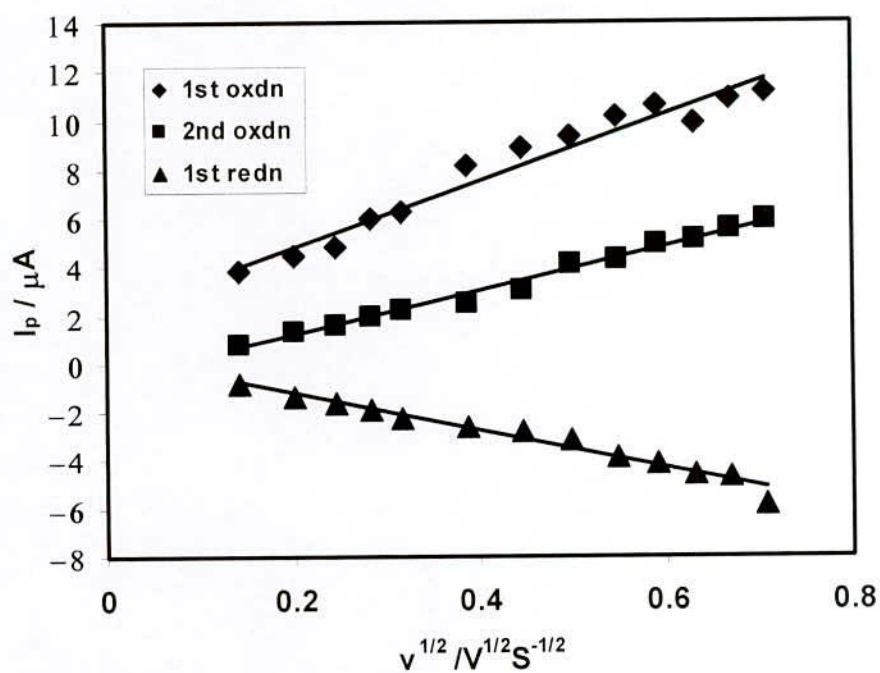
Figure 4.2 : Plots of peak current versus square root of scan rate of 2mM $CuCl_2$ in aqueous solution.
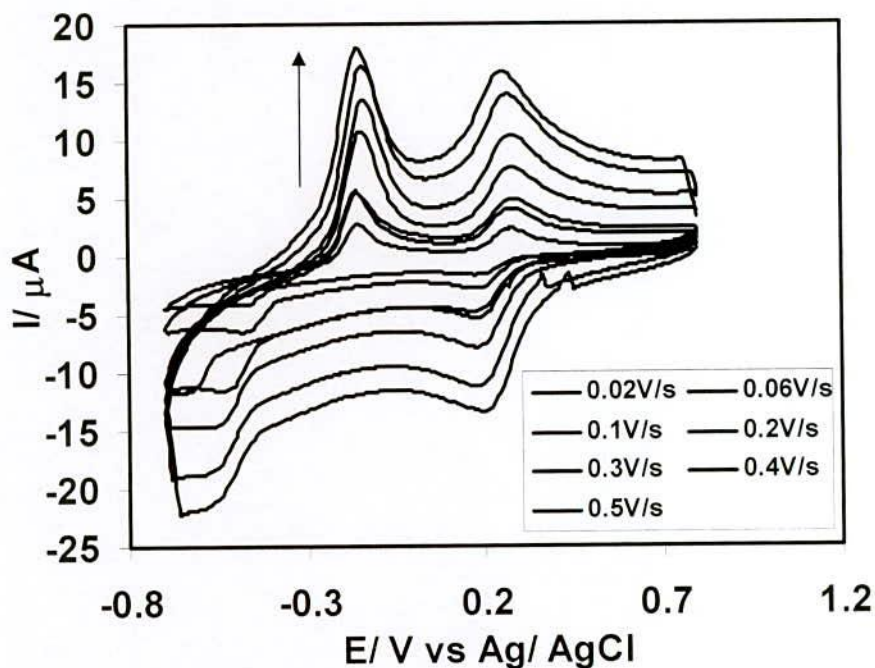
Figure 4.3 : Cyclic voltammogram of 2mM CuCl$_2$ in buffer solution (pH = 3) (acetate buffer) at different scan rate.
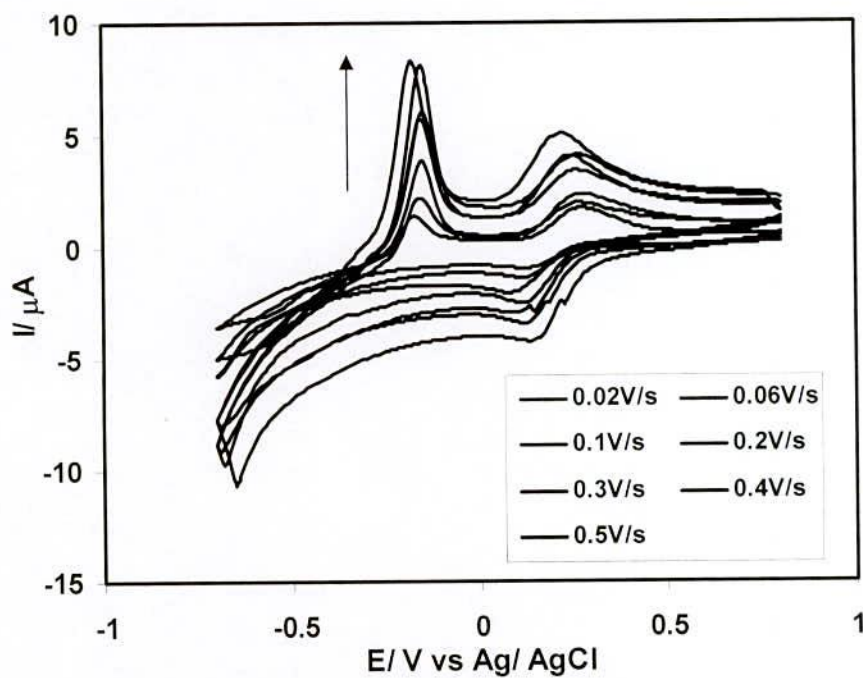
Figure 4.4: Cyclic voltammogram of 2mM CuCl$_2$ in buffer solution (pH = 6) (acetate buffer) at different scan rate.
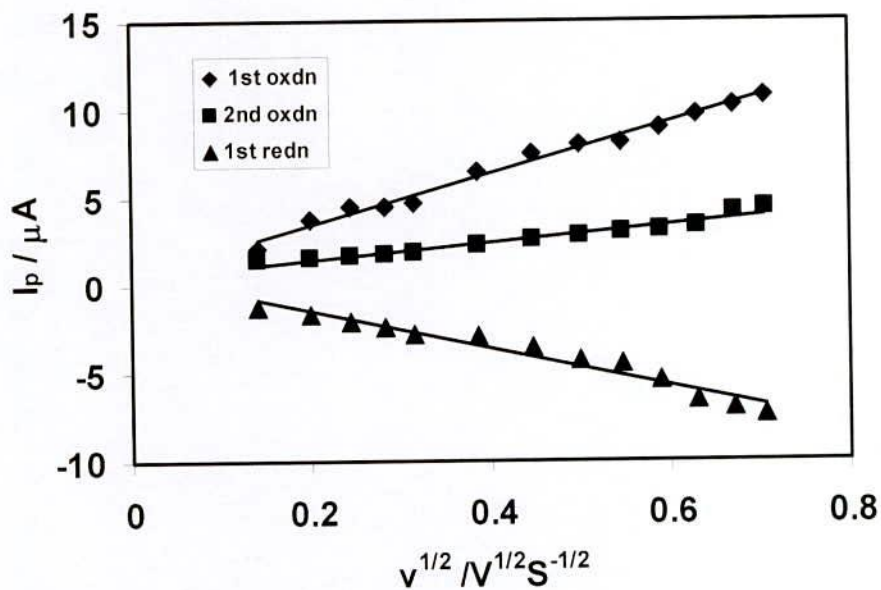
Figure 4.5 : Plots of peak current versus square root of scan rate of 2mM CuCl$_2$ in buffer solution (pH = 3) (acetate buffer).
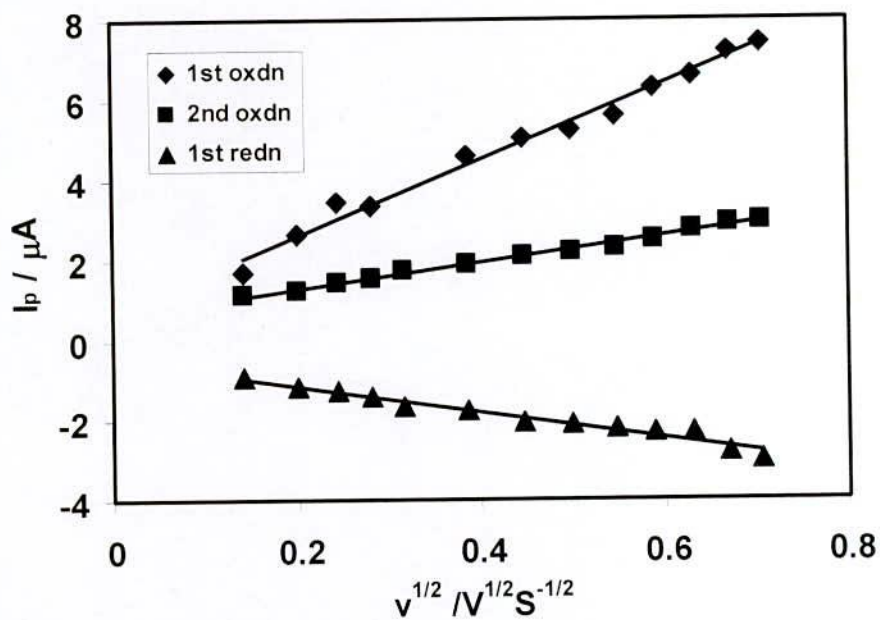
Figure 4.6 : Plots of peak current versus square root of scan rate of 2mM CuCl$_2$ in buffer solution (pH = 6) (acetate buffer).
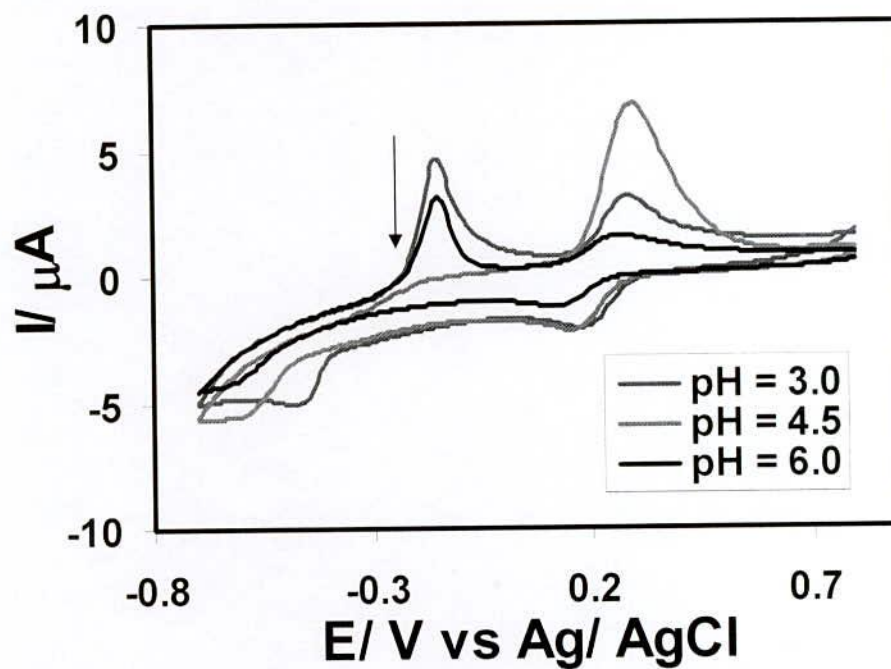
Figure 4.7 : Comparison of Cyclic voltammogram of $CuCl_2$ in different pH (3.0, 4.5, 6.0) at similar condition (Scan rate = 0.04V/s, Conc = 2mM).
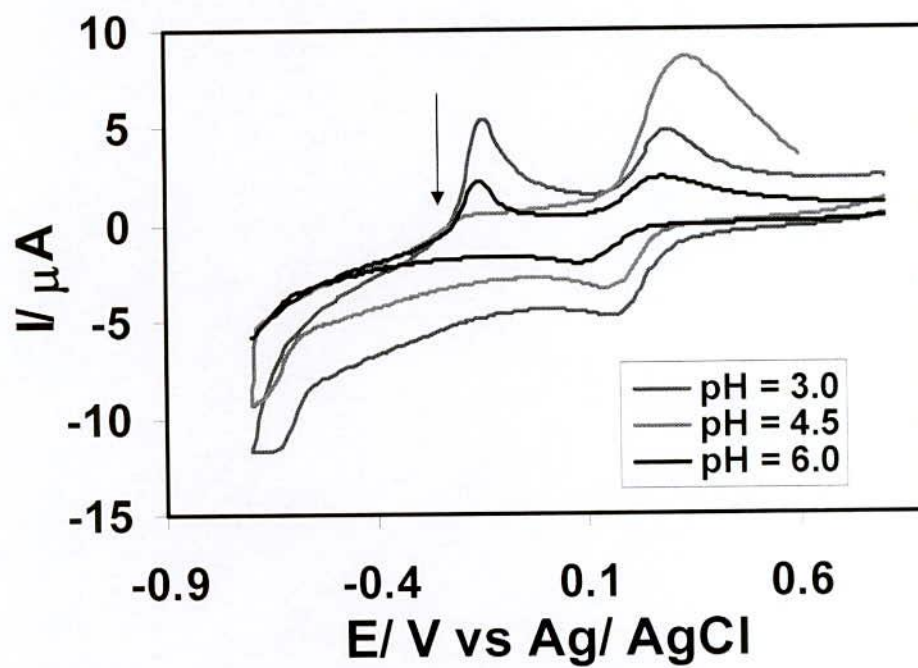
Figure 4.8 : Comparison of Cyclic voltammogram of $CuCl_2$ in different pH (3.0, 4.5, 6.0) at similar condition (Scan rate = 0.10V, Conc = 2mM).
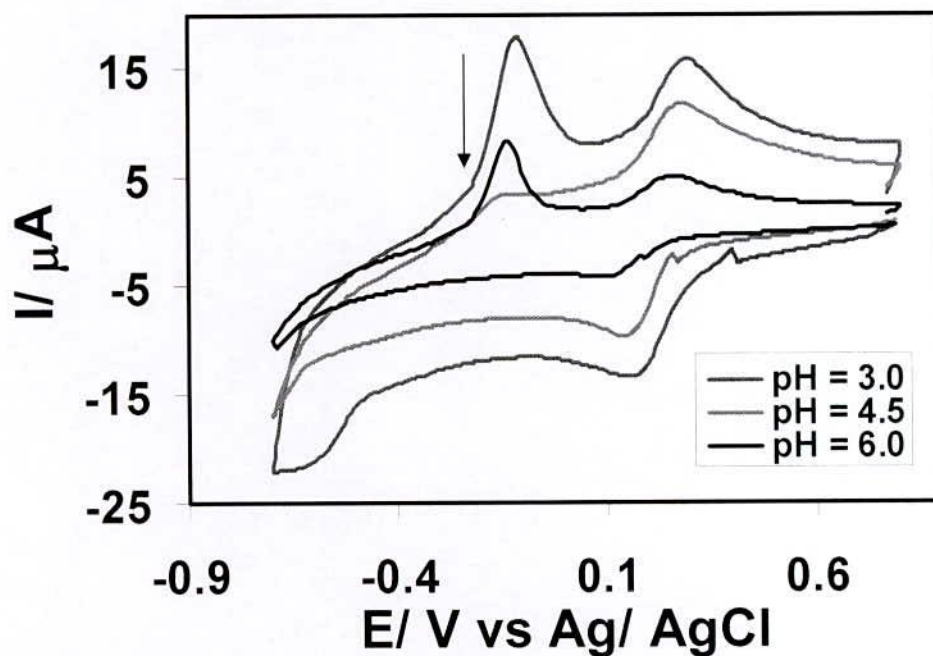
Figure 4.9 : Comparison of Cyclic voltammogram of CuCl$_2$ in different pH (3.0, 4.5, 6.0) at similar condition (Scan rate = 0.50V, Conc = 2mM).
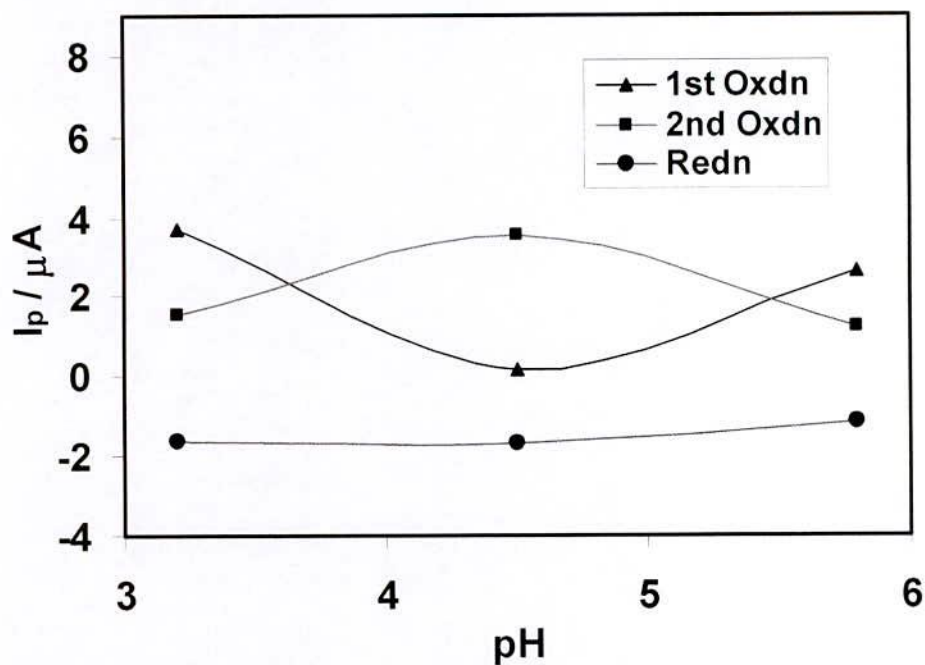
Figure 4.10 : Plots of peak current versus pH (3.0, 4.5, 6.0) of CuCl$_2$ at similar condition (Scan rate = 0.04V, Conc = 2mM).
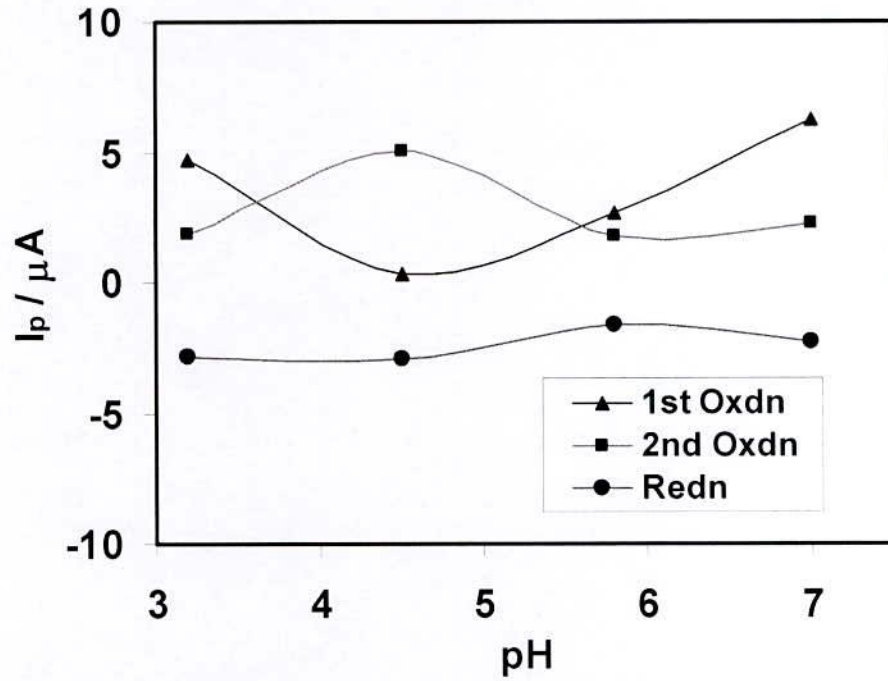
Figure 4.11 : Plots of peak current versus pH (3.0, 4.5, 6.0) of $CuCl_2$ at similar condition (Scan rate = 0.10V, Conc = 2mM).
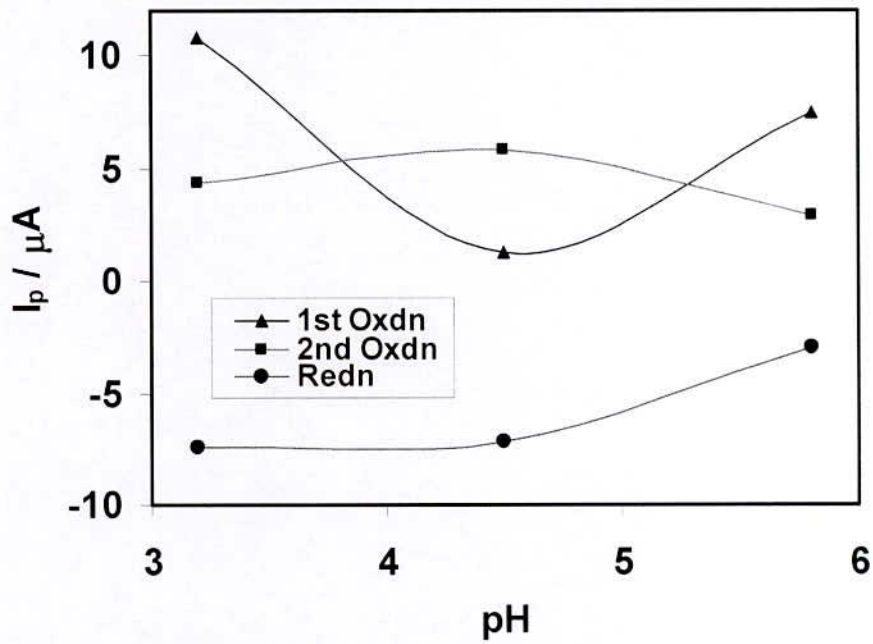
Figure 4.12 : Plots of peak current versus pH (3.0, 4.5, 6.0) of $CuCl_2$ at similar condition (Scan rate = 0.50V, Conc = 2mM).

111
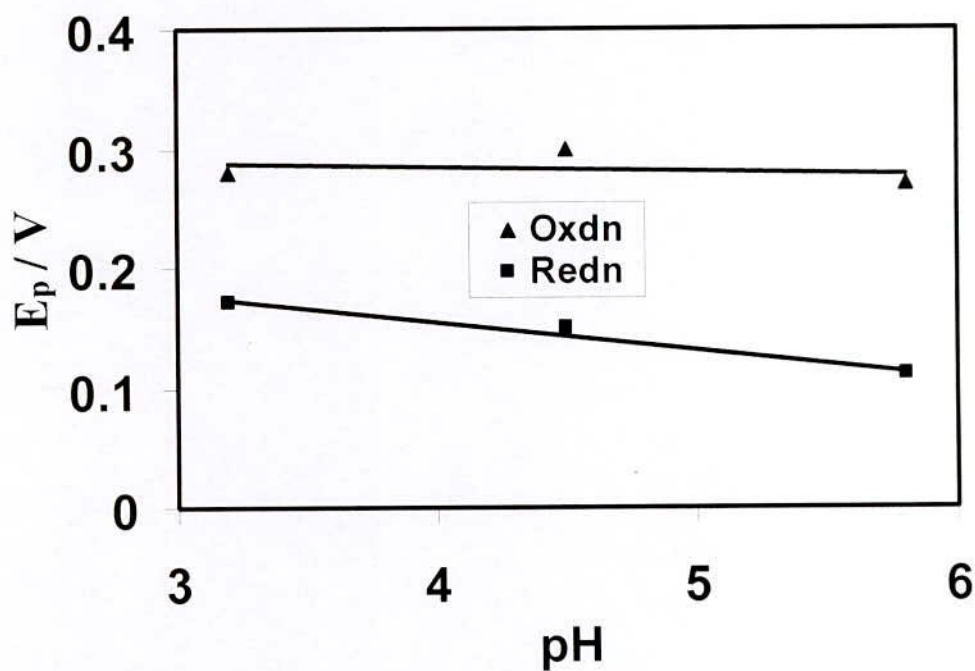
Figure 4.13 : Plots of peak potential (E/V) versus pH (3.0, 4.5, 6.0)   of CuCl$_2$ at similar condition (Scan rate= 0.04V, Conc = 2mM).
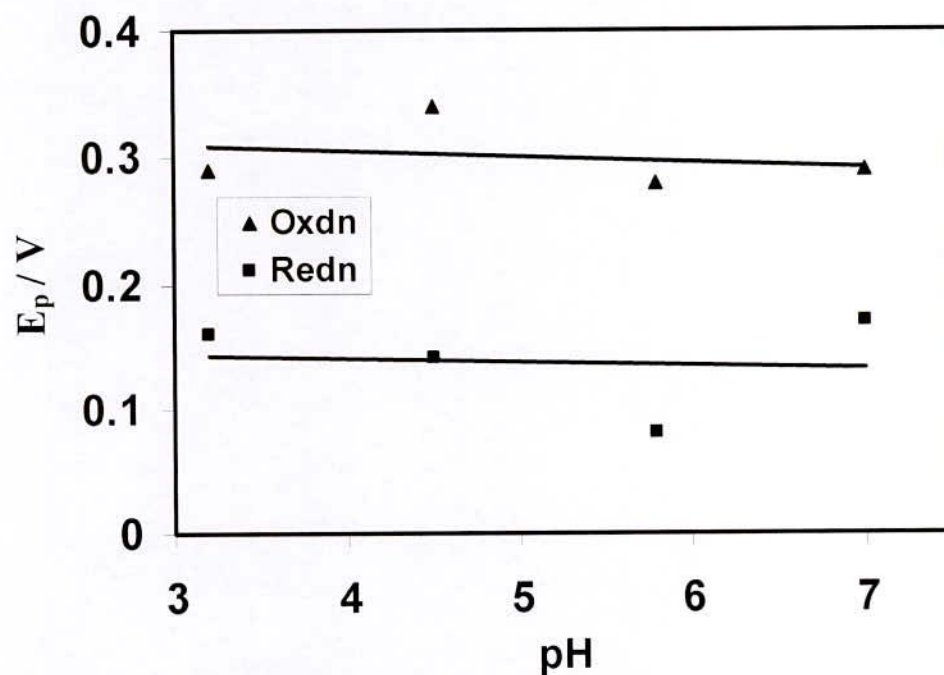
Figure 4.14 : Plots of peak potential (E/V) versus pH (3.0, 4.5, 6.0)   of CuCl$_2$ at similar condition (Scan rate = 0.10V, Conc = 2mM).

112
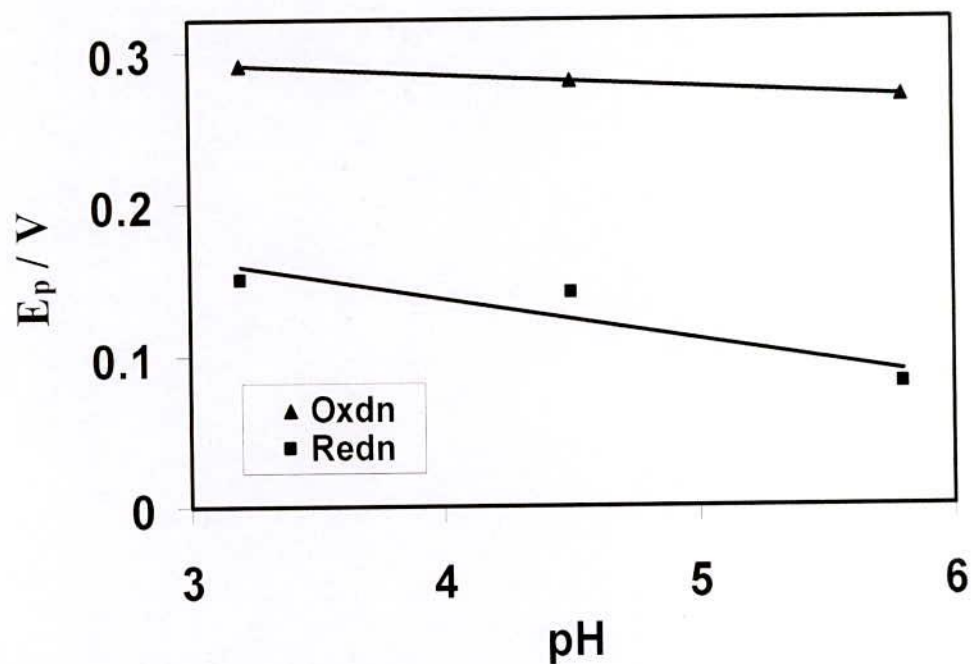
Figure 4.15: Plots of peak potential (E/V) versus pH (3.0, 4.5, 6.0) of CuCl$_2$ at similar condition (Scan rate = 0.50V, Conc = 2mM).
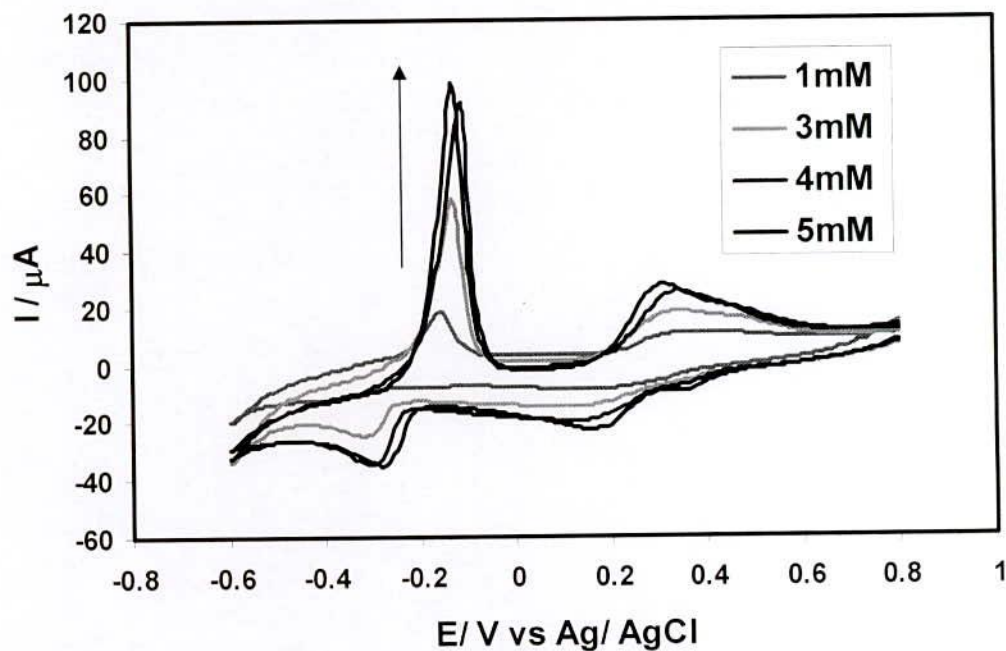
Figure 4.16 : Cyclic voltammogram of CuCl$_2$ in aqueous buffer solution (pH = 3.0) (acetate buffer) for concentration 1, 3, 4 and 5mM at scan rate 0.1Vs^{-1}.
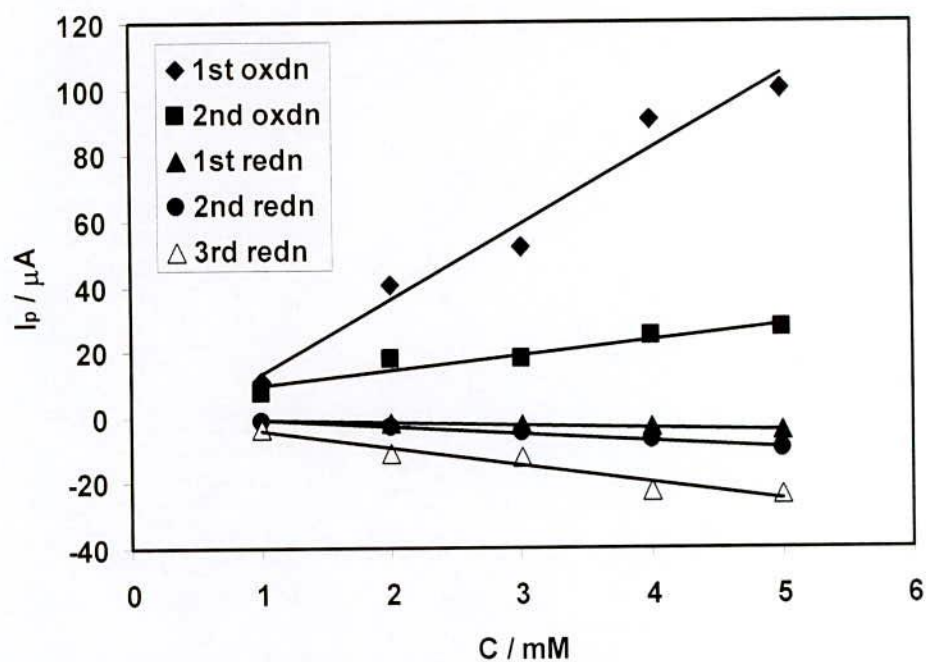
Figure 4.17 : Plots of peak current versus concentration of CuCl$_2$ in aqueous buffer solution (pH =3.0) (acetate buffer) at scan rate 0.1V.
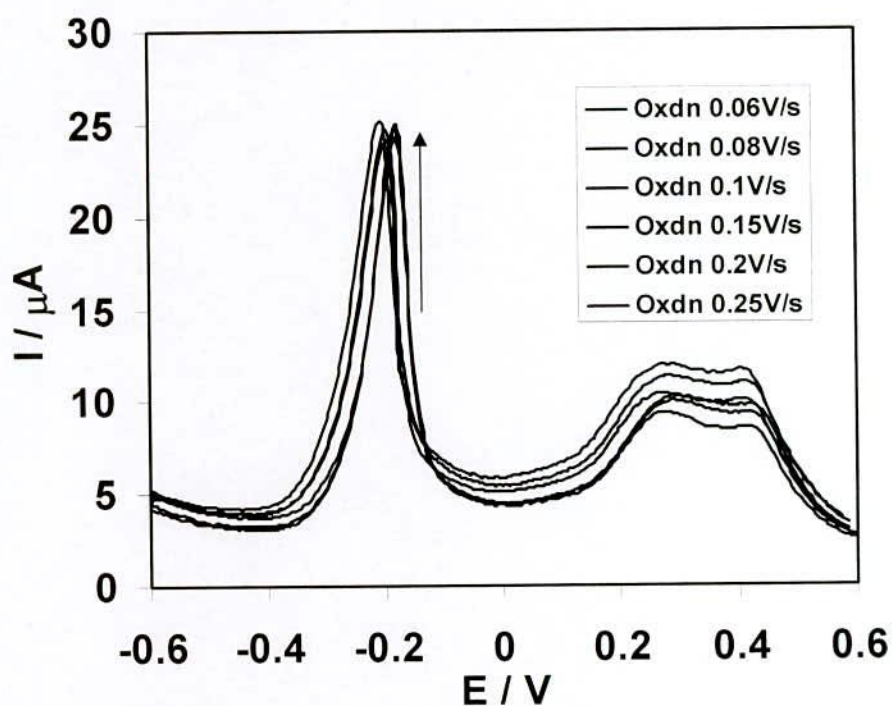
Figure 4.18 : Differential pulse voltammogram of 2mM CuCl$_2$ in buffer solution (pH = 3.0) (acetate buffer) for forward direction (oxidation) at different scan rate.

114
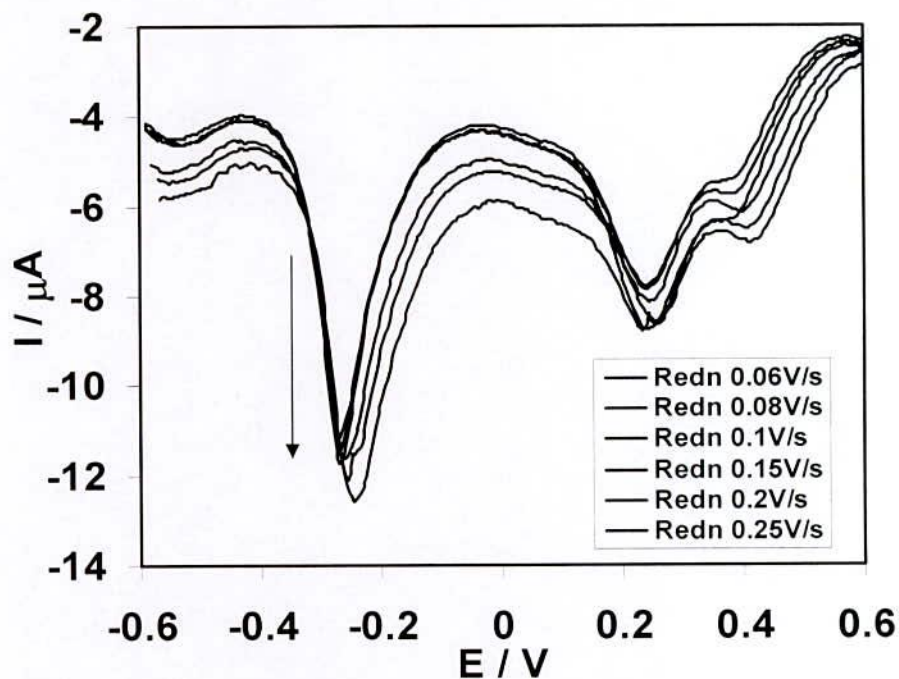
Figure 4.19 : Differential pulse voltammogram of 2mM $CuCl_2$ in buffer solution (pH = 3.0) (acetate buffer) for backward direction (reduction) at different scan rate.
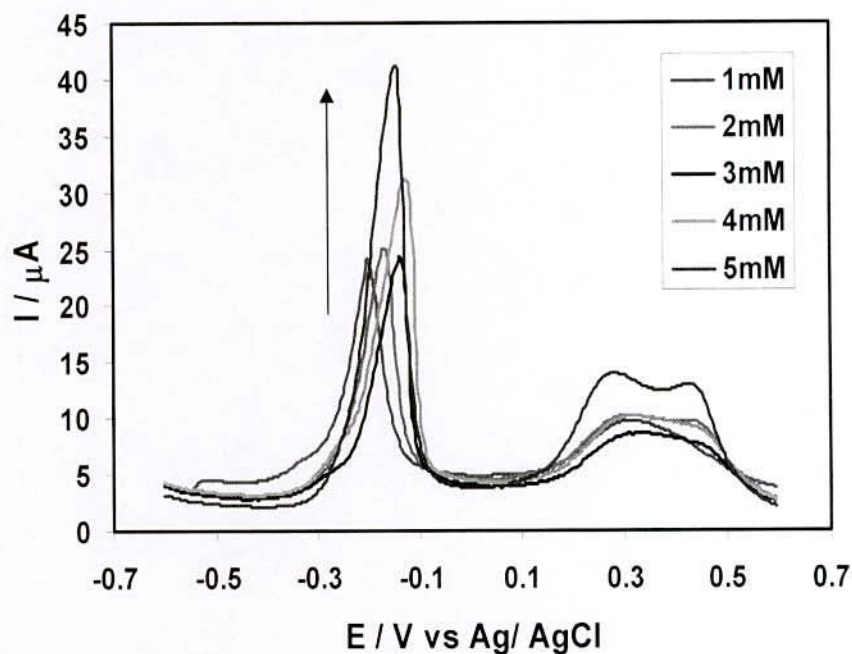
Figure 4.20 : Comparison of concentration of Differential pulse voltammogram of $CuCl_2$ in buffer solution (pH = 3.0) (acetate buffer) for forward direction (oxidation) at different concentration, scan rate 0.1V/s.
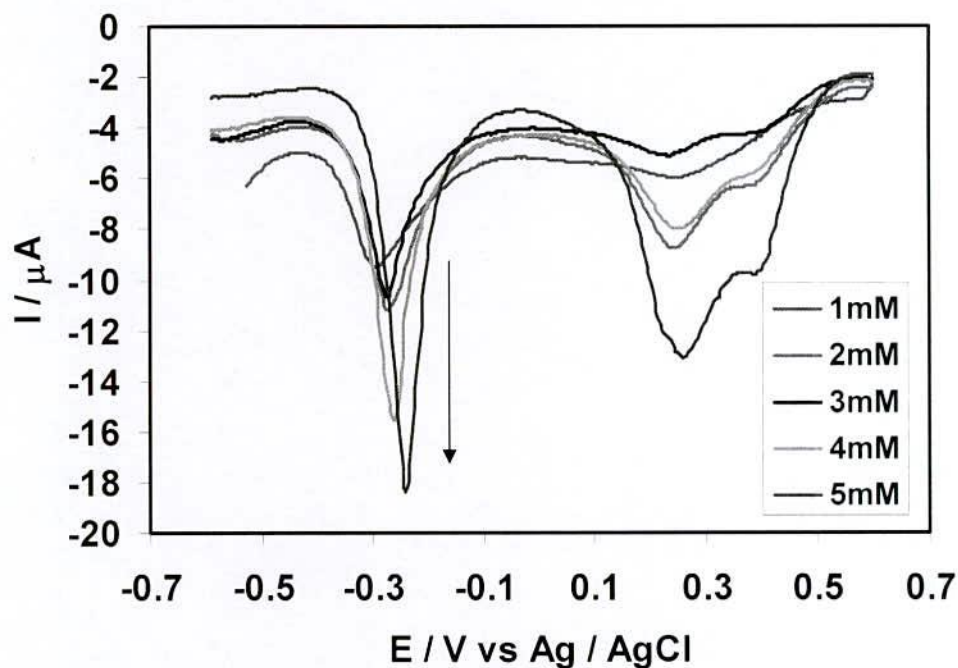
Figure 4.21 : Differential pulse voltammogram of CuCl₂ only in aqueous buffer solution (pH = 3.0) (acetate buffer) for backward direction (reduction) at different concentration, scan rate 0.1V/s.
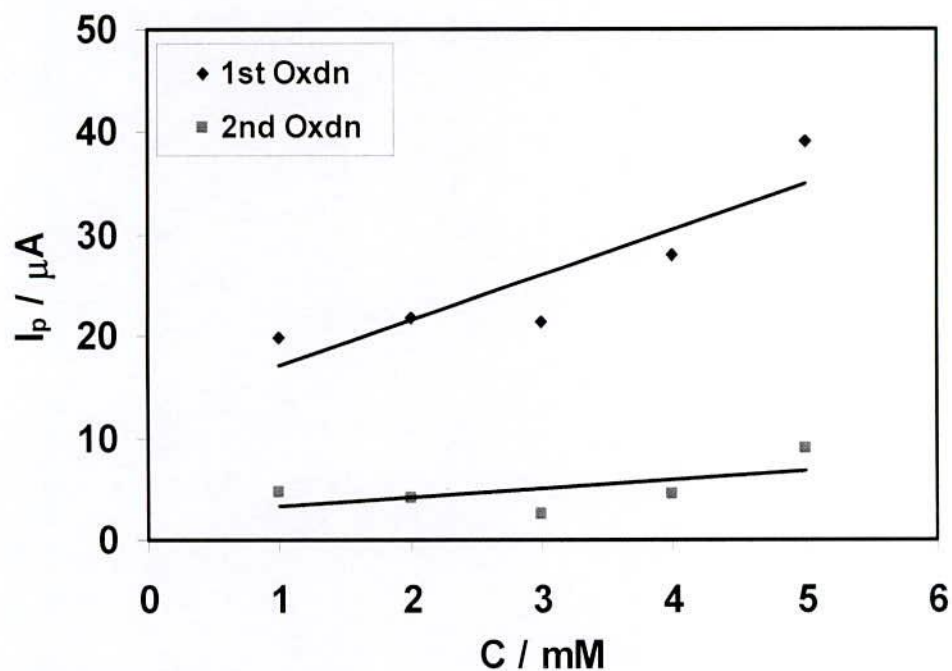
Figure 4.22 : Plots of peak current (Oxidation) versus concentration of DPV of CuCl₂ in buffer solution (pH =3.0) (acetate buffer) at scan rate 0.1V/s.
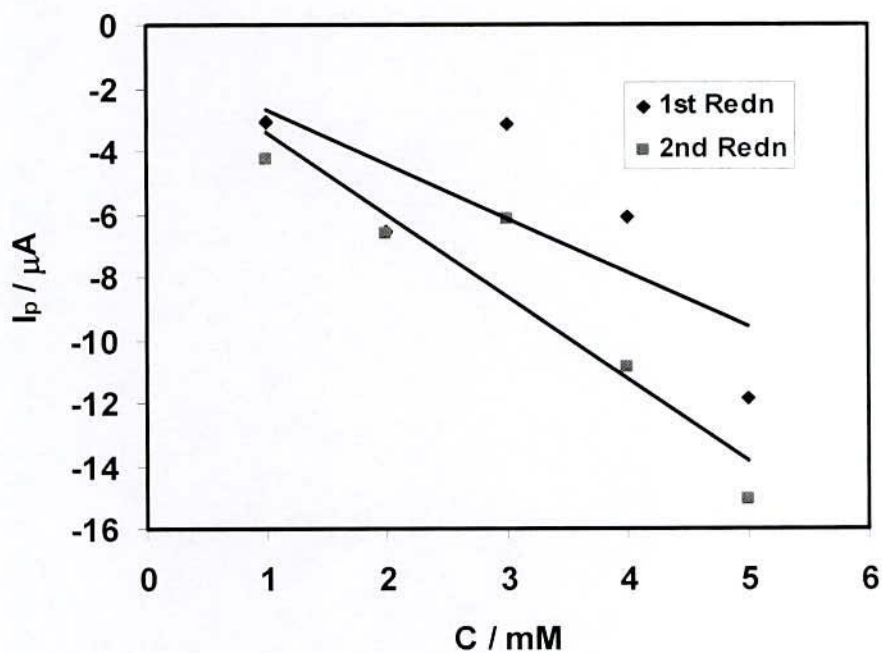
Figure 4.23 : Plots of peak current (Reduction) versus concentration of $CuCl_2$ in buffer solution (pH =3.0) (acetate buffer) at scan rate 0.1V/s.
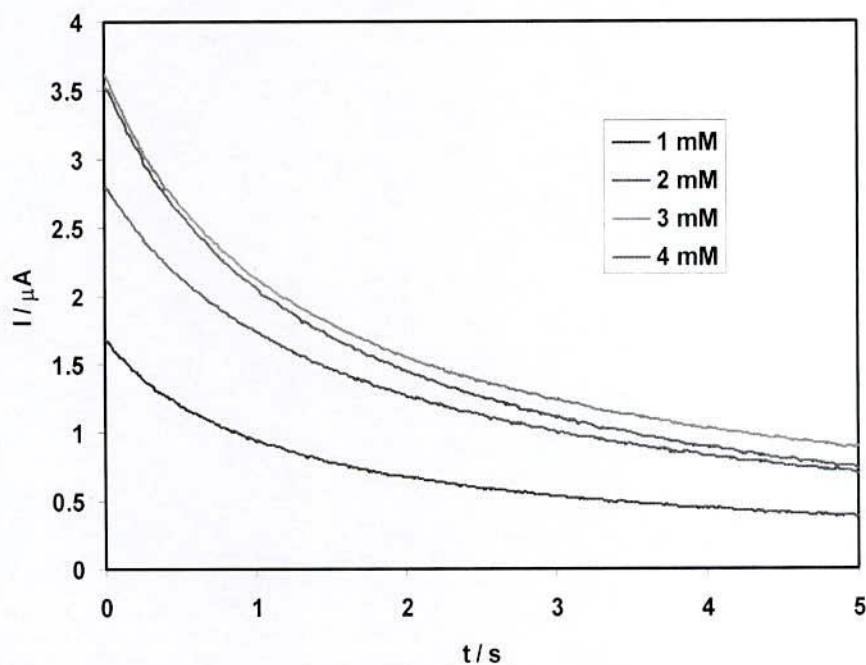
Figure 4.24 : Chronoamperometry curve of $CuCl_2$ in aqueous buffer solution (pH = 3.0) (acetate buffer) in different concentration stepping potential 0.4V.

117
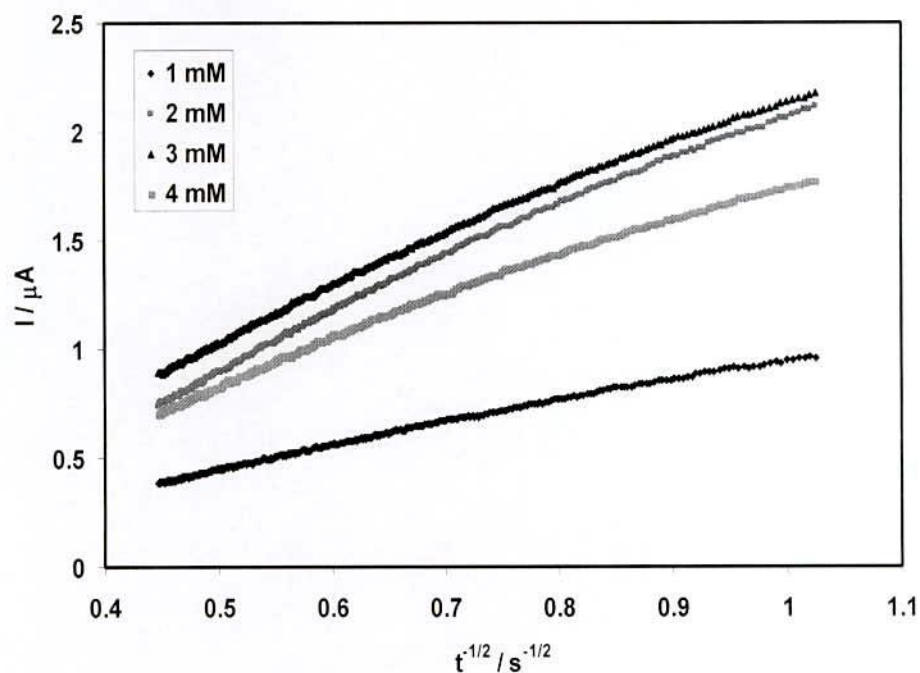
Figure 4.25 : Cottrel plots(I vs $t^{-1/2}$) of the back ground subtracted currents for $CuCl_2$ in buffer solution (pH = 3.0) (acetate buffer) at different concentration, stepping potential 0.4V.
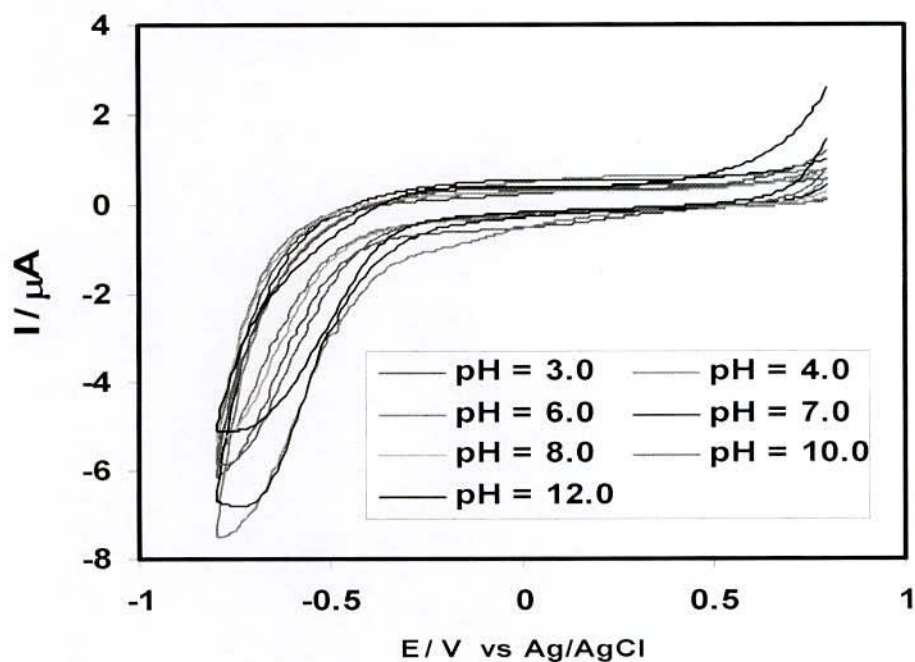
Figure 4.26 : Cyclic voltammogram of 2mM Aspartic acid in different pH at scan rate 0.1V/s.
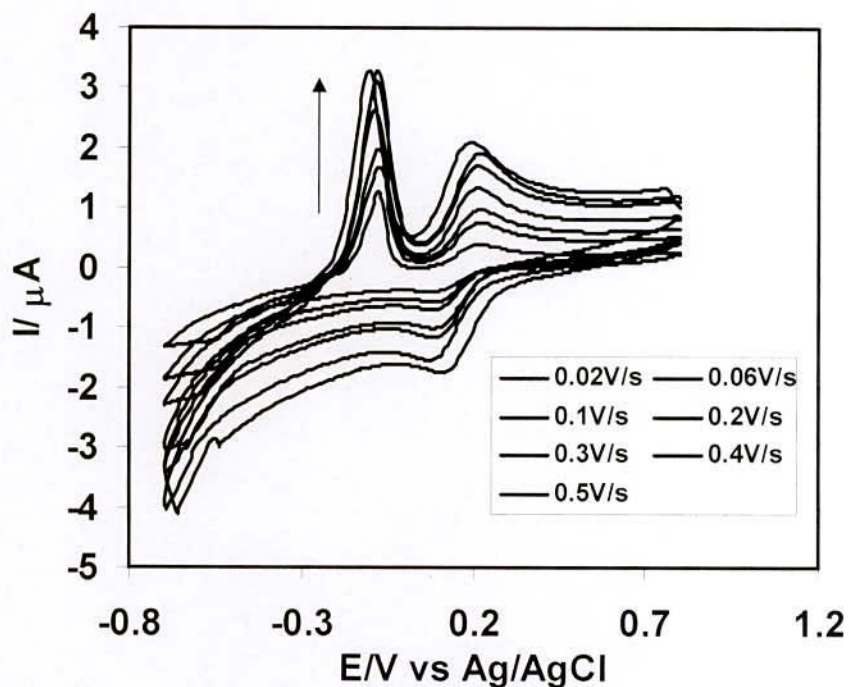
Figure 4.27 : Cyclic voltammogram of 2mM $CuCl_2$ +6mM aspartic acid (1:3) in aqueous solution at different scan rate.
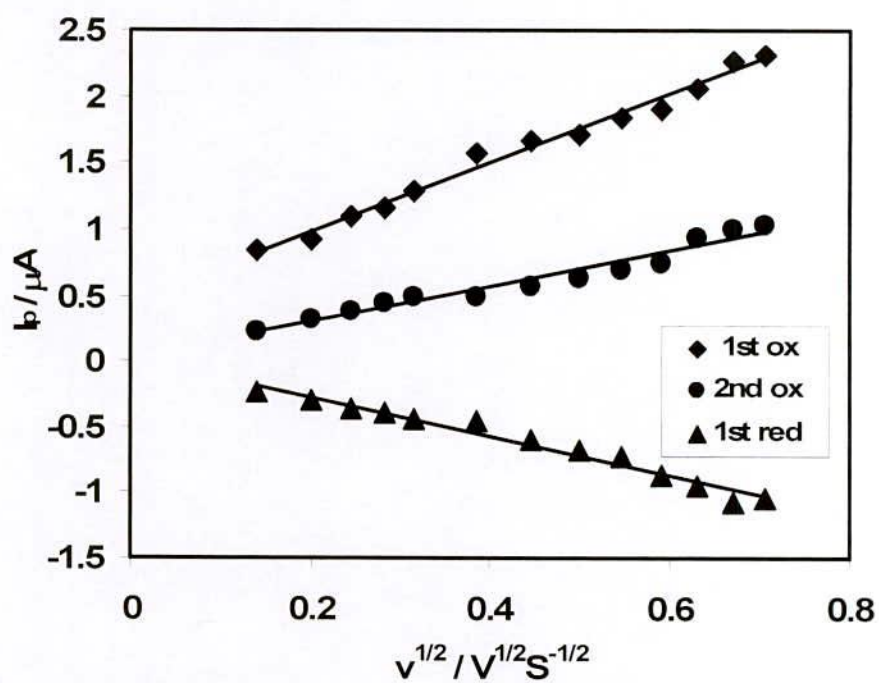
Figure 4.28 : Plots of peak current versus square root of scan rate of 2mM $CuCl_2$ + 6mM aspartic acid (1:3) in aqueous solution.
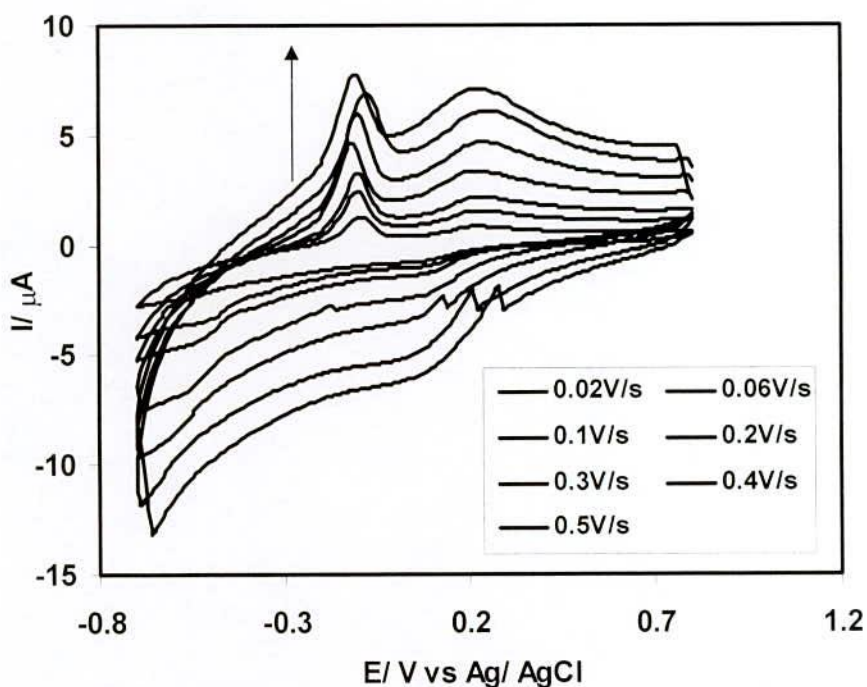
Figure 4.29 : Cyclic voltammogram of 2mM $CuCl_2$ + 6mM aspartic acid (1:3) in buffer solution (pH = 3.5) (acetate buffer) at different scan rate.
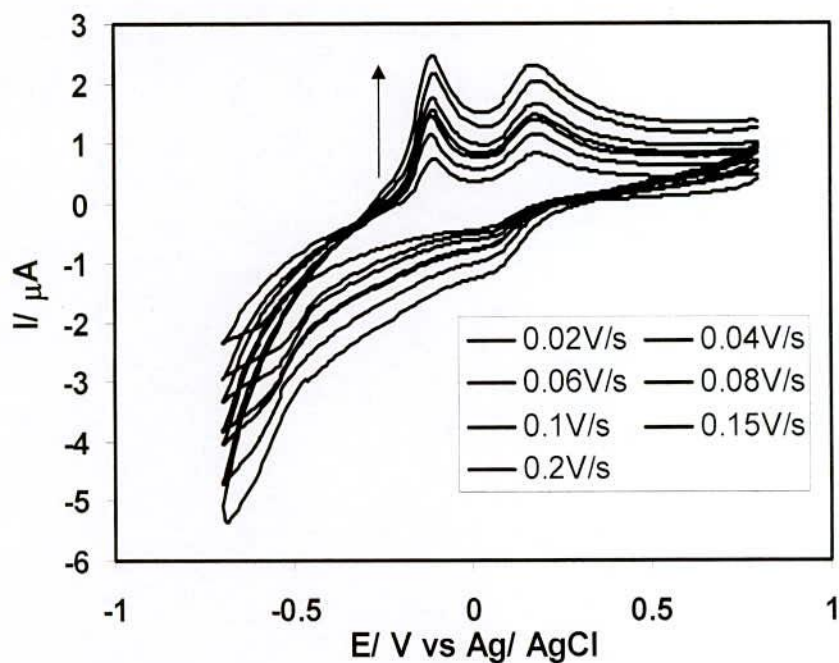
Figure 4.30 : Cyclic voltammogram of 2mM $CuCl_2$ + 6mM aspartic acid (1:3) in buffer solution (pH = 4.5) (acetate buffer) at different scan rate.
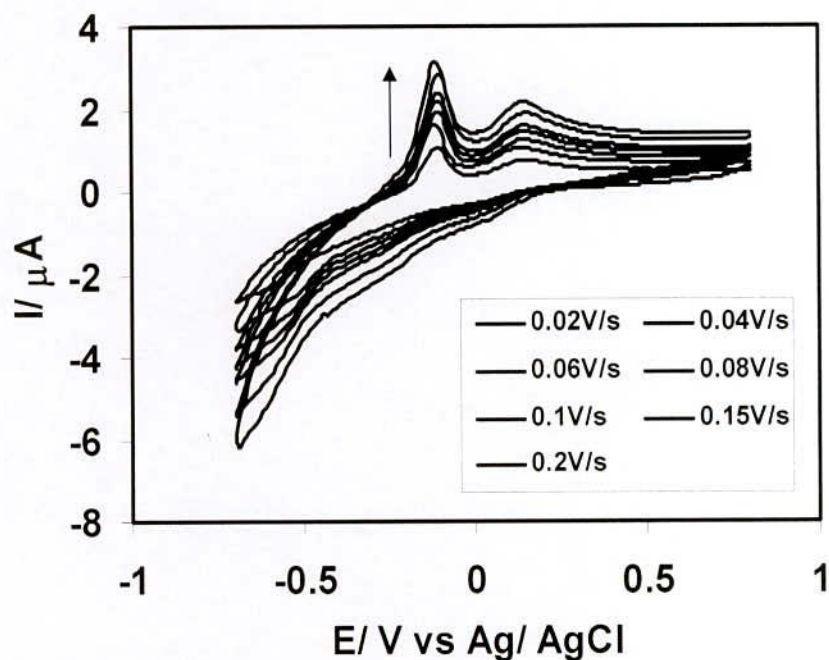
Figure 4.31 : Cyclic voltammogram of 2mM $CuCl_2$ + 6mM aspartic acid (1:3) in buffer solution (pH = 5.5) (acetate buffer) at different scan rate.
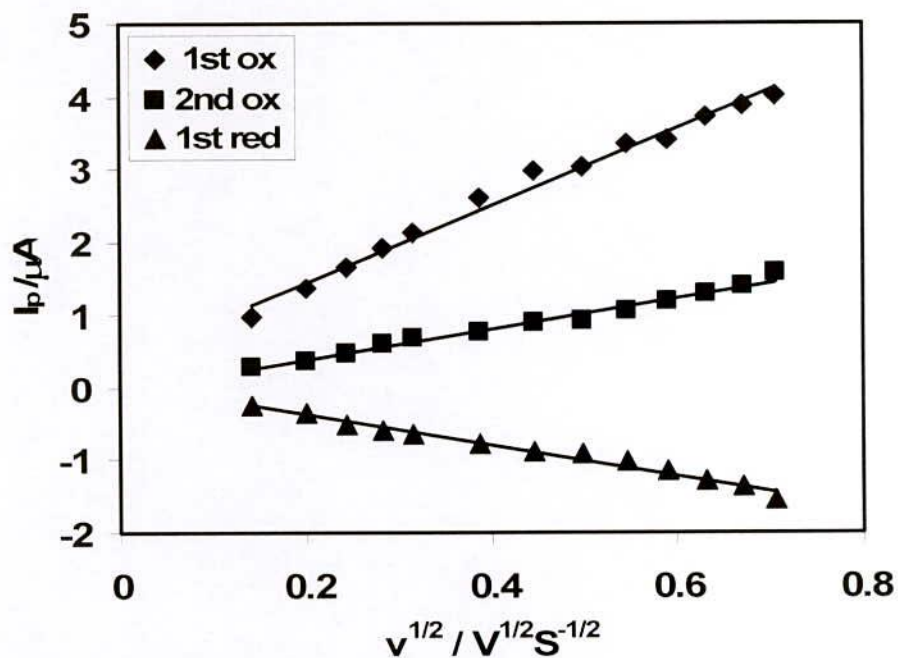
Figure 4.32 : Plots of peak current versus square root of scan rate of 2mM $CuCl_2$ + 6mM aspartic acid (1:3) in buffer solution (pH = 3.5) (acetate buffer).
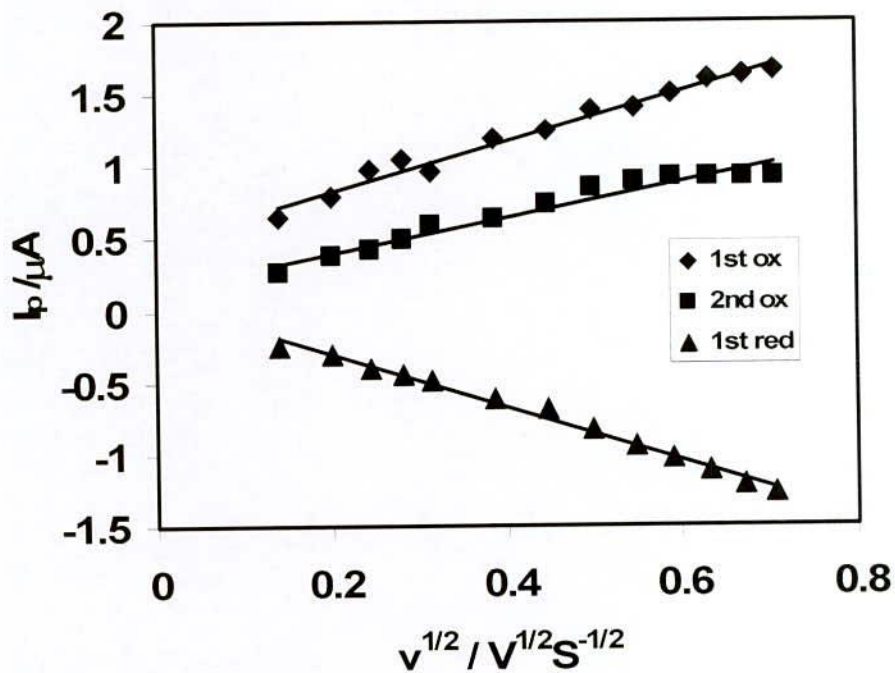
Figure 4.33 : Plots of peak current versus square root of scan rate of 2mM $CuCl_2$ + 6mM aspartic acid (1:3) in buffer solution   (pH = 4.5) (acetate buffer).
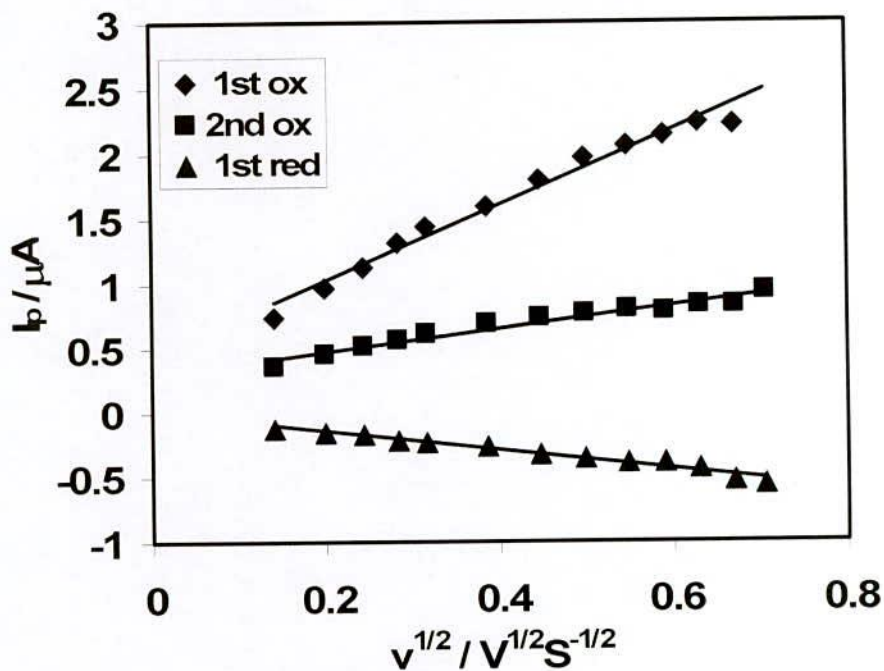
Figure 4.34 : Plots of peak current versus square root of scan rate of 2mM $CuCl_2$ + 6mM aspartic acid (1:3) in buffer solution   (pH = 5.5) (acetate buffer).
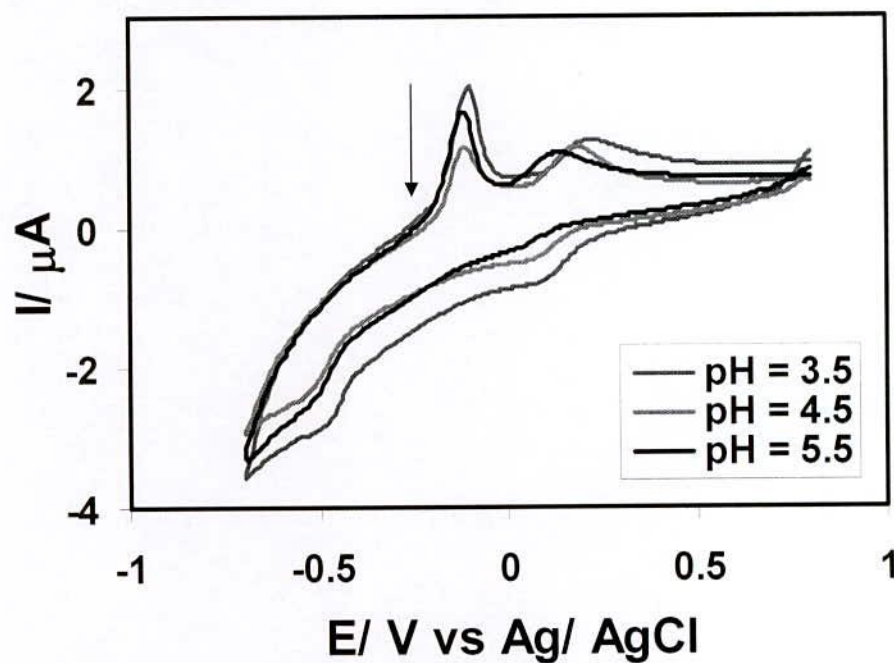
Figure 4.35 : Comparison of Cyclic voltammogram of Cu(II)-Aspartic acid(1:3) in different pH (3.5, 4.5, 5.5) at similar condition (Scan rate = 0.04V/s).
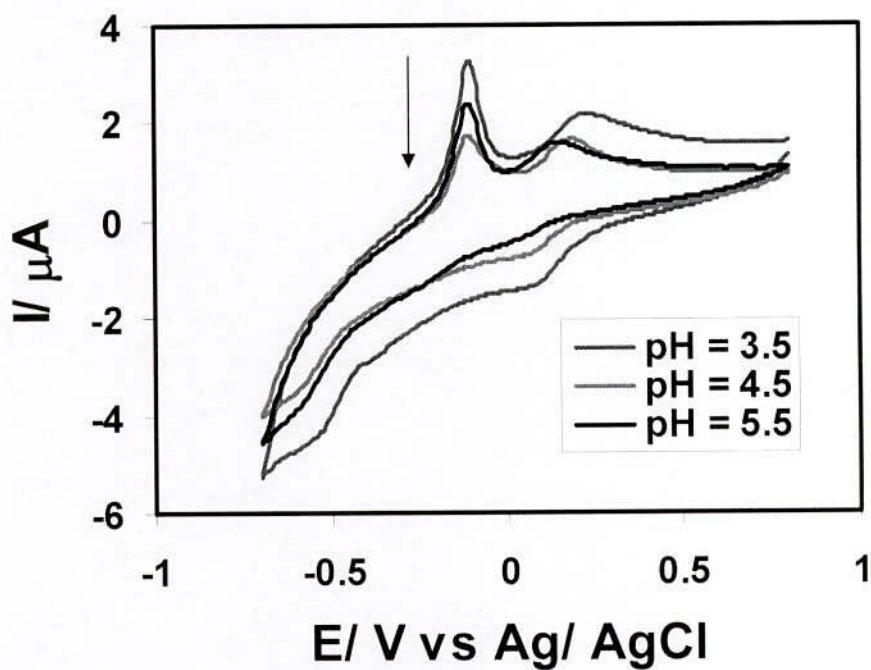
Figure 4.36 : Comparison of Cyclic voltammogram of Cu(II)-Aspartic acid(1:3) in different pH (3.5, 4.5, 5.5) at similar condition (Scan rate = 0.10V/s).
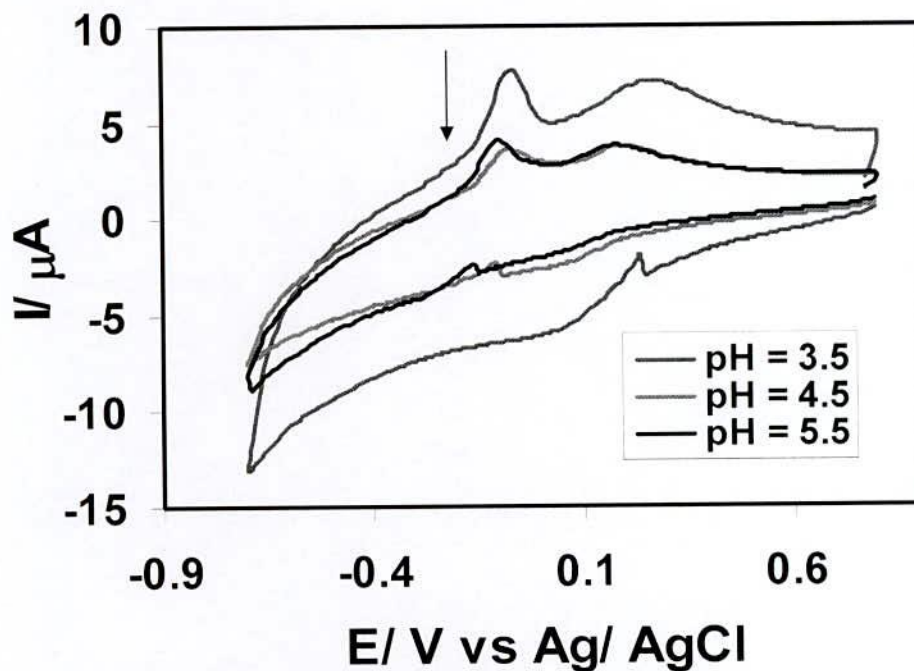
Figure 4.37 : Comparison of Cyclic voltammogram of Cu(II)-Aspartic acid(1:3) in different pH (3.5, 4.5, 5.5) at similar condition (Scan rate = 0.50V/s).
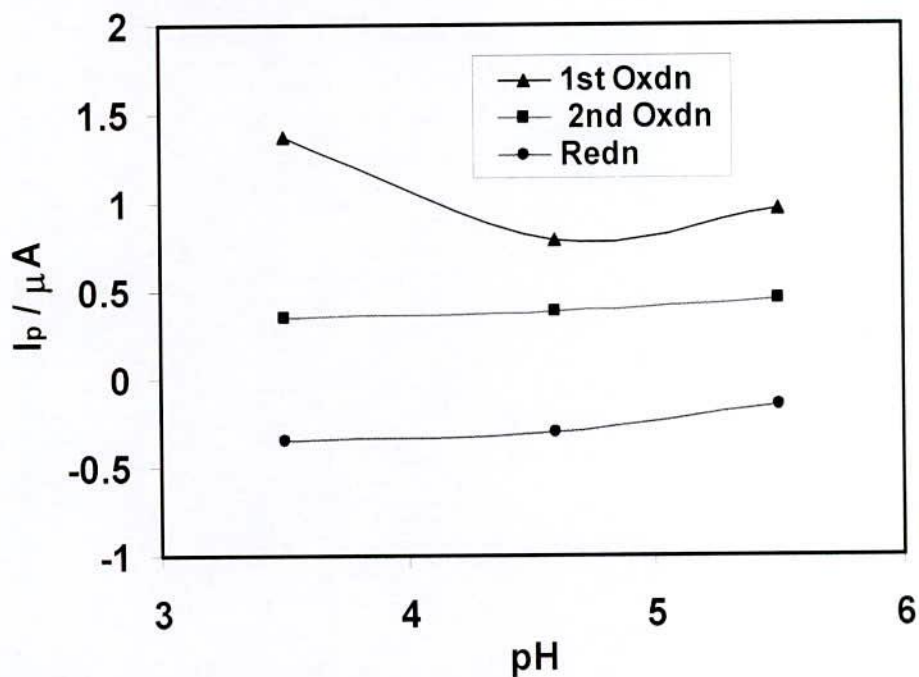
Figure 4.38 : Plots of peak current versus pH (3.5, 4.5, 5.5) of Cu(II)-Aspartic acid(1:3) at similar condition (Scan rate = 0.04V/s).
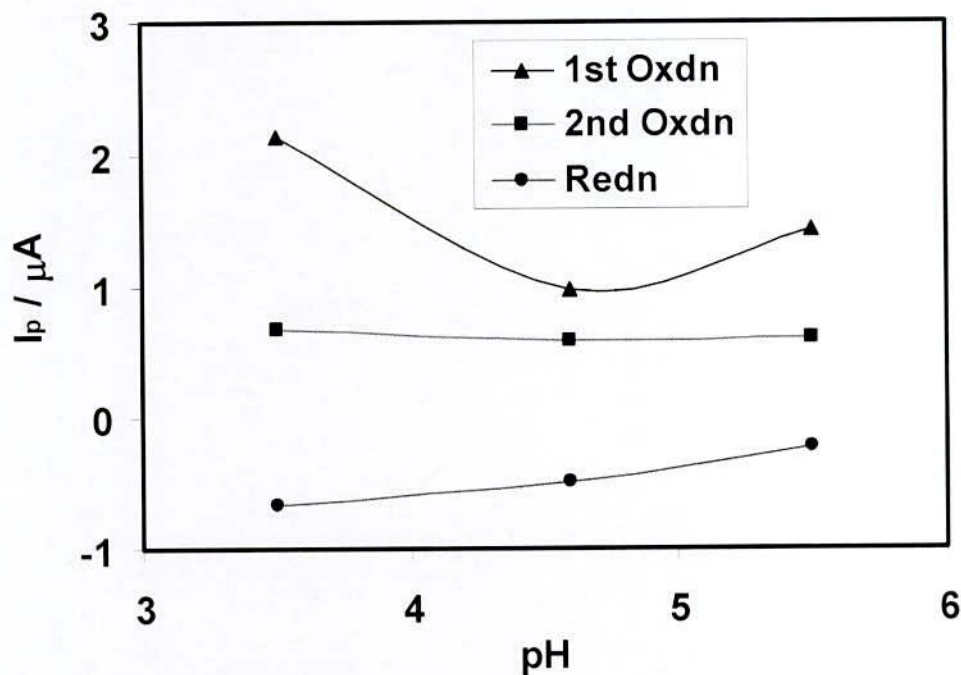
Figure 4.39 : Plots of peak current versus pH (3.5, 4.5, 5.5) of Cu(II)-Aspartic acid(1:3) at similar condition (Scan rate = 0.10V/s).
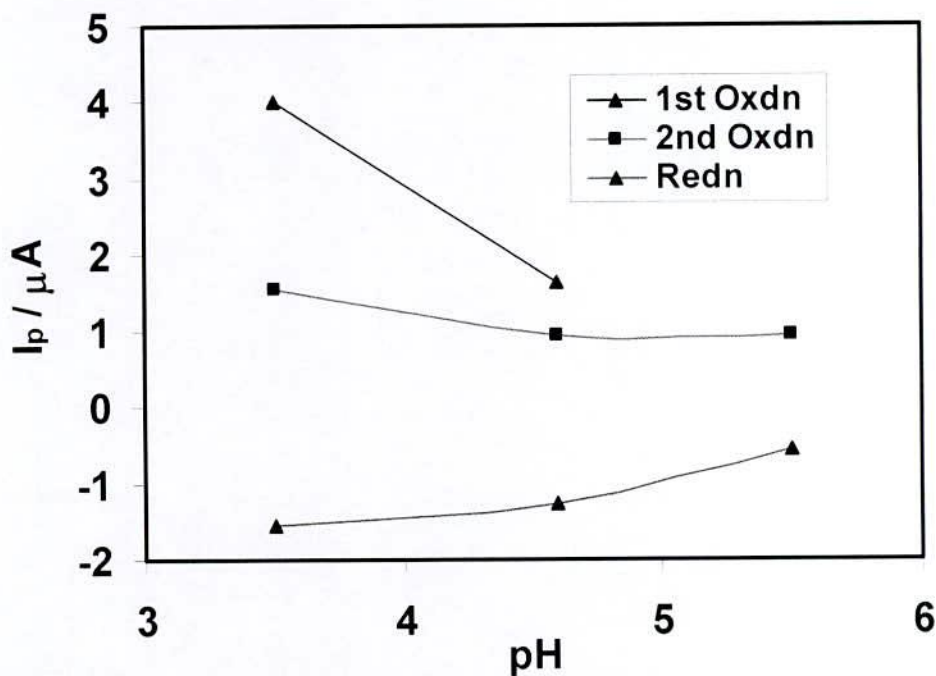
Figure 4.40 : Plots of peak current versus pH (3.5, 4.5, 5.5) of Cu(II)-Aspartic acid(1:3) at similar condition (Scan rate = 0.50V/s).
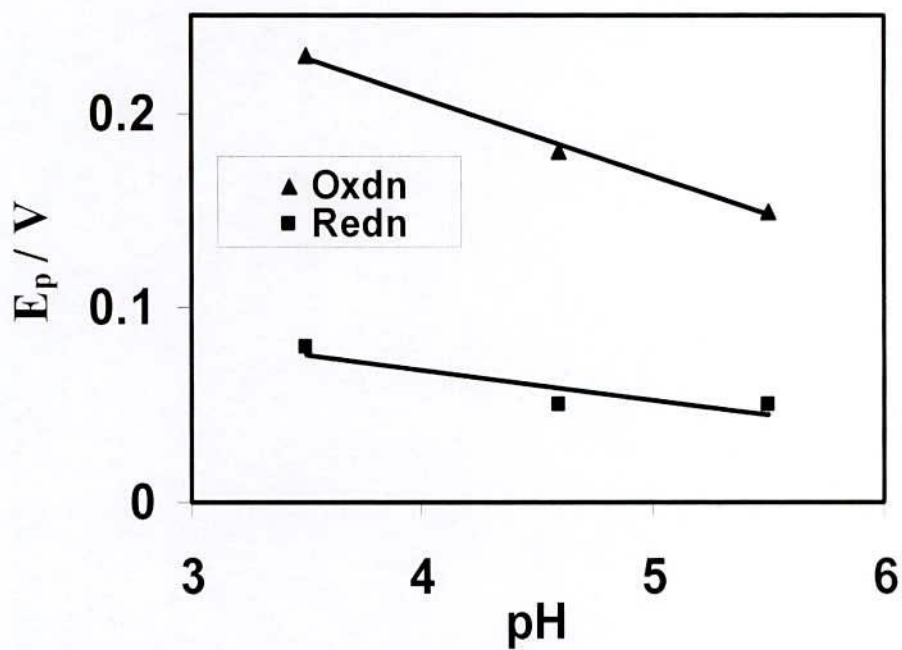
Figure 4.41 : Plots of peak potential (E /V) versus pH (3.5, 4.5, 5.5) of Cu(II)-Aspartic acid(1:3) at similar condition (Scan rate= 0.04V/s).
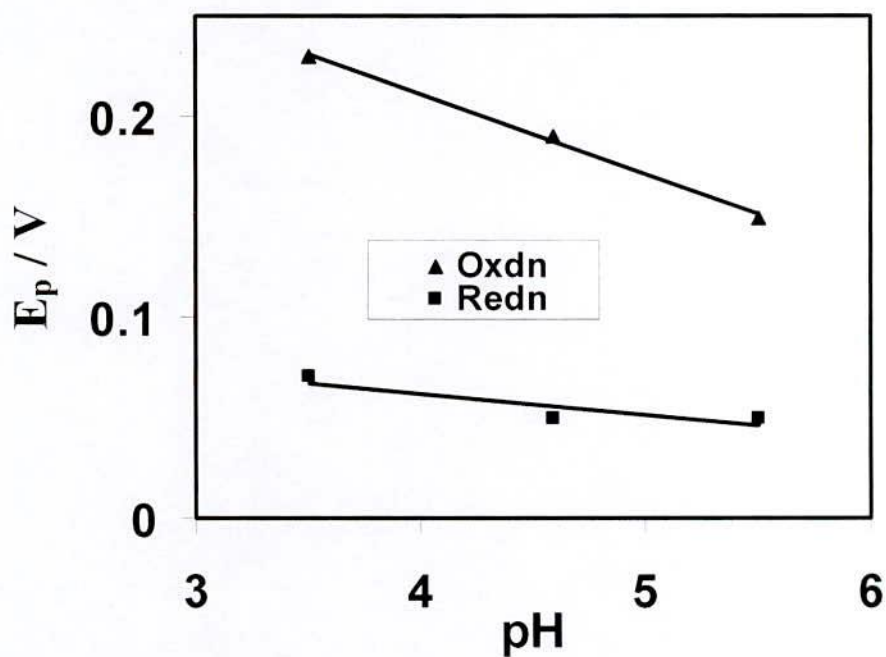
Figure 4.42 : Plots of peak potential (E /V) versus pH (3.5, 4.5, 5.5) of Cu(II)-Aspartic acid(1:3) at similar condition (Scan rate = 0.10V/s).
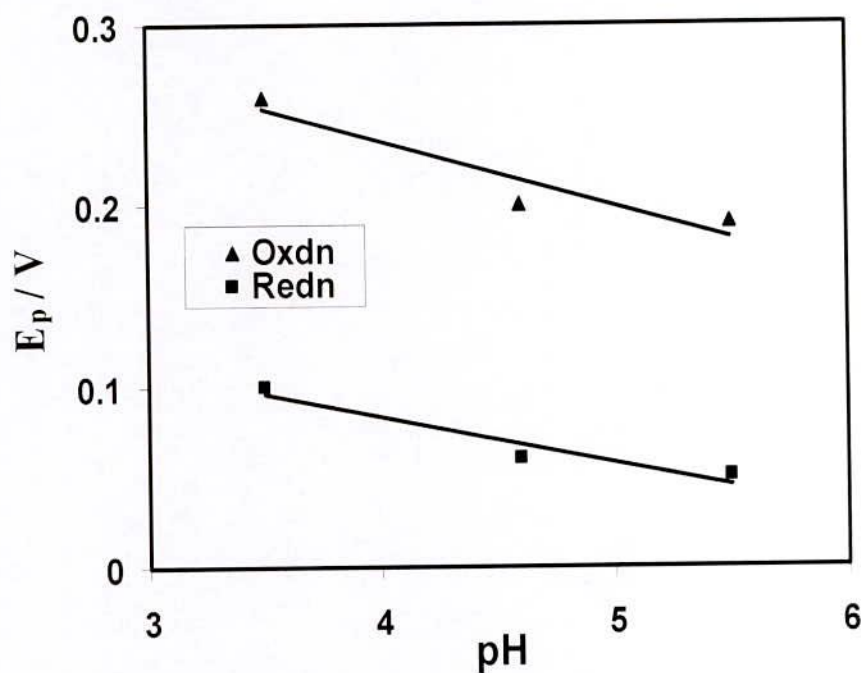
Figure 4.43 : Plots of peak potential (E /V) versus pH (3.5, 4.5, 5.5) of Cu(II)-Aspartic acid(1:3) at similar condition (Scan rate= 0.50V/s).
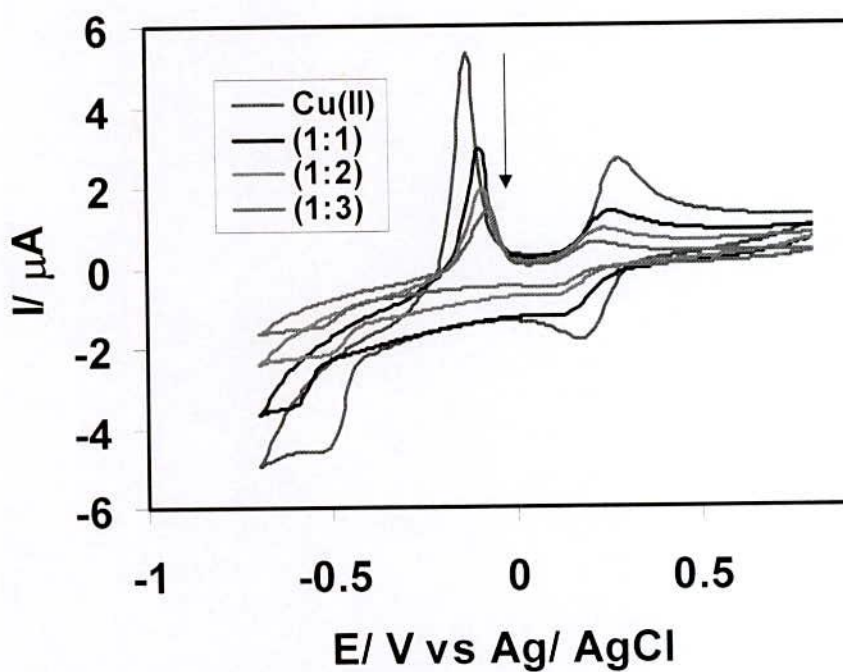
Figure 4.44 : Comparison of Cyclic voltammogram of Pure Cu(II), Cu(II)-Aspartic acid(1:1), (1:2) and (1:3) at similar condition (Scan rate = 0.04V/s).
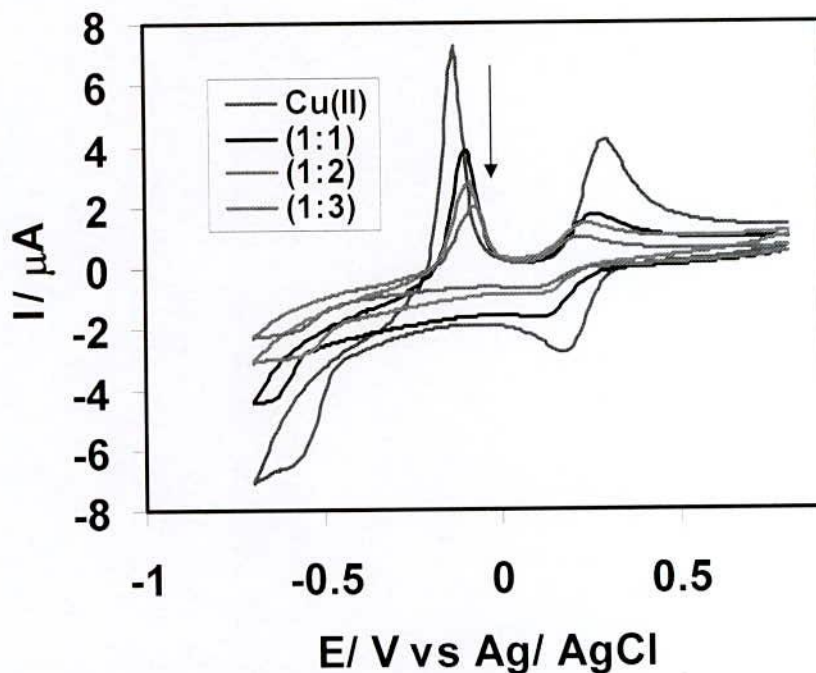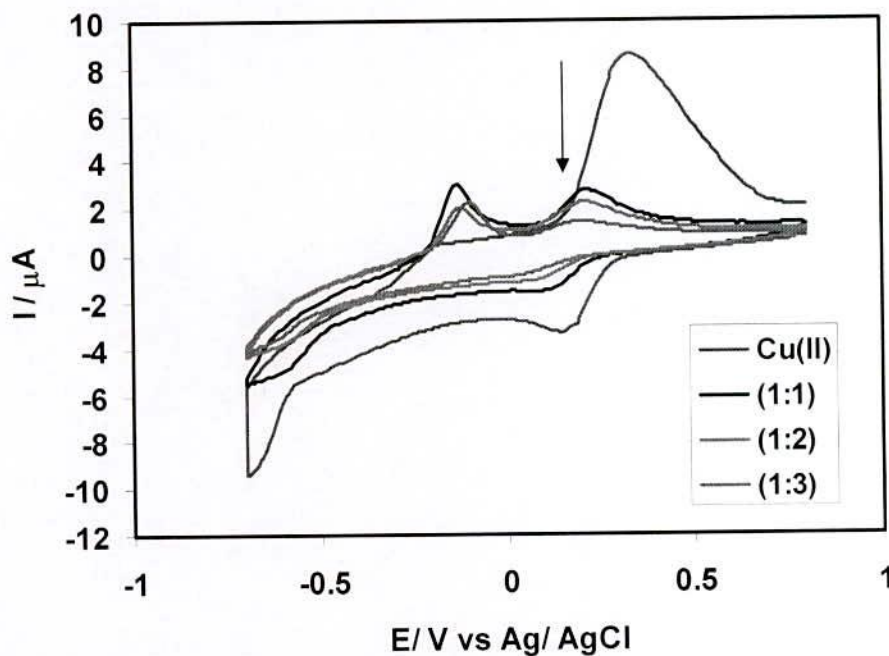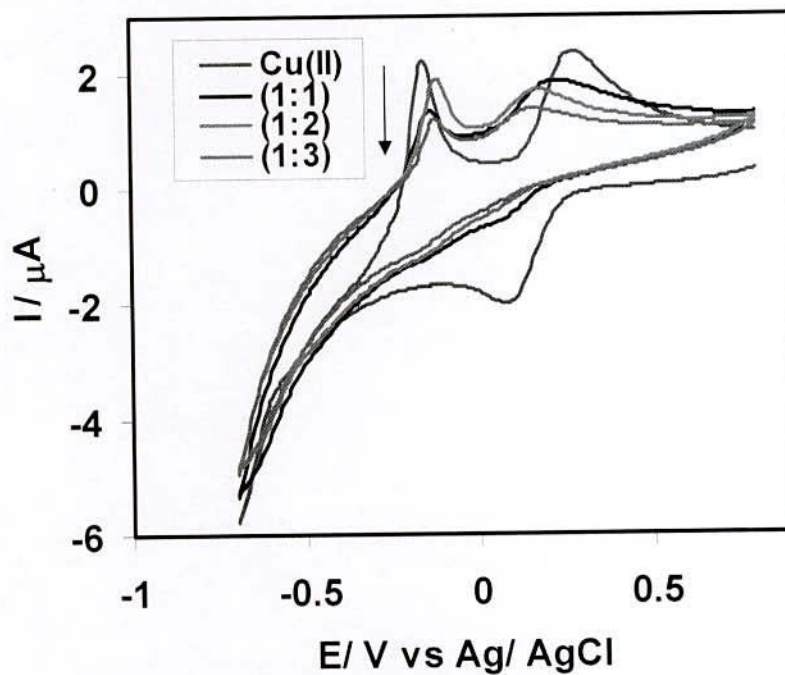
Figure 4.45 : Comparison of Cyclic voltammogram of Pure Cu(II), Cu(II)-Aspartic acid(1:1), (1:2) and (1:3) at similar condition (Scan rate = 0.10V/s).
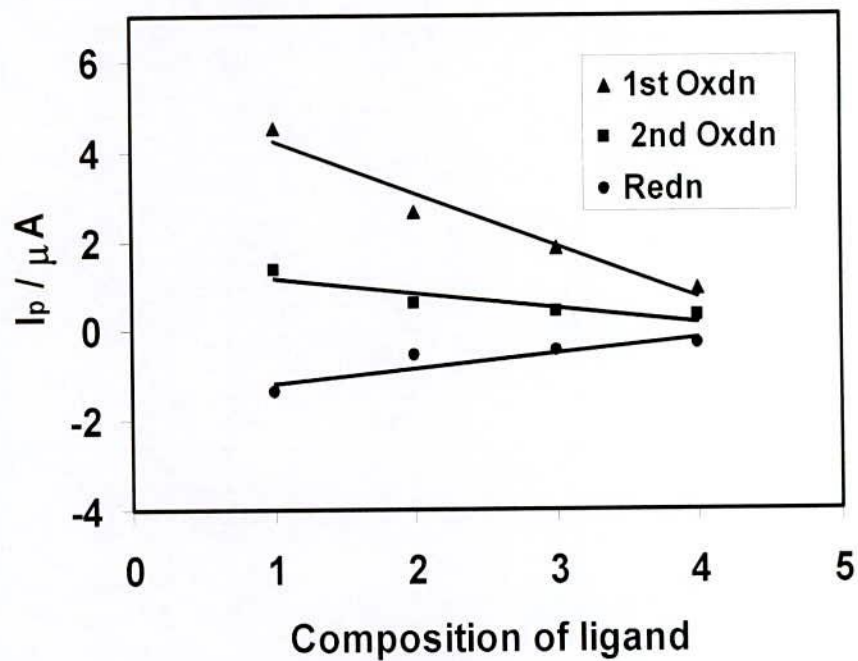
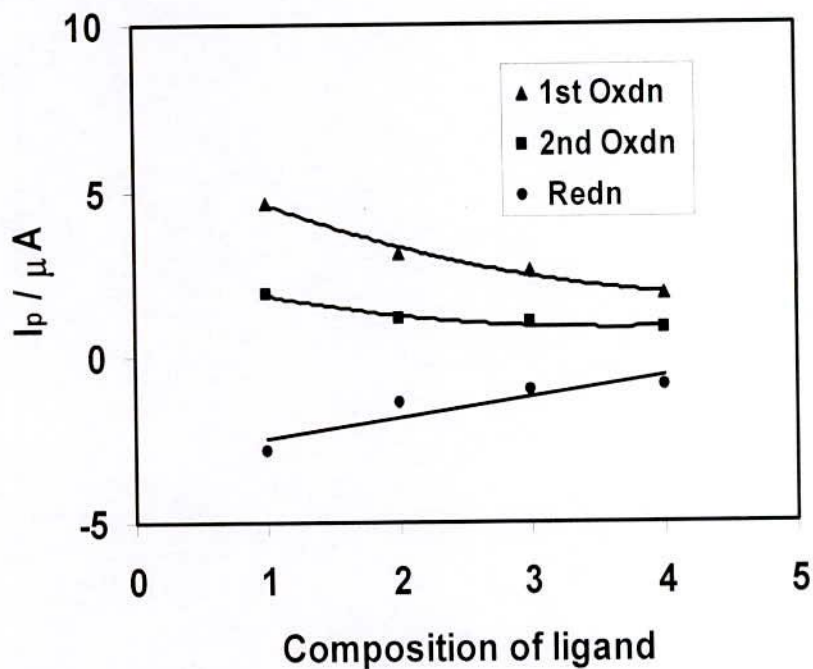Figure 4.46 : Plots of peak current versus composition of ligand(metal constant) of Pure Cu(II), Cu(II)-Aspartic acid(1:1), (1:2) and (1:3) at similar condition (Scan rate= 0.04V/s).
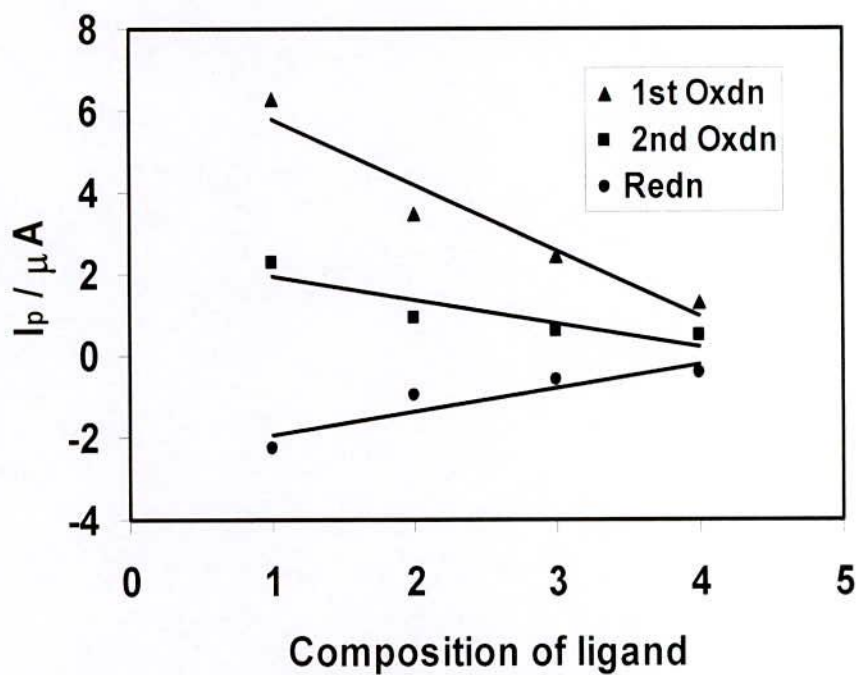
Figure 4.47 : Plots of peak current versus composition of ligand (metal constant) of Pure Cu(II), Cu(II)-Aspartic acid(1:1), (1:2) and (1:3) at similar condition (Scan rate = 0.10V/s).
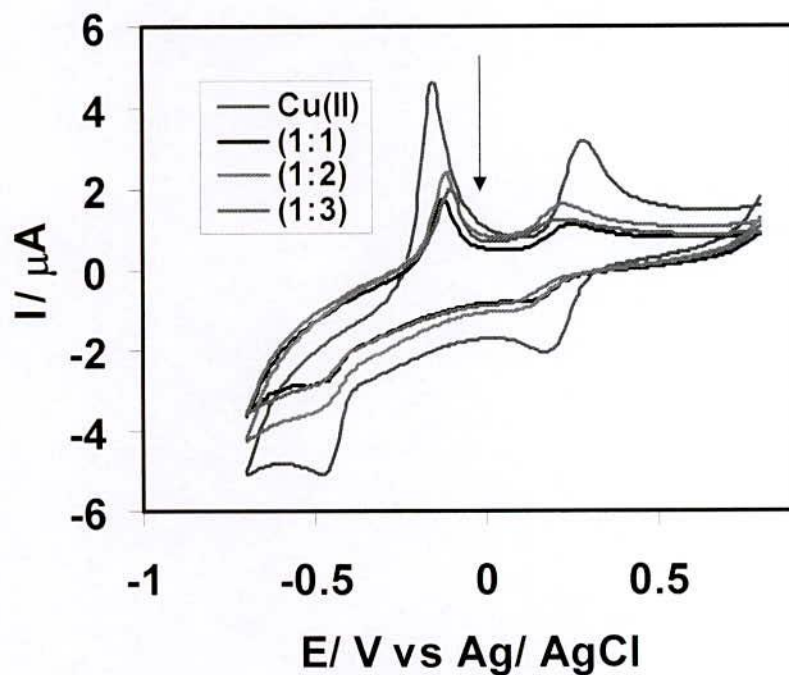
Figure 4.48 : Comparison of Cyclic voltammogram of Pure Cu(II), Cu(II)-Aspartic acid(1:1), (1:2) and (1:3) at similar condition (pH = 3.5, Scan rate = 0.04V/s).
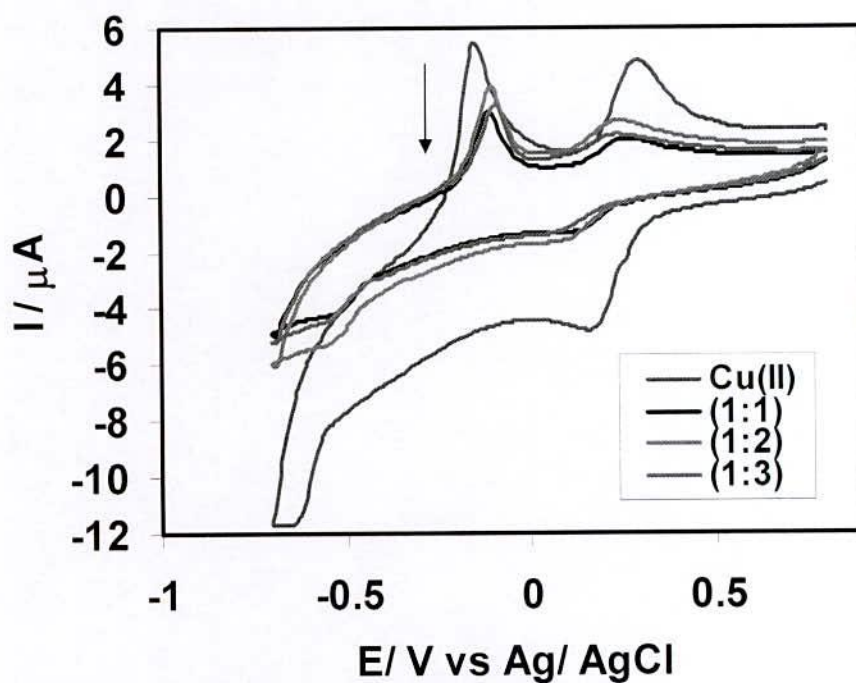
Figure 4.49 : Comparison of Cyclic voltammogram of Pure Cu Cu(II), Cu(II)-Aspartic acid(1:1), (1:2) and (1:3) at similar condition (pH = 3.5, Scan rate = 0.10V/s).
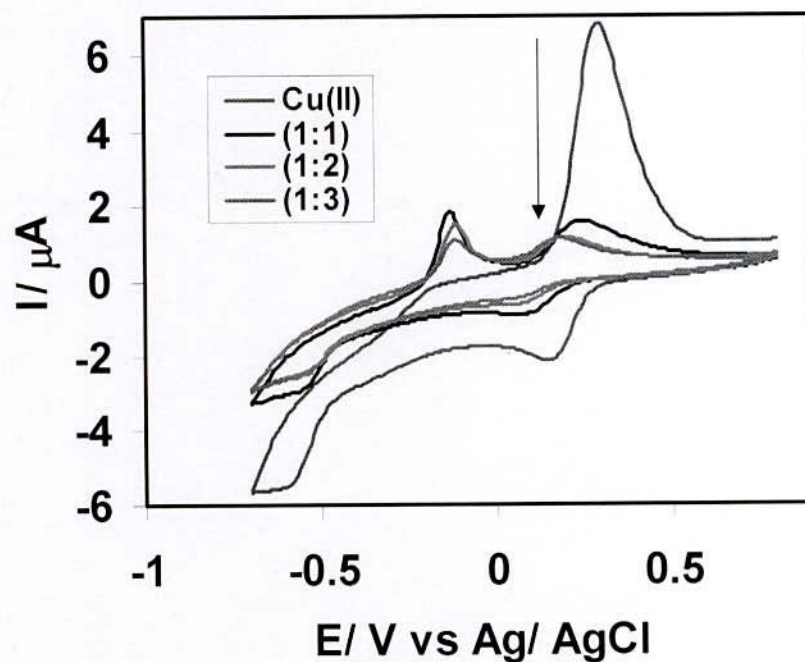
Figure 4.50 : Comparison of Cyclic voltammogram of Cu(II), Cu(II)-Aspartic acid(1:1), (1:2) and (1:3) at similar condition (pH = 4.5, Scan rate = 0.04V/s).
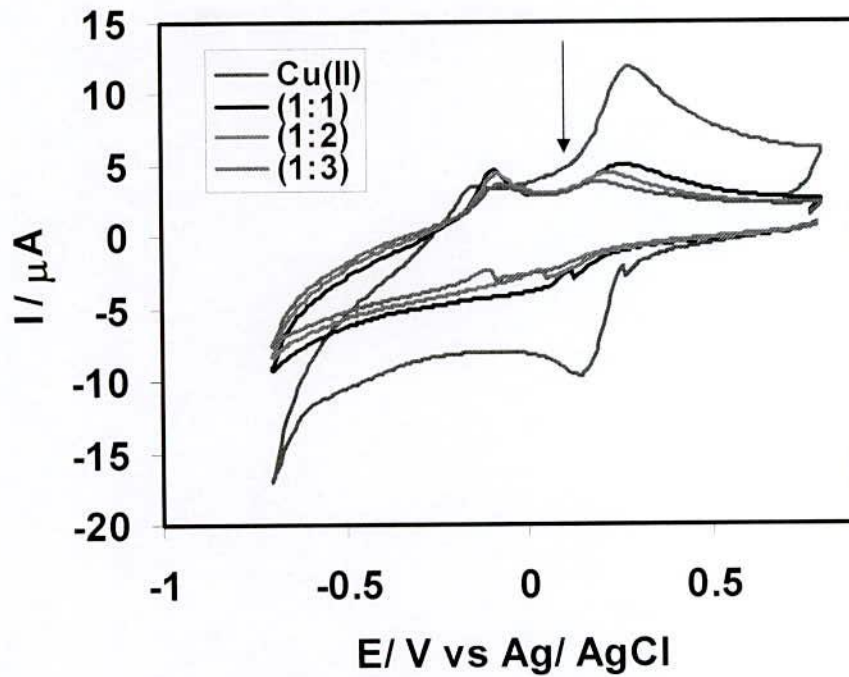
Figure 4.51 : Comparison of Cyclic voltammogram of Pure Cu(II), Cu(II)-Aspartic acid(1:1), (1:2) and (1:3) at similar condition (pH = 4.5, Scan rate = 0.50V/s).
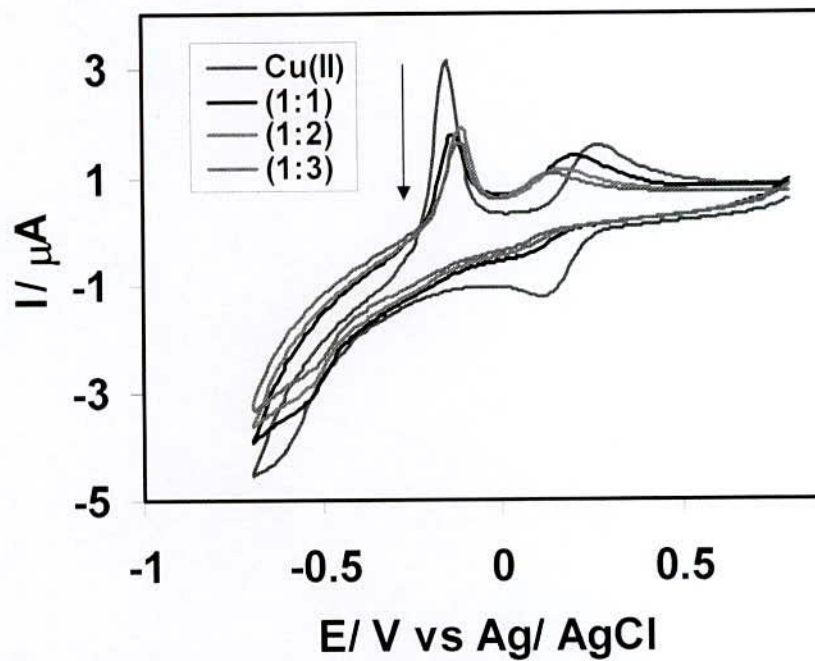
Figure 4.52 : Comparison of Cyclic voltammogram of Pure Cu(II), Cu(II)-Aspartic acid(1:1), (1:2) and (1:3) at similar condition (pH = 5.5, Scan rate = 0.04V/s).
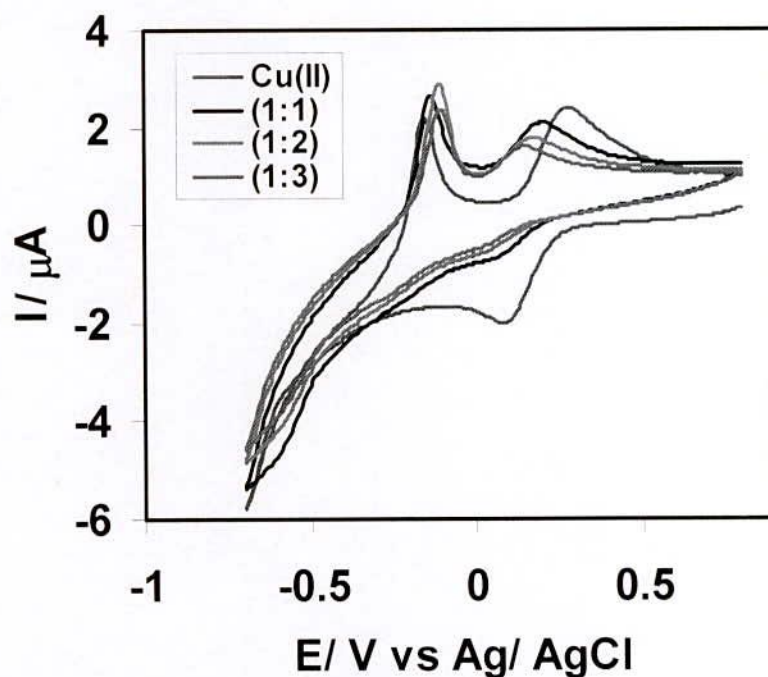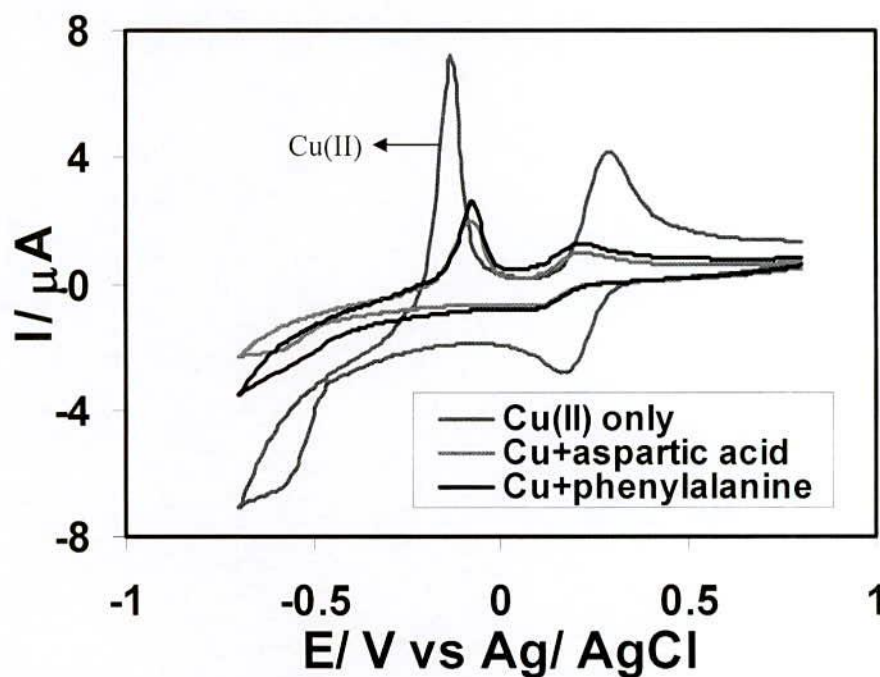
Figure 4.53 : Comparison of Cyclic voltammogram of Pure Cu(II), Cu(II)-Aspartic acid(1:1), (1:2) and (1:3) at similar condition (pH = 5.5, Scan rate = 0.10V/s).
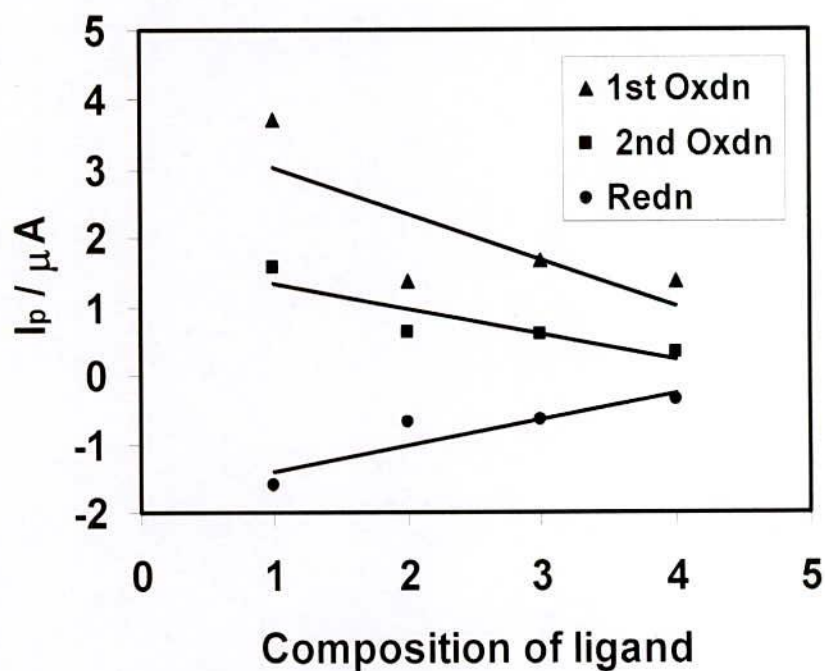

Figure 4.54 : Plots of peak current versus composition of ligand of Pure Cu(II), Cu(II)-Aspartic acid(1:1), (1:2) and (1:3) at similar condition (pH = 3.5, Scan rate = 0.04V/s).
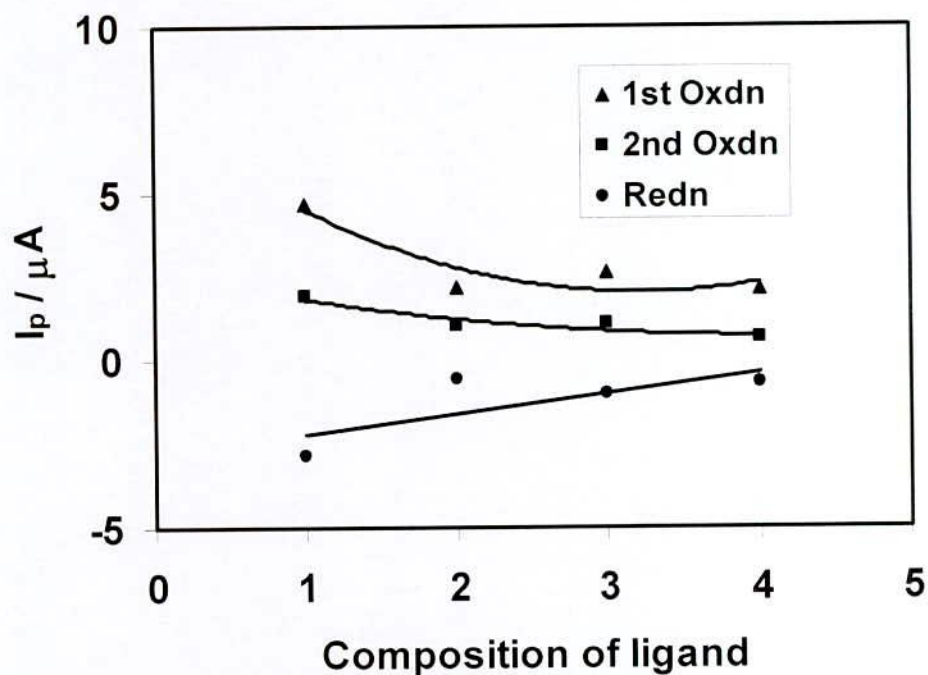
Figure 4.55 : Plots of peak current versus composition of ligand of Pure Cu(II), Cu(II)-Aspartic acid(1:1), (1:2) and (1:3) at similar condition (pH = 3.5, Scan rate = 0.10V/s).
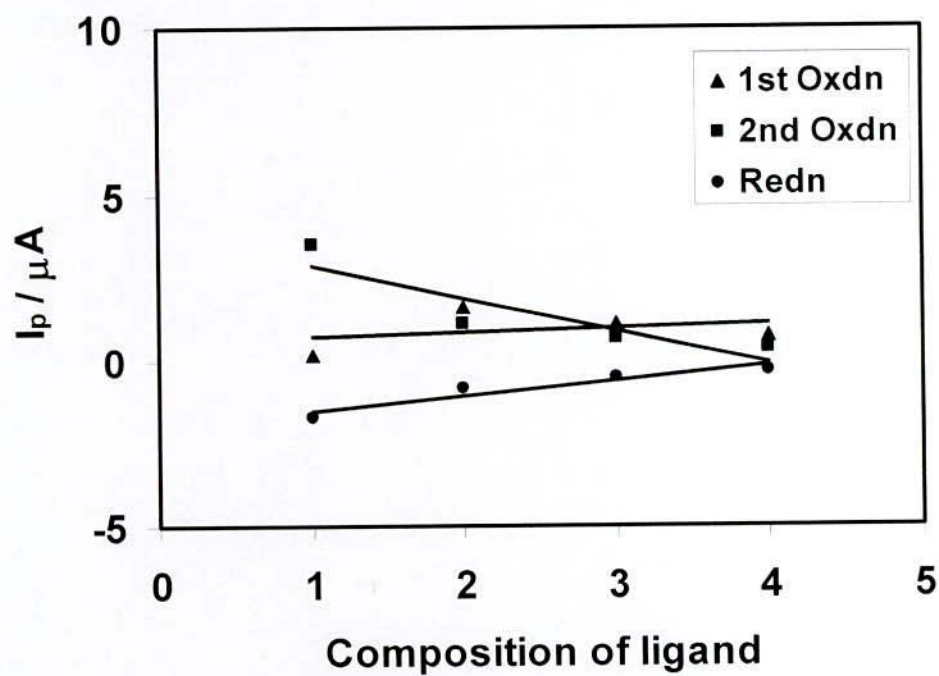
Figure 4.56 : Plots of peak current versus composition of ligand of Pure Cu(II), Cu(II)-Aspartic acid(1:1), (1:2) and (1:3) at similar condition (pH = 4.5,Scan rate = 0.04V/s).
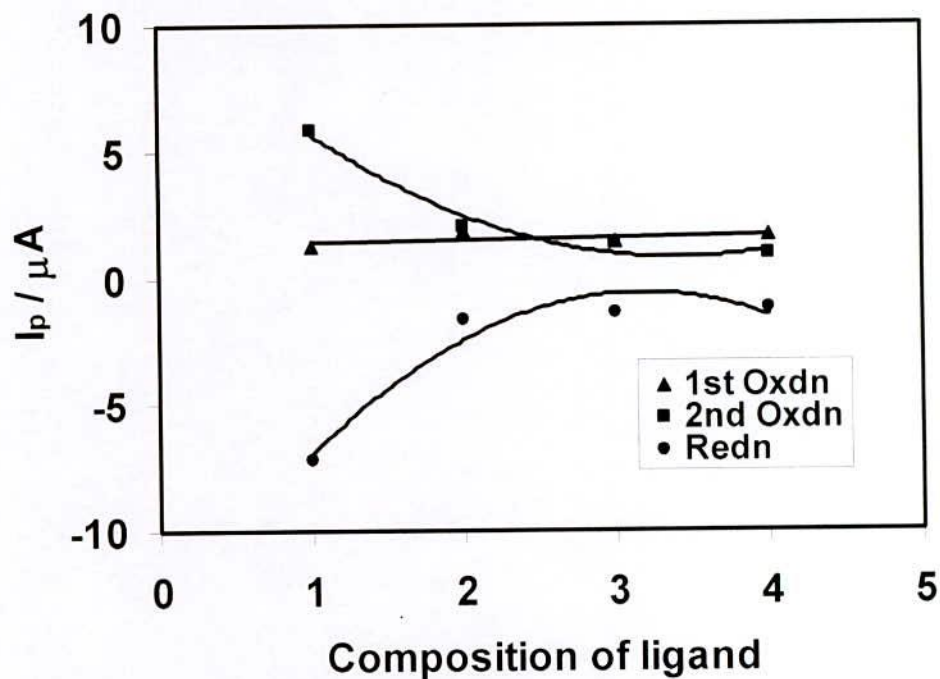
Figure 4.57 : Plots of peak current versus composition of ligand of Pure Cu(II), Cu(II)-Aspartic acid(1:1), (1:2) and (1:3) at similar condition (pH = 4.5, Scan rate = 0.50V/s).
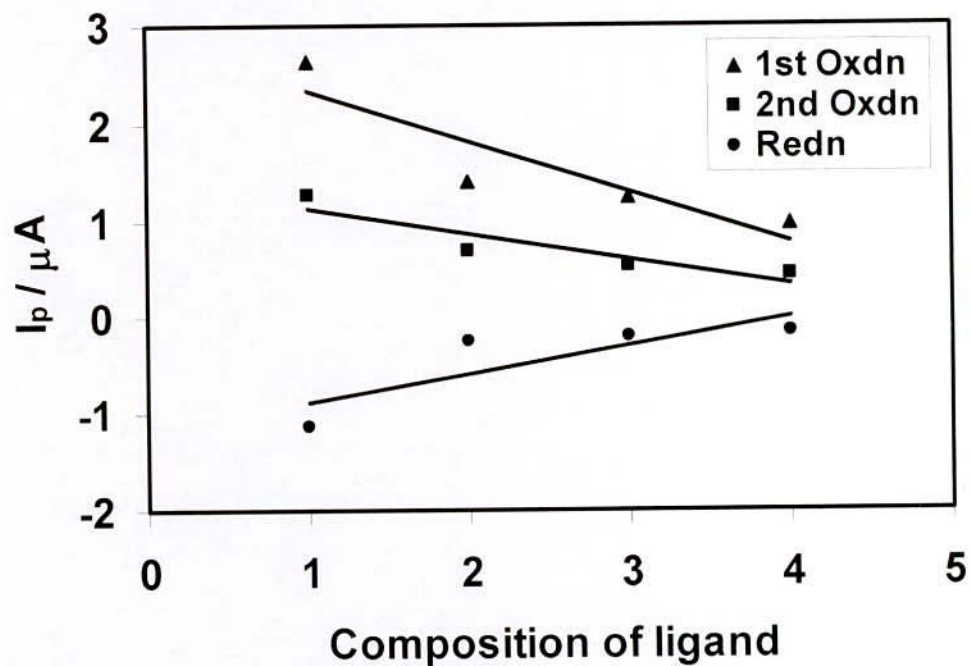
Figure 4.58 : Plots of peak current versus composition of ligand of Pure Cu(II), Cu(II)-Aspartic acid(1:1), (1:2) and (1:3) at similar condition (pH = 5.5, Scan rate = 0.04V/s).
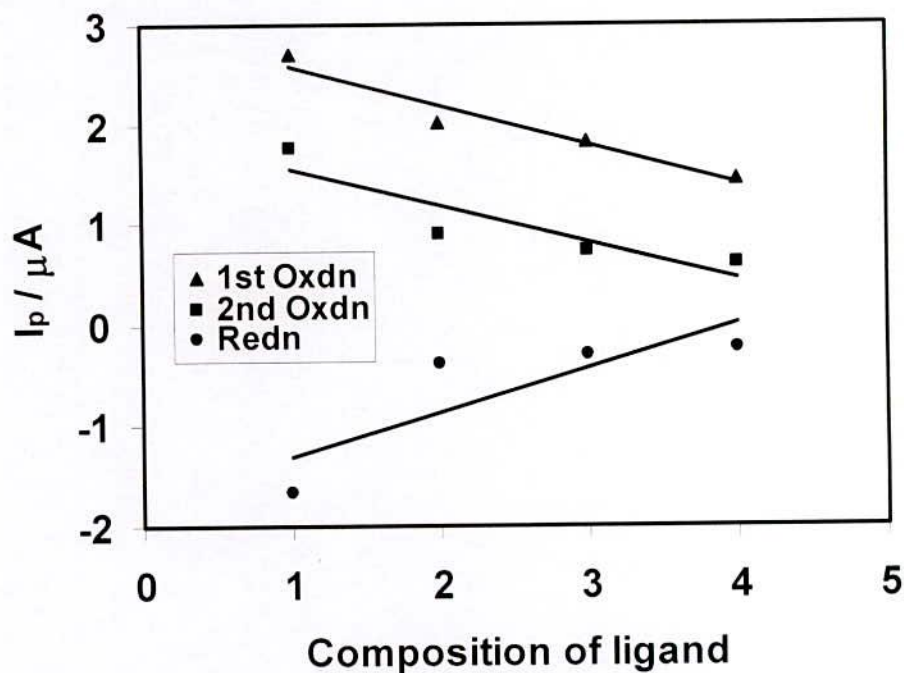
Figure 4.59 : Plots of peak current versus composition of ligand of Pure Cu(II), Cu(II)-Aspartic acid(1:1), (1:2) and (1:3) at similar condition (pH = 5.5, Scan rate = 0.10V/s).
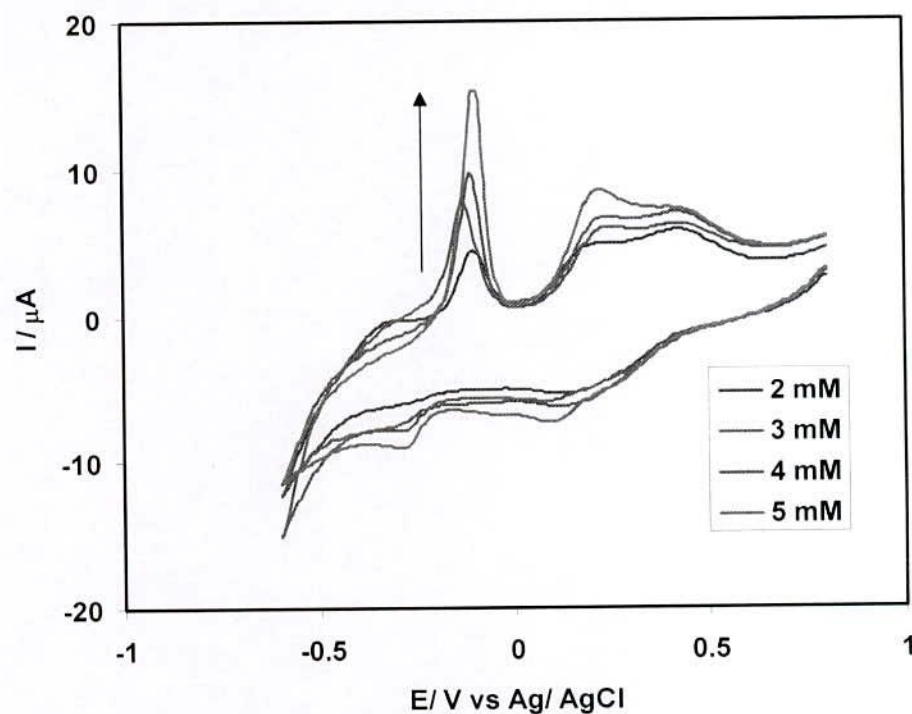
Figure 4.60: Cyclic voltammogram of Cu(II) + aspartic acid (1:3) in buffer solution (acetate buffer) pH = 3.5 at scan rate 0.1V/s.
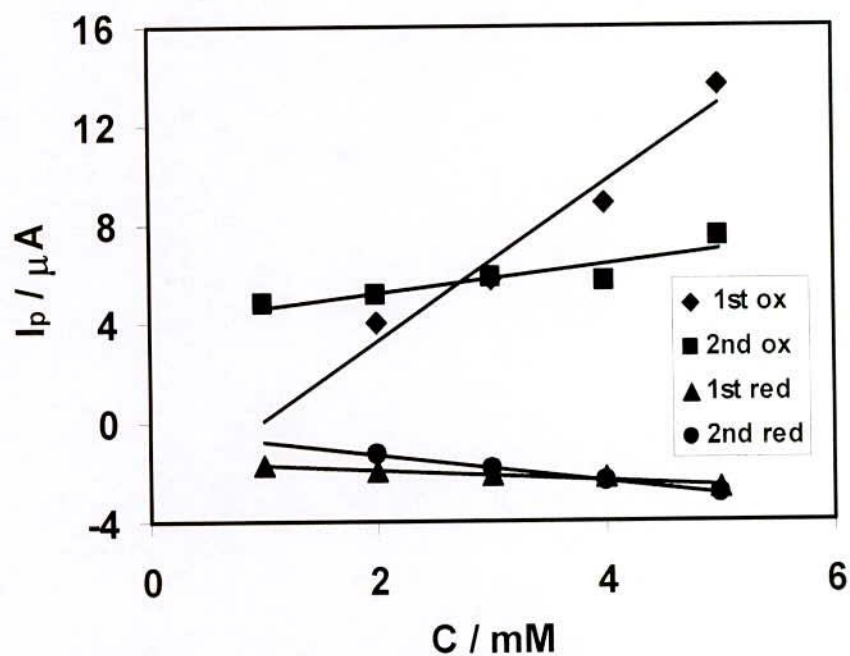
Figure 4.61 : Plots of peak current versus concentration of Cu(II) + aspartic acid (1:3) in buffer solution (acetate buffer) at pH = 3.5 at scan rate 0.1V/s.
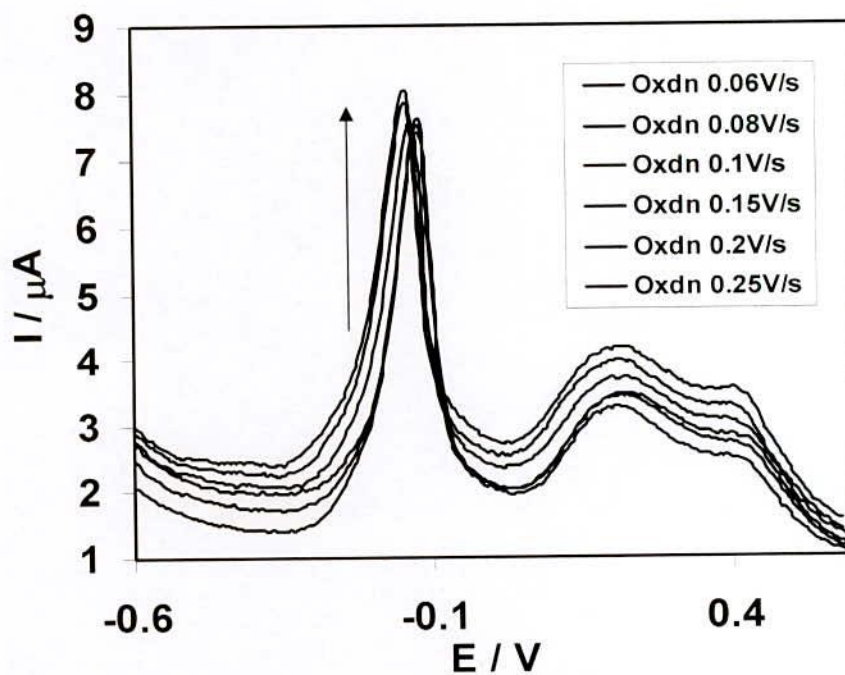
Figure 4.62 : Differential pulse voltammogram of Cu(II)+ aspartic acid (1:3) in buffer solution (pH = 3.0) (acetate buffer) for forward direction (oxidation) at different scan rate.
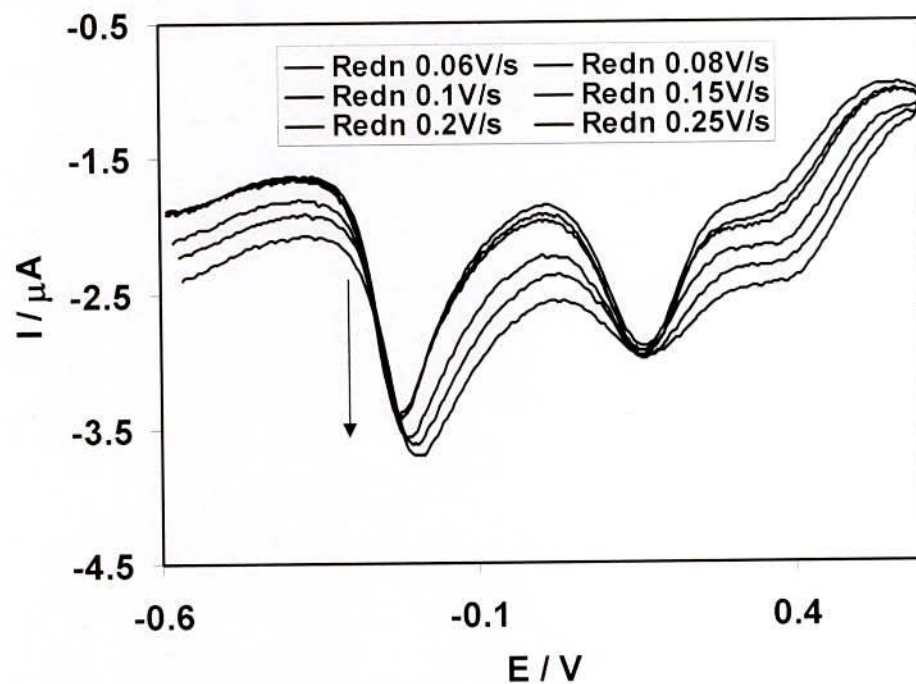
Figure 4.63 : Differential pulse voltammogram of Cu(II) + aspartic acid (1:3) in buffer solution (pH = 3.0) (acetate buffer) for backward direction (reduction) at different scan rate using.
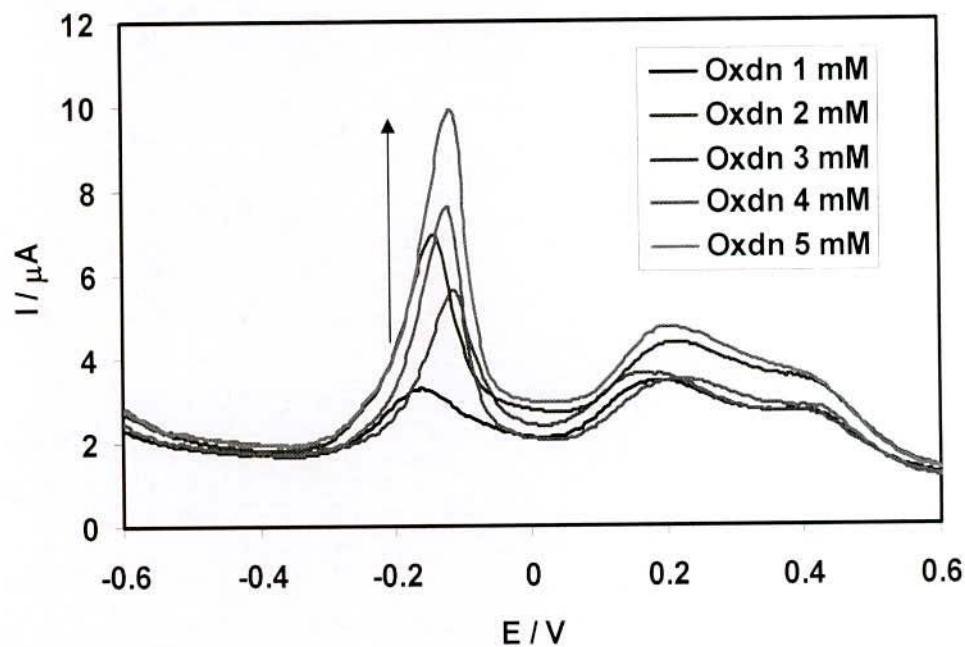
Figure 4.64 : Comparison of concentration of Differential pulse voltammogram of Cu(II) + Aspartic acid in buffer solution (pH = 3.5) (acetate buffer) for forward direction (oxidation) at different concentration, scan rate 0.1V/s.
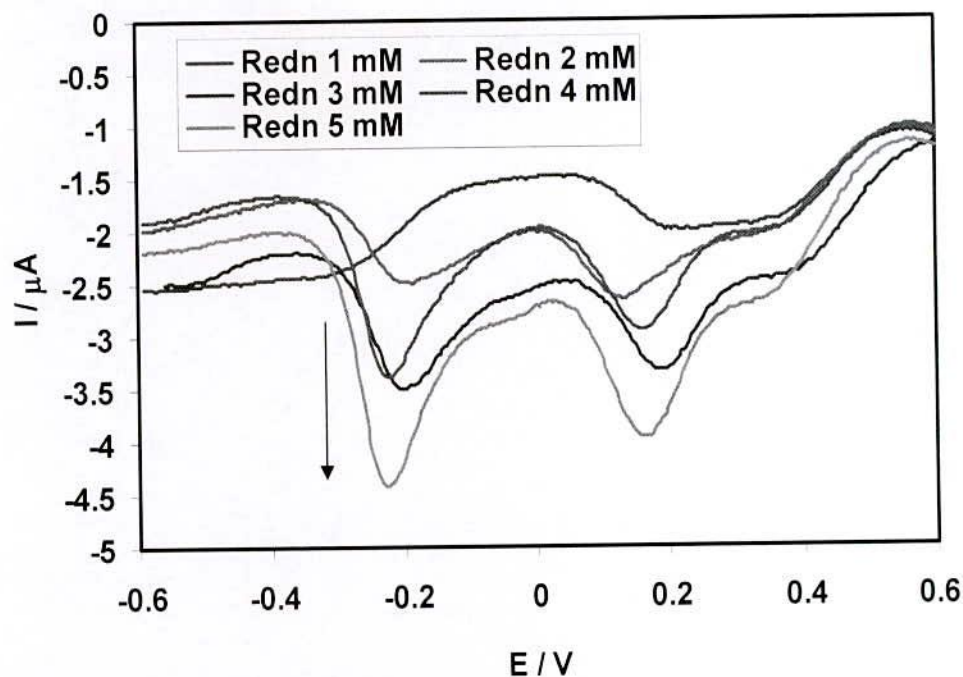
Figure 4.65 : Differential pulse voltammogram of CuCl$_2$ + Aspartic acid in buffer solution (pH = 3.5) (acetate buffer) for backward direction (reduction) at different concentration, scan rate 0.1V/s.
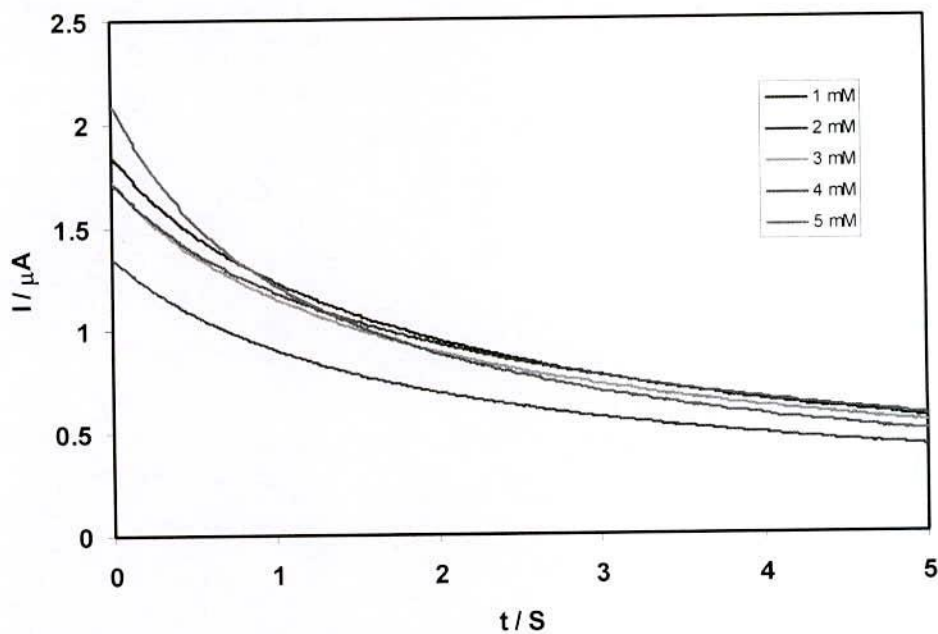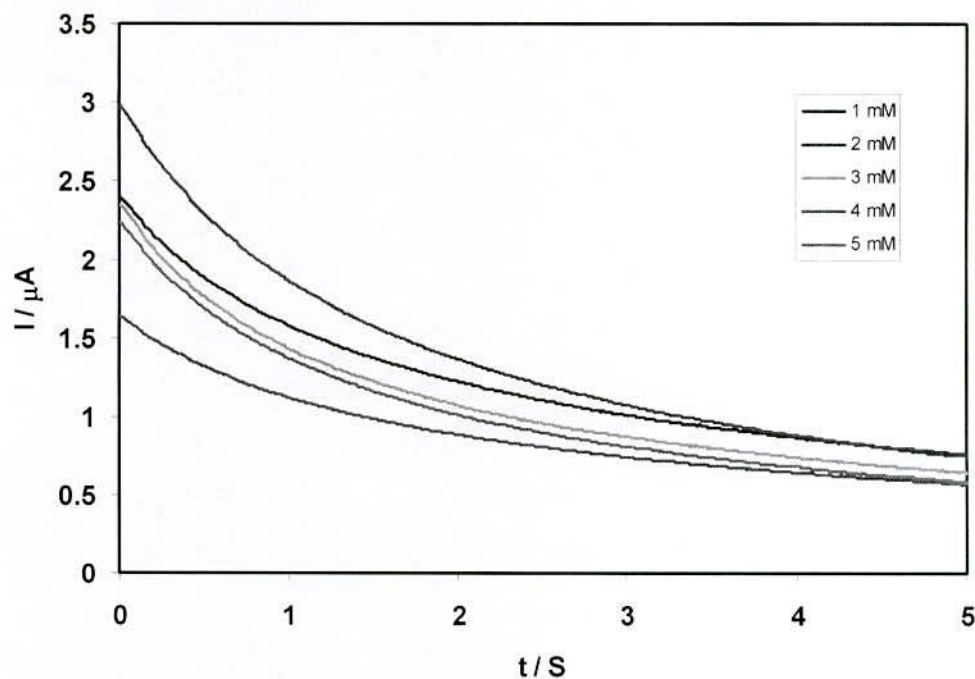

Figure 4.66 : Chronoamperometry curve of CuCl$_2$ + aspartic acid (1:3) in buffer solution (pH = 3.5) (acetate buffer) for forward direction (oxidation) different concentration at scan rate 0.4V/s.
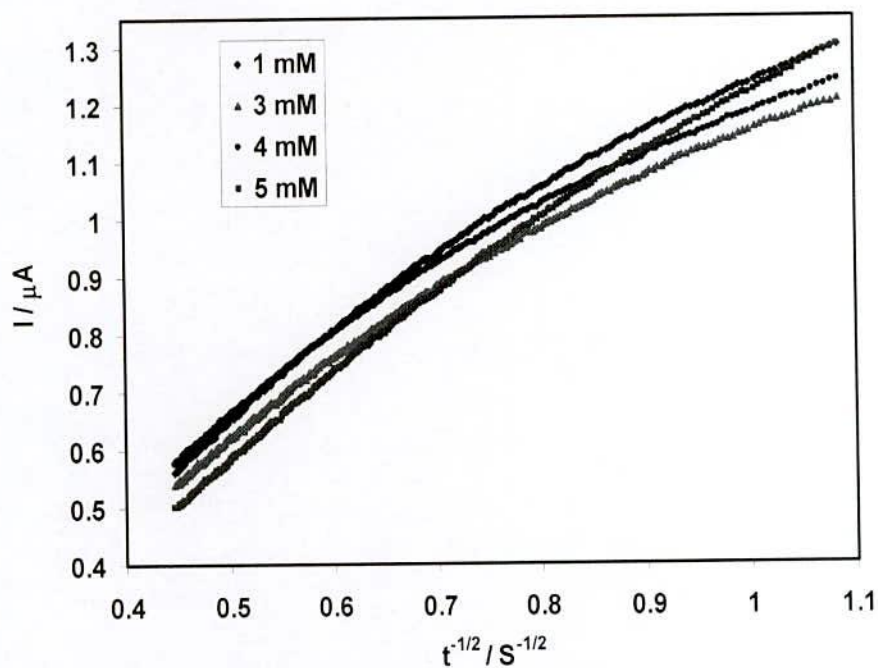
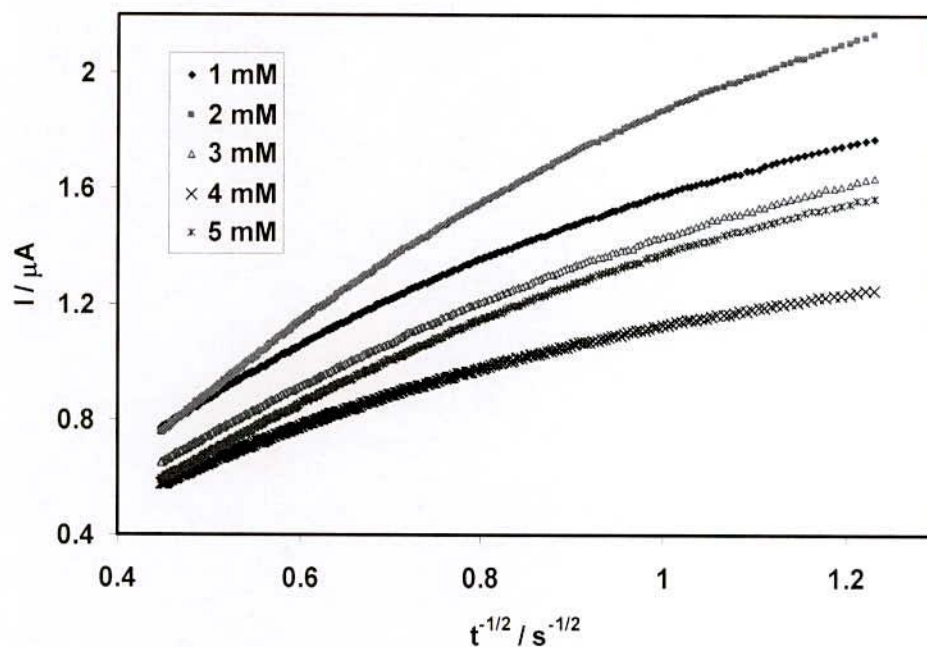Figure 4.67 : Cottrell plots of the back ground subtracted currents for $CuCl_2$ + aspartic acid (1:3) in buffer solution (pH = 3.5) (acetate buffer) when the potential was stepped from -0.3 to 0.4V
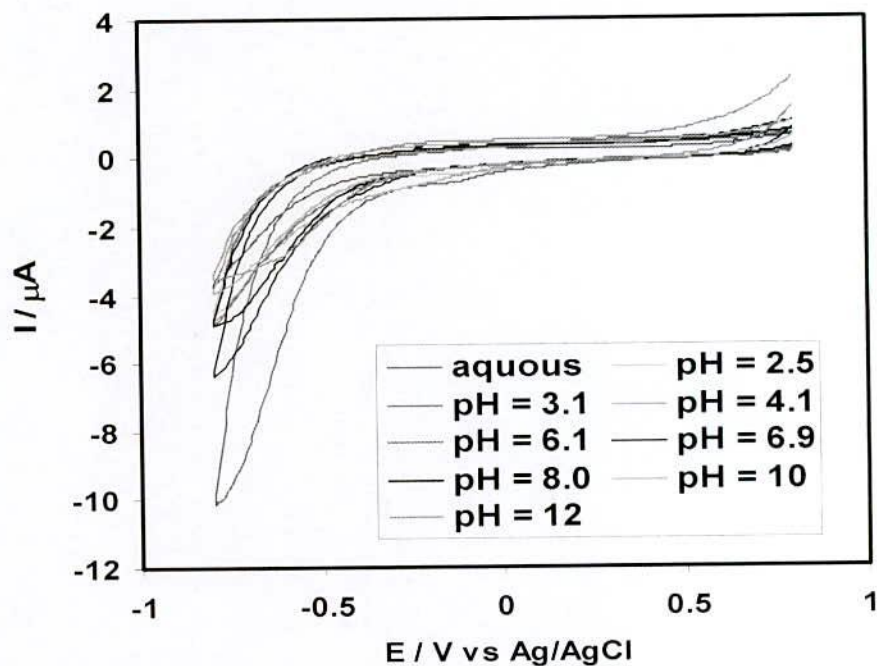
Figure 4.68 : Cyclic voltammogram of 2mM L-Phenylalanine in aqueous solution and different pH at scan rate 0.1V/s.

139
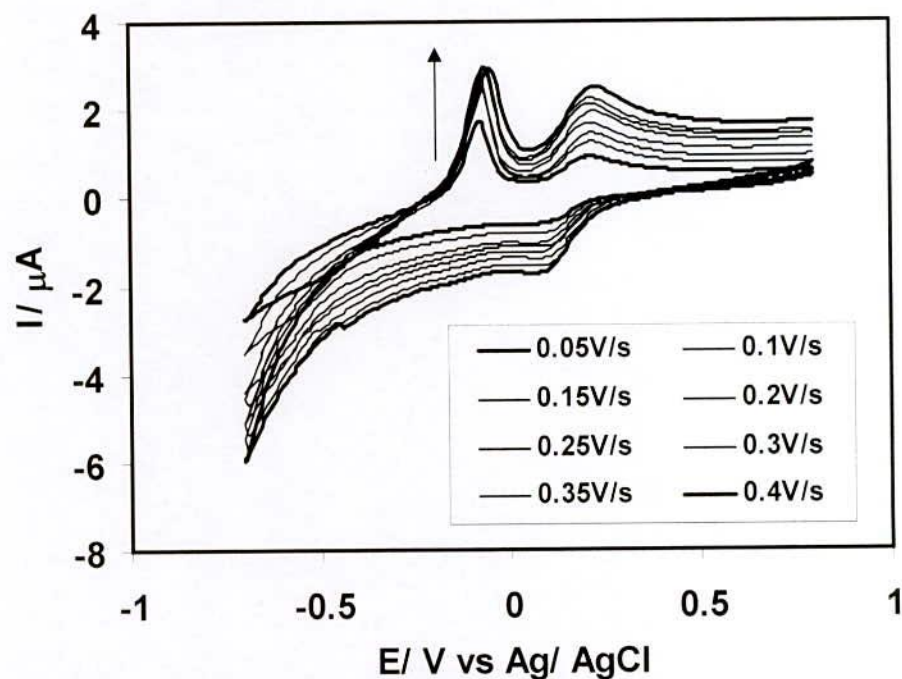
Figure 4.69 : Cyclic voltammogram of 2mM $CuCl_2$ + 6mM L-Phenylalanine (1:3) in aqueous solution at different scan rate.
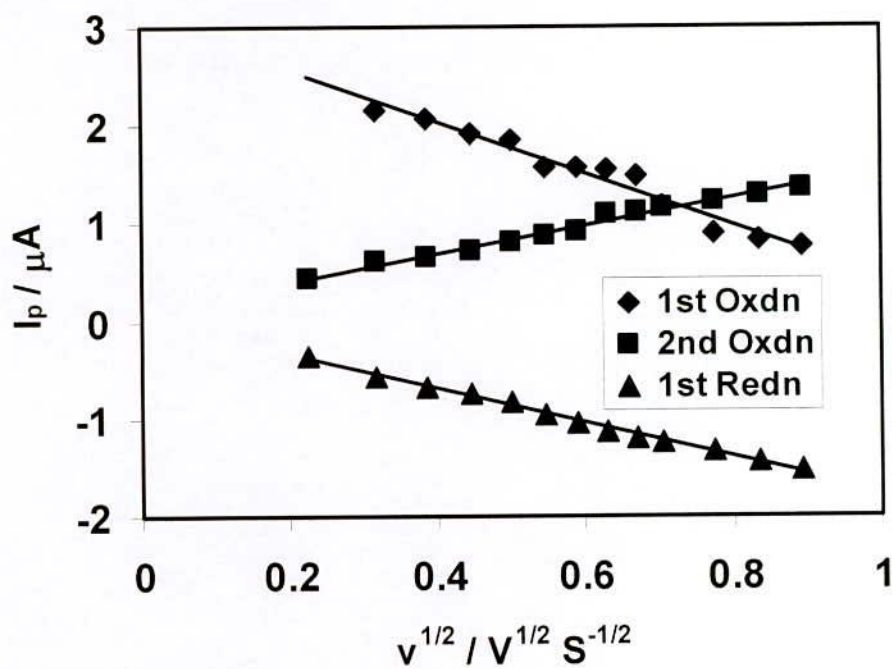
Figure 4.70 : Plots of peak current versus square root of scan rate of 2mM $CuCl_2$ + 6mM L-Phenylalanine (1:3) in aqueous solution.
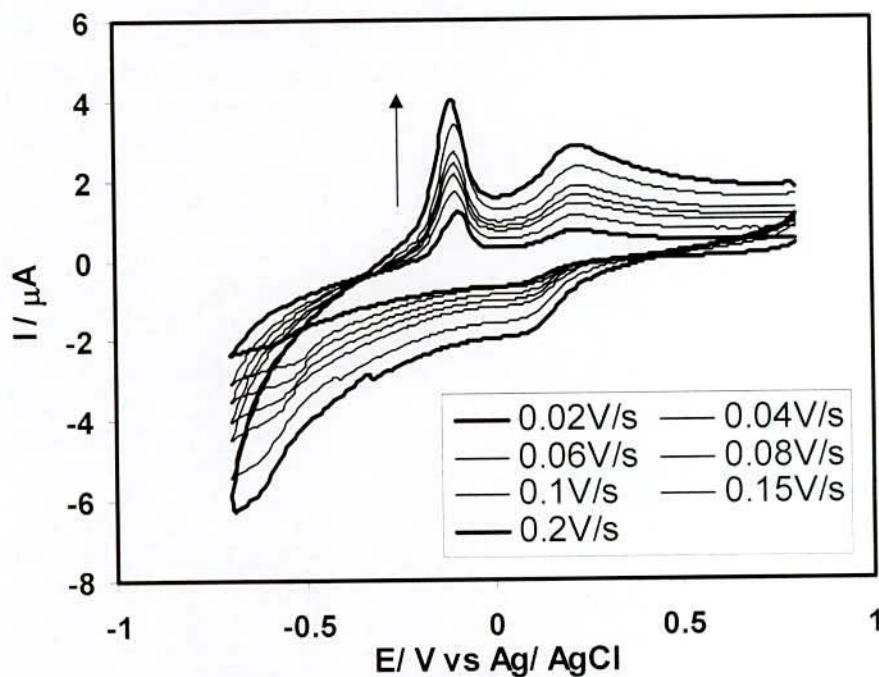
Figure 4.71 : Cyclic voltammogram of 2mM $CuCl_2$ + 6mM L-phenyl alanine (1:3) in buffer solution (pH = 3.5) (acetate buffer) at different scan rate.
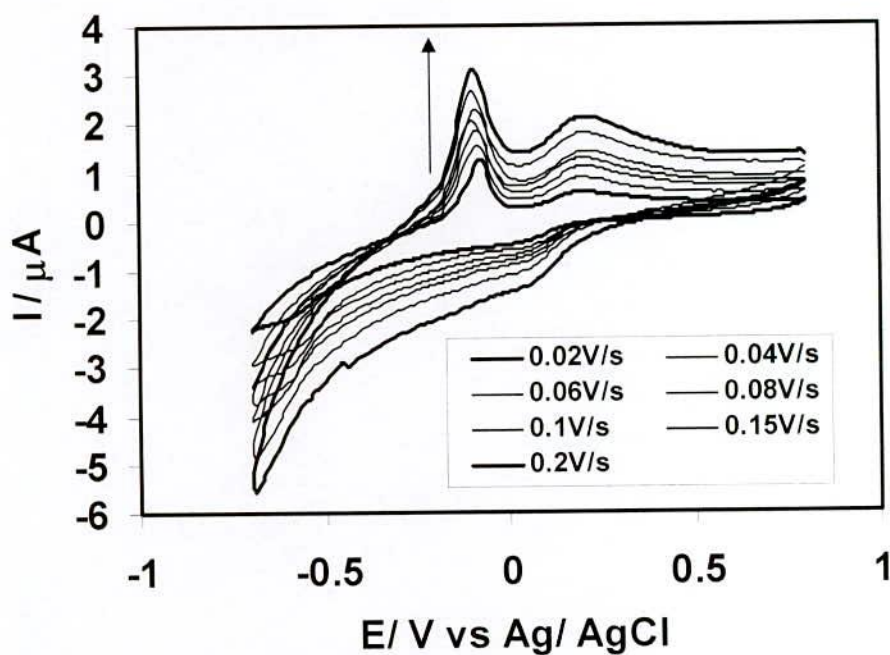
Figure 4.72 : Cyclic voltammogram of 2mM $CuCl_2$ + 6mM L-phenyl alanine (1:3) in buffer solution (pH = 4.5) (acetate buffer) at different scan rate.

141
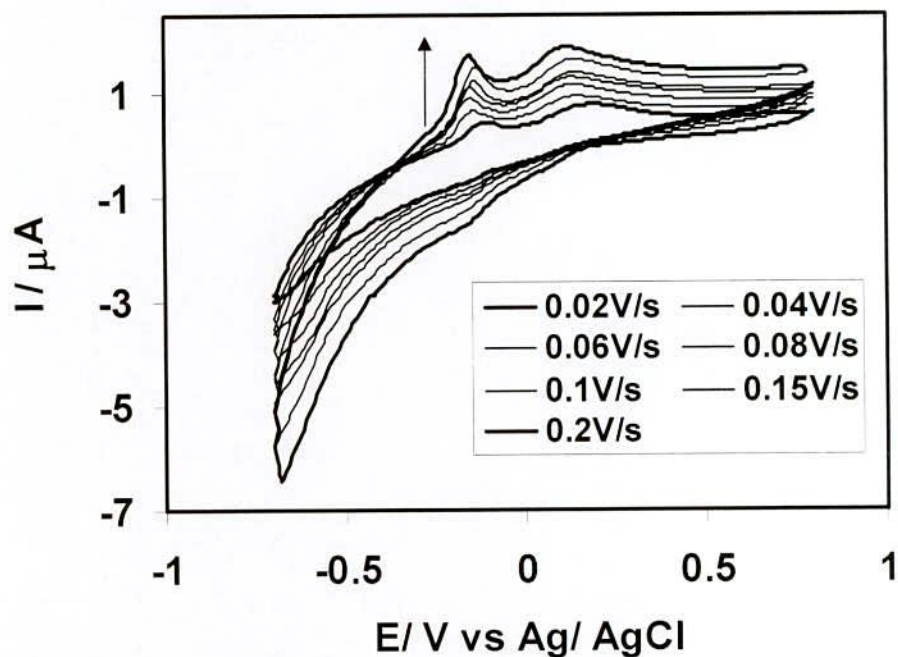
Figure 4.73 : Cyclic voltammogram of 2mM $CuCl_2$ + 6mM L-phenyl alanine (1:3) in buffer solution (pH = 6.0) (acetate buffer) at different scan rate.
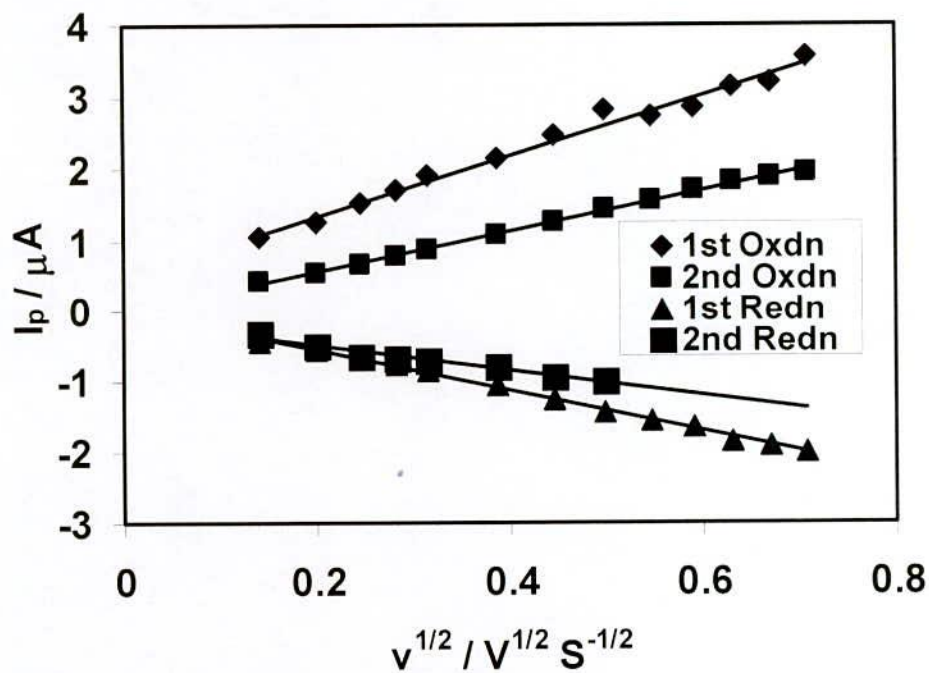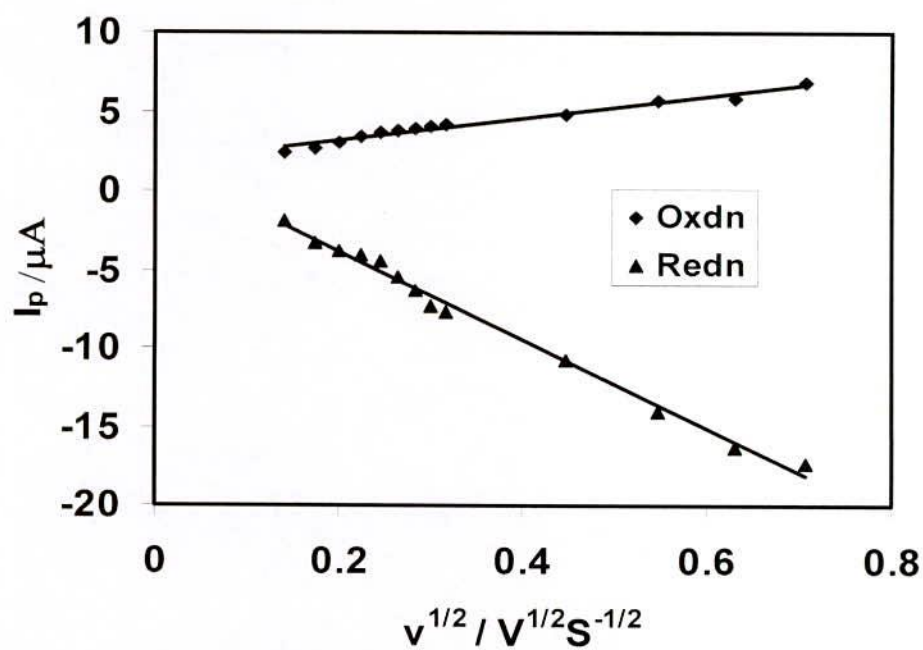

Figure 4.74 : Plots of peak current versus square root of scan rate of 2mM $CuCl_2$ + 6mM L-phenyl alanine (1:3) in buffer solution   (pH = 3.5) (acetate buffer).
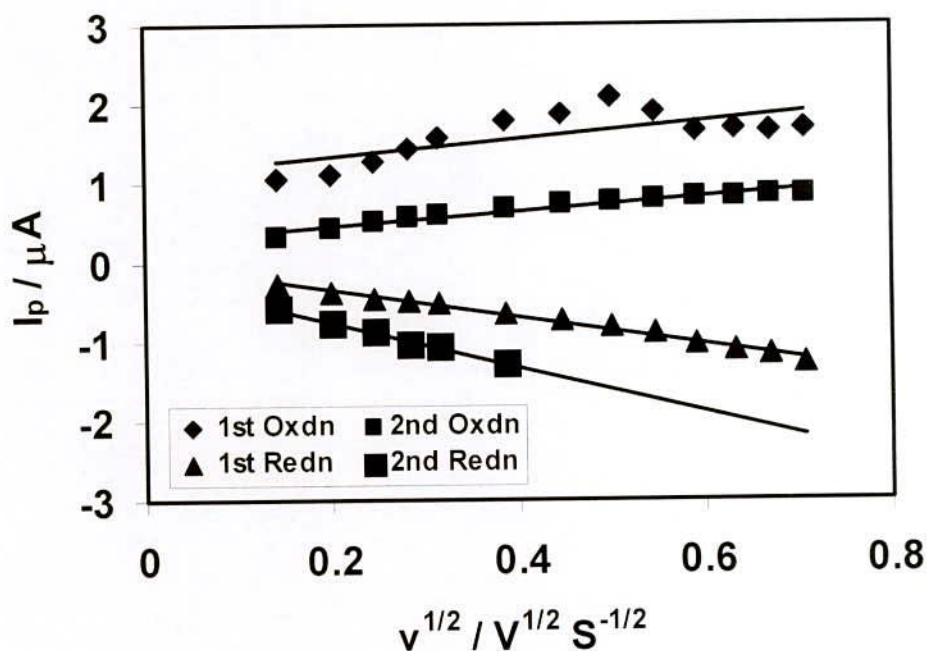
Figure 4.75 : Plots of peak current versus square root of scan rate of 2mM CuCl$_2$ + 6mM L-Phenyl alanine (1:3) in buffer solution (pH = 4.5) (acetate buffer).
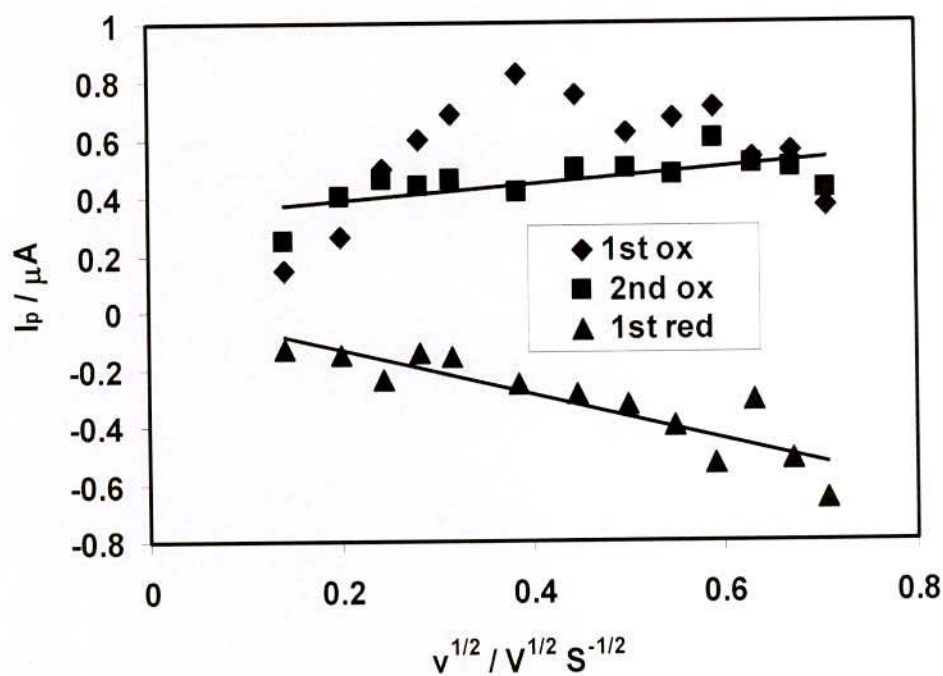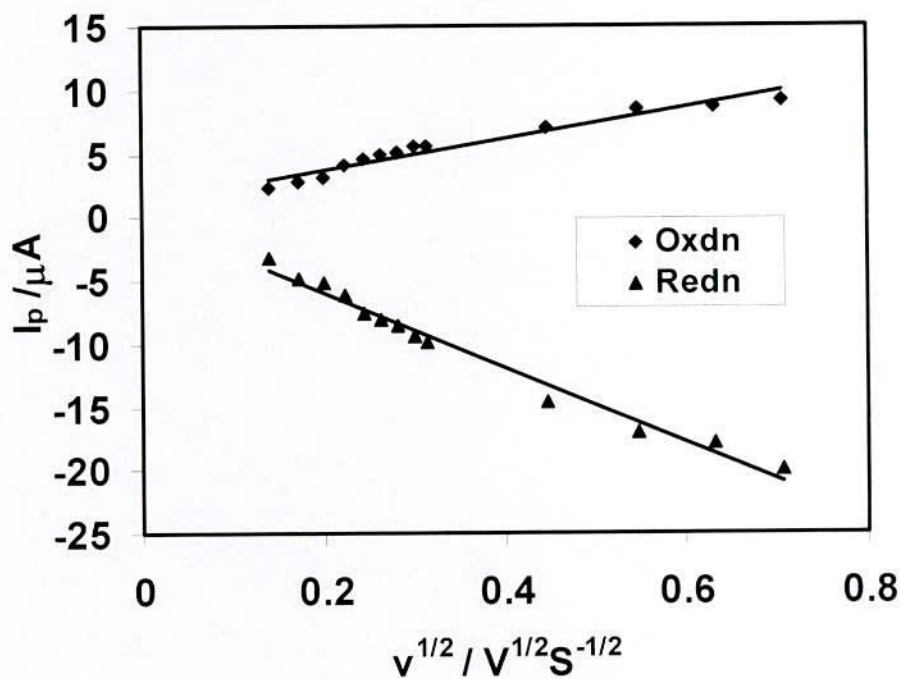

Figure 4.76 : Plots of peak current versus square root of scan rate of 2mM CuCl$_2$ + 6mM L-phenyl alanine (1:3) in buffer solution (pH = 6.0) (acetate buffer).
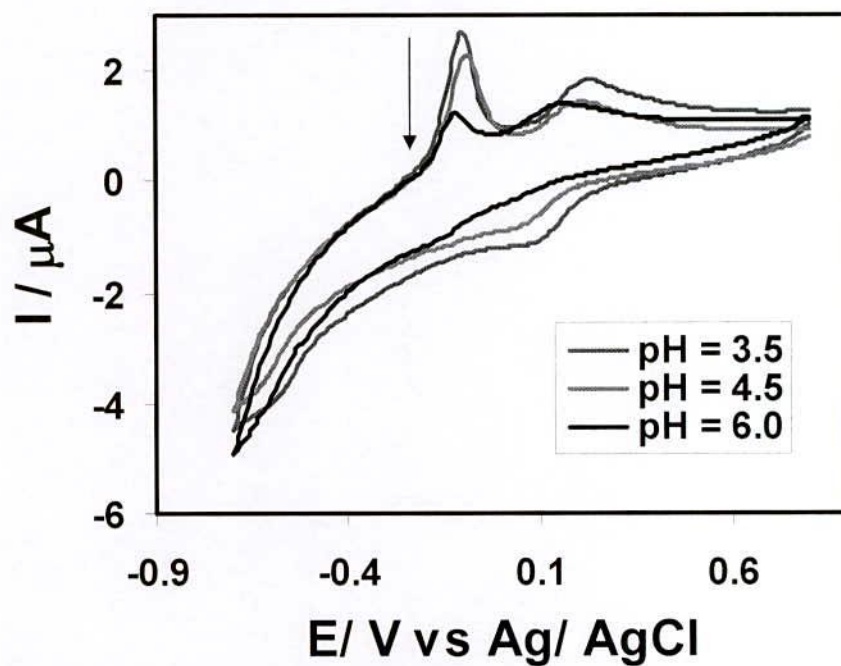
Figure 4.77 : Comparison of Cyclic voltammogram of Cu(II)-L-Phenyl alanine(1:3) in different pH (3.5, 4.5, 6.0) at similar condition (Scan rate = 0.04V/s).
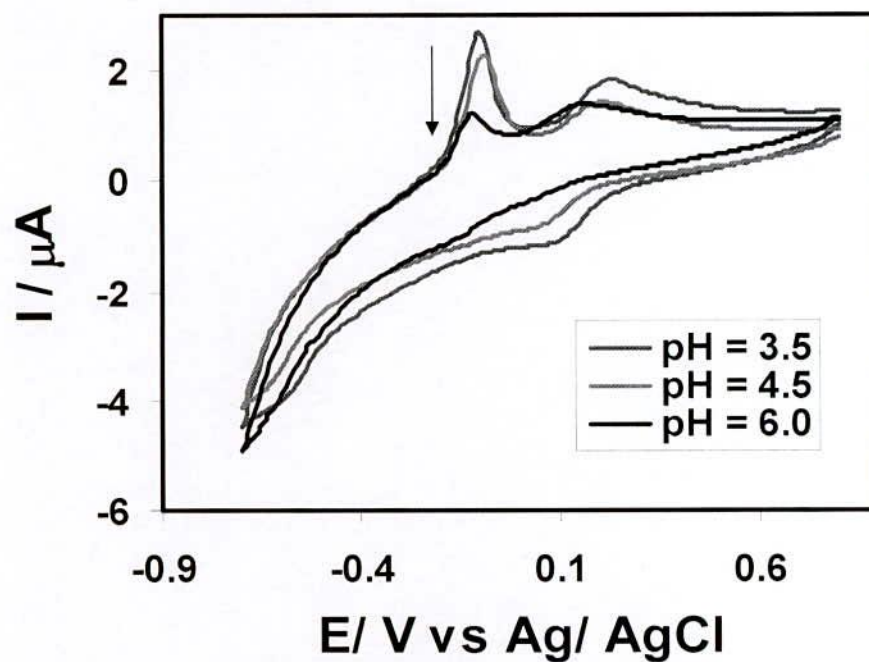
Figure 4.78 : Comparison of Cyclic voltammogram of Cu(II)- L-Phenyl alanine (1:3) in different pH (3.5, 4.5, 6.0) at similar condition (Scan rate = 0.10V/s).
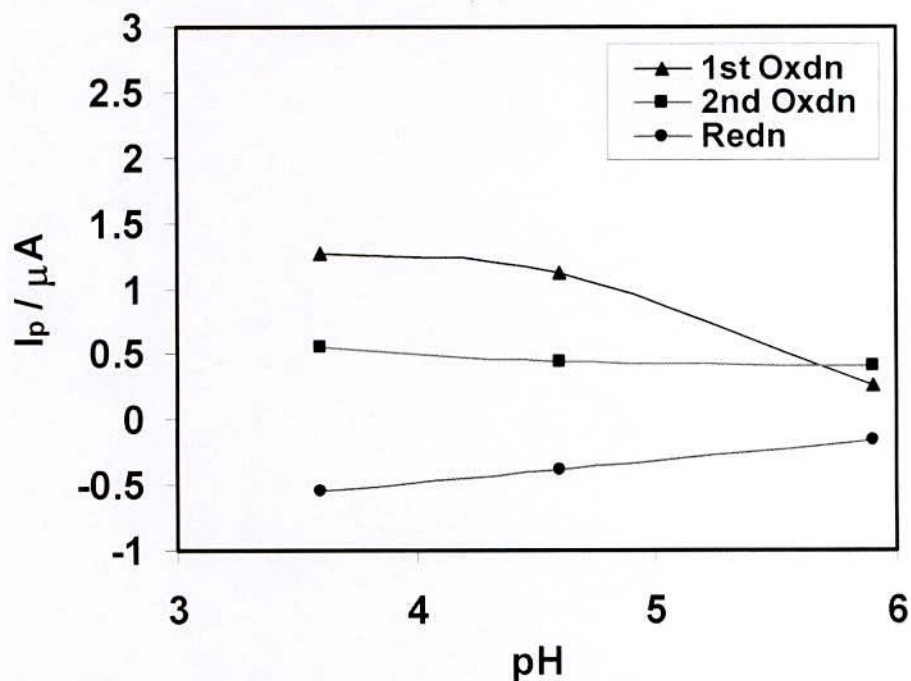
Figure 4.79 : Plots of peak current versus versus pH (3.5, 4.5, 6.0) of Cu(II)-L-Phenyl alanine (1:3) at similar condition (Scan rate = 0.04V/s).
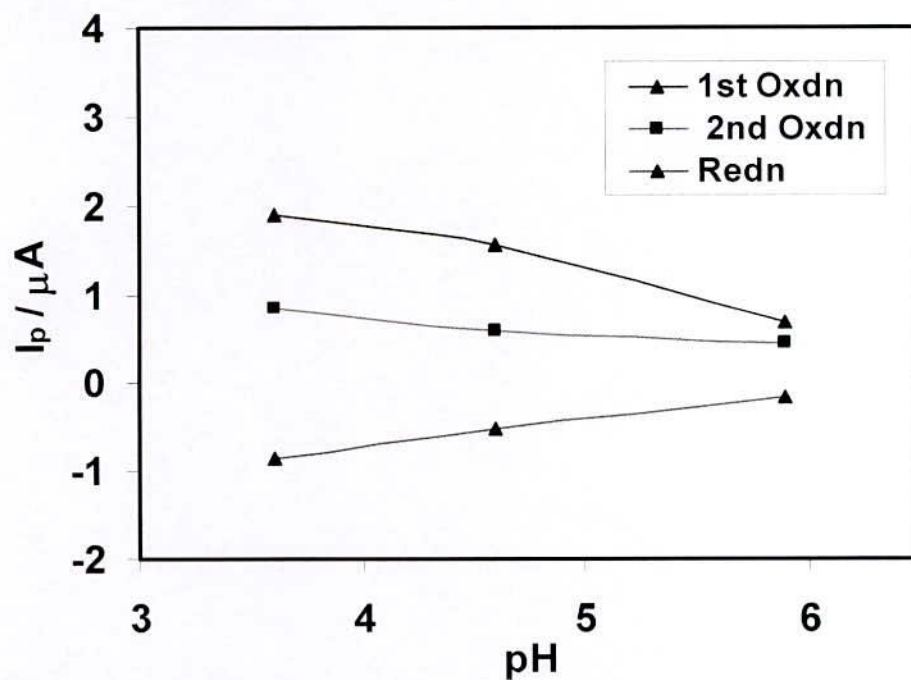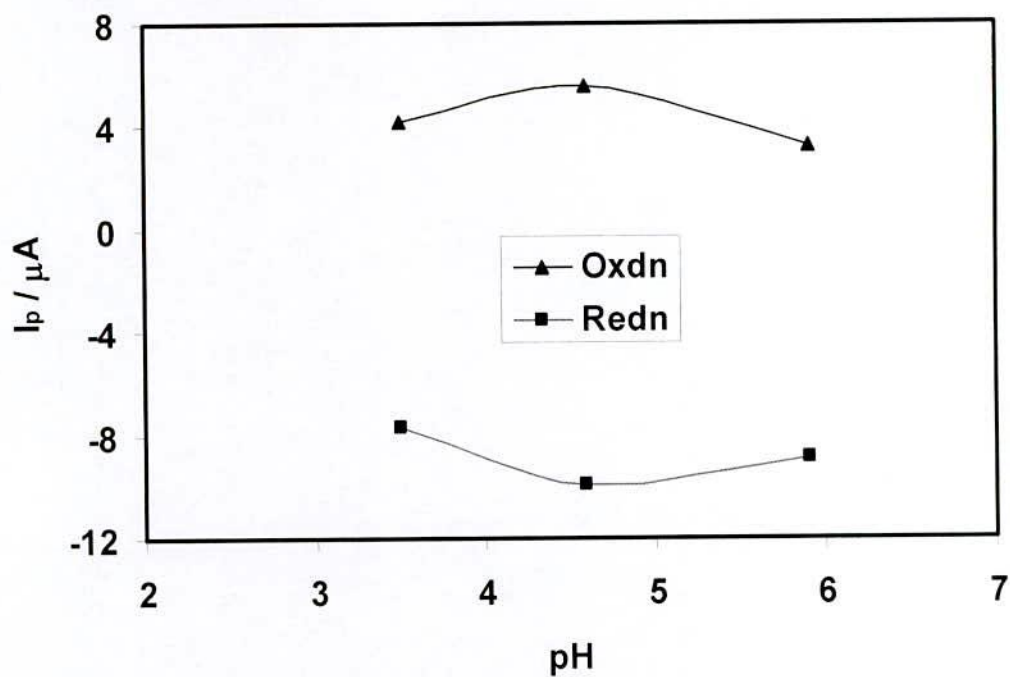

Figure 4.80 : Plots of peak current versus versus pH (3.5, 4.5, 6.0) of Cu(II)- L-Phenyl alanine(1:3) at similar condition (Scan rate = 0.10V/s).
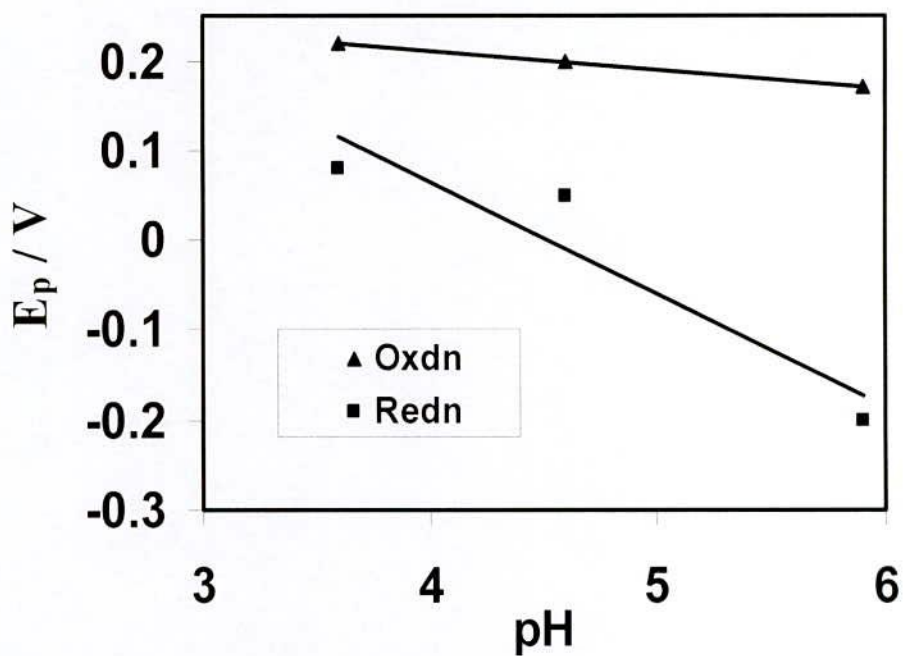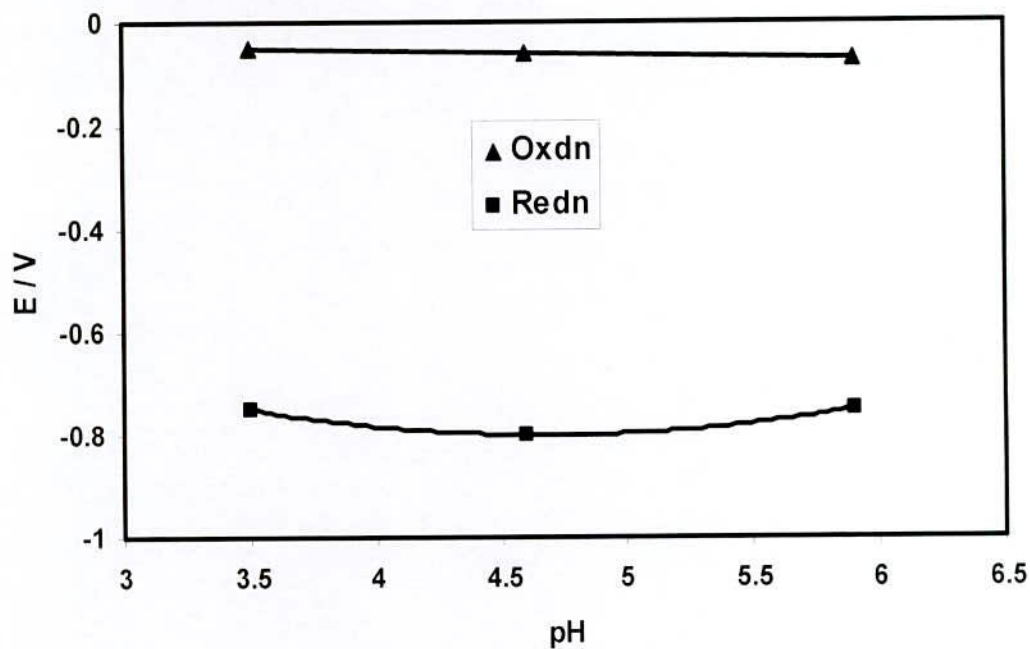
Figure 4.81 : Plots of peak potential (E/V) versus pH(3.5, 4.5, 6.0) of Cu(II)-L-Phenyl alanine (1:3) at similar condition (Scan rate = 0.04V/s).
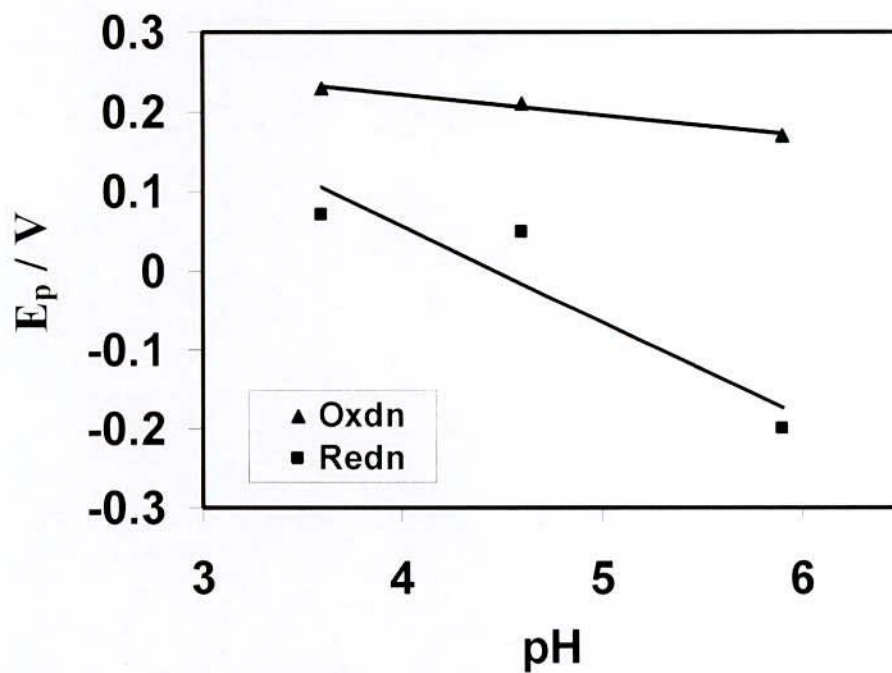
Figure 4.82 : Plots of peak potential (E /V) versus pH (3.5, 4.5, 6.0) of Cu(II)- L-Phenyl alanine (1:3) at similar condition (Scan rate = 0.10V/s).
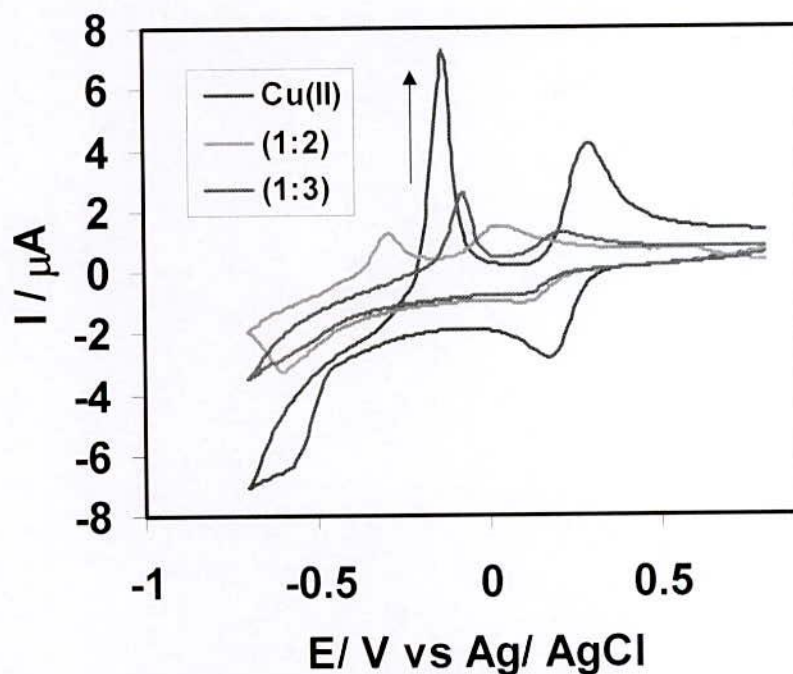
Figure 4.83 : Comparison of Cyclic voltammogram of Pure Cu(II), Cu(II)- L-Phenylalanine (1:2) and (1:3) in aqueous solution at similar condition (Scan rate = 0.1V/s).
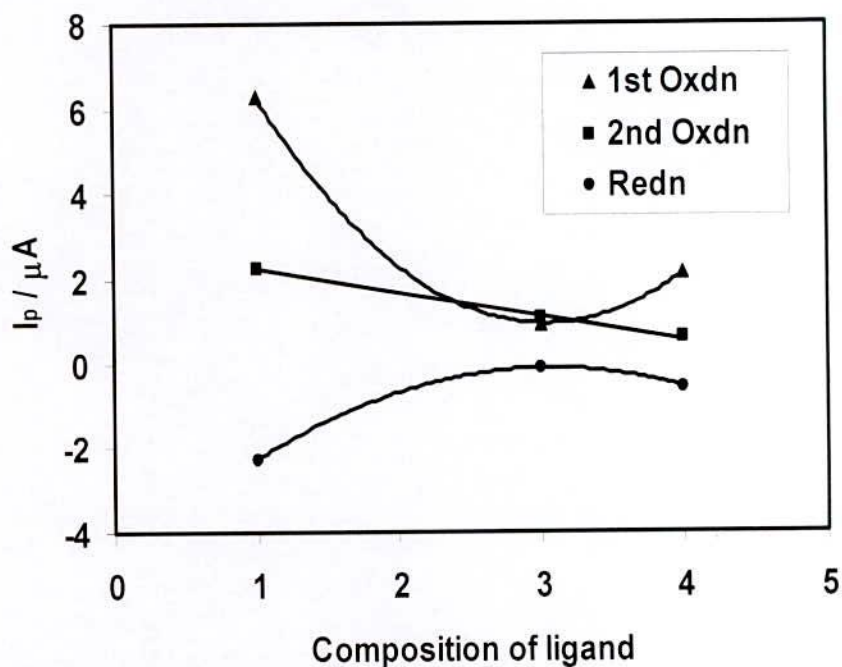
Figure 4.84: Plots of peak current versus composition of ligand of Pure Cu(II), Cu(II)- L-Phenylalanine (1:1), (1:2) and (1:3) at similar condition (Scan rate = 0.1V/s).
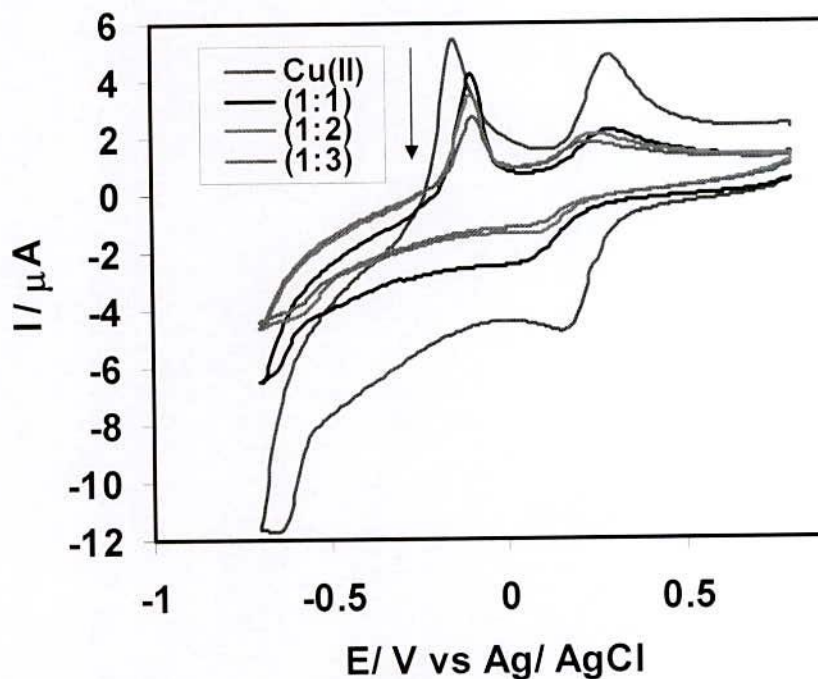
Figure 4.85 : Comparison of Cyclic voltammogram of Pure Cu(II), Cu(II)- L-Phenylalanine (1:1), (1:2) and (1:3) at similar condition (pH = 3.5, Scan rate = 0.1V/s).

Figure 4.86 : Comparison of Cyclic voltammogram of Pure Cu(II), Cu(II)- L-Phenylalanine (1:1), (1:2) and (1:3) at similar condition (pH = 4.5, Scan rate = 0.1V/s).

Figure 4.87 : Comparison of Cyclic voltammogram of Pure Cu(II), Cu(II)- L-Phenylalanine (1:1), (1:2) and (1:3) at similar condition (pH = 6.0, Scan rate = 0.1V/s).

Figure 4.88 : Plots of peak current versus composition of ligand of Pure Cu(II), Cu(II)- L-Phenylalanine (1:1), (1:2) and (1:3) at similar condition (pH = 3.5, Scan rate = 0.1V/s).
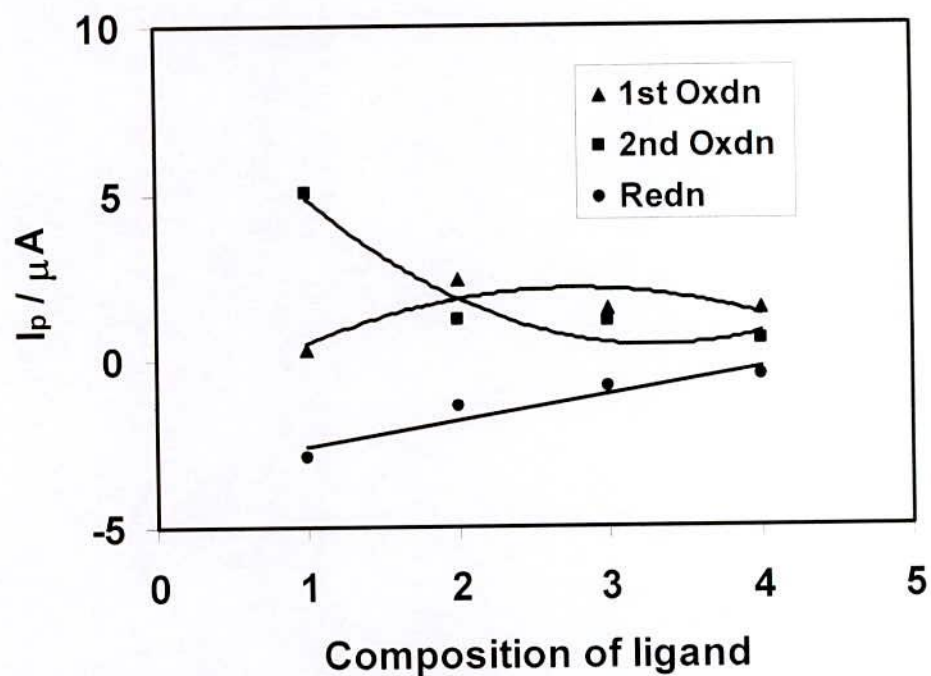
Figure 4.89 : Plots of peak current versus composition of ligand of Pure Cu(II), Cu(II)- L-Phenylalanine (1:1), (1:2) and (1:3) at similar condition (pH = 4.5, Scan rate = 0.1V/s).
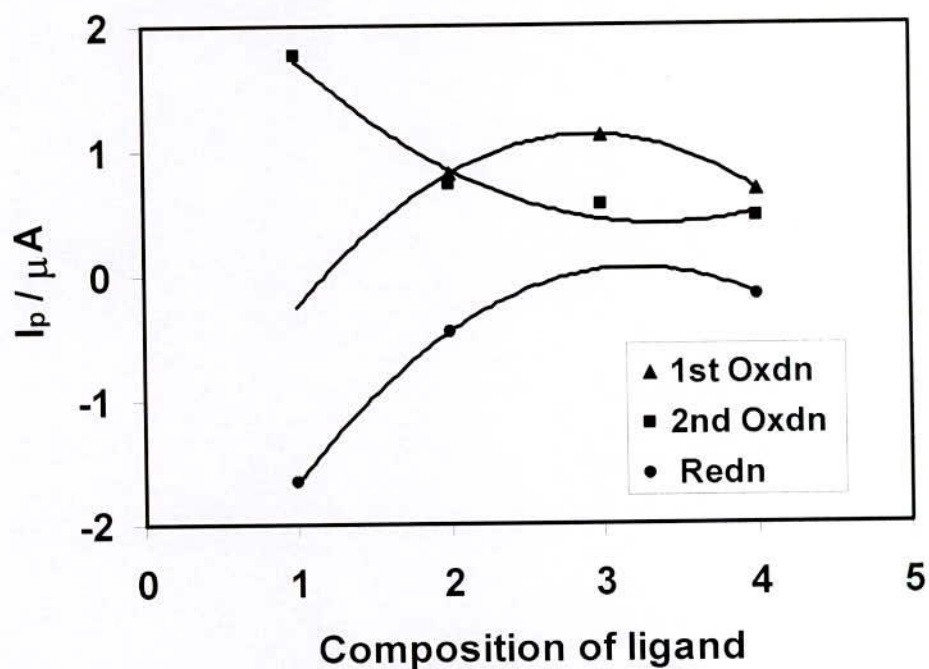
Figure 4.90 : Plots of peak current versus composition of ligand of Pure Cu(II), Cu(II)- L-Phenylalanine (1:1), (1:2) and (1:3) at similar condition (pH = 6.0, Scan rate = 0.1V/s).
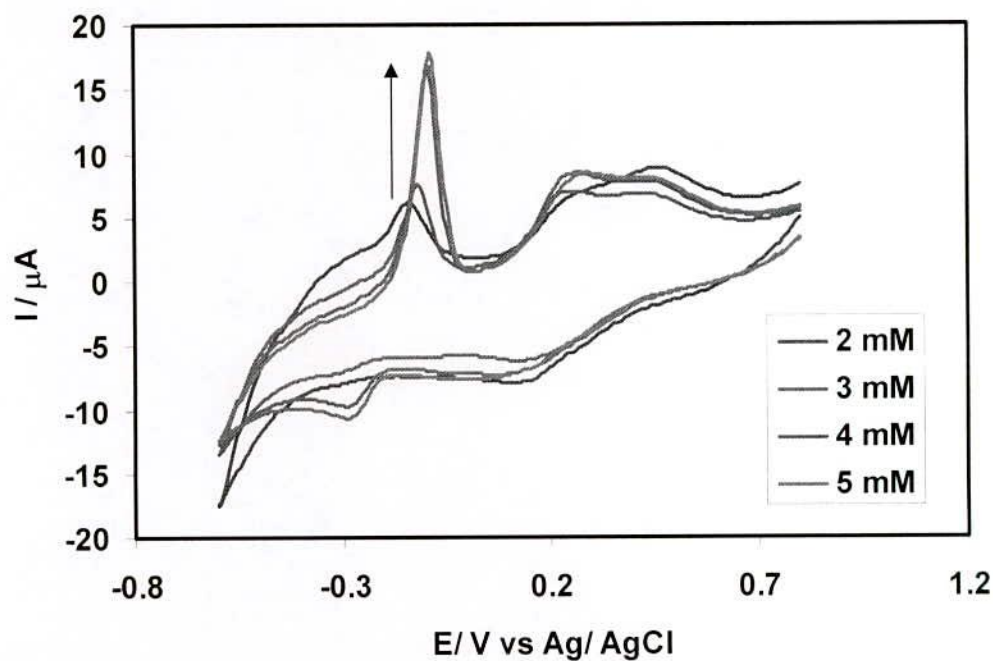
Figure 4.91 : Cyclic voltammogram of Cu(II) + L- Phenyl alanine (1:3 same concentration) in buffer solution (acetate buffer) pH = 3.5 at scan rate 0.1V/s.
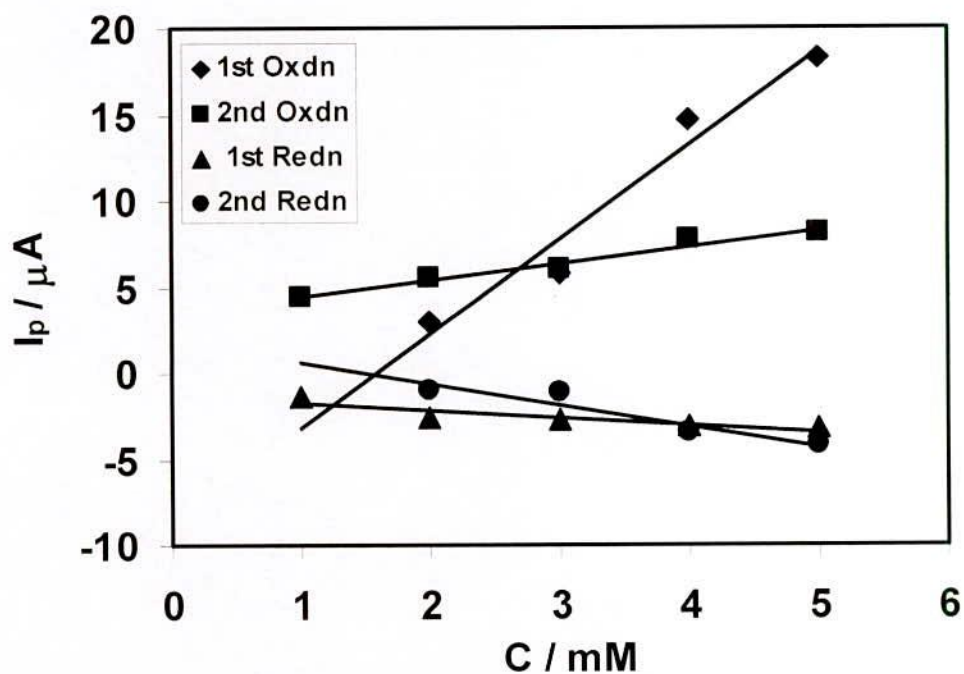
Figure 4.92 : Plots of peak current versus concentration of Cu(II) + L- Phenyl alanine (1:3 same concentration) in buffer solution (acetate buffer) pH = 3.5 at scan rate 0.1V/s.

151

Figure 4.93 : Comparison of Cyclic voltammogram of Pure Cu(II), Cu(II)-Aspartic acid(1:3), Cu(II)-L Phenyl alanine(1:3) at similar condition (Scan rate = 0.10V/s).
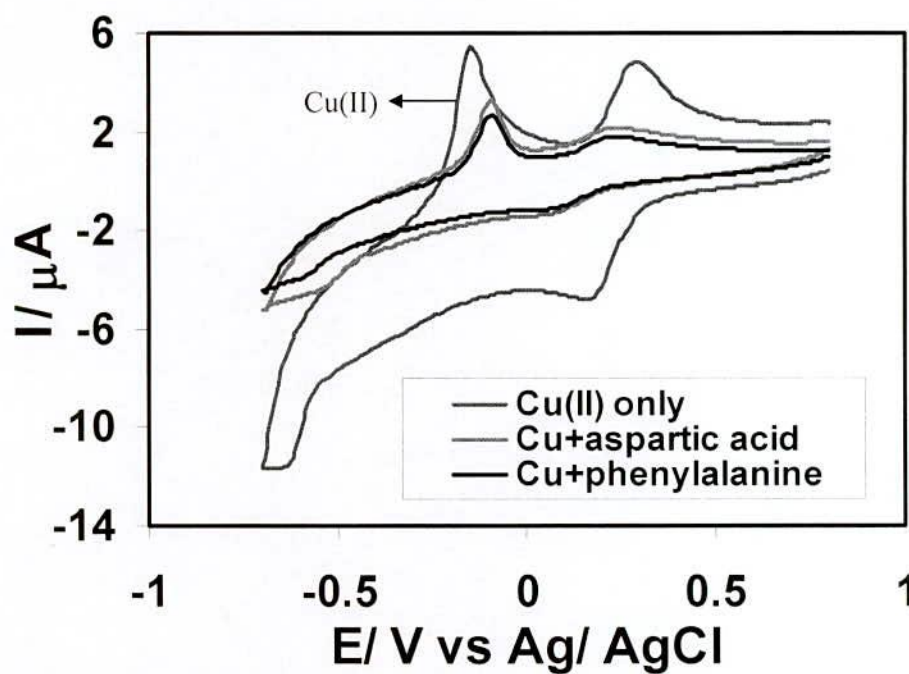
Figure 4.94 : Comparison of Cyclic voltammogram of Pure Cu(II), Cu(II)-Aspartic acid(1:3), Cu(II)-L Phenyl alanine(1:3) at similar condition (Scan rate = 0.10V/s, pH=3.5).
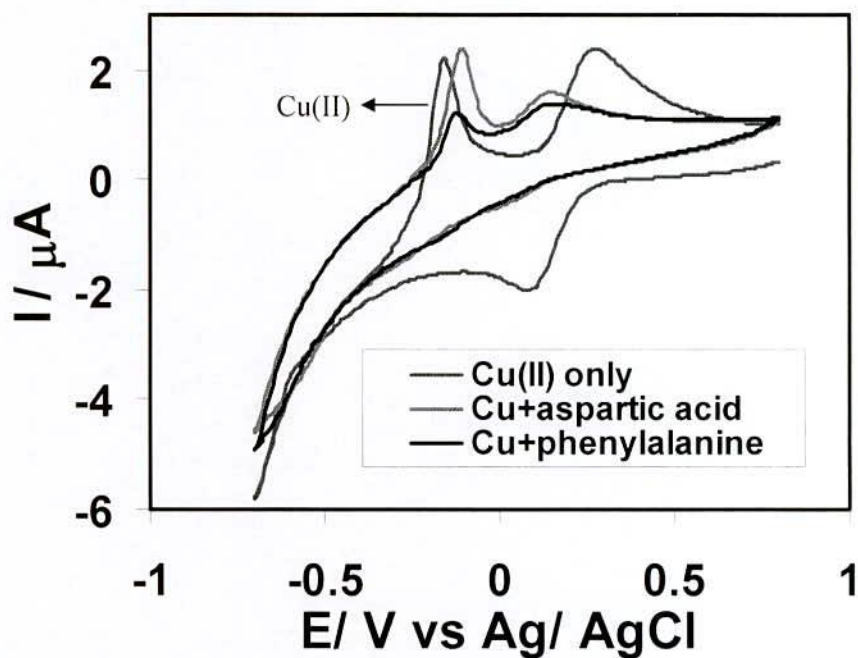
Figure 4.95 : Comparison of Cyclic voltammogram of Pure Cu(II), Cu(II)-Aspartic acid(1:3), Cu(II)-L Phenyl alanine(1:3) at similar condition (Scan rate = 0.10V/s, pH = 6.0).
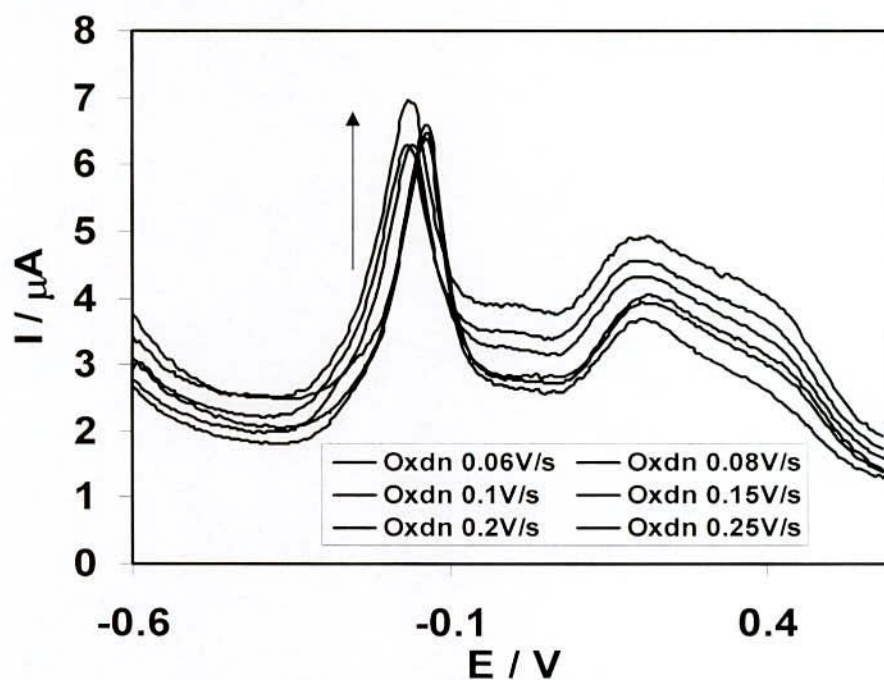
Figure 4.96 : Differential pulse voltammogram of Cu(II) + L- Phenyl alanine (1:3) in buffer solution (pH = 3.5) (acetate buffer) for forward direction (oxidation) at different scan rate using .
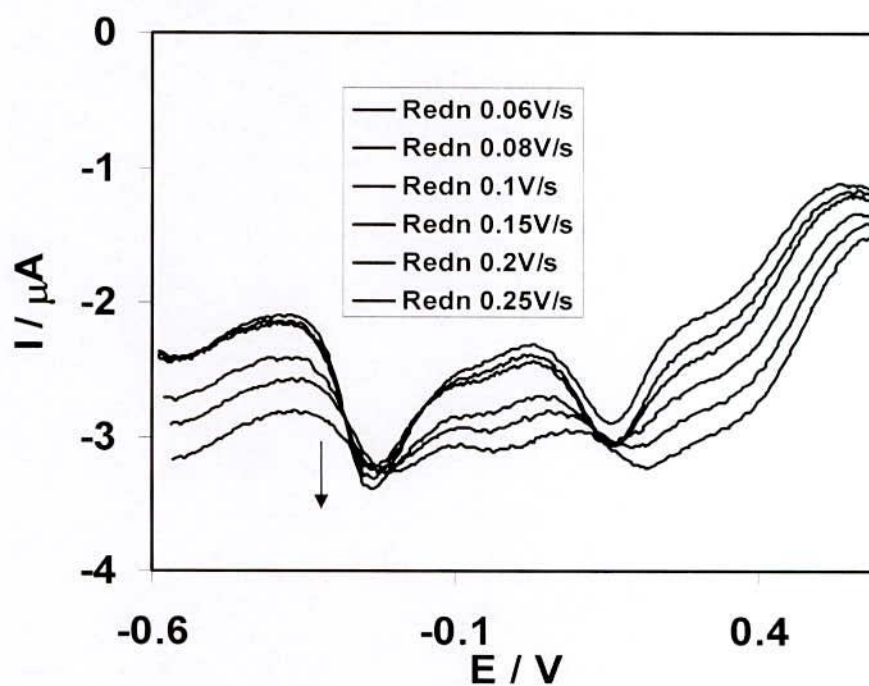
Figure 4.97 : Differential pulse voltammogram of Cu(II) + 3mM L- Phenyl alanine (1:3) in buffer solution (pH = 3.5) (acetate buffer) for backward direction (reduction) at different scan rate.
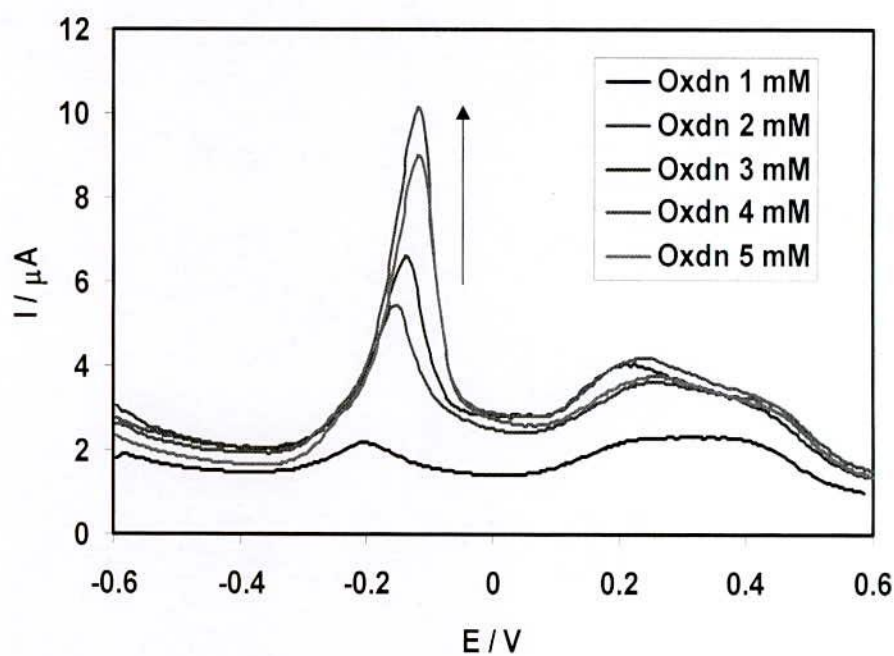
Figure 4.98 : Differential pulse voltammogram of Cu(II) + L- Phenyl alanine (1:3) in different concentration, buffer solution (pH = 3.5) (acetate buffer) for forward direction (oxidation) at scan rate 0.1V/s.
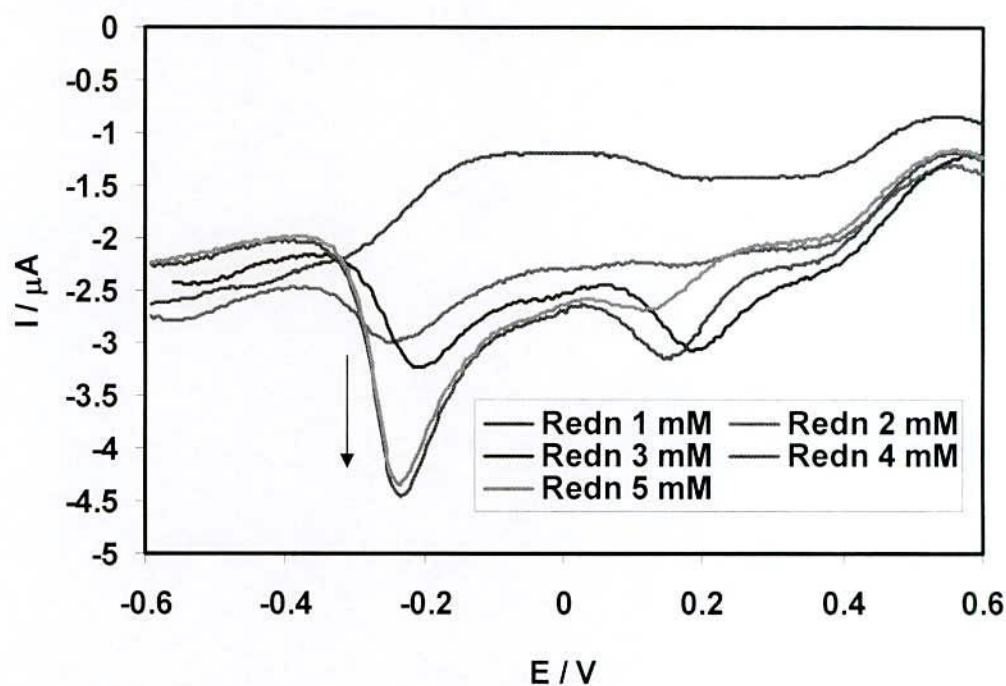
Figure 4.99 : Differential pulse voltammogram of Cu(II) + L- Phenyl alanine (1:3) in different concentration, buffer solution (pH = 3.5) (acetate buffer) for backward direction (reduction) at scan rate 0.1V/s.

Figure 4.100 : Chronoamperometry curve of $CuCl_2$ + L-Phenyl alanine (1:3) in buffer solution (pH= 3.5) (acetate buffer) for forward direction (oxidation) in different concentration at steping potential 0.4V.

155

Figure 4.101 : Cottrell plots of the back ground subtracted currents for $CuCl_2$ + L- Phenyl alanine (1:3) in different concentration, buffer solution (pH = 3.5) (acetate buffer) when the potential was stepped from -0.3 to 0.4V
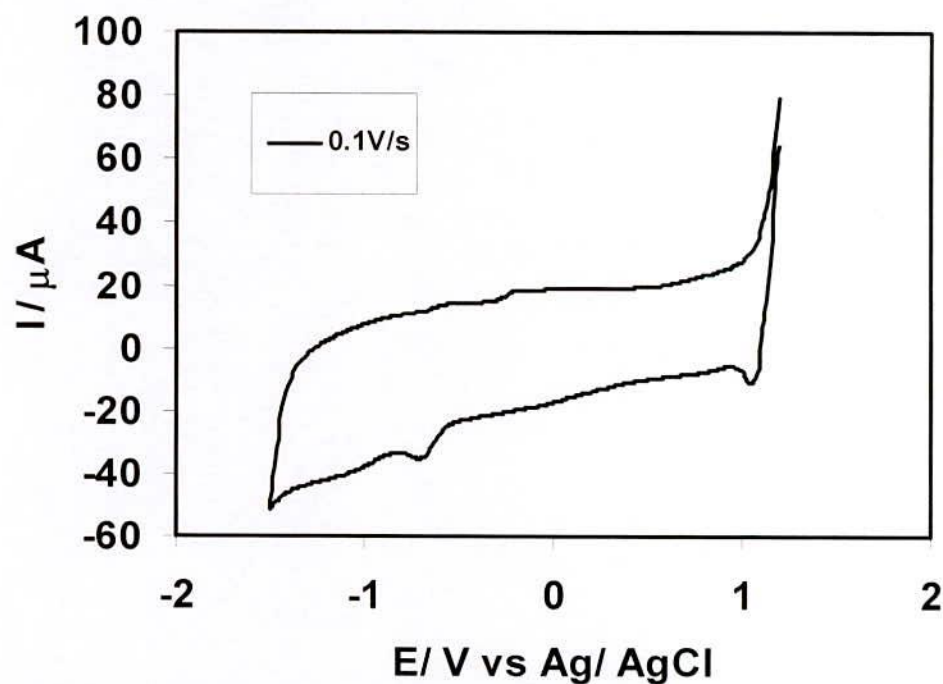
Figure 4.102 : Cyclic voltammogram of 3-Nitro benzene sulfonate only in buffer solution pH = 7.0 at scan rate 0.1V/s.
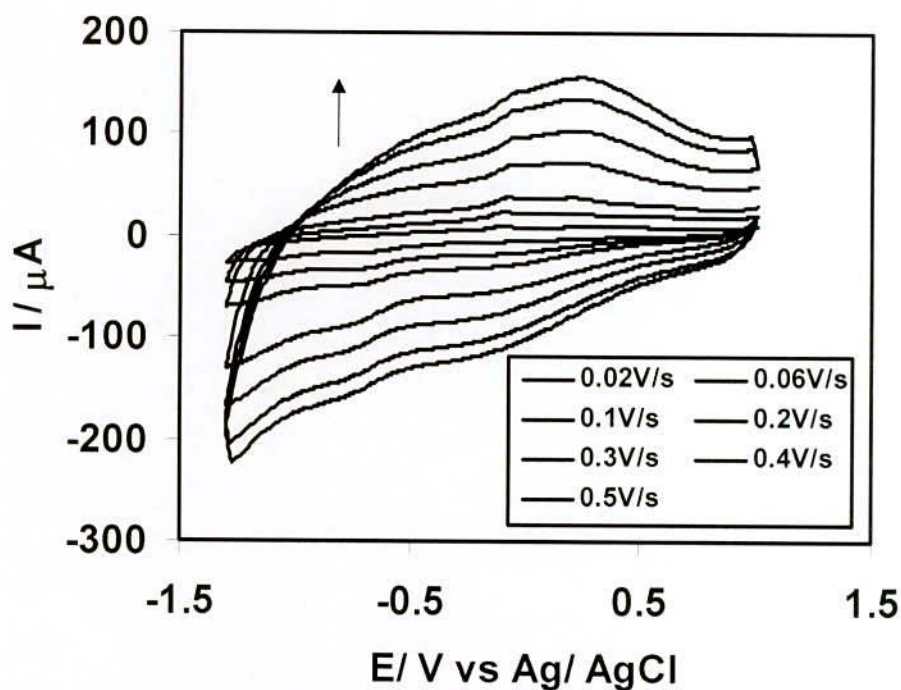
Figure 4.103 : Cyclic voltammogram of 2mM Cu(II) + 6mM 3-Nitro benzene sulfonate (1:3) in buffer solution (pH = 3.5) at different scan rate.
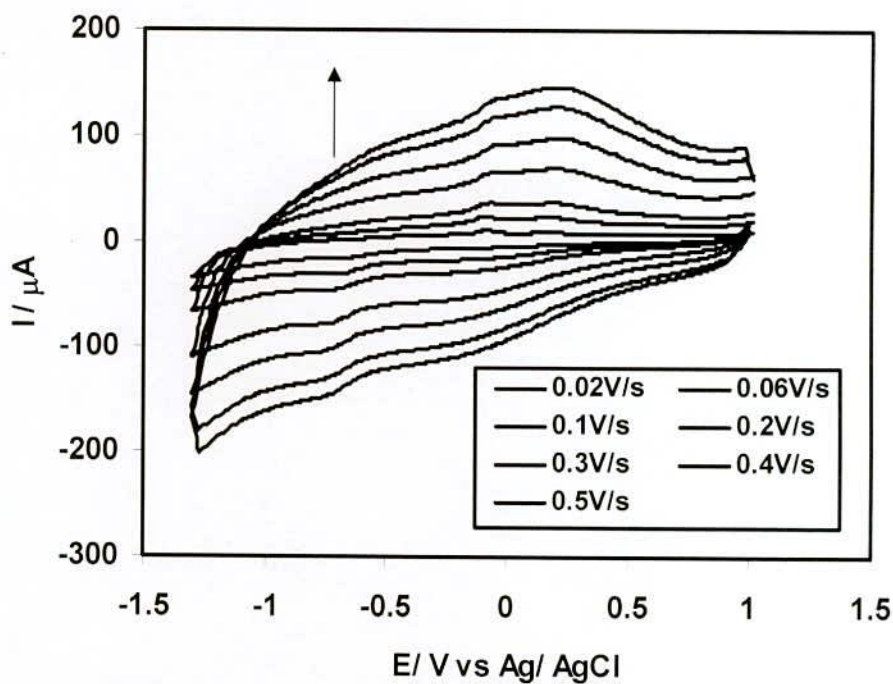
Figure 4.104 : Cyclic voltammogram of 2mM Cu(II) + 6mM 3-Nitro benzene sulfonate (1:3) in buffer solution (pH = 4.5) at different scan rate.

157
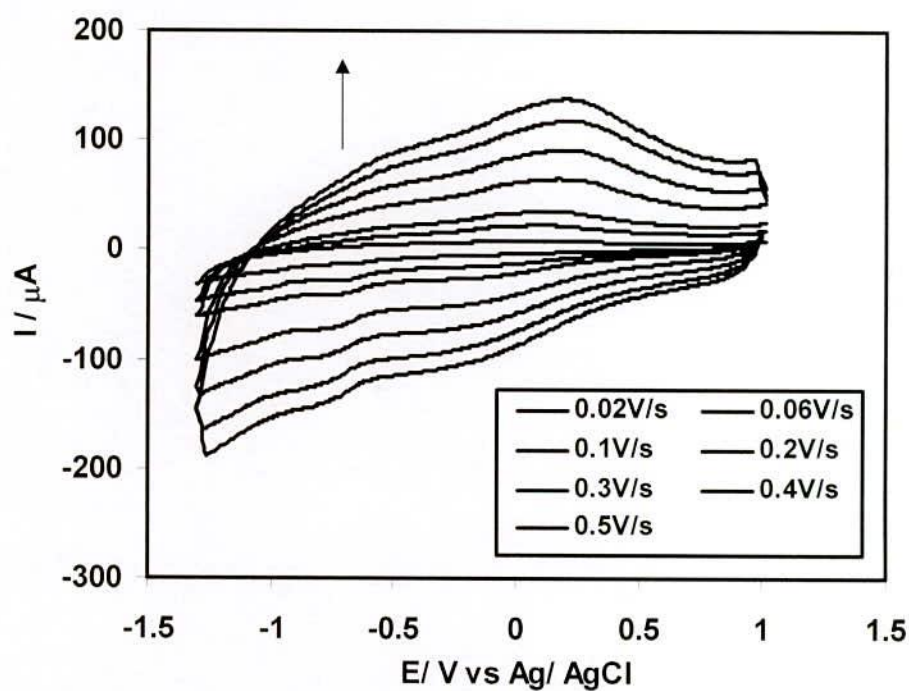
Figure 4.105 : Cyclic voltammogram of 2mM Cu(II) + 6mM 3-Nitro benzene sulfonate (1:3) in buffer solution (pH = 6.0) at different scan rate.

Figure 4.106 : Plots of peak current versus square root of scan rate of 2mM $CuCl_2$ + 6mM 3-Nitro benzene sulfonate (1:3) in buffer solution (pH = 3.5).

Figure 4.107 : Plots of peak current versus square root of scan rate of 2mM CuCl$_2$ + 6mM 3-Nitro benzene sulfonate (1:3) in buffer solution (pH = 4.5).
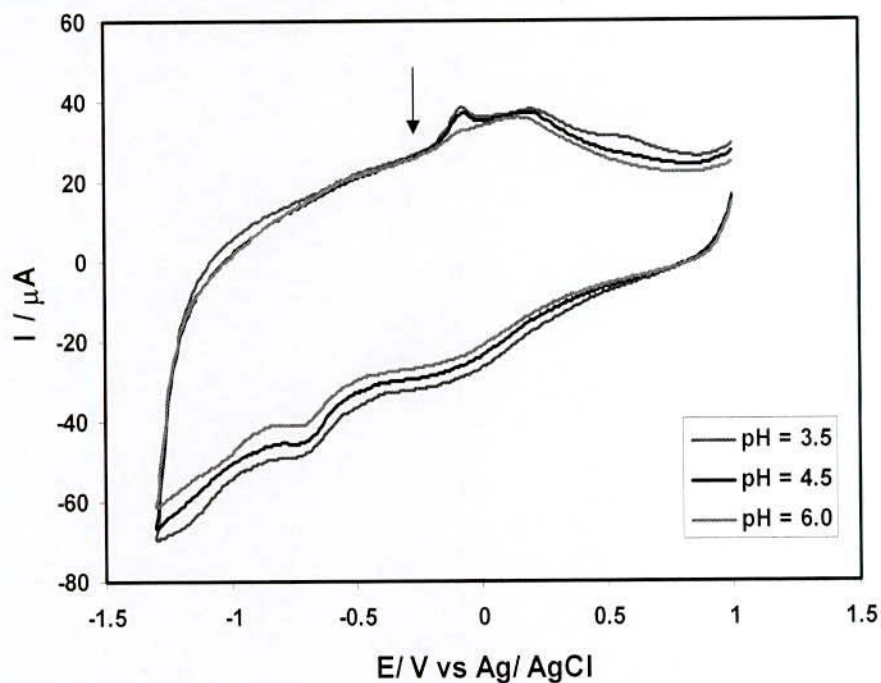
Figure 4.108 : Comparison of Cyclic voltammogram of Cu(II)- 3-Nitro benzene Sulphonate in different pH at similar condition (Scan rate = 0.1V/s).

159

Figure 4.109 : Plots of peak current versus versus pH (3.5, 4.5, 6.0) of Cu(II)- 3-Nitro benzene Sulphonate at similar condition (Scan rate = 0.1V/s).

Figure 4.110 : Plots of peak potential (E/V) versus pH (3.5, 4.5, 6.0) of Cu(II)- 3-Nitro benzene Sulphonate at similar condition (Scan rate = 0.1V/s).
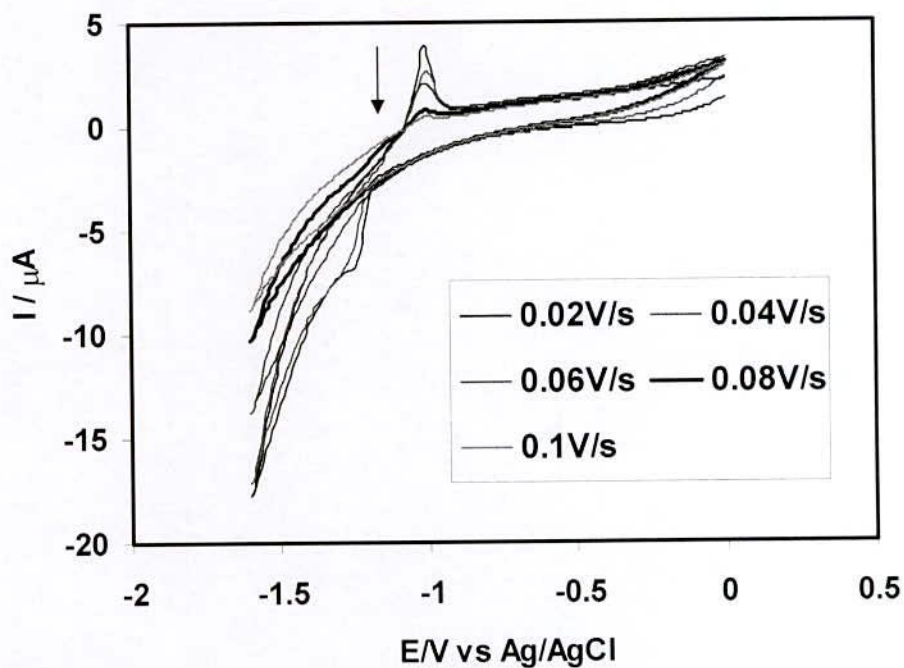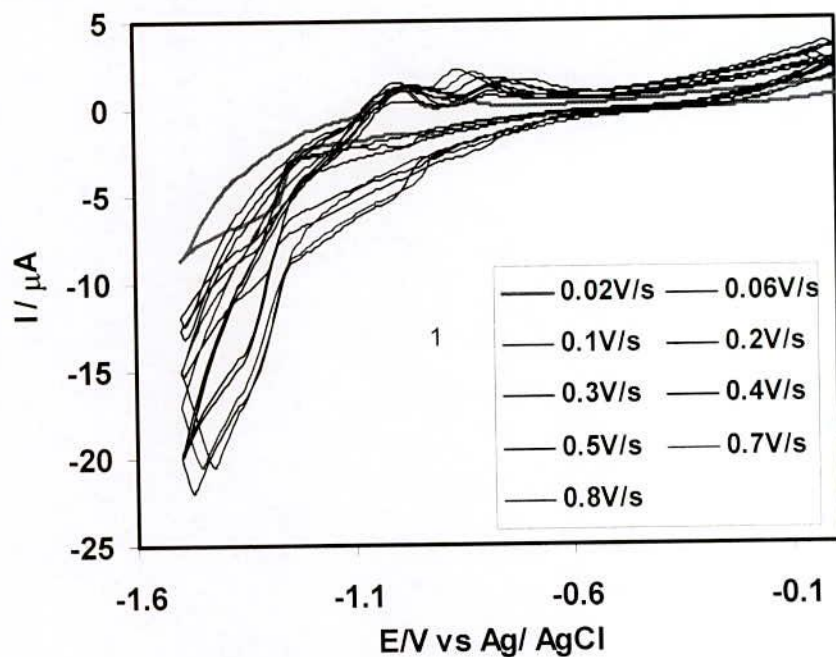
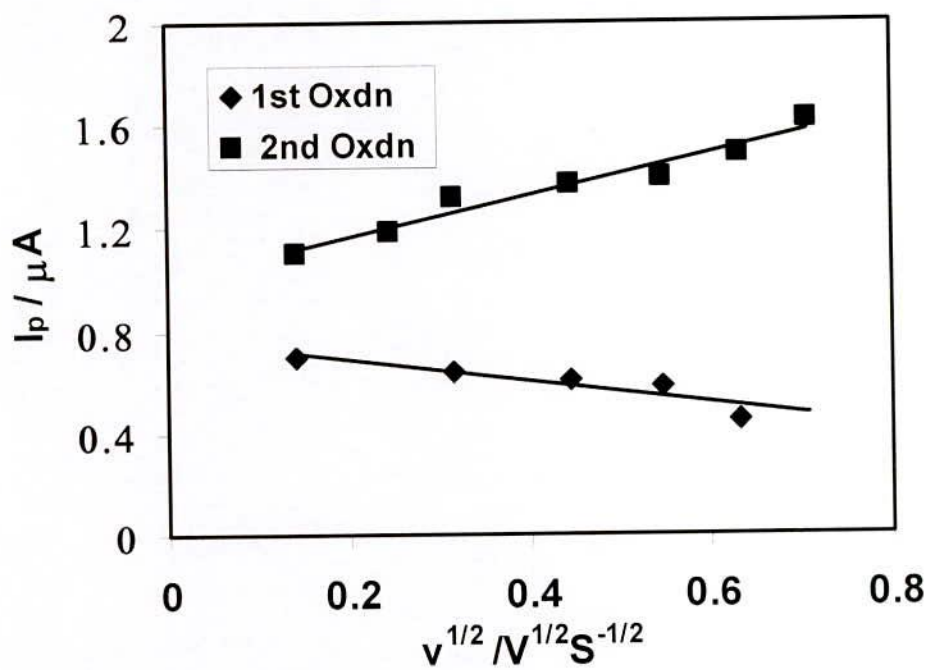Figure 4.111 : Cyclic voltammogram of 2mM Zn(II) in aqueous solution at different scan rate.
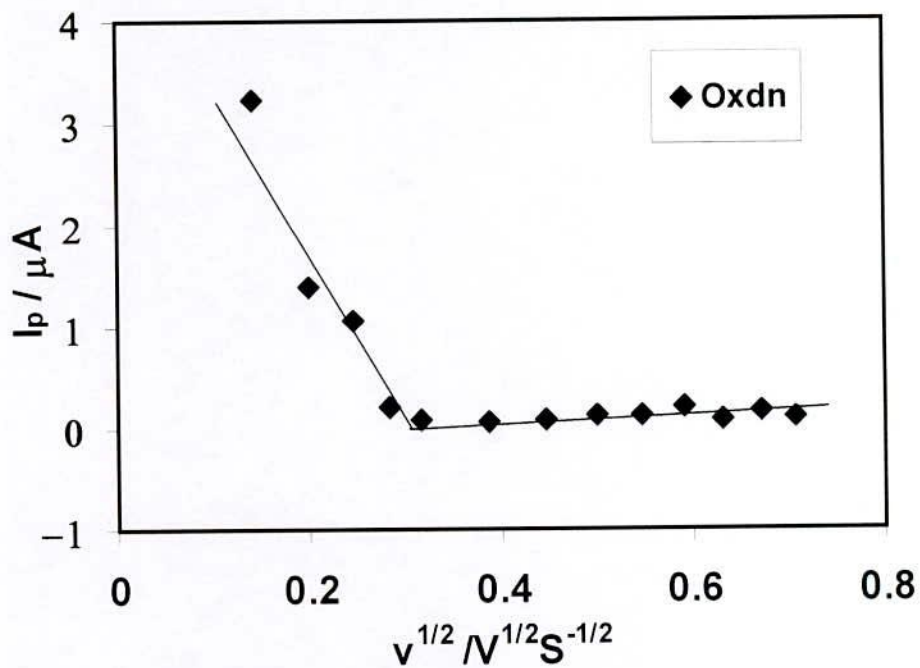
Figure 4.112 : Plots of peak current versus square root of scan rate of 2mM Zn(II) in aqueous solution.
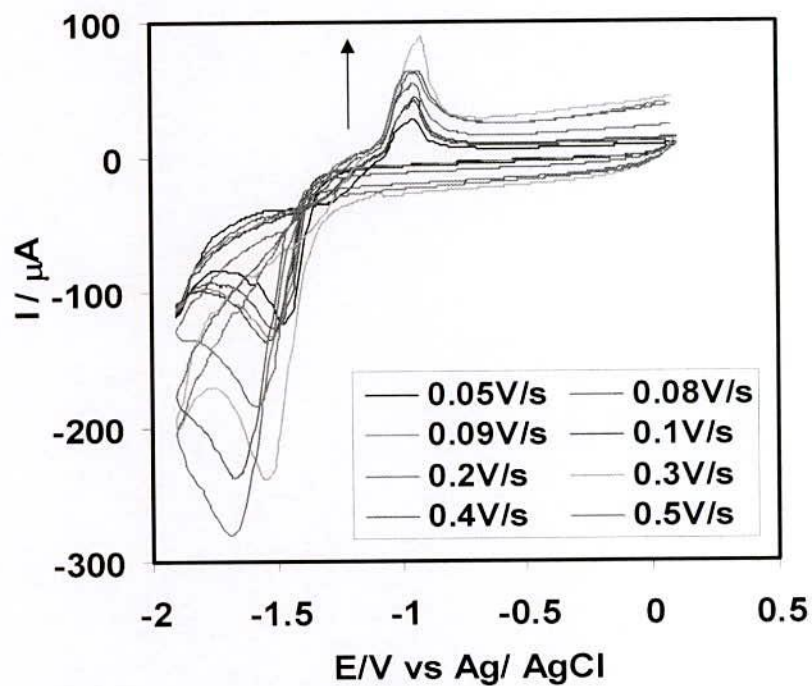
Figure 4.113 : Cyclic voltammogram of 2mM Zn(II) in buffer solution (pH = 1.5) (KCl + HCl buffer) at different scan rate.
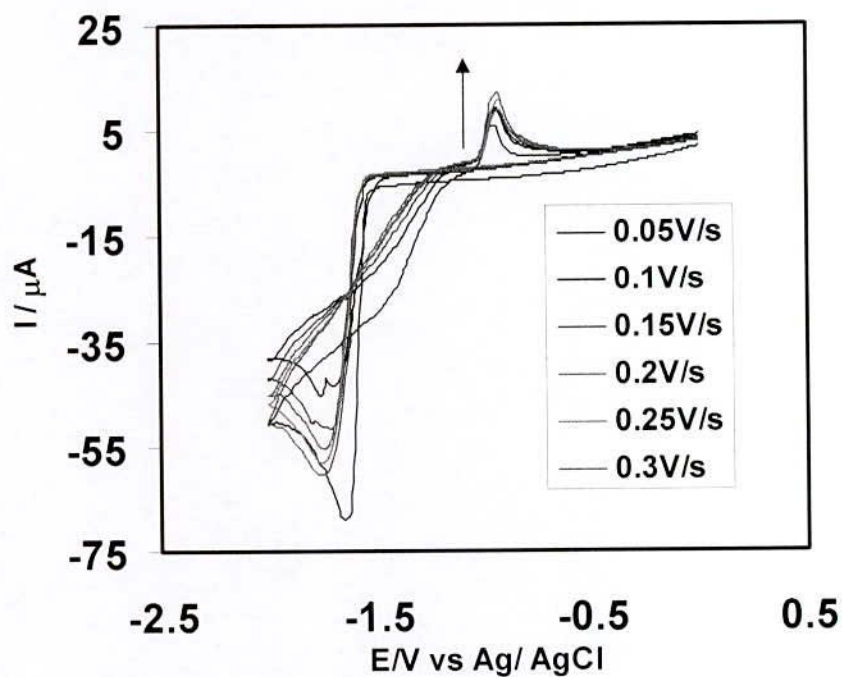
Figure 4.114 : Cyclic voltammogram of 2mM Zn(II) in buffer solution (pH = 2.0) (KCl + HCl buffer) at different scan rate.

162
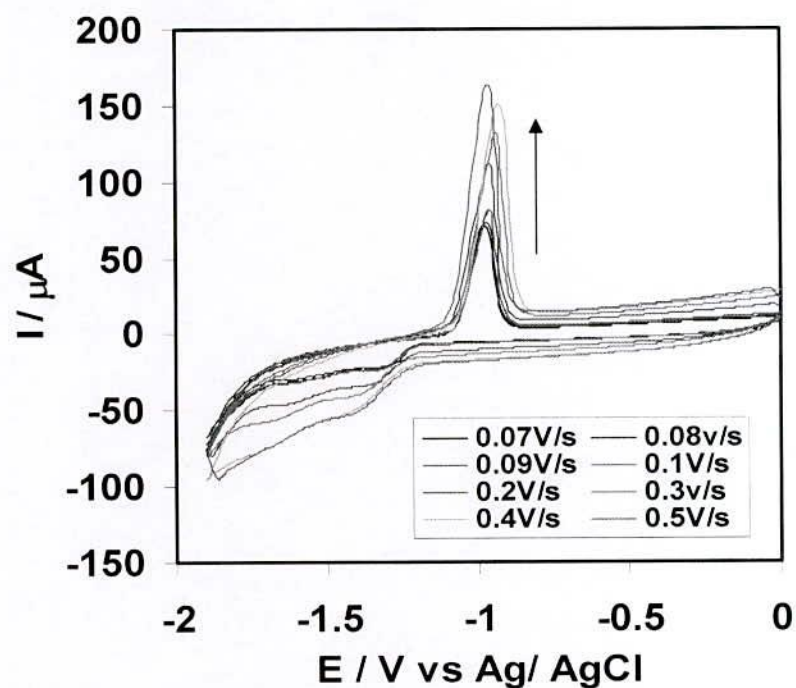
Figure 4.115 : Cyclic voltammogram of 2mM Zn(II) in buffer solution (pH = 4.5) (Acetate buffer) at different scan rate.
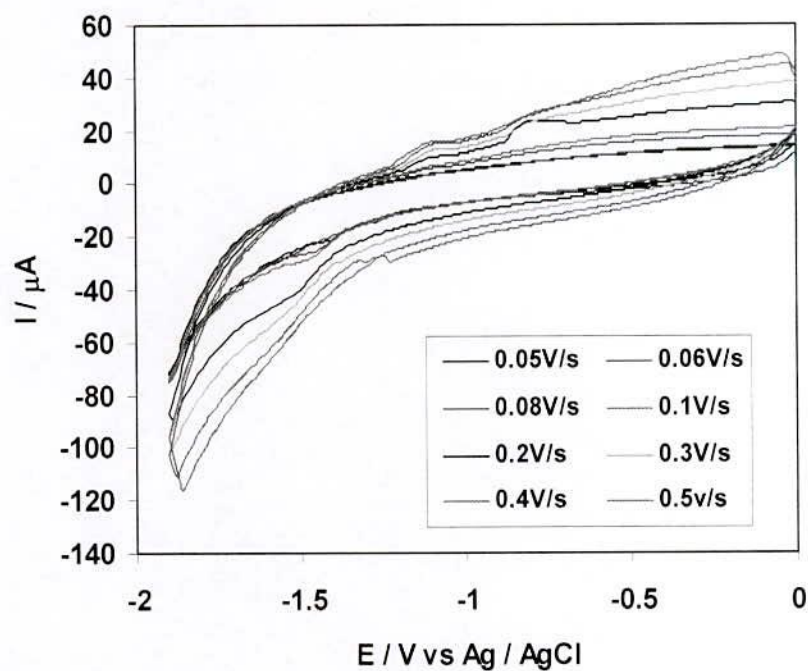
Figure 4.116 :   Cyclic voltammogram of 2mM Zn(II) in buffer solution (pH = 7.0) at different scan rate.

163
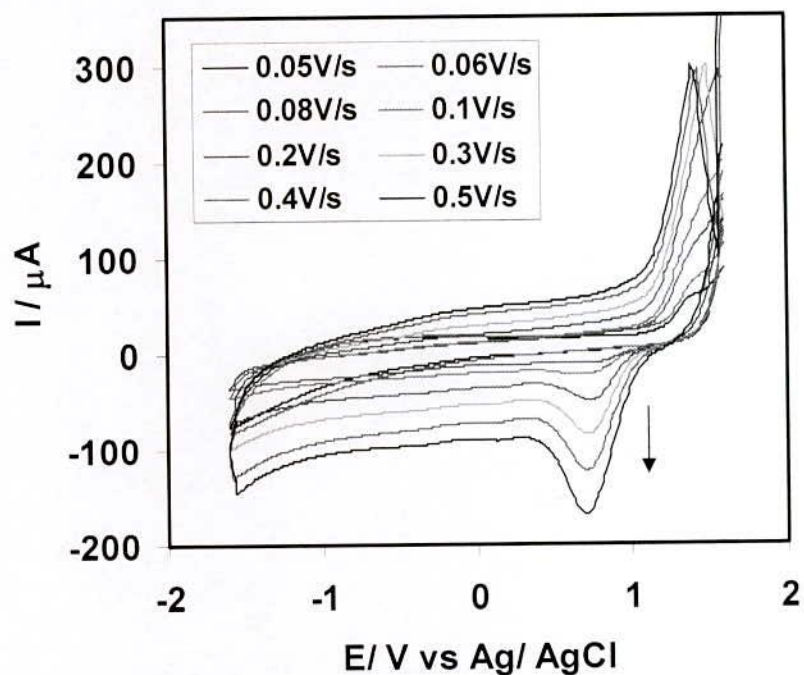
Figure 4.117 : Cyclic voltammogram of 2mM Zn(II) in buffer solution (pH = 11.0)   at different scan rate.
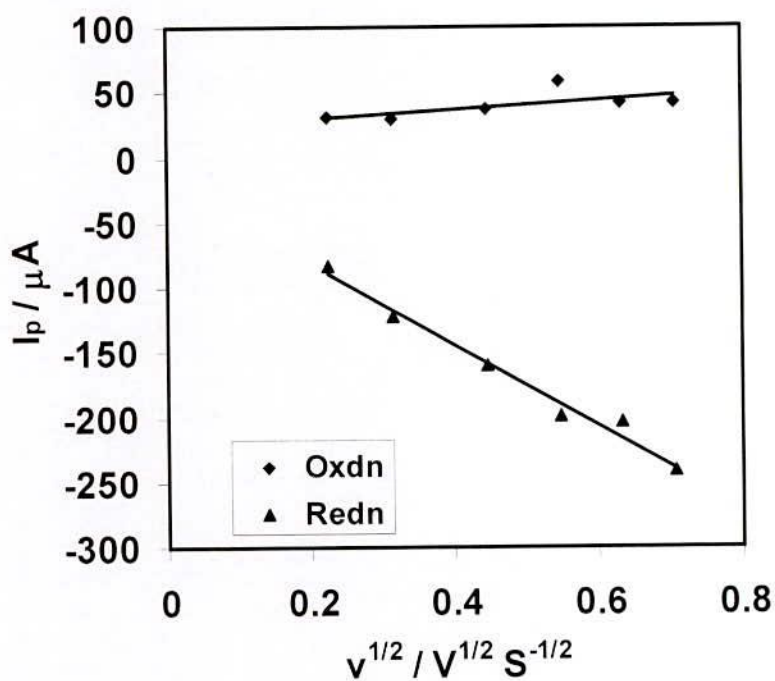
Figure 4.118 : Plots of peak current versus square root of scan rate of 2mM $ZnCl_2$ in buffer solution (pH = 1.5) (KCl + HCl buffer).
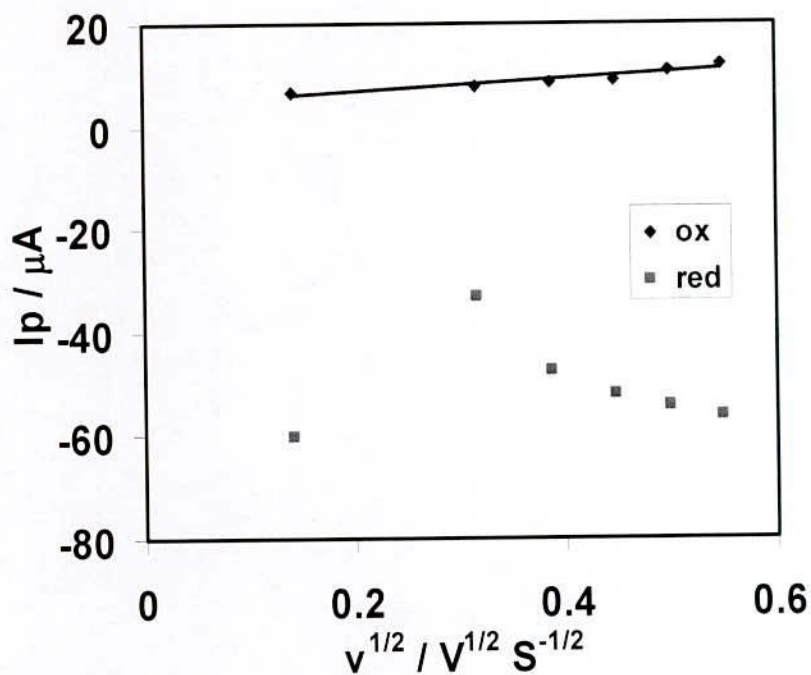
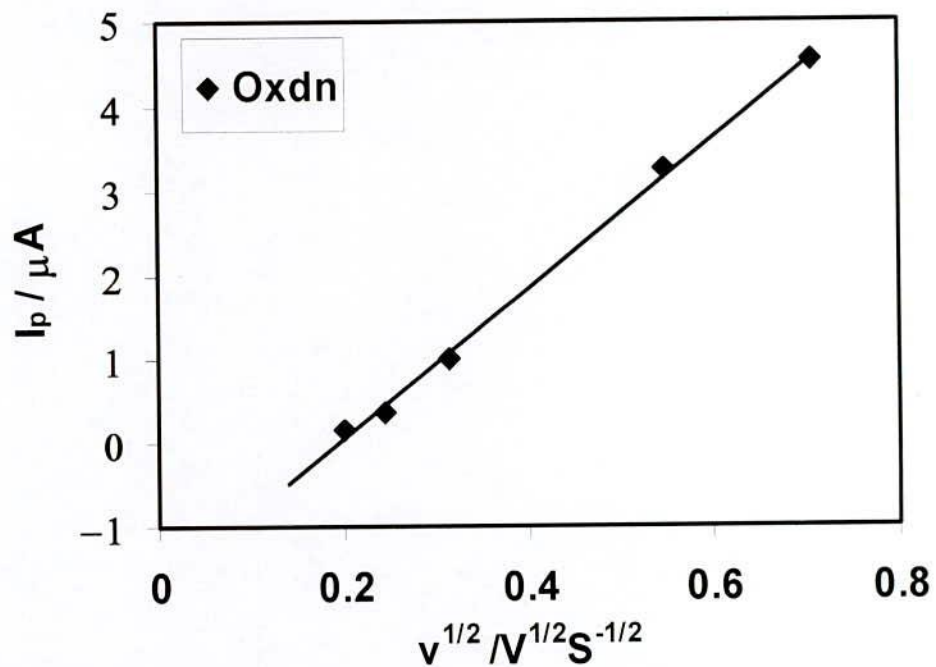Figure 4.119 : Plots of peak current versus square root of scan rate of 2mM Zn(II) in buffer solution (pH = 2.0) (KCl + HCl buffer).
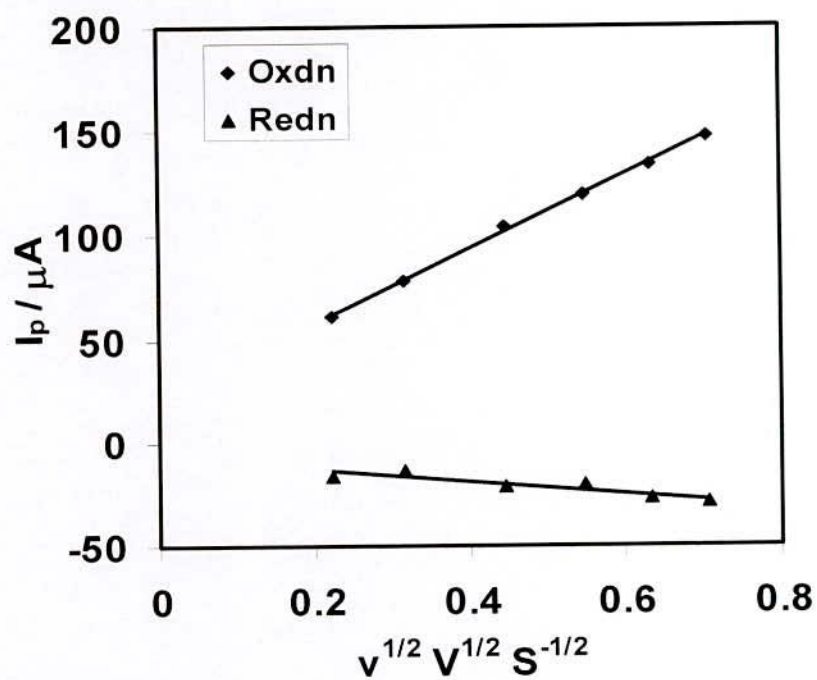
Figure 4.120 : Plots of peak current versus square root of scan rate of 2mM Zn(II) in buffer solution (pH = 4.5) (Acetate buffer).

165
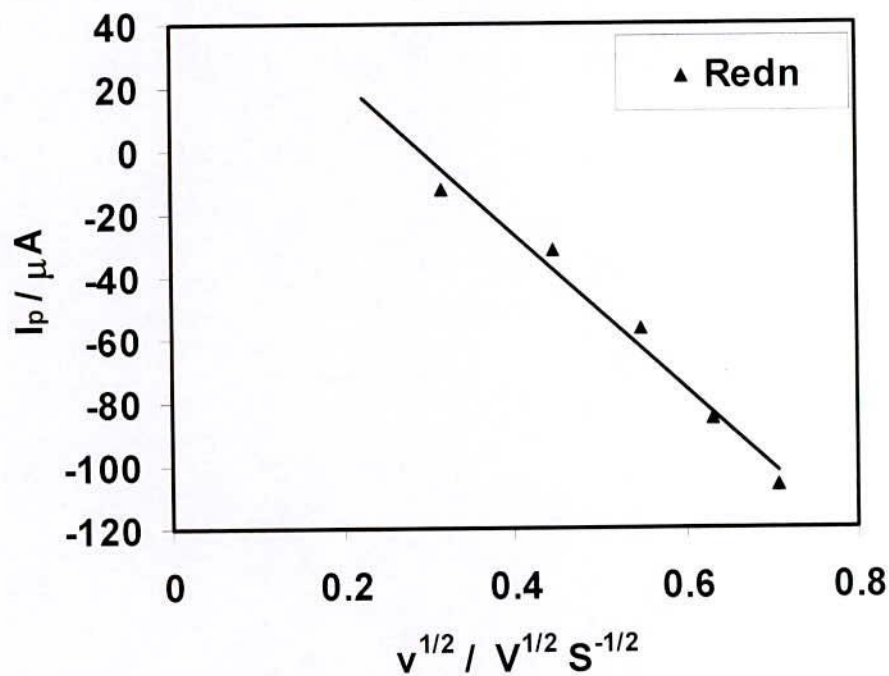
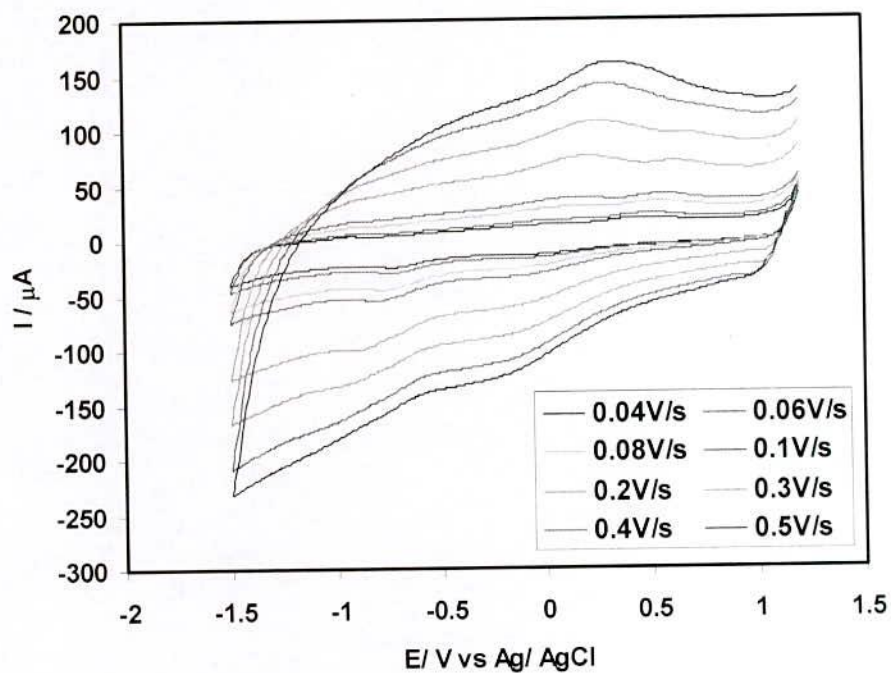Figure 4.121 : Plots of peak current versus square root of scan rate of 2mM Zn(II) in buffer solution (pH = 11.0).
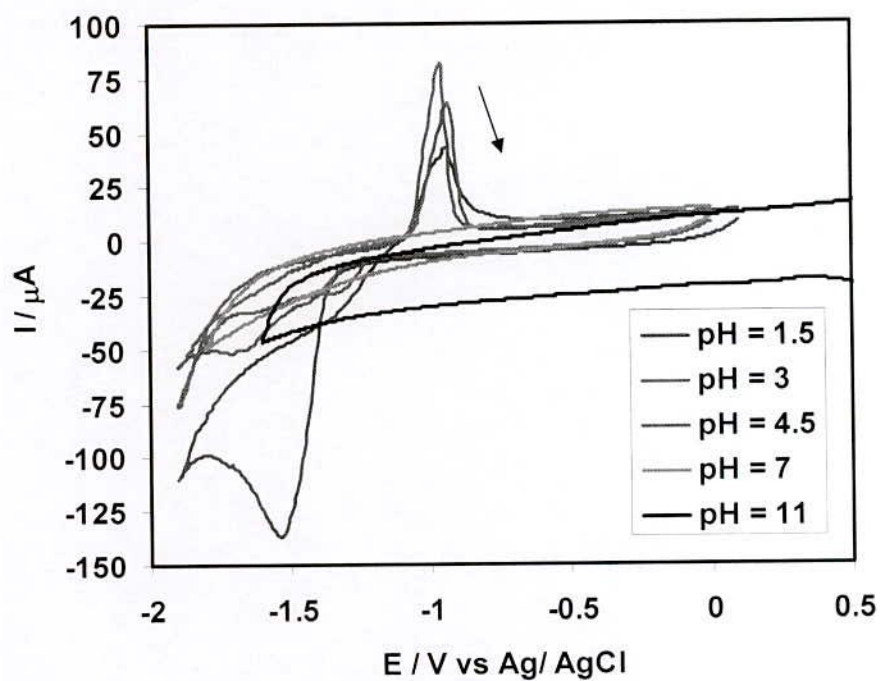
Figure 4.122 : Cyclic voltammogram of 2mM $ZnCl_2$ in buffer solution (pH = 1.5, 3, 4.5, 7 and 11) at scan rate $0.1 Vs^{-1}$.
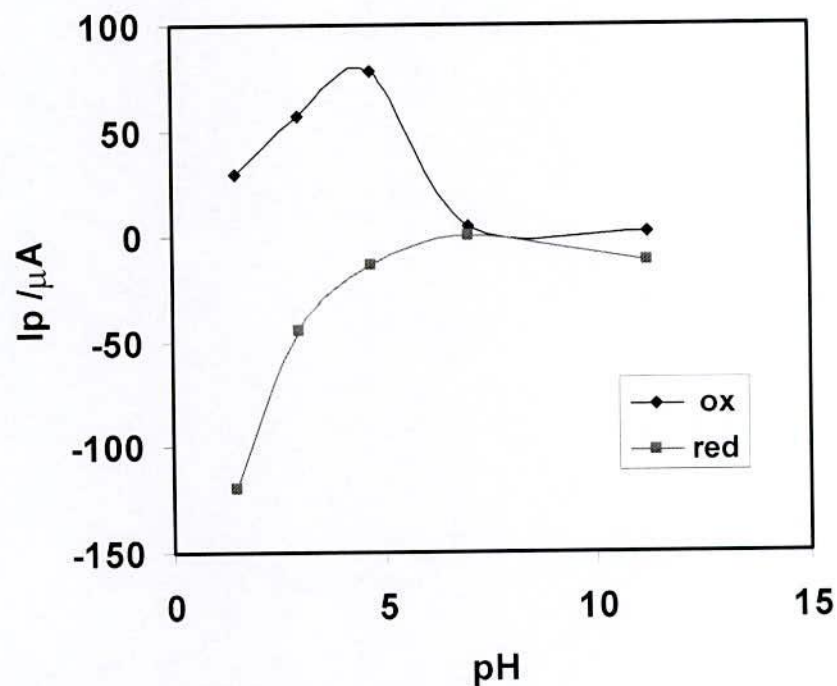
Figure 4.123 : Plots of peak current vs pH of 2mM $ZnCl_2$ in buffer solution (pH = 1.5, 3, 4.5, 7 and 11) at scan rate $0.1Vs^{-1}$.
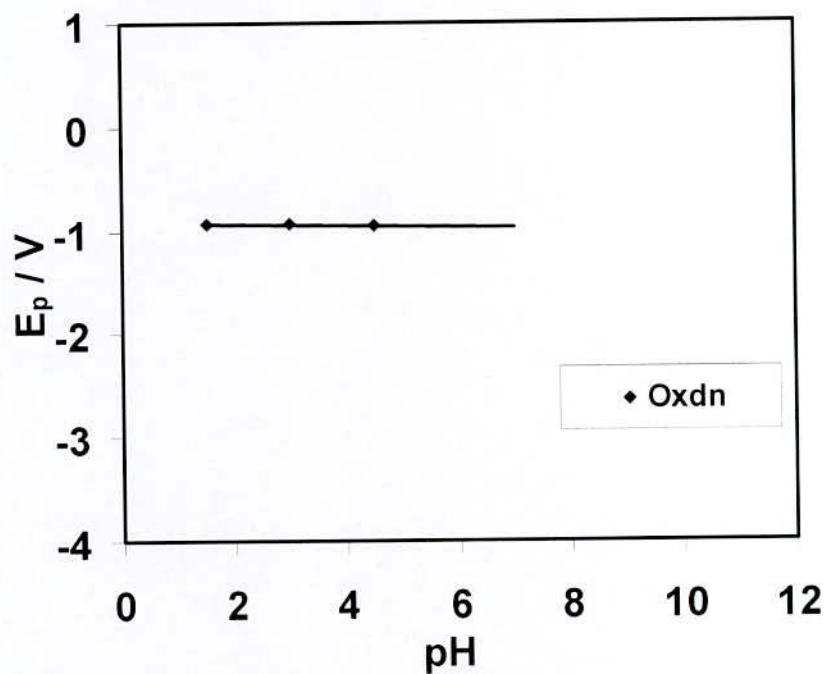
Figure 4.124 : Plots of peak potential vs pH of 2mM $ZnCl_2$ in buffer solution (pH = 1.5, 3, 4.7 and 11.2) at scan rate $0.1Vs^{-1}$.

167
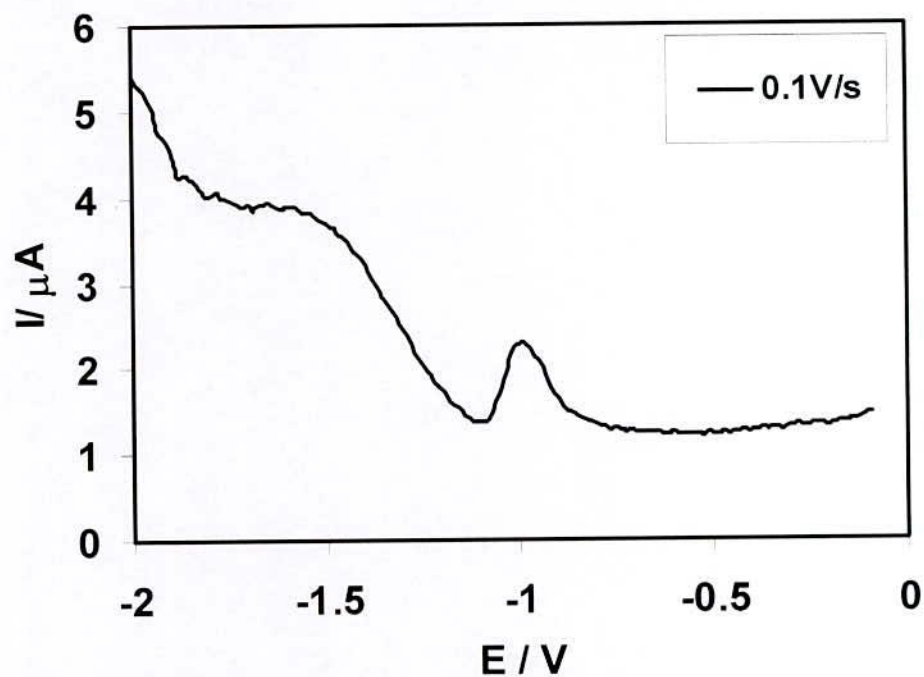
Figure 4.125 : Differential pulse voltammogram of 2mM $ZnCl_2$ in aqueous solution for forward direction (oxidation) at different scan rate.
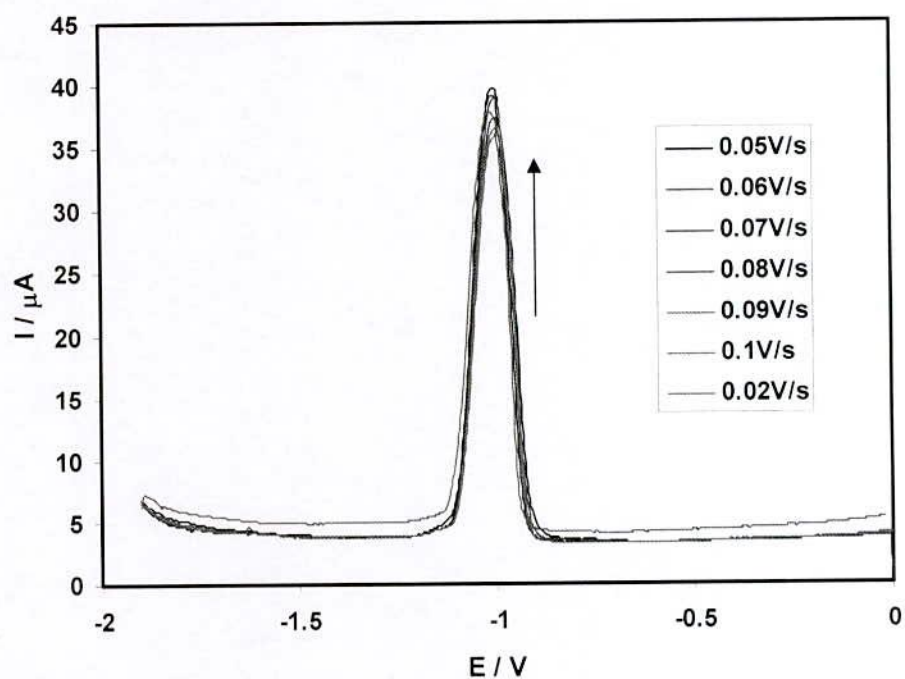
Figure 4.126 : Differential pulse voltammogram of 2mM Zn(II) only in buffer solution (pH = 4.5) (acetate buffer) at E_{puls} 0.02 V, t_{puls}= 20ms and scan rate 0.1V/s.
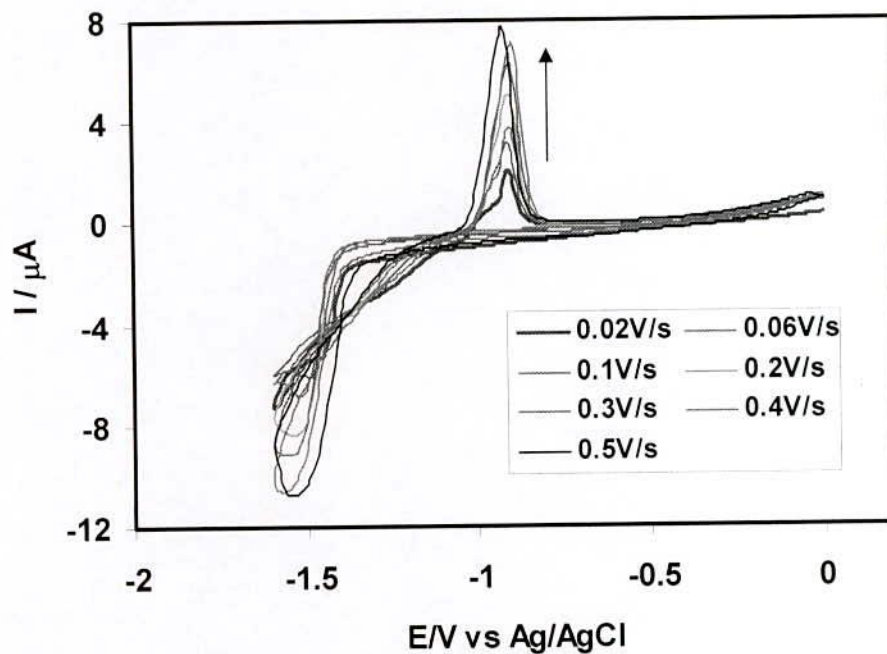
Figure 4.127 : Cyclic voltammogram of 2mM Zn(II) + 6mM aspartic acid (1:3) in aqueous solution at different scan rate.
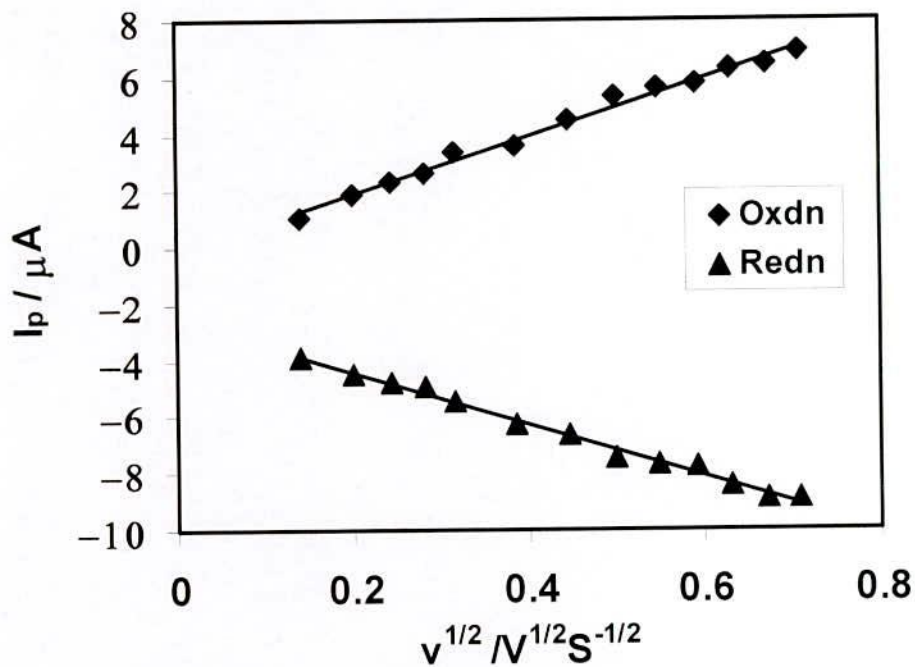
Figure 4.128 : Plots of peak current versus square root of scan rate of 2mM Zn(II) + 6mM aspartic acid (1:3) in aqueous solution.
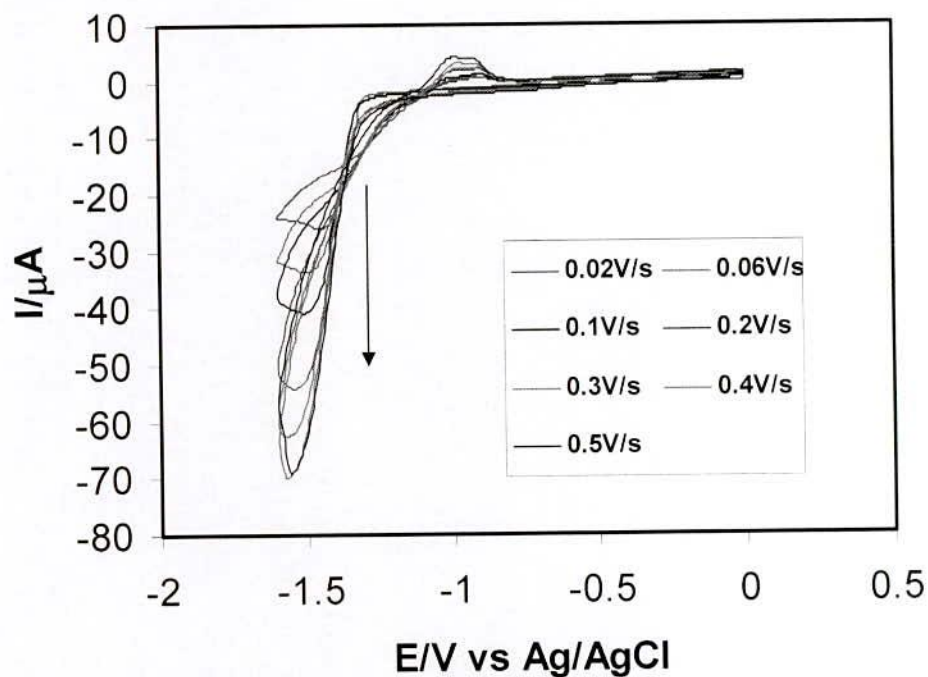
Figure 4.129 : Cyclic voltammogram of 2mM Zn(II) + 6mM aspartic acid (1:3) in buffer solution (pH = 3.5) (acetate buffer) at different scan rate.
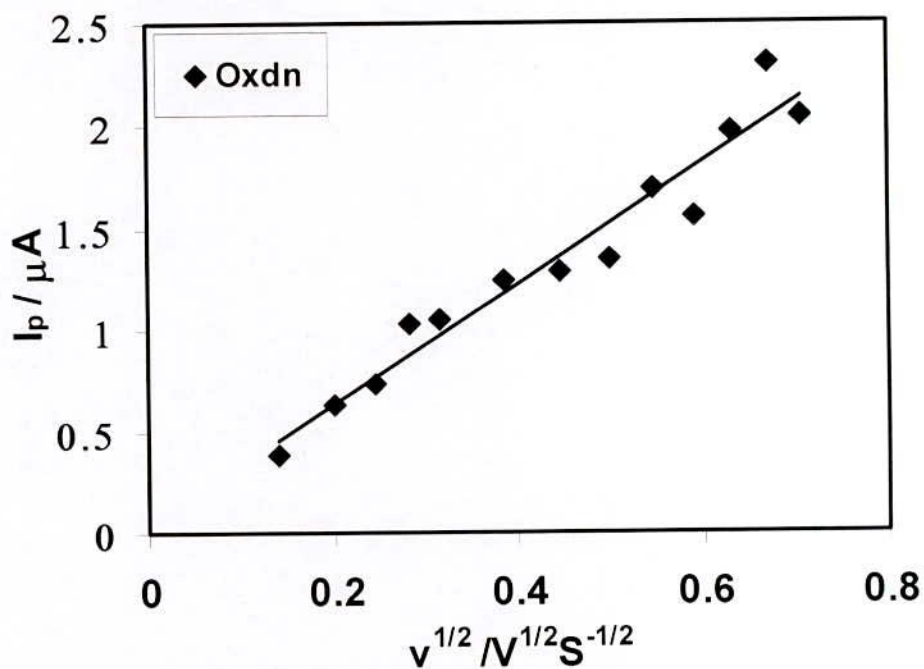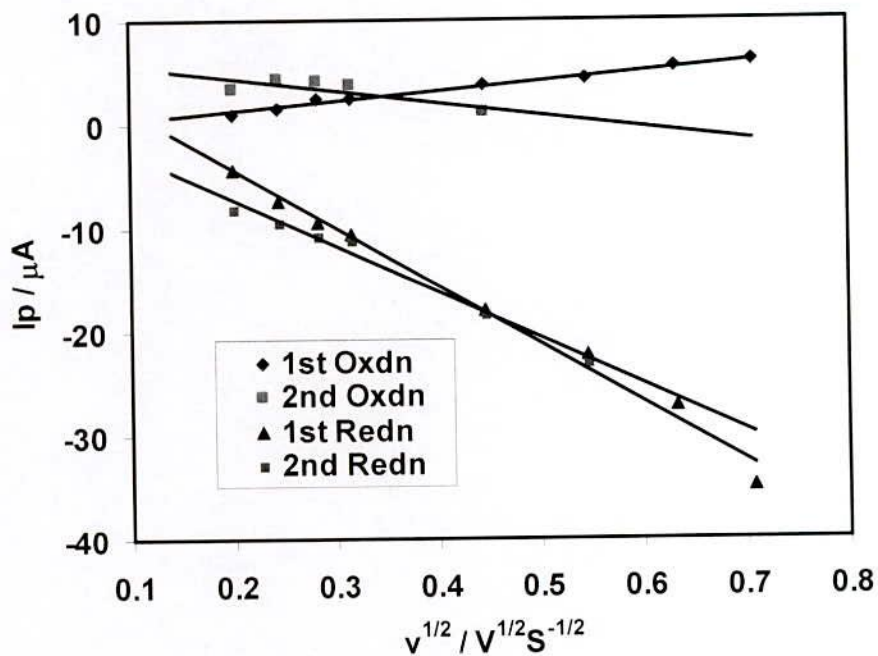

Figure 4.130 : Plots of peak current versus square root of scan rate of 2mM Zn(II) + 6mM aspartic acid (1:3) in buffer solution (pH = 3.5) (acetate buffer).
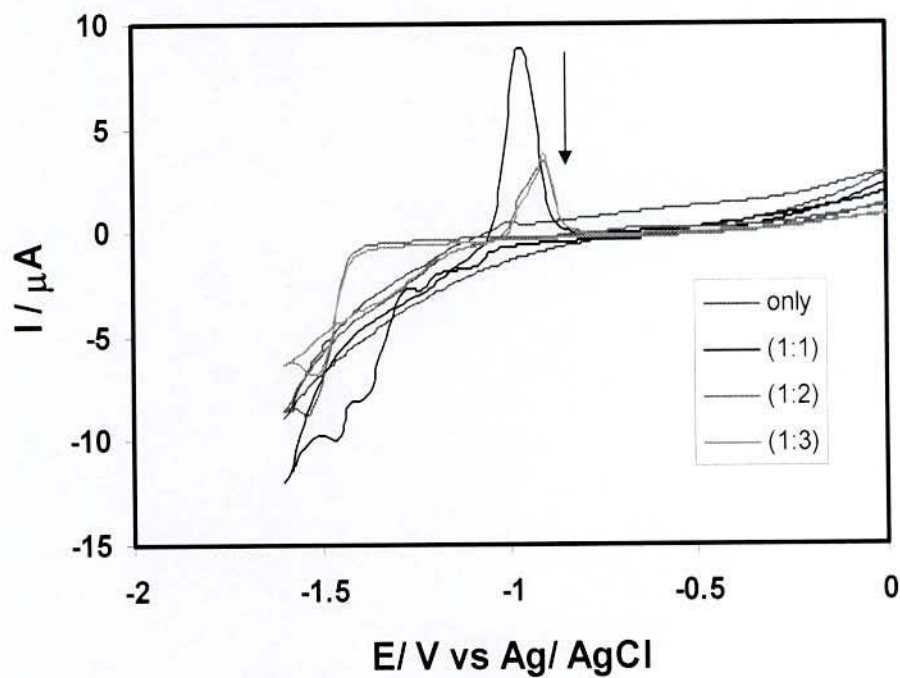
Figure 4.131 : Comparison of Zn(II) and Zn(II)-Aspartic acid(1:1), (1:2), (1:3), at scan rate 0.1V/s in aqueous solution.
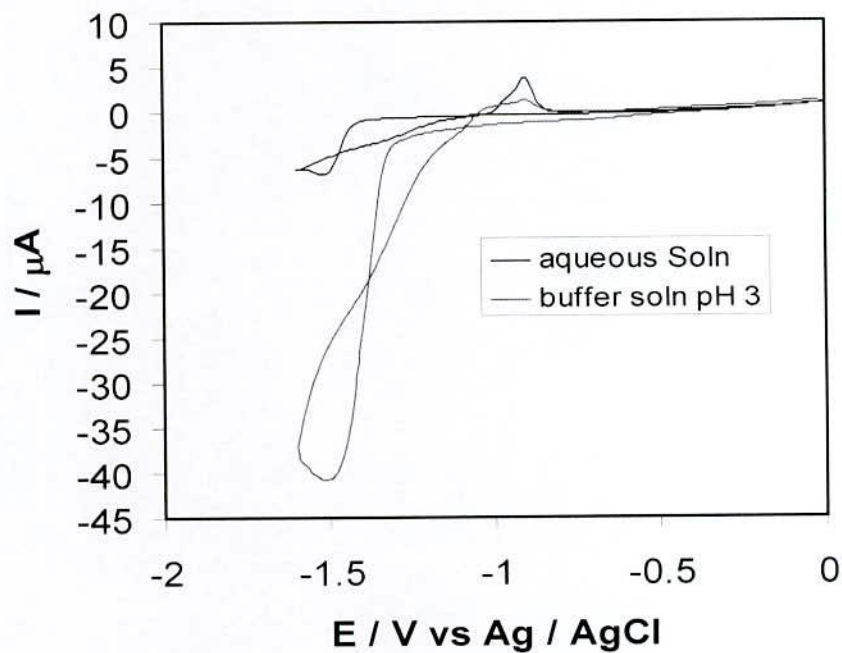
Figure 4.132 : Comparison cyclic voltammogram of Zn(II)-Aspartic acid in water and buffer solution (pH = 3.0)

171

Figure 4.133 : Cyclic voltammogram of 2mM Zn(II) + 6mM L-phenyl alanine (1:3) in aqueous solution at different scan rate.

Figure 4.134 : Plots of peak current versus square root of scan rate of 2mM Zn(II) + 6mM L-phenyl alanine (1:3) in aqueous solution.
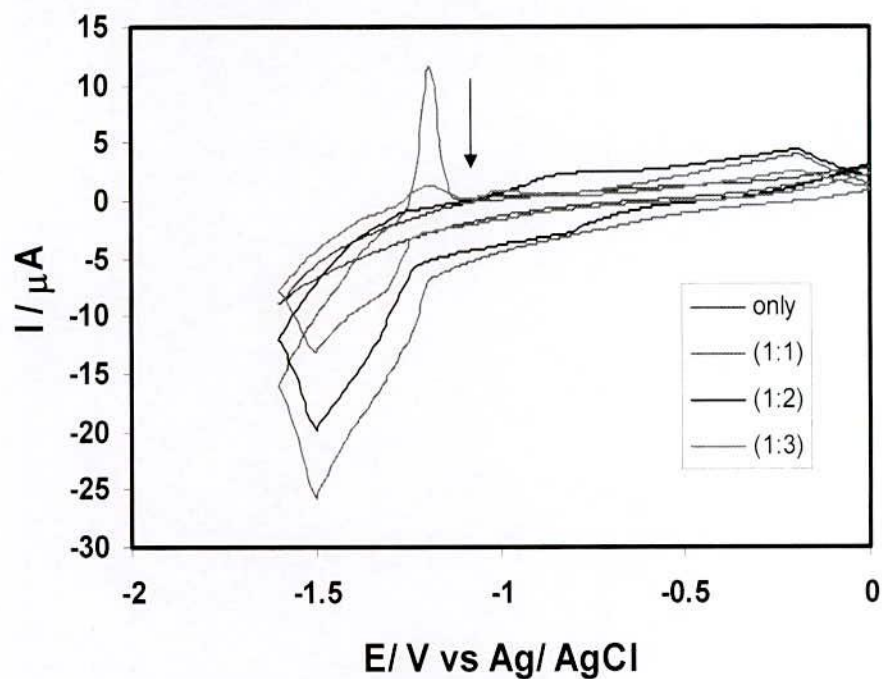
Figure 4.135 : Comparison cyclic voltammogram of Zn(II) and Zn(II)-L-phenyl alanine(1:1), (1:2), (1:3), at scan rate 0.1V/s in aqueous solution.
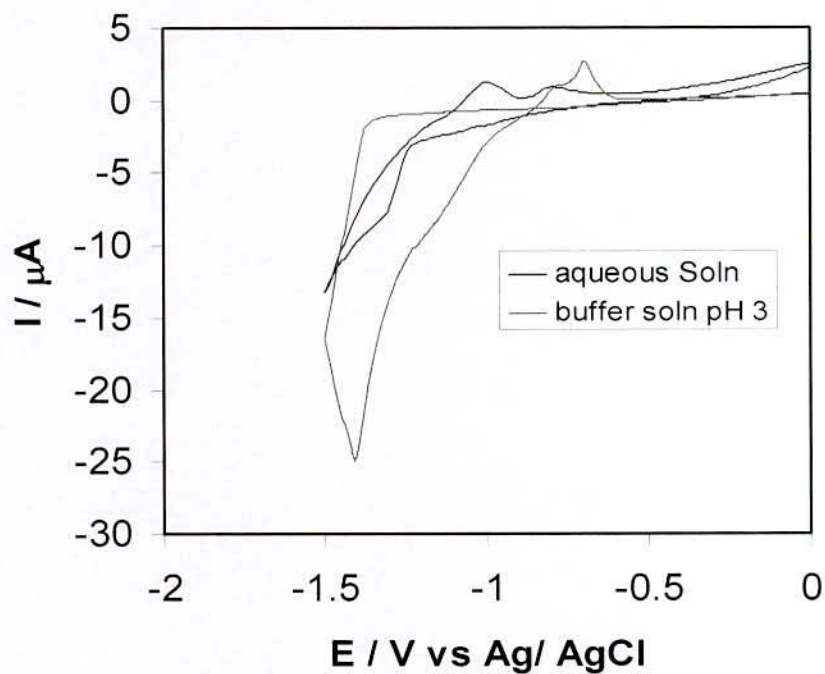
Figure 4.136 : Comparison cyclic voltammogram of Zn(II)-L Phenylalanine in water and buffer solution (pH = 3.0)
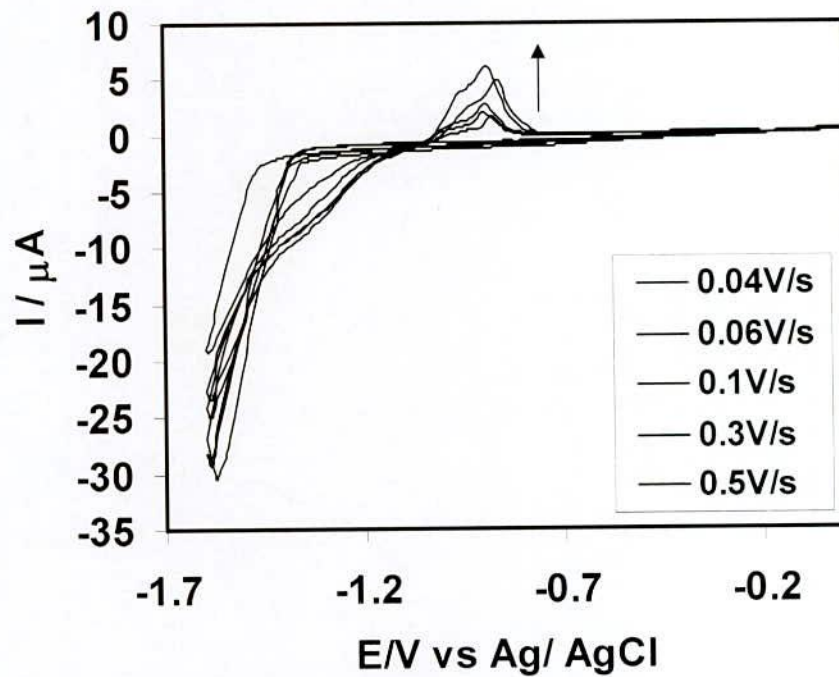
Figure 4.137 : Cyclic voltammogram of 2mM Zn(II) + 6mM L-phenyl alanine (1:3) in buffer solution (pH = 3.5) (acetate buffer) at different scan rate.

Figure 4.138 : Plots of peak current versus square root of scan rate of 2mM Zn(II) + 6mM L-phenyl alanine (1:3) in buffer solution (pH = 3.5) (acetate buffer).

174

Figure 4.139 : Cyclic voltammogram of 2mM Zn(II) + 6mM 3-Nitro benzene sulphonate(1:3) in buffer solution (pH = 3.5) (acetate buffer) at different scan rate.

Figure 4.140 : Plots of peak current versus square root of scan rate of 2mM Zn(II) + 6mM 3-Nitro benzene sulphonate(1:3) in buffer solution (pH = 3.5) (acetate buffer).
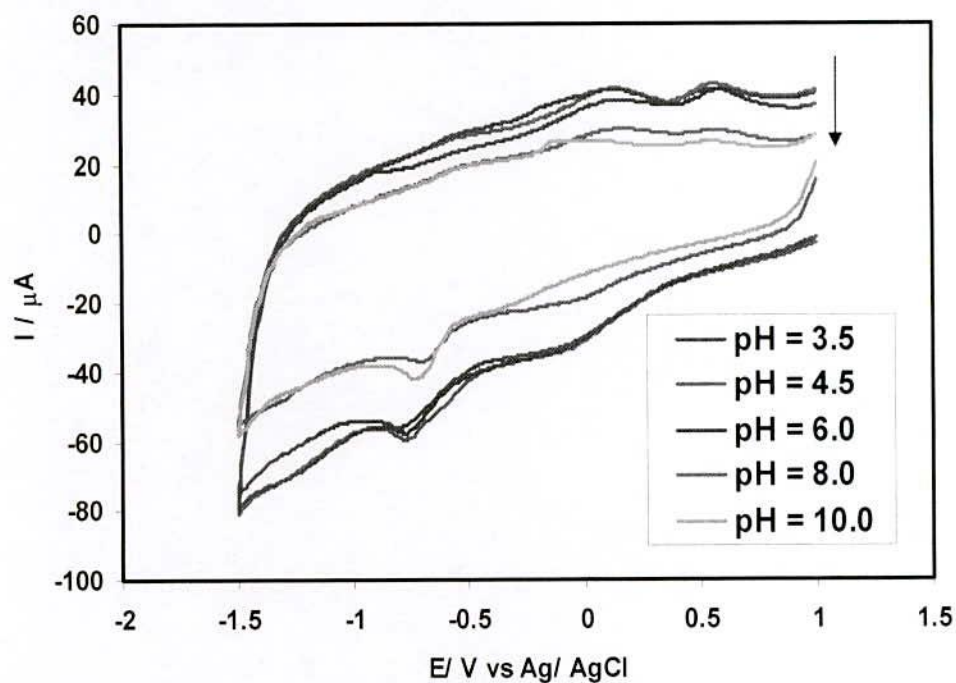
Figure 4.141 : Comparison of Cyclic voltammogram of Zn(II)-3-Nitro benzene Sulphonate(1:3) in different pH at similar condition (Scan rate = 0.1V/s).
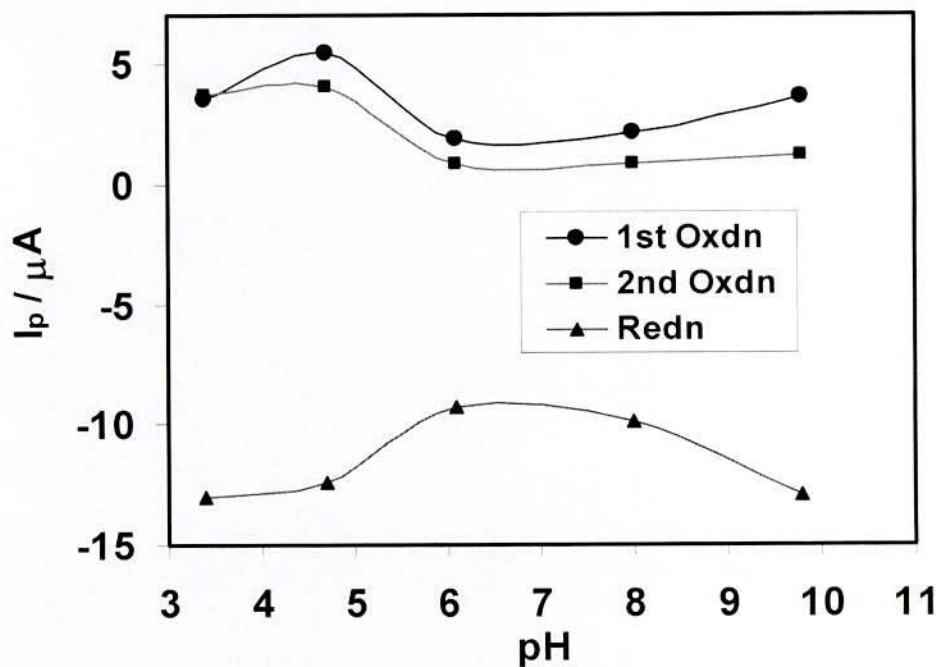
Figure 4.142 : Plots of peak current versus versus pH (3.5, 4.5, 6.0, 8.0, 10.0) of Zn(II)- 3-Nitro benzene Sulphonate(1:3) at similar condition (Scan rate = 0.1V/s).
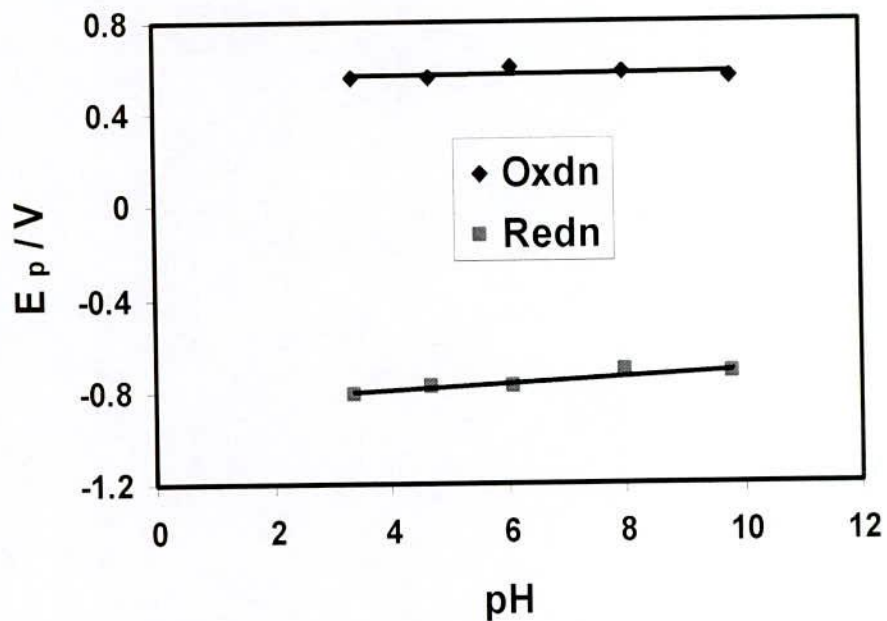
Figure 4.143 : Plots of peak potential (E/V) versus pH(3.5, 4.5, 6.0, 8.0, 10.0) of Zn(II)- 3-Nitro benzene Sulphonate(1:3) at similar condition (Scan rate = 0.1V/s).
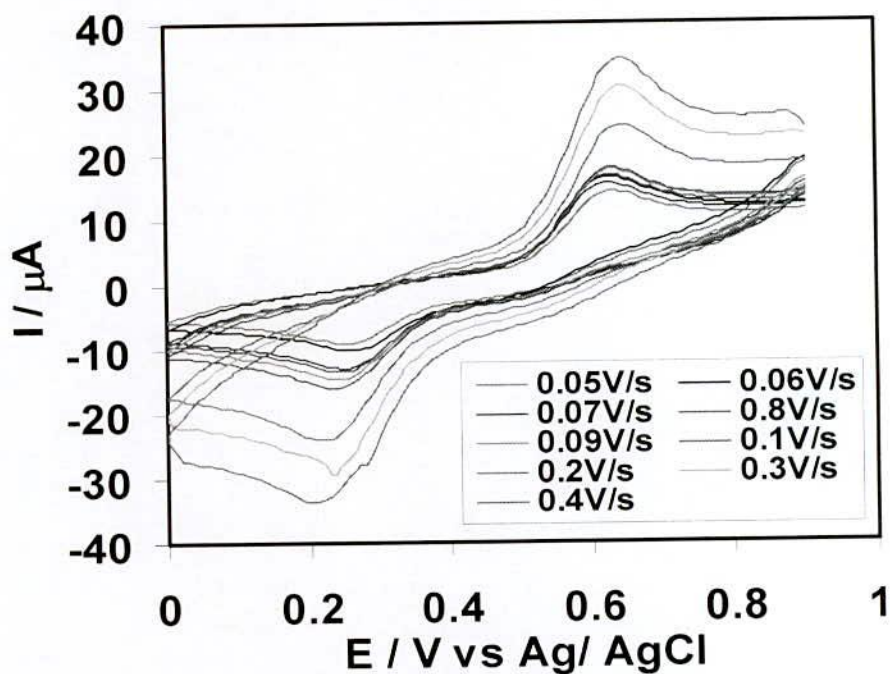
Figure 4.144 : Cyclic voltammogram of 2mM catechol in buffer solution (pH = 2.0) (KCl + HCl buffer) at different scan rate using pt electrode.

177
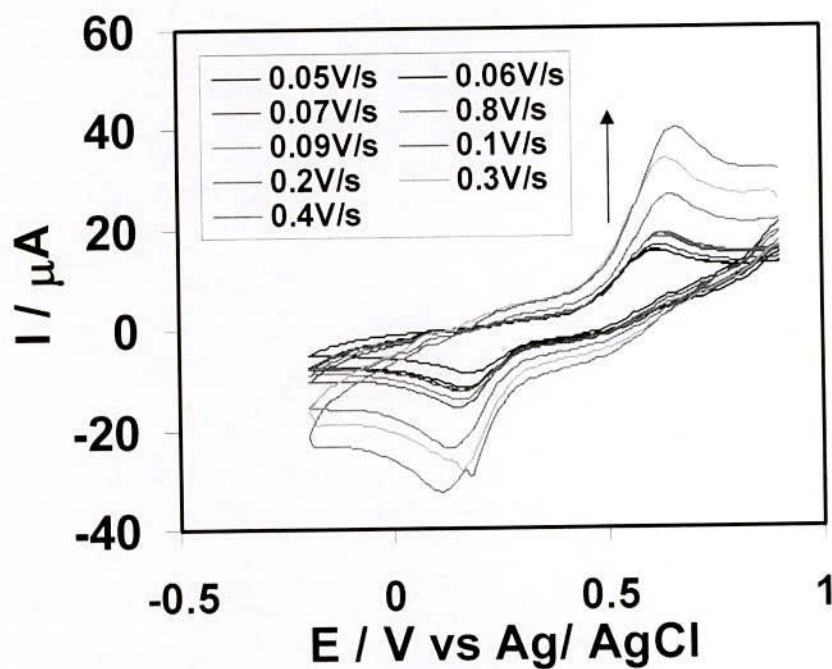
Figure 4.145 : Cyclic voltammogram of 2mM catechol in buffer solution (pH = 3.5) (Acetate buffer) at different scan rate.
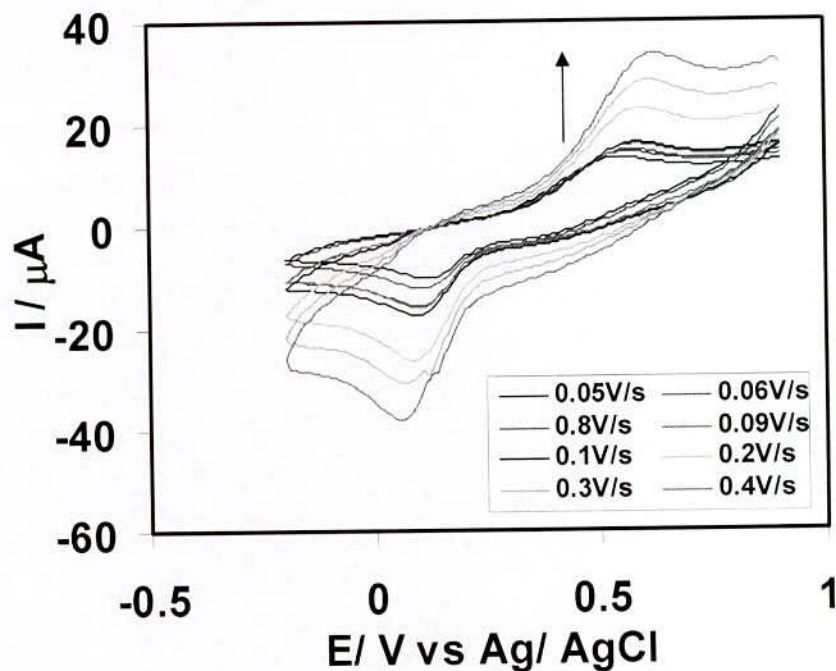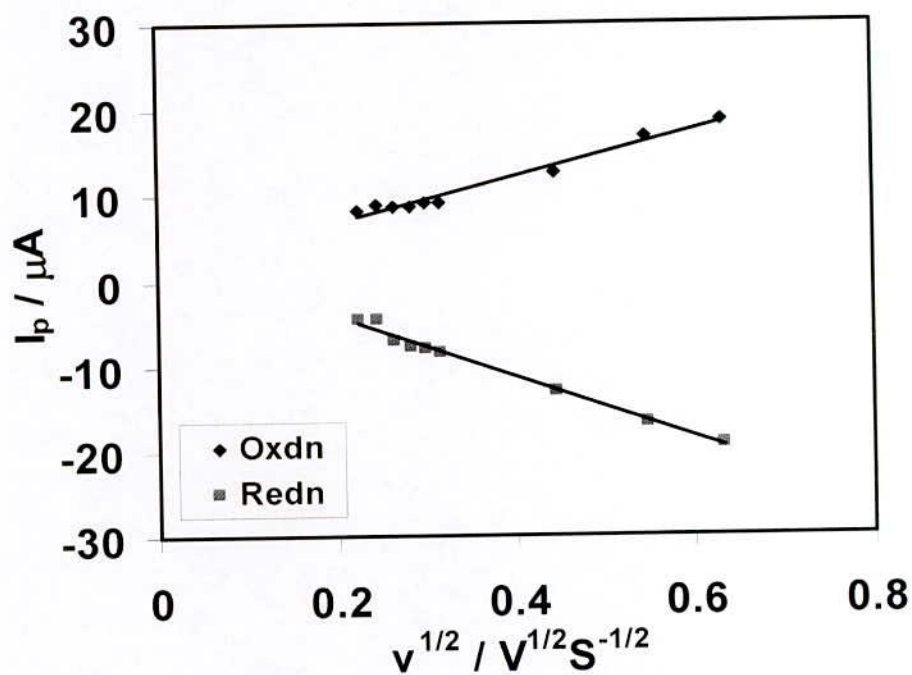

Figure 4.146 : Cyclic voltammogram of 2mM catechol in buffer solution (pH = 5.5) (Acetate buffer) at different scan rate.
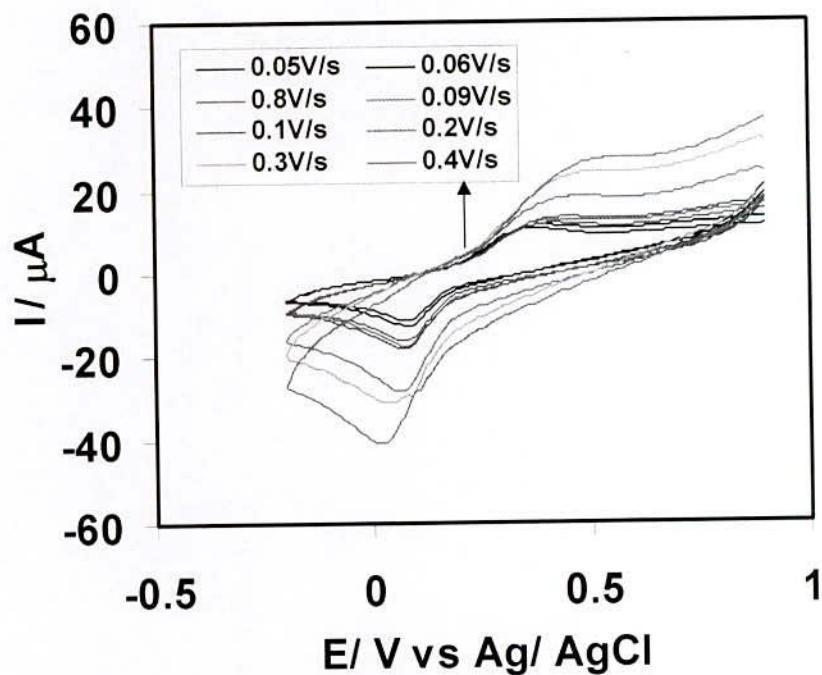
Figure 4.147 : Cyclic voltammogram of 2mM catechol in buffer solution (pH = 6.5) (Phosphate buffer) at different scan rate.
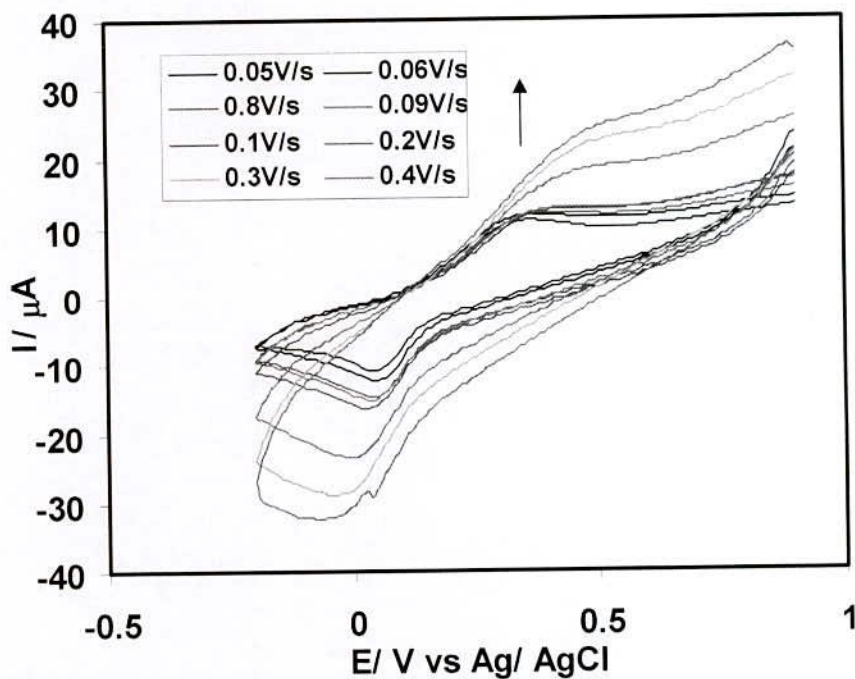
Figure 4.148 : Cyclic voltammogram of 2mM catechol in buffer solution (pH = 7.5) (Phosphate buffer) at different scan rate.
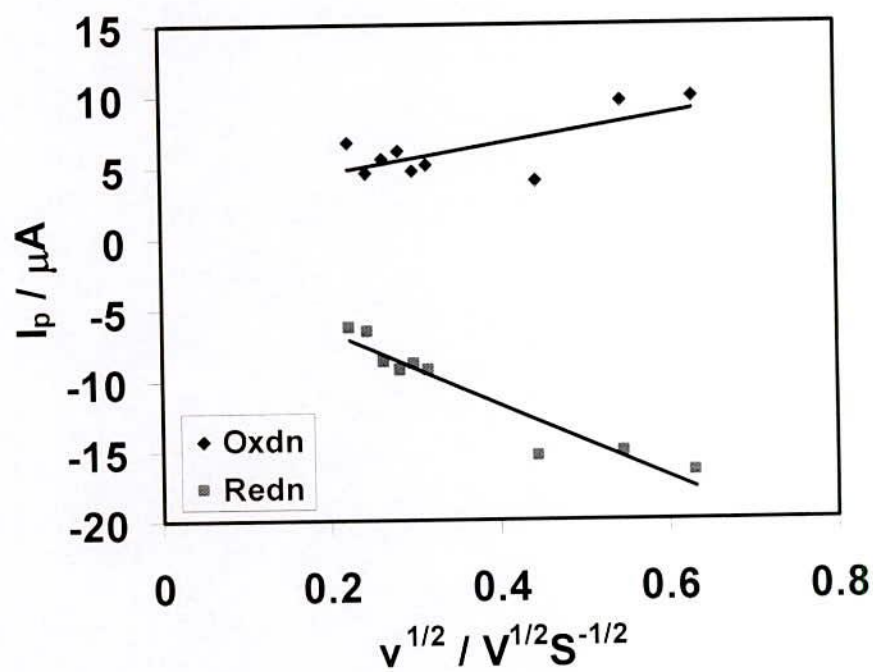
Figure 4.149 : Plots of peak current versus square root of scan rate of 2mM catechol in buffer solution (pH = 2.0) (KCl + HCl buffer).
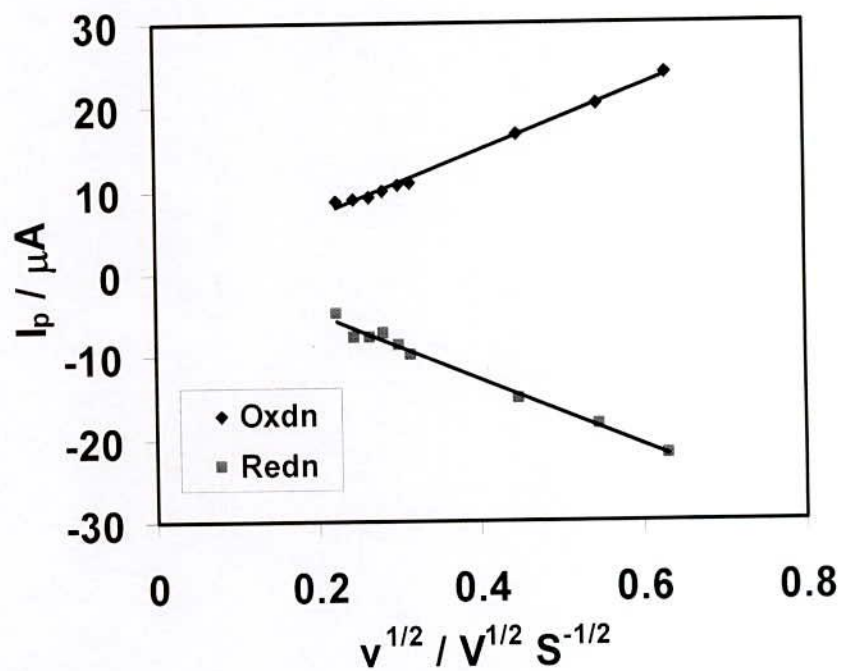
Figure 4.150 : Plots of peak current versus square root of scan rate of 2mM catechol in buffer solution (pH = 3.5) (Acetate buffer).
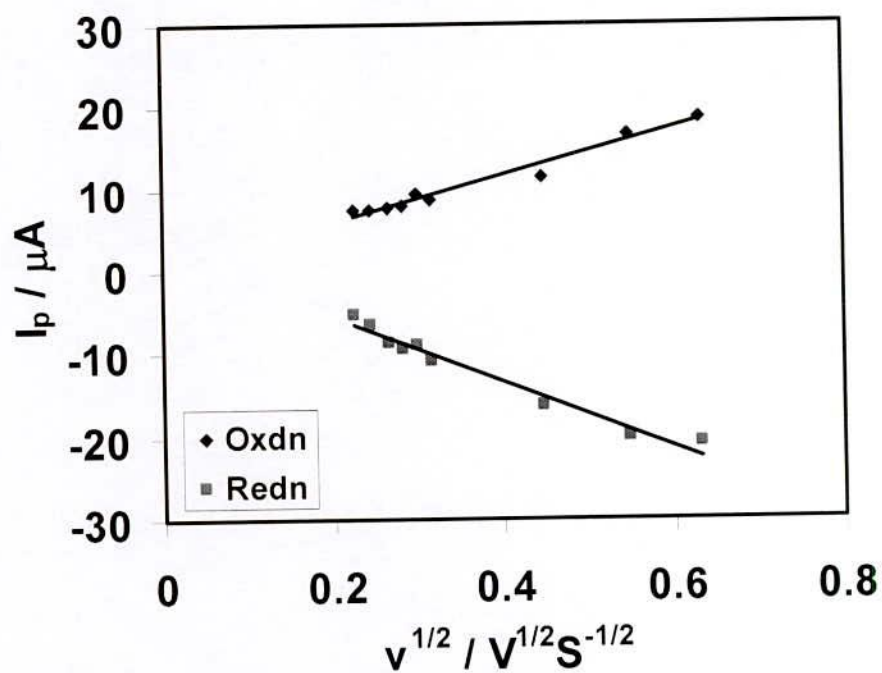
Figure 4.151 : Plots of peak current versus square root of scan rate of 2mM catechol in buffer solution (pH = 5.5) (Acetate buffer).
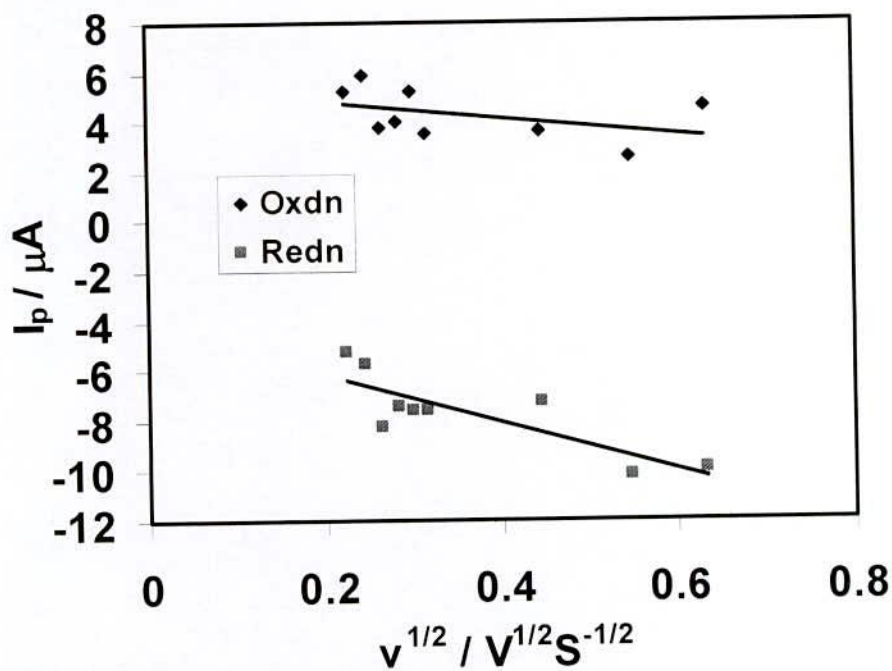

Figure 4.152 : Plots of peak current versus square root of scan rate of 2mM catechol in buffer solution (pH = 6.5) (Phosphate buffer).

Figure 4.153 : Plots of peak current versus square root of scan rate of 2mM catechol in buffer solution (pH = 7.5) (Phosphate buffer).
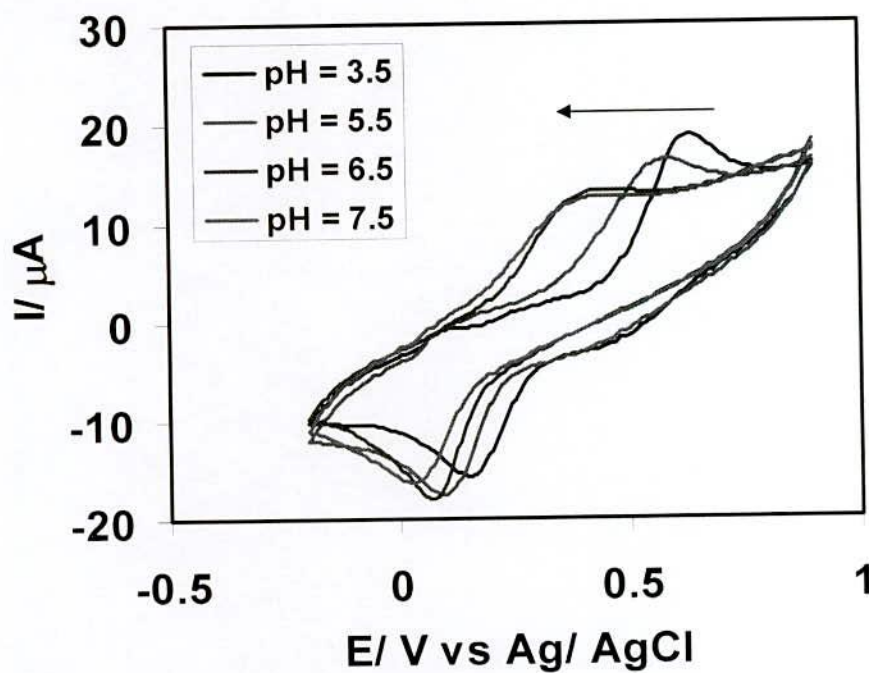

Figure 4.154: Cyclic voltammogram of 2mM Catechol in buffer solution (pH = 3.5, 5.5, 6.5 and 7.5) at 0.1Vs^{-1} scan rate.
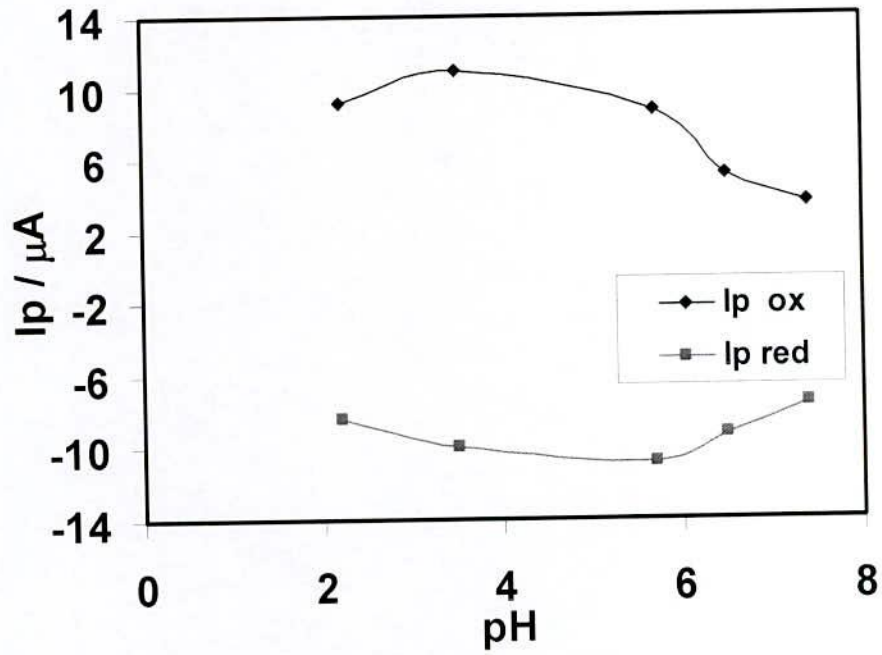
182

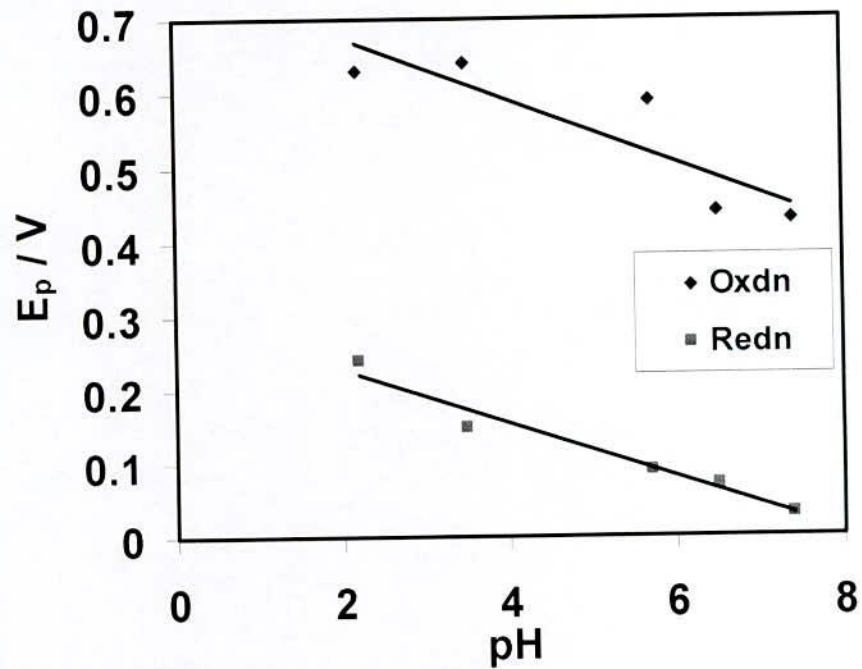Figure 4.155 : Plots of peak current vs pH of 2mM Catechol in buffer solution (pH = 3.5, 5.5, 6.5 and 7.5) at 0.1Vs⁻¹ scan rate.

Figure 4.156: Plots of peak potential vs pH of 2mM Catechol in buffer solution (pH = 3.5, 5.5, 6.5 and 7.5) at 0.1Vs⁻¹ scan rate.
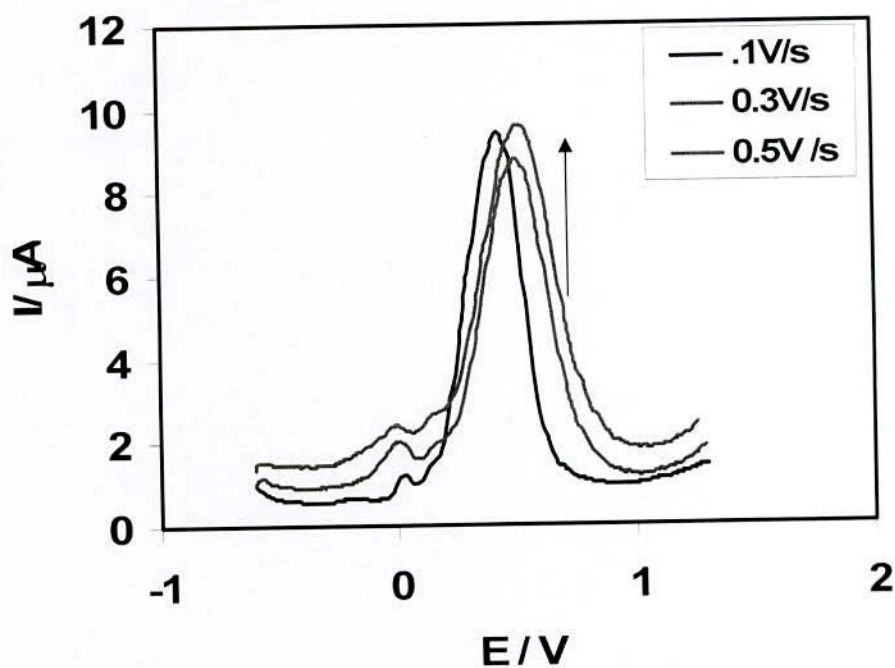
Figure 4.157 : Differential pulse voltammogram of 2mM catechol in buffer solution (pH = 7) (Phosphate buffer) for forward direction (oxidation) at different scan rate.
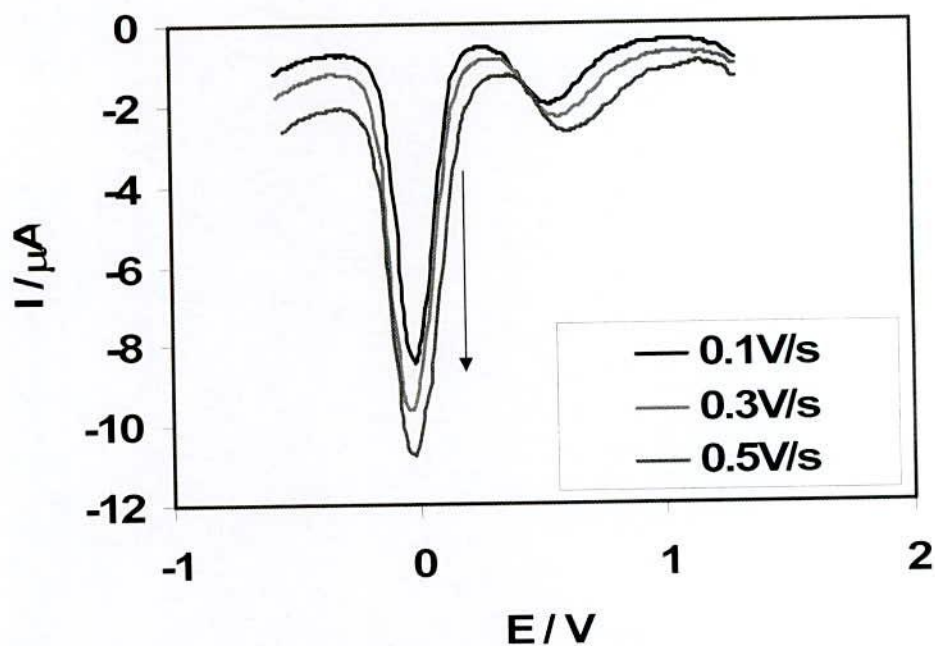

Figure 4.158 : Differential pulse voltammogram of 2mM catechol in buffer solution (pH = 7) (Phosphate buffer) for backward direction (reduction) at different scan rate.
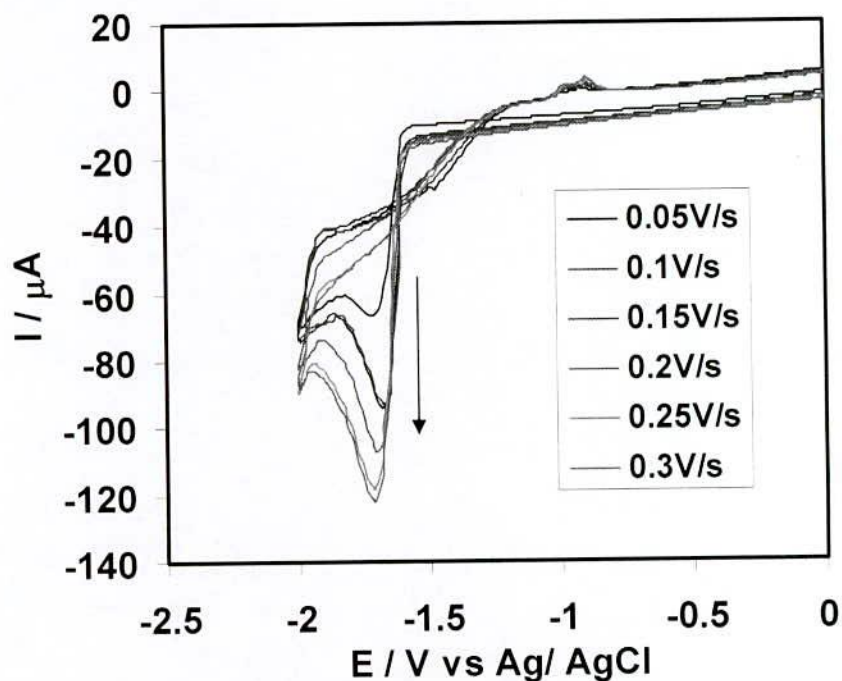
Figure 4.159 : Cyclic voltammogram of 2mM Zn(II) + 6mM catechol (1:3) in aqueous solution at different scan rate.
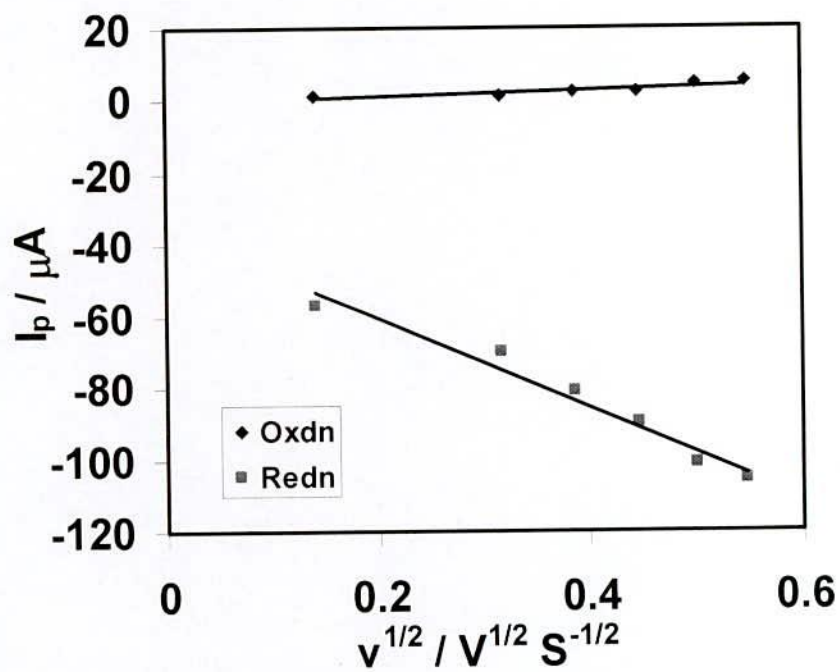

Figure 4.160 : Plots of peak current versus square root of scan rate of 2mM Zn(II) + 6mM catechol (1:3) in aqueous solution.
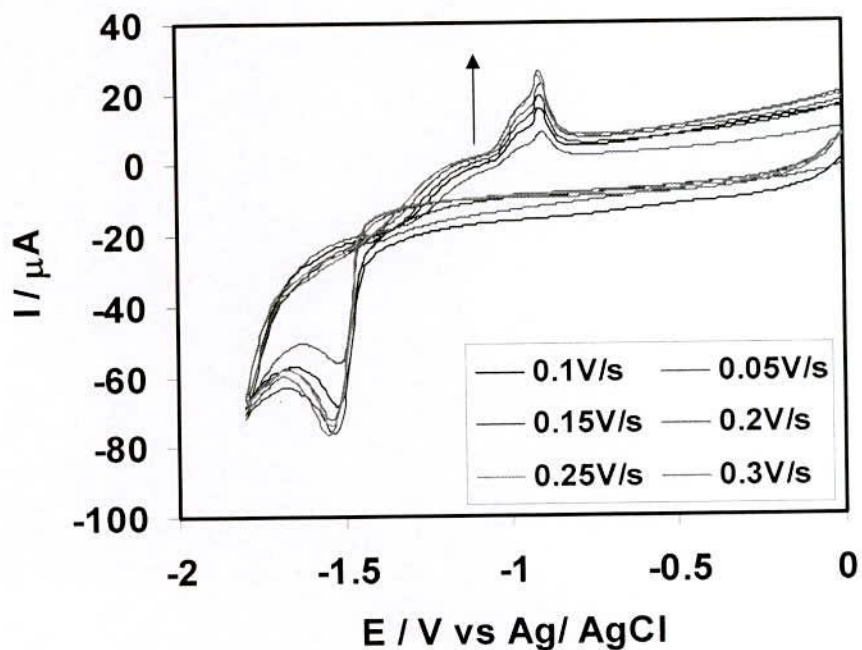
Figure 4.161 : Cyclic voltammogram of 2mM Zn(II) + 6mM catechol (1:3) in buffer solution (pH = 2) at different scan rate.
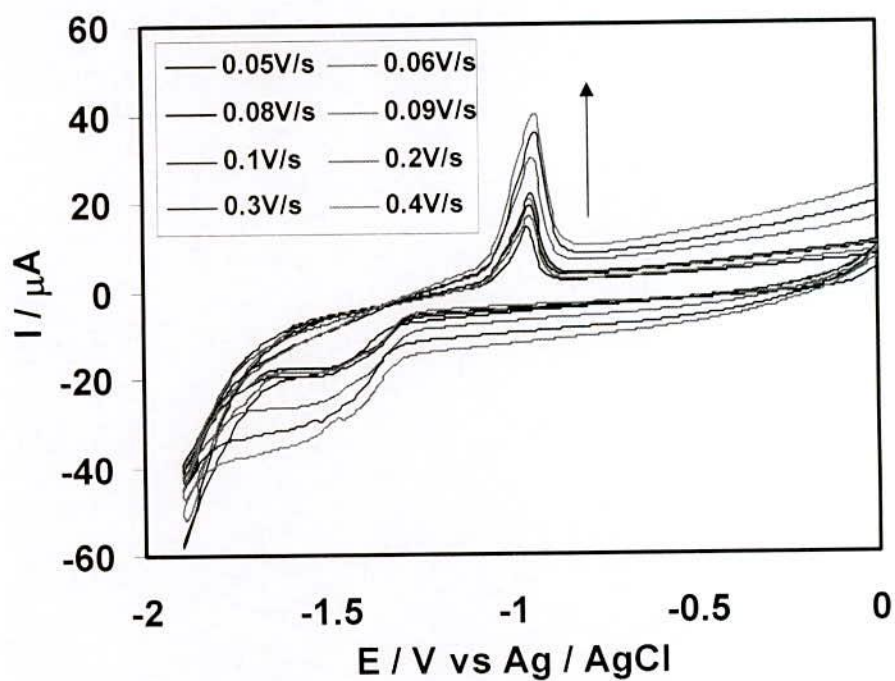

Figure 4.162 : Cyclic voltammogram of 2mM Zn(II) + 6mM catechol (1:3) in buffer solution (pH = 3) at different scan rate.
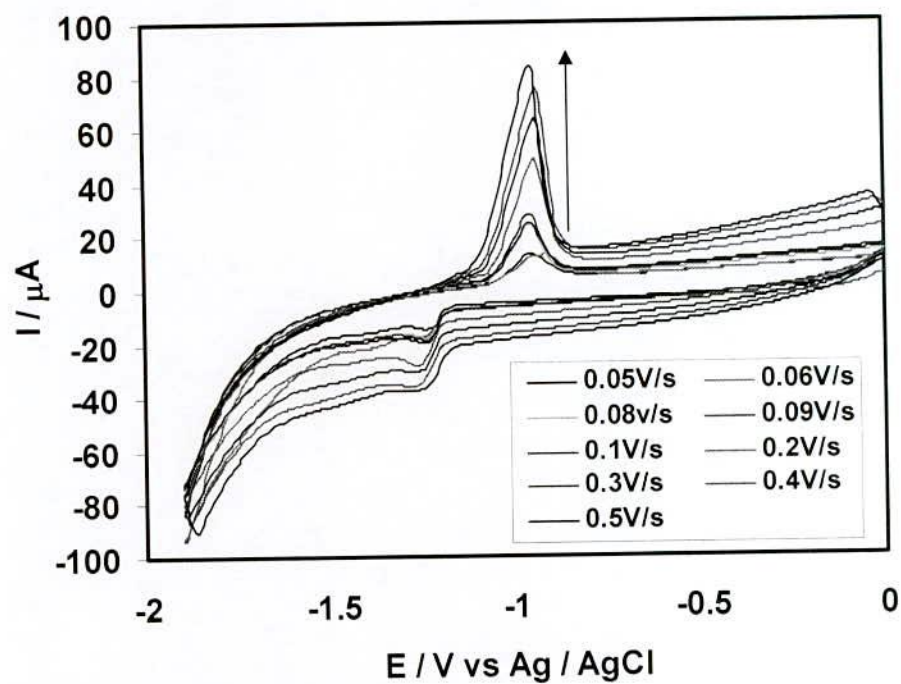
Figure 4.163 : Cyclic voltammogram of 2mM Zn(II) + 6mM catechol (1:3) in buffer solution (pH = 4.5) at different scan rate.
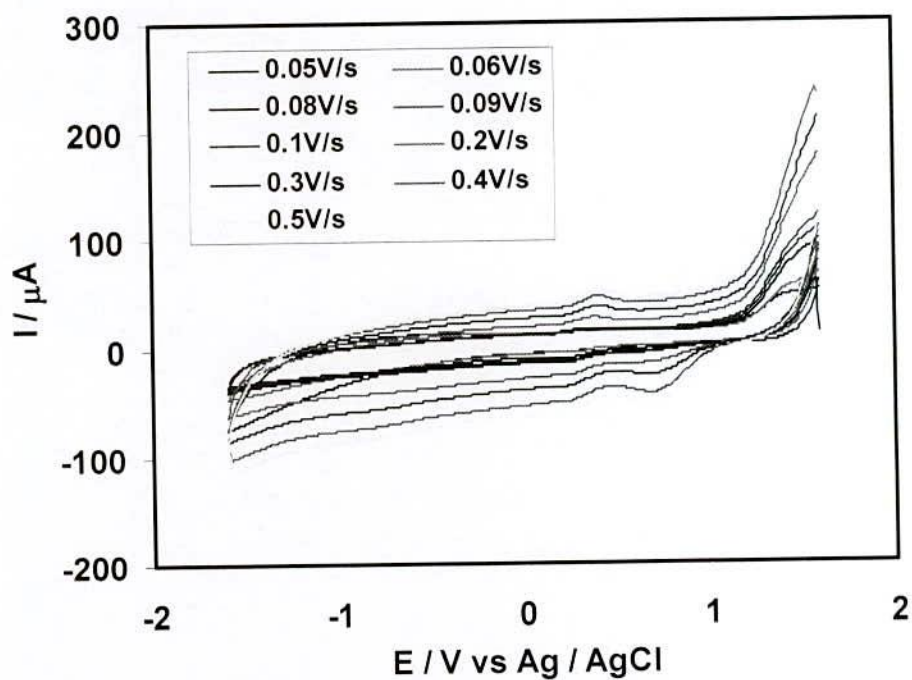

Figure 4.164 : Cyclic voltammogram of 2mM Zn(II) + 6mM catechol (1:3) in buffer solution (pH = 7.0) at different scan rate.

187
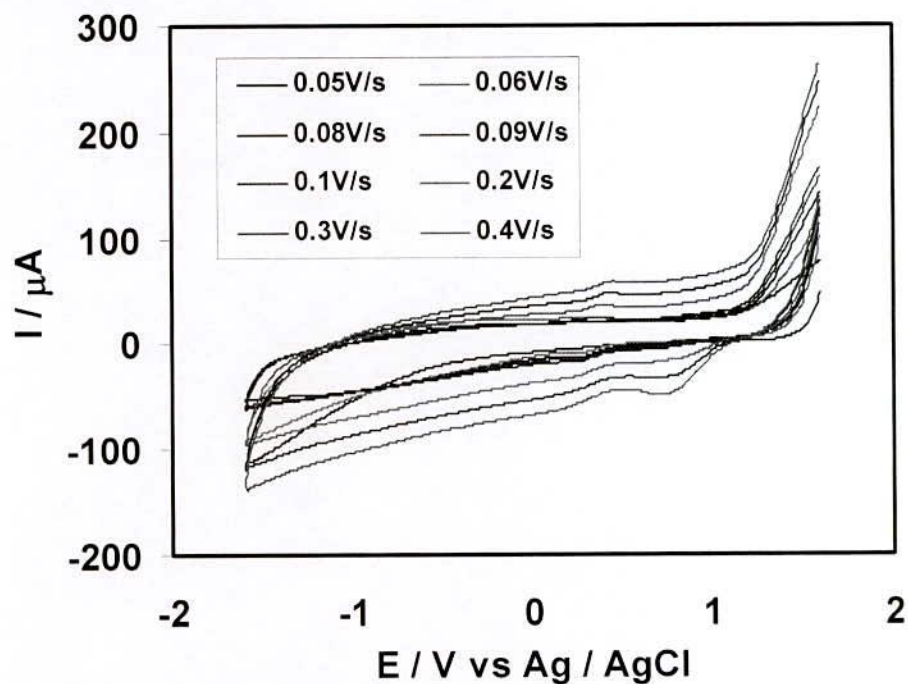
Figure 4.165 : Cyclic voltammogram of 2mM Zn(II) + 6mM catechol (1:3) in buffer solution (pH = 11.0) at different scan rate.

Figure 4.166 : Plots of peak current versus square root of scan rate of 2mM Zn(II) + 6mM catechol (1:3) in buffer solution (pH = 2).
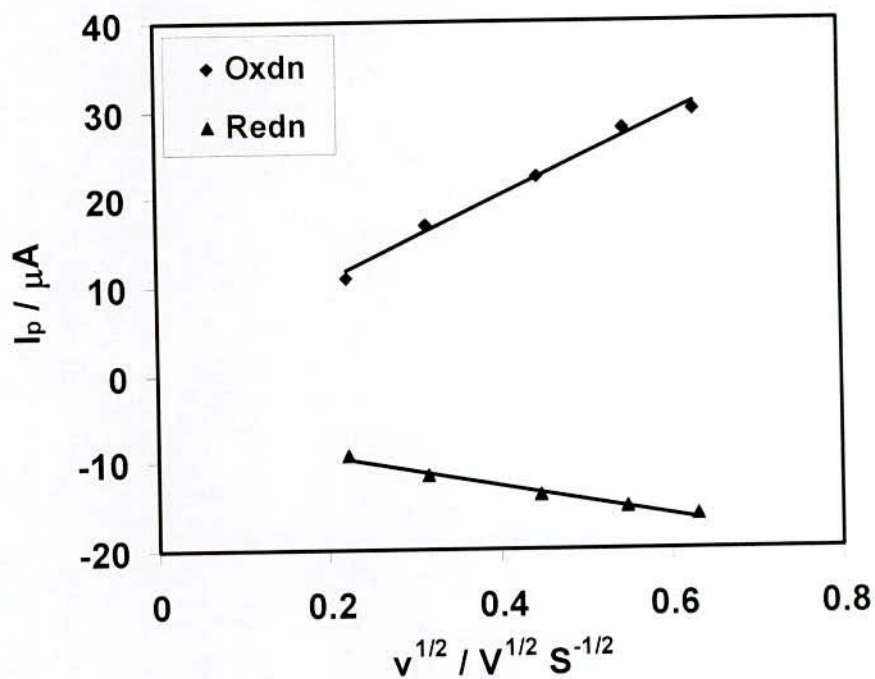
Figure 4.167 : Plots of peak current versus square root of scan rate of 2mM Zn(II) + 6mM catechol (1:3) in buffer solution (pH = 3).

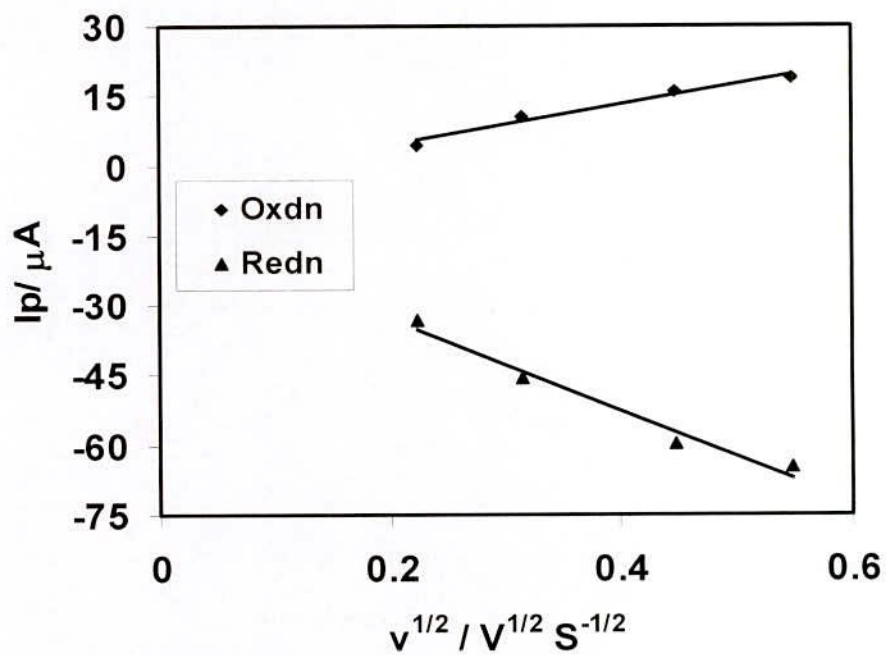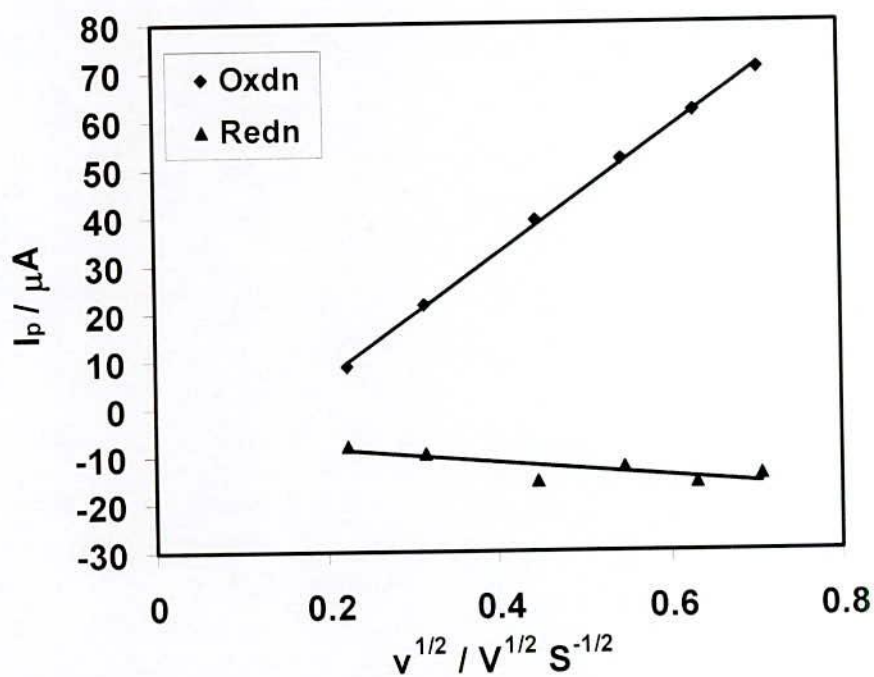Figure 4.168 : Plots of peak current versus square root of scan rate of 2mM Zn(II) + 6mM catechol (1:3) in buffer solution (pH = 4.5) at different scan rate.
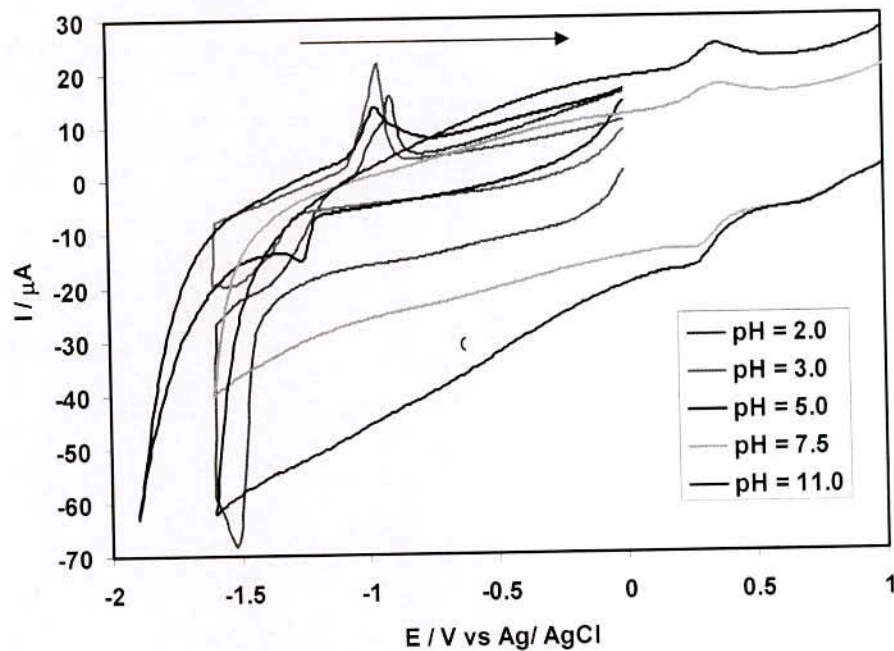
Figure 4.169 : Comparison cyclic voltammogram of Zn(II)-Catechol in buffer solution (pH = 2.0, 3.0, 5.0, 7.5 and 11.0) at scan rate $0.1Vs^{-1}$.
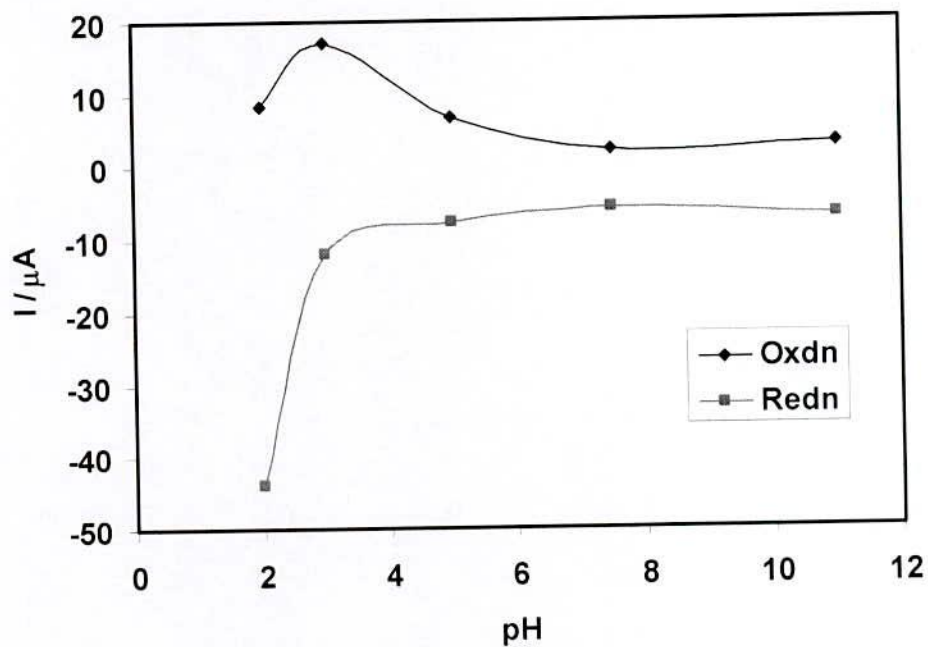
Figure 4.170 : Plots of peak current vs pH of Zn(II)-Catechol in buffer solution (pH = 2.0, 3.0, 5.0, 7.5 and 11.0) at scan rate $0.1Vs^{-1}$.
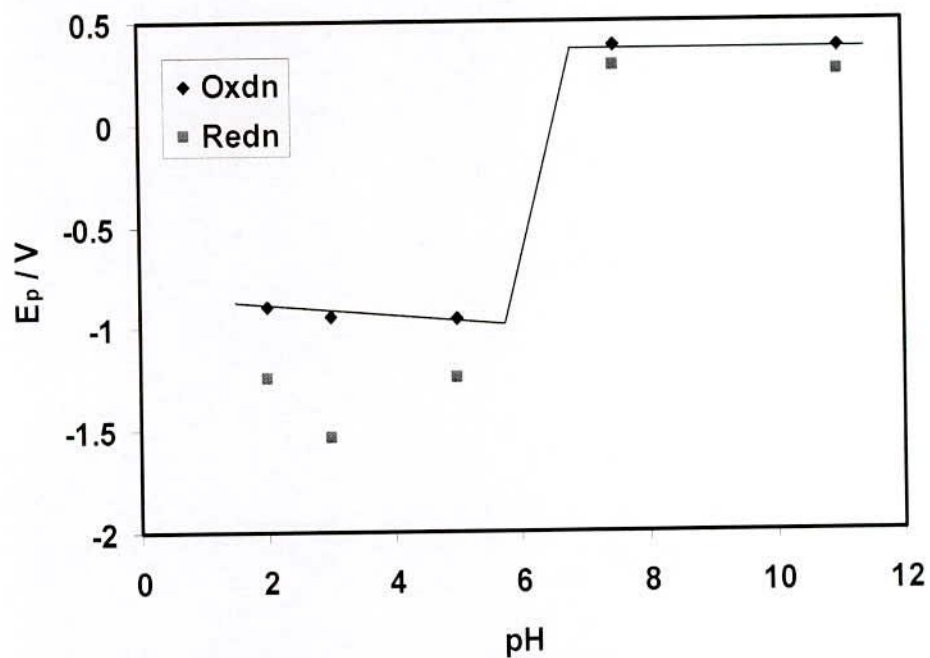
Figure 4.171: Plots of peak potential vs pH of Zn(II)-Catechol in buffer solution (pH = 2.0, 3.0, 5.0, 7.5 and 11.0) at scan rate $0.1 Vs^{-1}$.
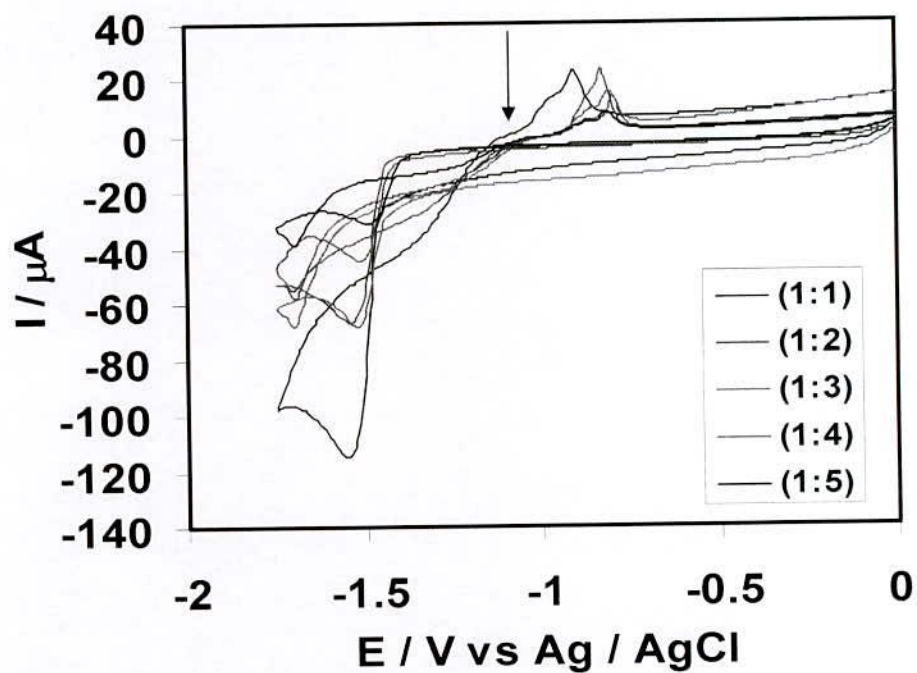
Figure 4.172 : Comparison of Cyclic voltammogram of $ZnCl_2$ + Catechol (1:1), (1:2), (1:3), (1:4) and (1:5) at similar condition (pH = 2, Scan rate = 0.1V/s).
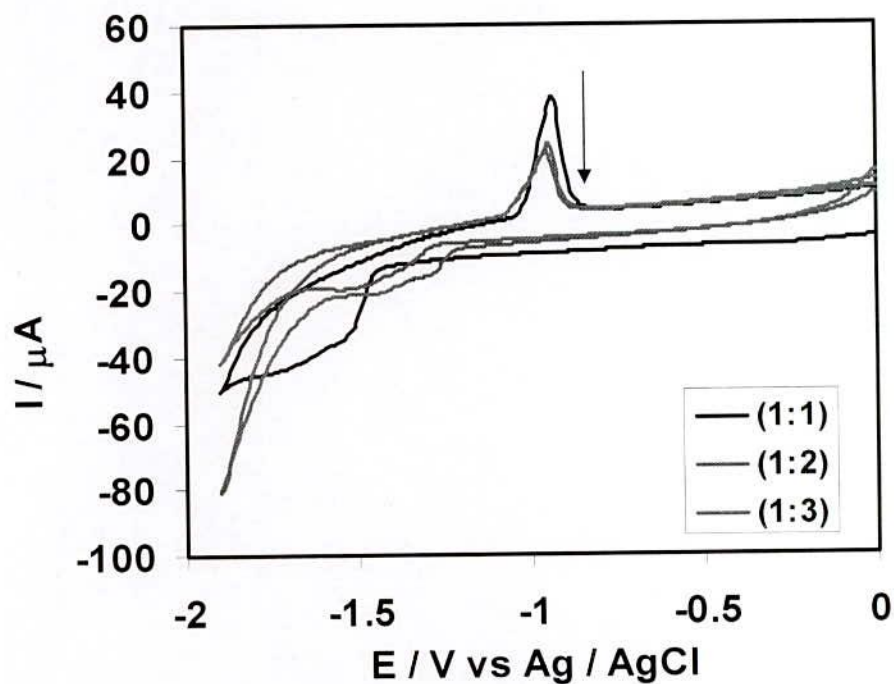
Figure 4.173 : Comparison of Cyclic voltammogram of $ZnCl_2$ + Catechol (1:1), (1:2) and (1:3) at similar condition (pH = 3, Scan rate= 0.1V/s).
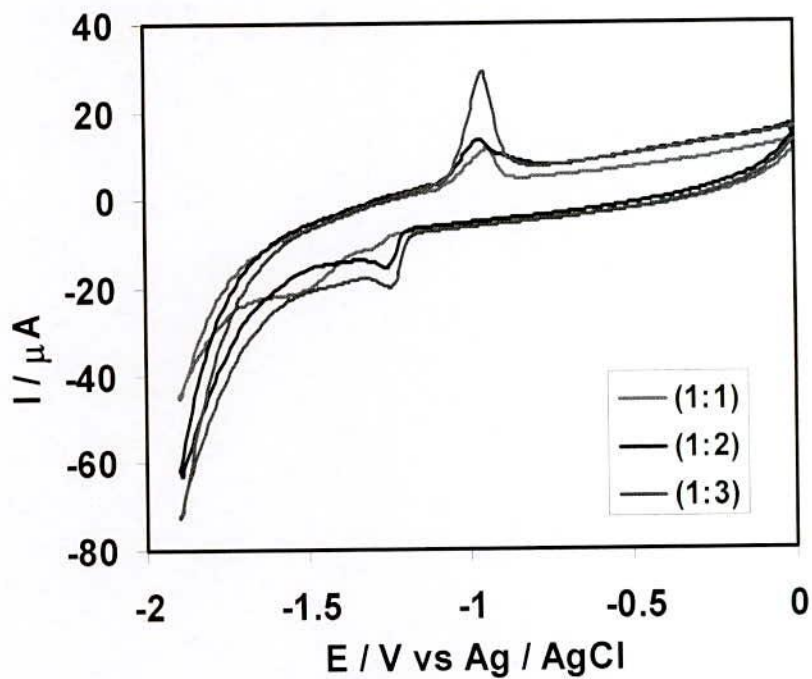
Figure 4.174 : Comparison of Cyclic voltammogram of $ZnCl_2$ + Catechol (1:1), (1:2) and (1:3) at similar condition (pH = 4.5, Scan rate= 0.1V/s).
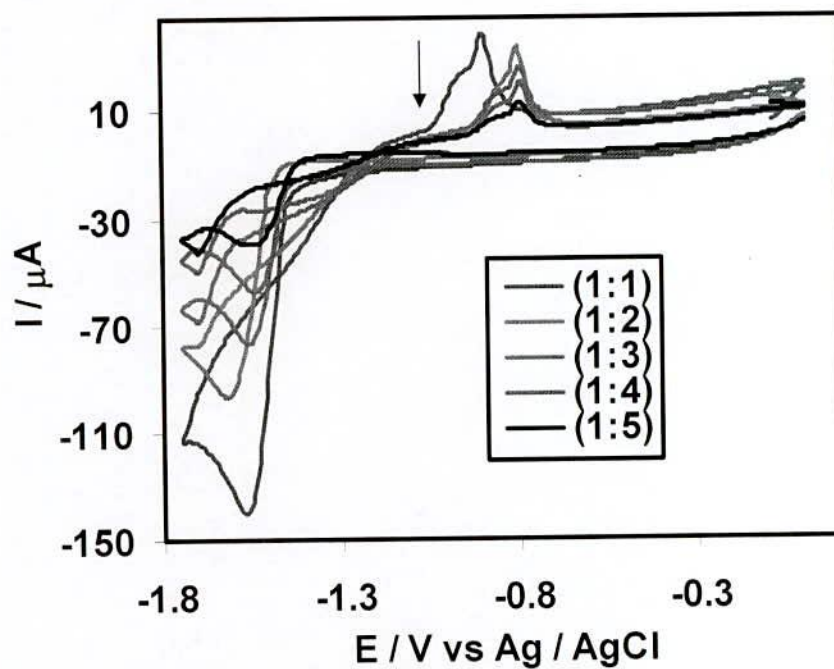
Figure 4.175 : Comparison of Cyclic voltammogram of Zn(II) + Catechol(1:1), (1:2), (1:3), (1:4) and (1:5) at similar condition (pH = 2, Scan rate = 0.30V/s).
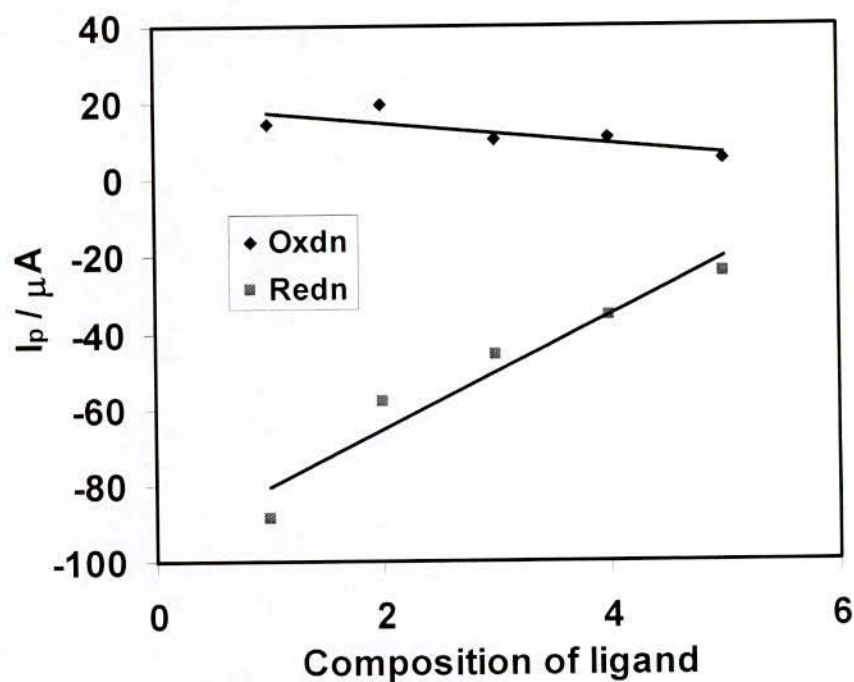
Figure 4.176 : Plots of peak current versus composition of ligand of $ZnCl_2$ + Catechol (1:1), (1:2), (1:3), (1:4) and (1:5) at similar condition (pH = 2, Scan rate = 0.1V/s).
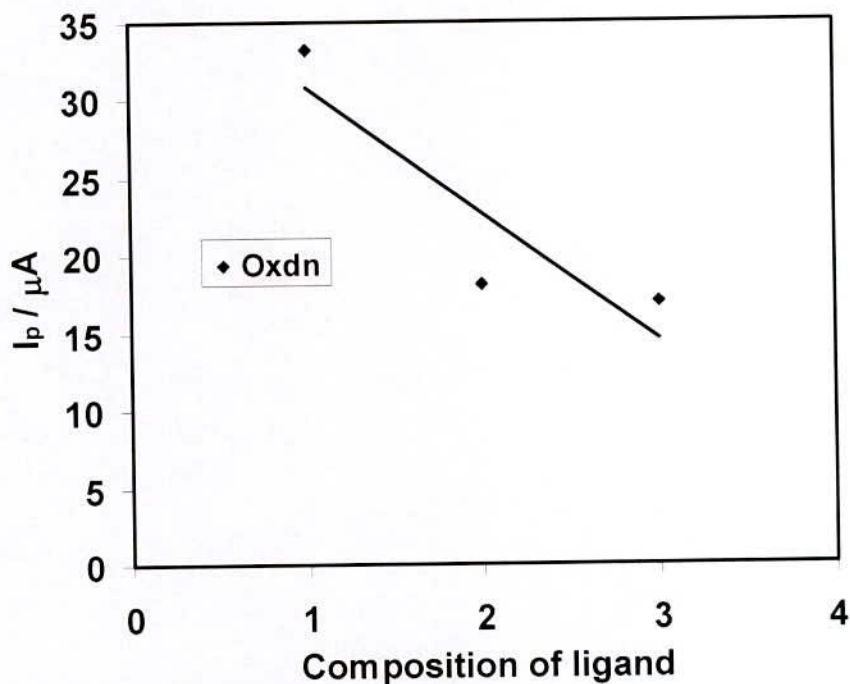
Figure 4.177 : Plots of peak current versus composition of ligand of $ZnCl_2$ + Catechol (1:1), (1:2) and (1:3) at similar condition (pH = 3.0, Scan rate= 0.1V/s).
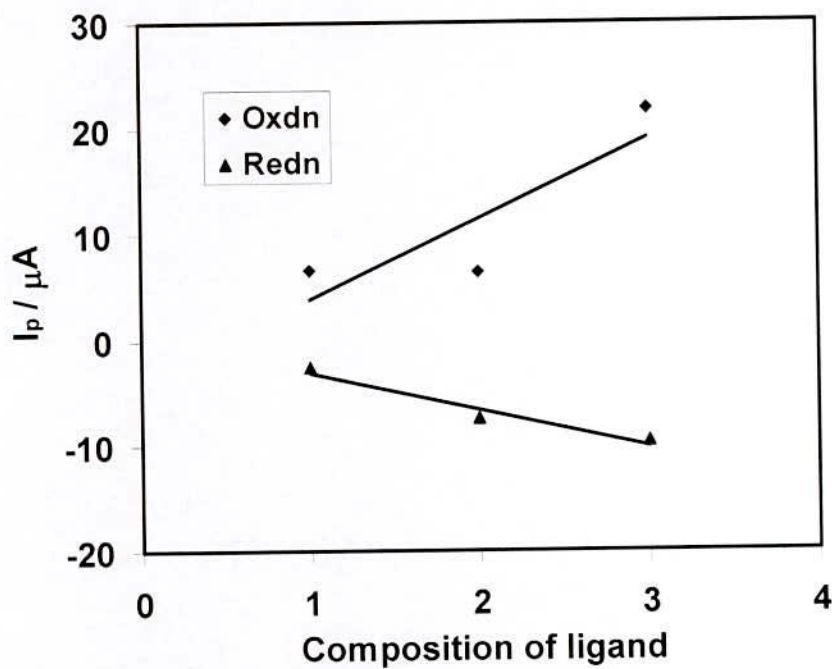
Figure 4.178 : Plots of peak current versus composition of ligand of $ZnCl_2$ + Catechol (1:1), (1:2) and (1:3) at similar condition (pH = 4.5, Scan rate= 0.1V/s).
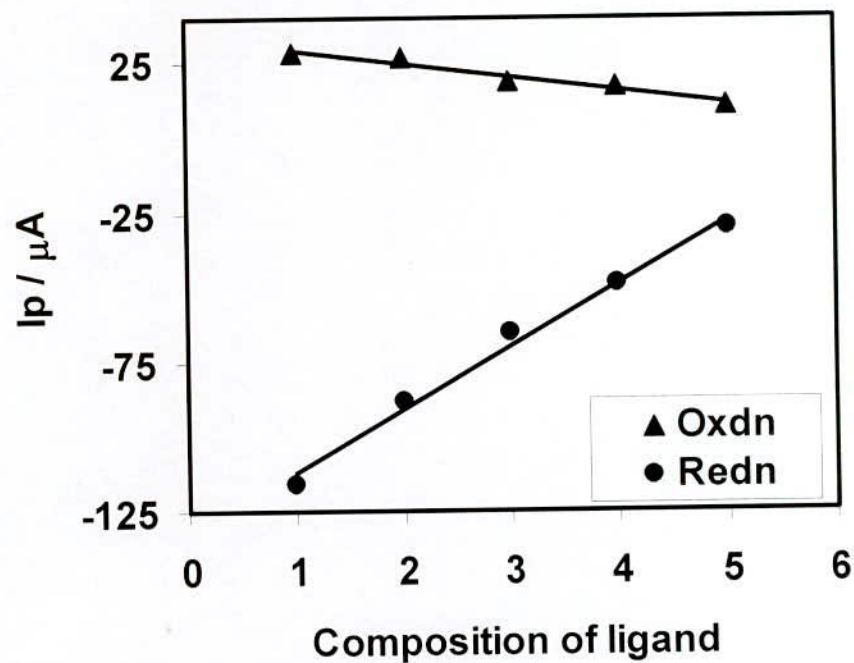
Figure 4.179 : Plots of peak current versus composition of ligand of Zn(II) + Catechol(1:1), (1:2), (1:3), (1:4) and (1:5) at similar condition (pH = 2, Scan rate= 0.30V/s).
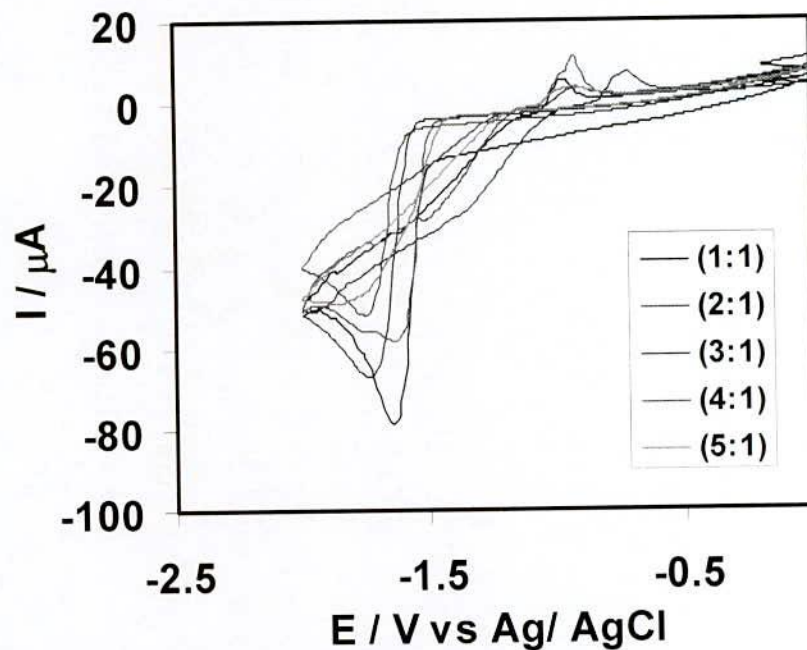
Figure 4.180 : Comparison of Cyclic voltammogram of ZnCl$_2$ + Catechol (1:1), (2:1), (3:1), (4:1) and (5:1) (metal composition change ligand fixed) at similar condition (pH = 2.0, Scan rate = 0.1V/s).
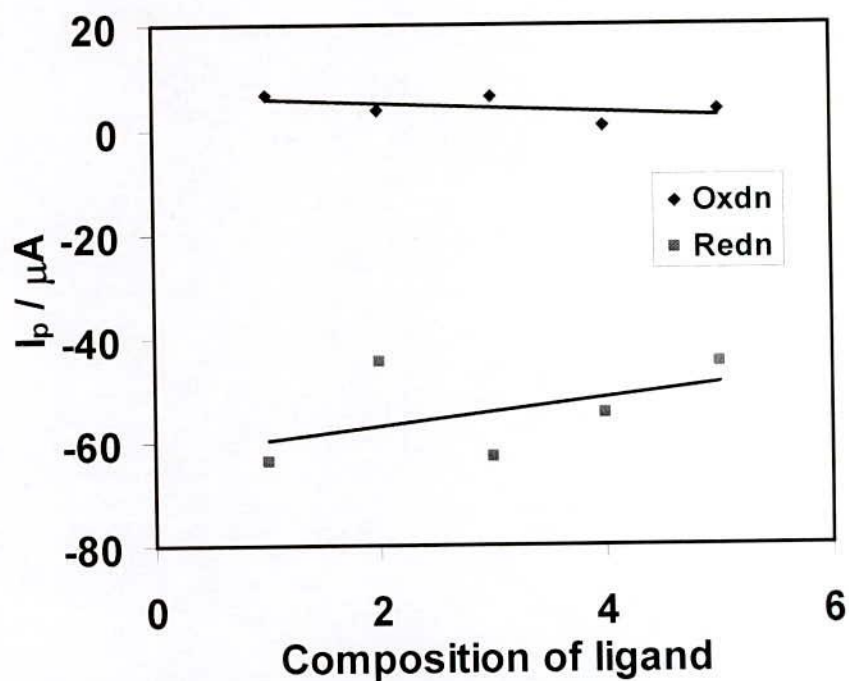
Figure 4.181 : Plots of peak current versus composition of ligand of $ZnCl_2$ + Catechol (1:1), (2:1), (3:1), (4:1) and (5:1) at similar condition (pH = 2, Scan rate = 0.1V/s).
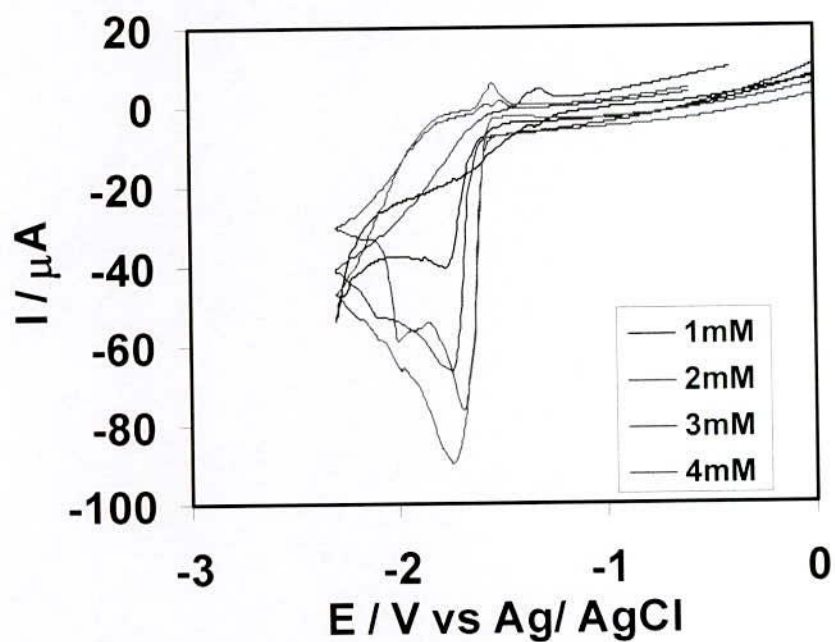
Figure 4.182: Cyclic voltammogram of $ZnCl_2$ + catechol (1:3 same concentration) in buffer solution pH = 2.0 at scan rate 0.1V/s.
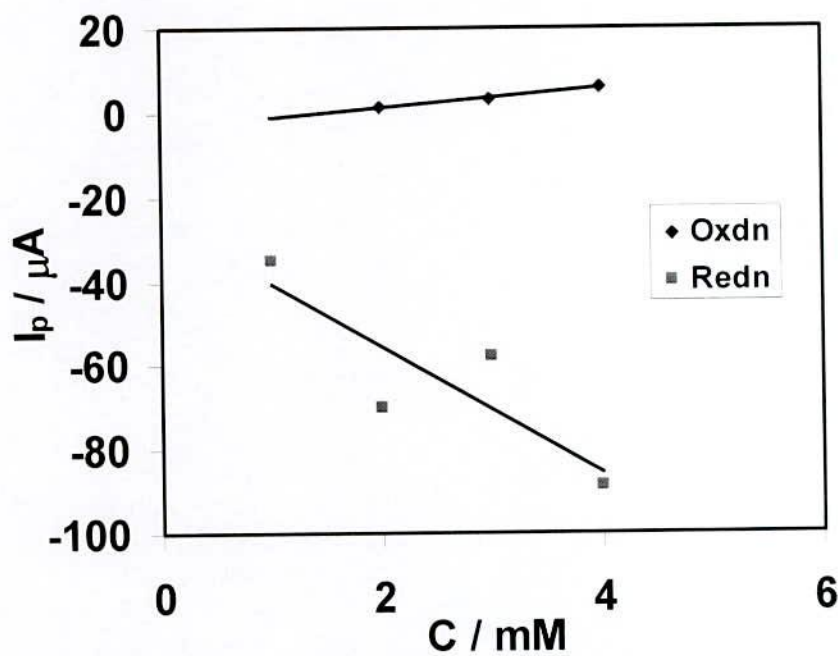
Figure 4.183 : Plots of peak current versus concentration of $ZnCl_2$ + Catechol (1:3) 1, 2, 3, 4mM concentration) in buffer solution pH = 2.0 at scan rate 0.1V/s.
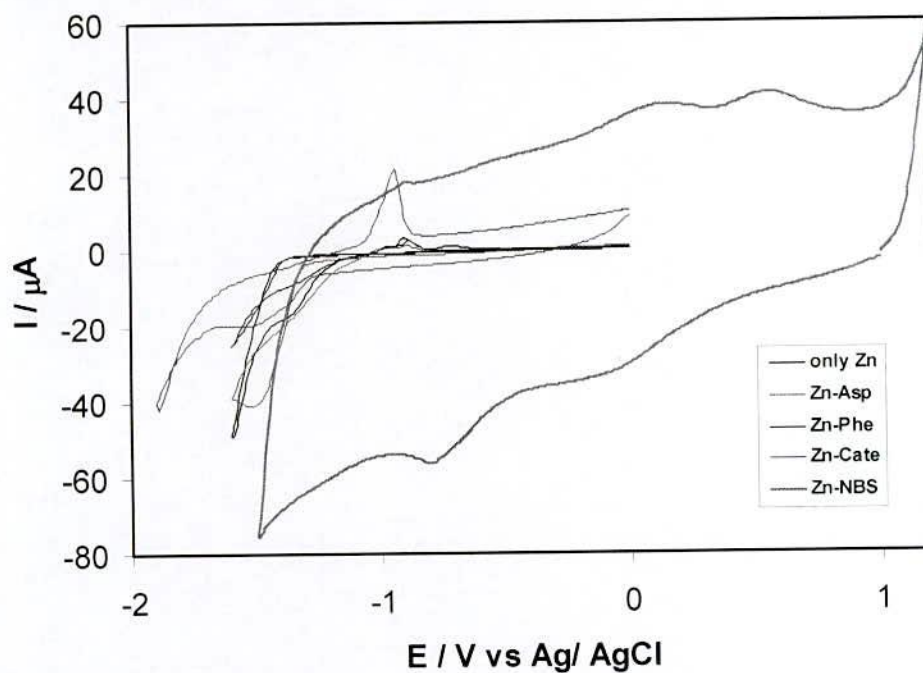
Figure 4.184 : Comparison of Cyclic voltammogram of Zn(II), Zn(II)-Apa, Zn(II)-Phe, Zn(II)-Cate and Zn(II)- 3-NBS at similar condition (pH =3, Scan rate= 0.10V/s,).
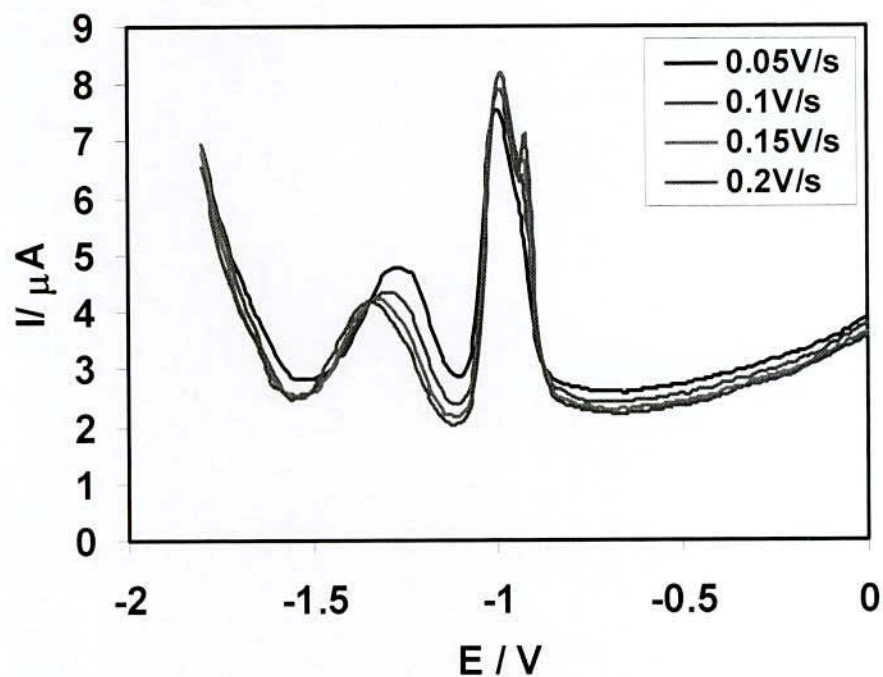
Figure 4.185 : Differential pulse voltammogram of 2mM Zn(II) + 2mM catechol in buffer solution (pH = 2) for forward direction (oxidation) at different scan rate.
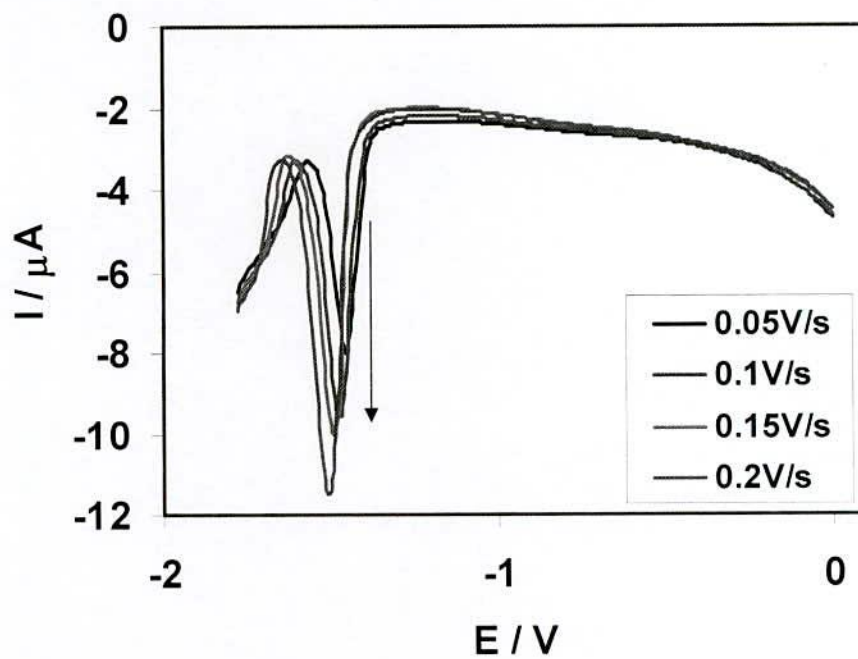
Figure 4.186 : Differential pulse voltammogram of 2mM Zn(II) + 2mM catechol in buffer solution (pH = 2) for backward direction (reduction) at different scan rate.
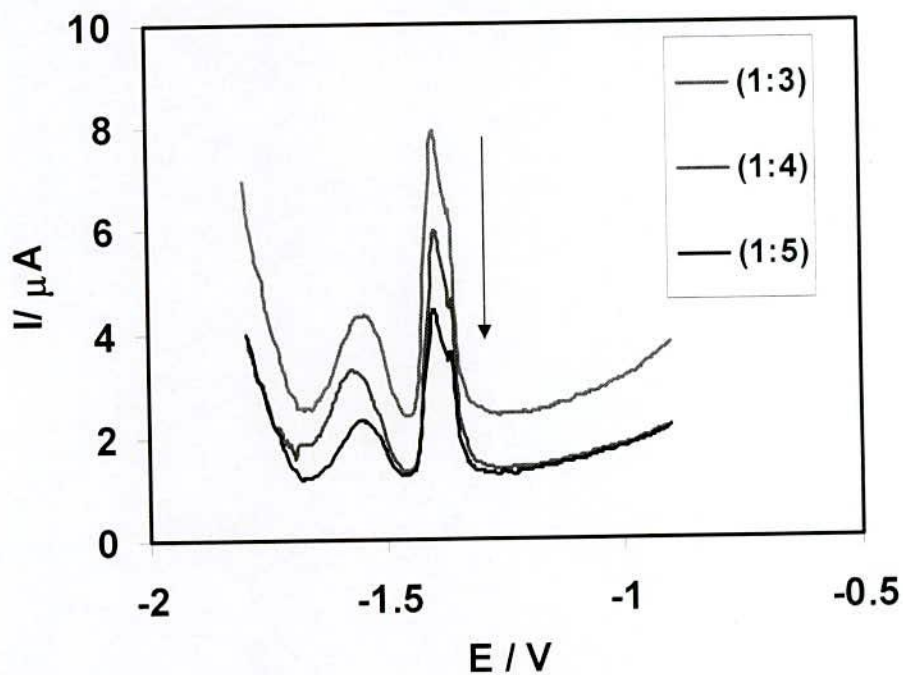
Figure 4.187 : Comparison of Differential pulse voltammogram of Zn(II) + catechol (1:3, 1:4, 1:5) in buffer solution (pH = 2) for forward direction (oxidation) at $0.1 vs^{-1}$ scan rate.
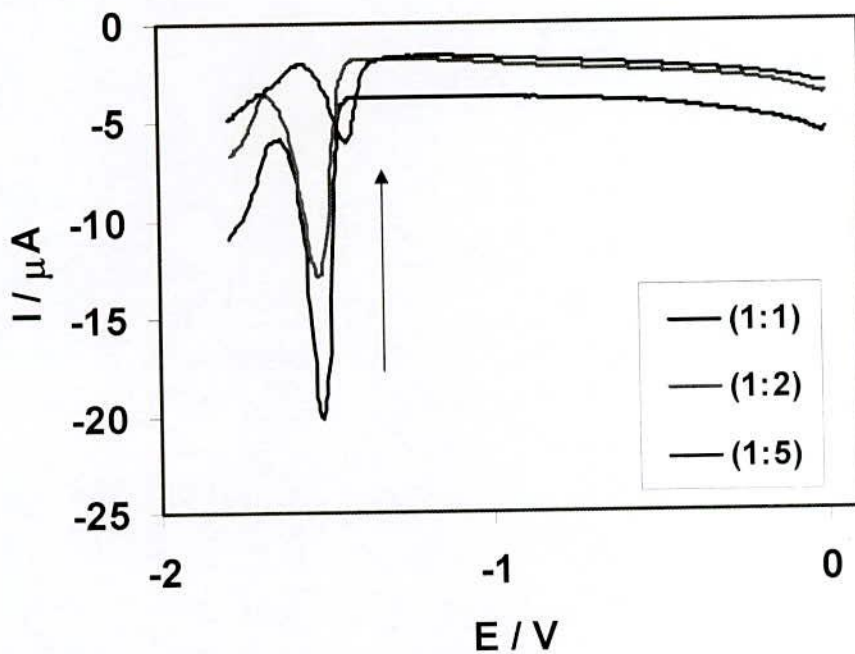
Figure 4.188 : Comparison of Differential pulse voltammogram of Zn(II) + catechol (1:1, 1:2, 1:5)) in buffer solution (pH = 2.0) for backward direction (reduction) at $0.1 Vs^{-1}$ scan rate.
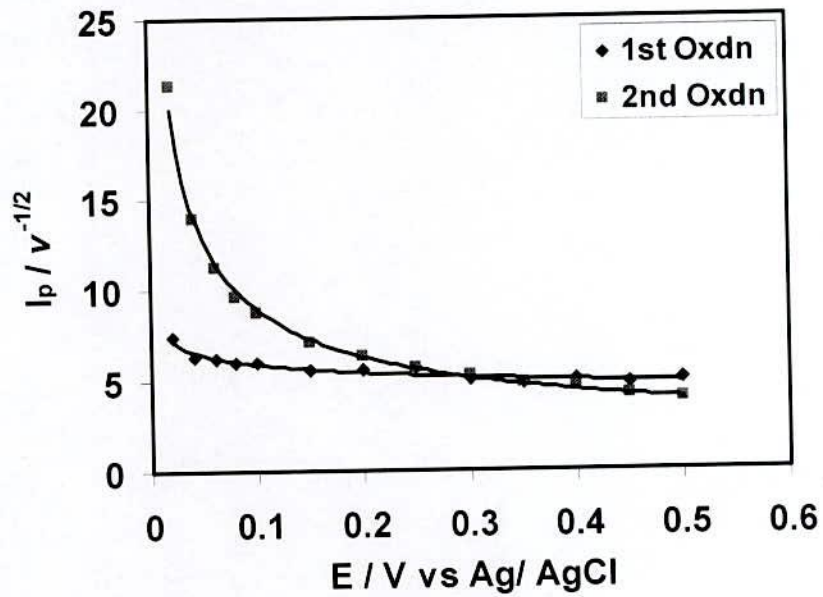
Figure 4.189 : Plots of $I_p/v^{-1/2}$ versus scan rate of $2mMCuCl_2$ + 6mM L-phenyl alanine (1:3) in buffer solution pH = 3.5.

CHAPTER V

Conclusion

Cyclic voltammetric and Differential pulse voltammetric studies were used to investigate the interaction behavior of biologically important metal ions such as Cu(II) and Zn(II) with aspartic acid (Apa), L-phenyl alanine (Phe), 3-nitrobenzene sulfonate (NBS) and/or Catechol (Cate). The interaction studies have been carried out in variation of metal ion concentration, ligand concentration, pH and scan rate. Apa and Phe are electroinactive ligands whereas Cate and NBS are electroactive ligands. The CV results indicated that Cu(II)-ligand systems and Zn(II)-ligand systems were quasireversible. The results indicated that both the cathodic and anodic peaks were shifted and sometimes developed new peaks upon the addition of the Apa, Phe, NBS, Cate. The development of the new peaks or shifted peaks suggested the formation of metal-ligand complex. The intensities of all the peaks are decreased compared to those of free metal ions upon the addition of ligands. The intensities of the peak current were increased with increasing both the concentrations of metal ions as well as ligands. This is due to the formation of more metal-ligand complex that enhanced the peak intensities. The effect of pH of metal-ligand complexes was studied by varying pH from 2.0 to 11. The peak current of metal-ligand complexes increases with the decrease of pH indicating that at the lower pH the metal-ligand complexes are highly electroactive. The maximum peak current was obtained at pH 3-4. This indicates that the electrochemical oxidation of metal-ligand complexes is facilitated in acid media and hence the rate of electron transfer is faster.

The plots of peak potential, E_p against pH of studied metal-ligands varies linearly and the slopes of the plot was determined graphically, which is close to 30 mV for a two-electron, two-proton transfer process which indicate that the oxidation of the metal -ligand proceeded via the $2e^-/2H^+$ processes. This also suggests that during the reaction not only electron but also protons are released from the metal-ligand complexes.

This is because the coordination sites of the ligands molecules were increased with decreasing pH that favored the formation of more metal-ligand complex. The intensities of the peak current were also increased with increasing scan rate that has been explained by the

Randles-Sevcik equation. A linear behavior of i_p vs. square root of scan rate plot indicated that the electrochemical processes were diffusion controlled. DPV of metal –ligand complexes showed similar nature of CV. The CV of the Cu (II)-ligands showed two pairs of signals for the both cathodic and anodic mode and every step is single electron transfer process. The electron transfer number was determined from the slope and intercept of Cottrell plot. From the studied of all systems it is seen that current functions ($1/v^{-1/2}$) decreased with the increasing of scan rate except Zn(II)- Cate. So the behavior of electrode reaction of Cu(II)- ligands and Zn(II)- ligands are of ECE mechanism and Zn(II)- Cate showed of CE mechanism.

REFERENCES

1. Zayas Blanco, F. De , García Falcón, M.S. and SimalGándara J., 2004, J. Food. Contr., Vol. 15, p. 375.

2. Bult, A. Metal Ions in Biological Systems, Sigel, H., Ed., New York: Marcel Dekker, 1983, vol. 16, p. 261.

3. Shashikala Devi, Ramaiah, K., Vanita, M., Veena G.K. and Vaidya, K., 2011, V.P.J. Chem. Pharm. Res., Vol. 3, pp. 445-451.

4. Amuthaselvi, M. Jothi, P. Dayalan, A. Duraipandiyan V. and Ignacimuthu, S. J. Chem. Pharm. Res., 2011, 3(1), 382-387.

5. Gutierrez, L. Alzuet, G. Borras, J. Castiñeiras, A. Fortea, A. R. Ruiz, E., 2001, Inorg. Chem., Vol. 40, p. 3089.

6. Shivhareand Mangla S. and Gautam, D., 2011, J. Chem. Pharm. Res., Vol. 3, pp. 682-688.

7. M. E. Hossain, 2010, study of interaction between metals and phenylalanine and isolation, characterization and properties of the complex, Dhaka University.

8. Pandeya, S.N., Sriram, D., Declecq, E.C., Pannecouque, M. Mitvrouw, 1999, Indian J. Pharm. Sci., Vol. 60, p. 207.

9. Cerchiaro, G., Aquilano, K., Filomeni, G., Rotilio, G., Ciriolo, M.R. Ferreira, A.M.D.C., 2005, J. Inorg. Biochem., Vol. 99, p. 1433.

10. Stickely, K. R., Selby, T. D. and Blackstock, S. C., 1997, J. Org. Chem., Vol. 62, p. 448.

11. Nishiumi, T., Nomura, Y., Chimoto, Y., Higuchi, M. and Yamamoto, K., 2004, J. Phys. Chem. B, Vol. 108, p. 7992.

12. Nishiumi, T., Motin, M.A. and Aoki K, 2005., Electrochem. Commun., Vol. 7, p. 1213.

13. Motin, M.A. Nishiumi, T., and Aoki K, 2007, J. of Electroanal. Chem. Vol. 601, pp 139–147.

14. IUPAC-IUBMB Joint Commission on Biochemical Nomenclature and Symbolism for Amino Acids and Peptides, 2007.

15. D.L Nelson, M.M Cox. and A.L. Lehninger, 2000, "Principle of Biochemistry", pp. 679. Worth Publishing , New York, 3rd Ed,

16. http://en.wikipedia.org/wiki/Catechol.

17. Briggs, D.E.G., 1999, "Molecular taphonomy of animal and plant cuticles selective preservation and diagenesis". Philosophical Transactions of the Royal Society B: Biological Sciences 354, 7.

18. B.A. Barner, 2004, "Catechol" in Encyclopedia of Reagents for Organic Synthesis Wiley & Sons, New York, (Ed: L. Paquette),

19. Fahlbusch, K.G. Hammerschmidt, F. J. and Panten, J., 2005, "Horst SurburgFlavors and Fragrances" in Ullmann's Encyclopediaof Industrial Chemistry, Wiley- VCH.

20. Fiegel, H., Voges,H. W., Hamamoto, T., Umemura, S. and Lwata, T., 2002, "Phenol Derivatives" in Ullmann's Encyclopedia of Industrial Chemistry, Wiley- VCH.

21. Nomenclature and symbolism for amino acids and peptides (IUPAC-IUB Recommendations 1983)", 1984, Pure Appl. Chem. Vol. 56, pp. 595–624, doi:10.1351/pac198456050595

22. http://datasheets.scbt.com/sc-229293.pdf

23. A.J. Bard and L.R. Faulkner, 2001, Electrochemical Methods: Fundamentals and applications, John Wiley & Sons, Hobokon, Nj. 2nd Ed,

24. M. E. Hossain, 2014, Electrochemical sensor simultaneous detection and estimation of environmental toxic pollutants, M.Phil Thesis, KUET.

25. http://www.drhuang.com/science/chemistry/electrochemistry/polar.doc.htm

26. Zhang, L. and .in,X., 2001, Analyst, Vol. 126, pp. 367-370.

27. Santos, D.P., Fogg, A.G. and Zanoni, B., 2005, Microchim. Acta., Vol. 151. pp. 127-134.

28. Kakihana, M., Ikeuchi, H., Satoh, G. P. and Tokuda, K., 1981, *J. Electroanal. Chem. Vol.* 117, p. 201.

29. Ikeuchi, H., 2005, *J. Electroanal. Chem. Vol.* 577, p. 55.

30. A.S. Brill (Ed.), Transition Metals in Biochemistry, Springer Verlag, New York, 1977.

31. Huerta, F., Morallon, E., Vazquez, J. L. and Aldaz, A., 1999, *J. Electroanal. Chem.* Vol. 475, p. 38.

32. E. J. Underwood, 1977, Trace Elements in Human and Animal Nutritions, Academic Press, New York, 4th Ed.

33. West, D.X., El-Sawaf, A.K. and Bain, G.A., 1998, *Tran. Met. Chem., Vol.* 23, p. 1.

34. Oljan, R., Kapa, P. and George, T.L., 2001, *Org. Process Research & Development,* 5, p. 519.

35. Thompson, K.H. and Orvig, C., 2006, *J. Chem. Soc., Dalton Trans.,* 761.

36. Ferrari, M.B., Fava, G.G., Tarasconi, P., Albertini, R., Pinelli, S. and Starcich, R., 1994, *J. Inorg. Biochem., Vol.* 53, p. 13.

37. Rodrigues-Arguelles, M.C., Ferrari, M.B., Bisceglie, F., Pelizzi, C., Pelosi, G., Pinelli, S. and Sassi, M., 2004, *J.Inorg. Biochem., Vol.* 98, p. 313.

38. Cerchiaro, G., Aquilano, K., Filomeni, G., Rotilio, G., Ciriolo, M.R. and Ferreira, A.M.D.C., 2005, *J. Inorg.Biochem., Vol.* 99, p. 1433.

39. Kauffmann, J.M. and Vire, J.C., 1993, *Anal. Chim. Acta., Vol,* 273, p. 329

40. J. Wang, (Ed.), 1988, *Electroanalytical Techniques in Clinical Chemistry and Laboratory Medicine,* VCH, New York,

41. P.T. Kissinger, W.R. Heineman, 1966, *Laboratory Techniques in Electroanalytical Chemistry,* Marcel Dekker, New York, 2nd Ed.

42. Mannan, R.J. and Sarker, G.C., 1997, *J. Bangladesh Acad. Sci, Vo.* 21, pp. 35-41.

43. A.L. Crumbliss, in: G. Winkelmann (Ed.), 1991.Handbook of Microbial Iron Chelates, CRC Press, New York.

44. Raymond, K.N. , 1994, Pure Appl. Chem., Vol. 66, p. 773.

45. A.-M. Albrecht-Gary, A.L. Crumbliss, in: A. Sigel, H. Sigel (Eds.), 1998, Metal Ions in Biological Systems, vol. 35, p. 239, Marcel Dekker, New York,,

46. A.E. Martell, W.F. Anderson, D.G. Badman (Eds.), 1981, Development of Iron Chelators for Clinical Use, Elsevier, New York,

47. G. Winkelman, D. Van der Helm, J.B. Neilands (Eds.), 1987, Iron Transport in Microbes, Plants and Animals, VCH, Weinheim, Germany.

48. V. Braun, K. Hantke, in: G. Winkelmann, C.J. Carrano (Eds.), 1997, Transition Metals in Microbial Metabolism, p. 81, Harwood Academic Publishers, London.

49. Gobinda, N.P., Bakshi, P.K., and Khair, A., *J. Bangladesh Chem. Soc.,* 2002, vol. 15, no. 2, p. 134.

50. Romman, U.K.R., Malik, K.M.A., Haider, S.Z., and Hursthouse, M.B., 1992, *J. Bangladesh Acad Sci.,* vol. 16, p. 159.

51. Romman, U.K.R., Malik, K.M.A., and Haider, S.Z., *J., 1993, Bangladesh Chem. Soc.,* vol. 6, p. 43.

52. Romman, U.K.R., Malik, K.M.A., and Haider, S.Z., 1999, *J. Bangladesh Acad. Sci.,* vol. 23, p. 155.

53. Montazerozohori, M., Hojjati, A., Joohari, S. and Ebrahimi, H.R. 2012, Synthesis and Electrochemical Behavior of Some New Four Coordinated IIB Transition Metal Ions Complexes, Int. J. Electrochem. Sci., Vol. 7, pp. 11758 – 11767

54. Montazerozohori, M, Nozarian, K. and Ebrahimi, H.R., 2013, Theoretical, and Electrochemical Studies of Zn(II), Cd(II), and Hg(II) Azide and Thiocyanate Complexes of a New Symmetric Schiff-Base Ligand, Journal of Spectroscopy, Vol. 2013, pp, 9.

55. Mamun, M.A., Ahmed, O., Bakshi, P.K. and Ehsan, M.Q., 2010, Synthesis and spectroscopic, magnetic and cyclic voltammetric characterization of some metal complexes of methionine: $[(C_5H_{10}NO_2S)_2M^{II}]$; M^{II} = Mn(II), Co(II), Ni(II), Cu(II), Zn(II), Cd(II) and Hg(II), Journal of Saudi Chemical Society, Vol. 14, pp. 23–31

56. Kulkarni, A.D., Patil, S.A. and Badami, P.S., 2009, Electrochemical Properties of some Transition Metal Complexes: Synthesis, Characterization and In-vitro antimicrobial studies of Co(II), Ni(II), Cu(II), Mn(II) and Fe(III) Complexes. Int. J. Electrochem. Sci.,Vol. 4, pp. 717 – 729

57. Haque, F., Rahman, M.S., Ahmed, E., Bakshi, P.K. and Shaikh, A.A., 2013, A Cyclic Voltammetric Study of the Redox Reaction of Cu(II) in Presence of Ascorbic Acid in Different pH Media, Dhaka Univ. J. Sci. vol. 61, pp. 161-166.

58. Afzal Shah, 2010, Redox Behavior and DNA Binding Studies of Some Electroactive Compounds, Ph.D Thesis, Department of Chemistry, Quaid-i-Azam University, Islamabad.

59. C.M.A. Brett and A.M.O. Brett, 1993, Electrochemistry Principles, Methods and Applications, Oxford University Press.

60. P.T. Kissinger and W.R. Heineman, 1996, Laboratory Techniques in Electroanalytical Chemistry, Marcel Dekker, Inc.

61. C.M.A. Brett and A.M.O. Brett, 1998, Electroanalysis, Oxford University Press.

62. J.B. Chaires, N. Dattagupta and D.M. Crothers, 1982, Biochemistry, 21, 3933.

63. Randles, J.E.B., 1948, Trans. Faraday, Soc., Vol. 44, pp. 327.

64. Sevcik, A., 1948, Collec. Czech. Chem. Common., Vol. 13, pp. 349.

65. Bott, A.W., 1994, Curr. Seps., 13, 49.

66. Klinger, R.J., and Kochi, J.K., 1981, J. Phy. Chem., Vol. 85, p. 12.

67. Delahay, E. J.,1953, Am. Chem. Soc., Vol. 75, p. 1190.

68. A.J. Bard and L.R. Faulkner, 1980, Electrochemical Methods, Fundamentals and Applications, John Wiley, New York.

69. Hush, N.S., 1958, J Chem. Phys., Vol. 28, p. 962.

70. Palecek, E. and Fojta, M., 2001, Anal. Chem., Vol. 73, p. 74.

71. Matsuda, H. and Ayabe, Y.Z., 1955, J. Electrochim., Vol. 59, p. 494.

72. Reinmuth, W.H., 1961, Anal.Chem., Vol. 33, p. 1793.

73. Nicholson, R.S., 1965, Anal. Chem., Vol. 37, p. 135.

74. Andrews, L. J., 1954, Chem. Revs., Vol. 54, p. 713.

75. Eyring, H. Glasstone, S. and Laidler, K.J., 1939, J. Chem. Phys.,Vol. 7, p.1053.

76. Reinmuth, W.H., 1962, Anal.Chem., Vol. 34, p. 144.

77. Laviron, E., 1983, J. Electrochim. Interfac. Electrochim., Vol. 1, p. 148.

78. Polcyn, D.S. and Shain, I.,1966, Anal. Chem., Vol. 38, p. 370.

79. Nicholson, R.S., and Shain, I., 1964, Anal. Chem., Vol. 36, p. 706.

80. Gileadi, E. and Eisner, U. J., 1970, Electroanal. Chem., Vol. 28, p. 81.

81. Klinger, R.J. and Kochi, J.K., 1981, J. Phy. Chem., Vol. 85, p. 1731.

82. J. Wang, 1994, Analytical Electrochemistry, VCH Publishers, New York.

83. Aoki, K. and Osteryoung, J., 1981, J. Electroanal. Chem. Vol. 122, p. 19.

84. Aoki, K. and Osteryoung, J., 1984, J. Electroanal. Chem. Vol. 160, p. 335.

85. Flanagan, J.B. and Marcoux, L., 1973, J. Phys. Chem. Vol. 77, p. 1051.

86. Heinze, J., 1981, J. Electroanal. Chem., Vol. 124, p. 73.

87. Shoup, D. and Szabo, A., 1982, J. Electroanal. Chem., Vol. 140, p. 237.

88. Gavaghan, D. J. and Rollett, J. S., 1990, J. Electroanal. Chem. Vol. 295, p. 1.

89. Qian, W., Jin, B., Diao, G., Zhang, Z. and Shi, H., 1996, J. Electroanal. Chem. Vol. 414, p. 1.

90. Ikeuchi, H. and Kanakubo, M., 2000, J. Electroanal. Chem. Vol. 493, p. 93.

91. D.A. Skoog, F.J. Holler and T.A. Nieman, 2007, Principles of Instrumental Analysis, pp. 349-351, Thomson Brooks/ Cole, 6th Ed.,

92. Gosser, Jr. D.K., 1993, Cyclic Voltammetry (Simulation and analysis of reaction mechanisms), Wiley-VCH, Inc.

93. F.M. Hawkridgein, P.T. inKissinger, and W.R.(Eds.) Heieman, 1996, Laboratory Techniques in Electroanalytical chemistry , Marcel Dekker Inc., New York. 2nd Ed.

94. J. Wang, 1994, Analytical Electrochemistry, VCH Publishers Inc., New York.

95. E.R. Brown, and R.F. Larg, A. inWeissberger and B.(Eds.) Rossiter, 1971, Physical Methods of chemistry, Vol.1-Part IIA, Wiley-Interscience, New York.

96. Armada, P.G., Losada, J. and Perez, S. V., 1996, "Cation analysis scheme by differential pulse polarography", Vol. 73, pp. 544-546.

97. Zhang, J., 1972, Electroanal. Chem., Vol. 331, p. 945.

98. Brown, G.M., Meyer, T.J., Cowan, D.O., Levanda, C., Kaufman, F., Roling, P.V. and Rausch, M. D., 1975, Inorg. Chem. Vol. 14, p. 3.

99. Barlow, S. and Ohare, D., 1997, Chem. Rev. Vol. 97, p. 637.

100. Wienk, M.M. and Janssen, R.A., 1997, J. Am. Chem. Soc., Vol. 119, p. 4492.

101. Aoki, K., Akimoto, K., Tokuda, K., Matsuda, H. and Osteryoung, J., 1984, J. Electroanal. Chem., Vol. 171, p. 219.

102. Kakihana, M., Ikeuchi, H., Satoh, G.P. and Tokuda, K., 1981, J. Electroanal. Chem. Vol. 117, p. 201.

103. Guang-Jun Xu, Ying-Ying Kou, Li Feng, Shi-Ping Yan, Dai-Zheng Liao, Zong-Hui Jiang and Peng Cheng, 2006, Cu(II) and Ni(II)-1,10-phenanthroline- 5,6-dione-amino acid ternary complexes exhibiting pH-sensitive redox properties, Appl. Organometal. Chem. Vol. 20, pp. 351–356.